

# **Understanding the mode of action of TRPC1/4/5 ion channel modulators**

Aisling Minard

Submitted in accordance with the requirements for the degree of  
Doctor of Philosophy

The University of Leeds  
School of Chemistry

September 2018

## Intellectual property and publication statements

The candidate confirms that the work submitted is her own, except where work which has formed part of jointly-authored publications has been included. The contribution of the candidate and the other authors to this work has been explicitly indicated below. The candidate confirms that appropriate credit has been given within the thesis where reference has been made to the work of others.

Portions of Chapter 1 were adapted from a review article that was published in June 2018 (Minard, A., Bauer, C.C., Wright, D.J., Rubaiy, H.N., Muraki, K., Beech, D.J., Bon, R.S., Remarkable Progress with Small-Molecule Modulation of TRPC1/4/5 Channels: Implications for Understanding the Channels in Health and Disease. *Cells* **7**, 52–72 (2018)). AM (the candidate) prepared a draft of section 3 (Recent Progress with Small-Molecule Modulators of TRPC1/4/5 Channels) which was edited into its final form by RSB. The draft originally prepared by AM was then re-written as Section 1.3 of Chapter 1.

The majority of the work described in Chapter 3 formed the basis of a research article which was published in February 2016 (Naylor, J., Minard, A., Gaunt, H.J., Amer, M.S., Wilson, L.A., Migliore, M., Cheung, S.Y., Rubaiy, H.N., Blythe, N.M., Musialowski, K.E., Ludlow, M.J., Evans, W.D., Green, B.L., Yang, H., You, Y., Li, J., Fishwick, C.W., Muraki, K., Beech, D.J., Bon, R.S., Natural and synthetic flavonoid modulation of TRPC5 channels. *Br. J. Pharmacol.* **173**, 562–574 (2016)). The contributions of the authors are as follows: JN, HJG, MSA, LAW, SYC, HNR, BLG, HY, YY, JL performed screening of natural products and evaluation of flavonols by calcium recording assays in HEK cells and mouse primary cells; MM performed synthesis of library of mono-substituted flavonols and SAR analysis; AM (the candidate) performed synthesis of AM12 with assistance of route development from WDE and calcium recording assays of AM12 with assistance from HG; NMB, KEM and MJL developed TRPC4/5-C1 concatemers and stable cell lines, HNR and KM performed electrophysiology assays; CWF supervised MM; HY, DJB and RSB provided project design and leadership; DJB and RSB prepared the manuscript.

This copy has been supplied on the understanding that it is copyright material and that no quotation from the thesis may be published without proper acknowledgement.

## Acknowledgments

Firstly, I would like to thank my primary supervisor Dr Robin Bon for the opportunity to work on this project and all the help and support he has given me throughout my PhD. Secondly, I would like to thank my co-supervisors Dr Stuart Warriner and Prof David Beech for all the incredibly useful ideas and suggestions for the project. I would also like to thank AstraZeneca and Dr Matt Burnham for a brilliant opportunity to undertake a placement within the safety screening department and for all of your useful tips for the project.

Work in this thesis would not have been possible without all the technical staff in the School of Chemistry, Faculty of Biological Sciences and LICAMM. In particular, Simon Barrett and Mark Howard for help with NMR experiments, Martin Huscroft for HPLC analysis and purification, Alan Burnett for organisation of cell culture and calcium recording facilities and Dr Rachel George for performing tandem mass spectrometry experiments.

I would also like to thank Hannah Gaunt for teaching me cell culture and calcium recording assays, Kat Miteva, Lucia Pedicini, Claudia Bauer and David Wright for helping me with calcium recording assays, immunoprecipitations and western blots, and all members of the Beech group (past and present) who have helped me in the lab. Thanks to Dr Shahrzad Mohamadi for her help with the electrochemical biosensor assays. I would also like to thank Ann Woods for teaching me automated electrophysiology. I would like to acknowledge Dr Megan Wright for providing YnMyr tagged protein lysates for click experiments and all the useful suggestions and discussions which really helped the project move forwards.

Special thanks to all members of the Bon group (past and present) for all the useful discussions and advice. Particularly, Jake Hauser for all your random facts and interesting office discussions and Hester Beard my 'partner in crime', you have made the past four years so much fun.

Finally, thank you Mum, Dad and John (Jack and Sam) for all the love and support you have always given me.

## Abstract

Calcium ions are critical for cellular signalling and impact almost all aspects of cellular life. TRPC channels are non-selective cation channels permeable to both Na<sup>+</sup> and Ca<sup>2+</sup>. TRPC channels are ubiquitously expressed in mammalian tissue and are linked to a wide range of pathological and physiological mechanisms. TRPC proteins can form both homo- and hetero-tetrameric channels. The natural composition and heteromerization of TRPC channels is poorly understood. However, they have been reported to be particularly promiscuous in the formation of heteromers. Over recent years numerous modulators of TRPC1/4/5 channels have been published; among them (-)-Engelrin A and Pico145 have emerged as particularly potent and specific activators and inhibitors of TRPC1/4/5 channels, respectively. However there still lacks evidence around the mode of action of these modulators and the ability to differentiate between TRPC1, TRPC4 and TRPC5 homomers and heteromers.

This thesis explores approaches to unravel the mechanism of action of TRPC1/4/5 modulators. Firstly, recently published TRPC1/4/5 modulators, along with the pathology and advancements in structural information are reviewed in *Chapter 1*. Secondly, current approaches towards chemical labelling of target proteins is explored in Section 1.6 of *Chapter 1*. A range of cellular and biochemical techniques have been used in this thesis to unravel the mechanism of action of ion channel modulators and these have been briefly explained in *Chapter 2*. *Chapter 3* details the development of novel TRPC5 modulators and investigation of the mechanism of action through calcium recording, electrophysiology and cyclic voltammetry experiments. Findings from these experiments suggest that the synthetic flavonol-based TRPC5 modulators act directly on the channel. The work in *Chapter 4* details the use of photoaffinity probes based on the TRPC1/4/5 channel inhibitor, Pico145, to indicate a direct interaction with TRPC5. The work in this chapter identified that a known TRPC5 channel activator can distinguish between the closely related TRPC4 and TRPC5 proteins (~70% sequence identity). Structure activity relationships were explored on a series of TRPC5 inhibitors in *Chapter 5*. Overall this thesis demonstrates how multiple approaches can be used to unravel the mechanism of action of ion channel modulators in a synergistic manner.



## Table of Contents

Intellectual property and publication statements.....	i
Acknowledgments.....	ii
Abstract .....	iii
Abbreviations .....	x
Chapter 1- Introduction .....	1
1.1 TRP Channels.....	1
1.2 TRPC Channels .....	2
1.3 Pharmacology of TRPC1/4/5 Channels.....	4
1.3.1 Pharmacology 1: Activators.....	4
1.3.1.1 (-)-Englerin A .....	5
1.3.1.2 Tonantzitolone .....	6
1.3.1.3 Riluzole.....	7
1.3.1.4 BTD .....	7
1.3.2 Pharmacology 2: Inhibitors.....	8
1.3.2.1 A54.....	9
1.3.2.2 ML204 .....	10
1.3.2.3 Benzimidazoles .....	10
1.3.2.4 Xanthines .....	11
1.3.3 Comparison of TRPC1/4/5 channel modulators.....	13
1.4 Disease relation of TRPC1/4/5 channels.....	14
1.5 Composition and recent structural studies of TRPC1/4/5 Channels.....	17
1.6 Ligand-directed labelling in target- and binding-site identification .....	21
1.6.1 Genetic manipulation methods.....	22
1.6.2 Biochemical approaches .....	23
1.6.3 Target engagement studies of membrane protein modulators.....	25
1.6.4 Binding site identification of ion channel modulators.....	27
1.6.5 Considerations for photoaffinity labelling experiments .....	29
1.6.6 Photo-induced crosslinking chemistries.....	30

1.6.6.1	Aryl azides .....	31
1.6.6.2	Benzophenones.....	32
1.6.6.3	Diazirines.....	33
1.6.6.4	Summary of photoaffinity labelling functional groups .....	34
1.6.7	Traceless affinity labelling chemistries .....	36
1.7	Project aims .....	40
Chapter 2 - Techniques and Methods .....		41
2.1	Intracellular calcium measurements .....	41
2.2	Manual electrophysiology .....	44
2.3	Automated electrophysiology .....	46
2.3.1	Cardiac safety .....	47
2.3.2	Experimental protocols.....	49
2.4	Electrochemical biosensor assays.....	51
2.5	Photoaffinity labelling experiments .....	52
Chapter 3 - Modulation of TRPC5 using natural and synthetic flavonols .....		55
3.1	Introduction .....	55
3.2	Synthesis of galangin analogues AM12 and AM13.....	59
3.3	Identification of AM12 and AM13 as synthetic flavonols that selectively inhibit TRPC5 .....	61
3.3.1	Comparison of AM12 and AM13 to a known TRPC5 inhibitor, 2-APB ..	61
3.3.2	Evaluation of the potency of AM12 and AM13 on TRPC5 .....	62
3.3.3	Evaluation of the activity of AM12 on TRPC5 in the presence of alternative activators .....	63
3.3.4	AM12 inhibits TRPC1/4/5 channels relatively directly .....	64
3.3.5	Investigation into the effect of AM12 on other TRP channels.....	66
3.4	Effect of AM12 and AM13 on a series of cardiac ion channels .....	67
3.5	Electrochemical biosensor assays.....	70
3.6	Summary and Conclusions.....	73
Chapter 4 - Pico145 based photoaffinity probes to elucidate the mechanism of action of Pico145.....		74

4.1	Introduction .....	74
4.2	Design and synthesis of photo-reactive Pico145 derivatives .....	76
4.2.1	Design.....	76
4.2.2	Synthesis .....	78
4.3	Evaluation of the activity of Pico145 photoaffinity probes .....	81
4.3.1	Investigations into the activity of Pico145-DA and Pico145-DAAIk against TRPC5.....	81
4.3.2	Investigation of Pico145-DA and Pico145-DAAIk on calcium elevation mechanisms .....	83
4.3.3	Evaluation of the potency of Pico145-DA and Pico145-DAAIk on TRPC5 84	
4.3.4	Inhibition of the Pico145-DA and Pico145-DAAIk activated calcium entry <i>via</i> TRPC5 with Pico145 .....	86
4.3.5	Inhibition of the Pico145-DA and Pico145-DAAIk activated calcium entry <i>via</i> TRPC5 with ML204 .....	88
4.3.6	Evaluation of the potency of the photoaffinity probes against TRPC4...89	
4.3.7	Evaluation of the potency of the photoaffinity probes against heteromeric channels TRPC5:C1 and TRPC4:C1 .....	91
4.4	Characterisation of a TRPC5 agonist .....	94
4.4.1	Evaluation of the potency of AM237 on TRPC5.....	95
4.4.2	Evaluation of the potency of AM237 on TRPC4.....	96
4.4.3	Evaluation of the potency of AM237 against heteromeric channels TRPC5-C1 and TRPC4-C1 .....	97
4.5	Sequence mapping of TRPC5 protein .....	99
4.5.1	Identification of TRPC4/5 protein <i>via</i> immunoprecipitation and mass spectrometry.....	101
4.5.2	Sequence coverage optimisation.....	102
4.6	The use of photoaffinity probes to confirm target engagement with TRPC5 105	
4.6.1	Irradiation of photoaffinity probes and mass spectrometric analysis ...	105
4.6.2	Click chemistry using alkyne tagged protein lysates .....	106

4.6.3 Photoaffinity labelling followed by click chemistry with Azide-fluor-545 for target engagement studies .....	107
4.7 Conclusions.....	110
Chapter 5 - Synthesis of a library of novel TRPC5 inhibitors .....	113
5.1 Introduction .....	113
5.2 Design and synthesis of a third series of piperazine inhibitors of TRPC5 ..	115
5.3 Evaluation of the potency of piperazine and piperidine inhibitors.....	120
5.3.1 Evaluation of potency of Gd <sup>3+</sup> -evoked TRPC5 activity .....	120
5.3.2 Evaluation of potency of (-)-EA-evoked TRPC5 activity .....	122
5.4 Evaluation of the selectivity of piperazine and piperidine inhibitors.....	123
5.5 Future work and conclusions.....	125
Chapter 6 - Thesis summary and future directions .....	126
Experimental Section .....	129
7.1 Experimental section applying to all chapters .....	129
7.1.1 General materials and methods for organic synthesis .....	129
7.1.2 Ionic Solutions.....	130
7.1.3 Chemicals and reagents.....	130
7.1.4 Cell Culture .....	131
7.1.5 Intracellular calcium measurements .....	131
7.1.5.1 Fura-2 acetoxymethyl ester (Fura-2 AM) .....	131
7.1.5.2 High throughput Ca <sup>2+</sup> measurement using the FlexStation II <sup>384</sup> /FlexStation III <sup>384</sup> .....	132
7.1.5.3 Experimental protocol .....	133
7.1.5.4 Data Analysis.....	134
7.1.6 Automated electrophysiology .....	135
7.1.6.1 Cell culture .....	135
7.1.6.2 Experimental protocol for IonWorks HT system <sup>272</sup> .....	136
7.1.6.3 Voltage protocols.....	140
7.2 Experimental section for Chapter 3 .....	143
7.2.1 Organic synthesis.....	143

7.2.2	Chemicals and reagents.....	148
7.2.3	Cell Culture .....	148
7.2.4	Manual electrophysiology .....	148
7.2.5	Rapid cyclic voltammetry experiments .....	149
7.3	Experimental section for Chapter 4 .....	150
7.3.1	Organic synthesis.....	150
7.3.2	Solutions .....	158
7.3.3	Chemicals and reagents.....	158
7.3.4	Cell Culture .....	159
7.3.5	Photoaffinity labelling experiments .....	160
7.3.5.1	Photoaffinity labelling in cells and lysis .....	160
7.3.5.1	DC protein quantification assay .....	161
7.3.5.2	CuAAC .....	162
7.3.5.3	SDS-PAGE.....	162
7.3.5.4	Fluorescence Gel .....	163
7.3.5.5	Western blotting.....	163
7.3.6	Peptide mapping of TRPC5-SYFP2 .....	163
7.3.6.1	Immunoprecipitation .....	164
7.3.6.2	In-gel digestion .....	164
7.3.6.3	In-Gel Digestion Protocol – ProteaseMax .....	165
7.3.6.4	On-bead digestion <sup>278</sup> .....	166
7.3.6.5	Sep-Pak C18 Purification.....	167
7.3.6.6	Liquid chromatography-mass spectrometry .....	167
7.4	Experimental Section for Chapter 5.....	169
7.4.1	Organic synthesis.....	169
Appendix I	.....	182
Appendix II	.....	200
Appendix III	.....	201
Appendix IV	.....	202
Appendix V	.....	208

Appendix VI .....	210
Bibliography .....	216

## Abbreviations

(-)-EA	(-)-Englerin A
(-)-EB	(-)-Englerin B
2-APB	2-Aminoethoxydiphenyl borate
AGD	Affinity guided DMAP catalysis
AGOX	Affinity guided oxime catalysis
ALS	Amyotrophic lateral sclerosis
AT1R	angiotensin type 1 receptor
CA12	Carbonic anhydrase 12
CA2	Carbonic anhydrase 2
Ca <sup>2+</sup>	Calcium ion
Ca <sup>2+</sup> <sub>e</sub>	Extracellular calcium
Ca <sup>2+</sup> <sub>i</sub>	Intracellular calcium
CBB	Coomassie Brilliant Blue
Cch	Carbachol
CCK-4	Cholecystokinin tetrapeptide
COSY	Correlation spectroscopy
CuAAC	copper(I)-catalysed azide-alkyne cycloaddition
DEPT	Distortionless enhancement by polarisation transfer
DMAP	4-Dimethylaminopyridine
DMSO	Dimethyl sulfoxide
DOPC	Dioleoyl phosphatidylcholine
EC <sub>50</sub>	Half maximal effective concentration
EDTA	Ethylenediaminetetraacetic acid
ESI	Electrospray Ionisation
Fluo-4 AM	Fluo-4 acetoxymethyl ester
FSGS	Focal segmental glomerulosclerosis
Fura-2 AM	Fura-2 acetoxymethyl ester

Gd <sup>3+</sup>	Gadolinium ion
GPCR	G protein-coupled receptor
HEK	Human embryonic kidney
hERG	Human ether-à-go-go-related gene
Hg	Mercury
HMBC	Heteronuclear multiple bond correlation
HMQC	Heteronuclear multiple quantum coherence
HPLC	High performance liquid chromatography
HRMS	High resolution mass spectrometry
IR	Infrared (spectroscopy)
K <sub>v</sub>	Potassium voltage-gated channels
IC <sub>50</sub>	Half maximal inhibitory concentration
LC-MS	Liquid chromatography–mass spectrometry
LDAI	Ligand-directed acyl imidazole chemistry
LDBB	Ligand-directed (di)bromophenyl benzoate
LDNASA	Ligand-directed <i>N</i> -acyl- <i>N</i> -alkyl sulfonamide
LDPE	Ligand-directed phenyl ester chemistry
LDSP	Ligand-directed <i>N</i> -sulfonyl pyridine
LDT	Ligand-directed tosyl chemistry
MeOH	Methanol
MS	Mass spectrometry
Na <sup>+</sup>	Sodium ion
Na <sub>v</sub>	Sodium voltage-gated channels
PAL	Photoaffinity labelling
PBS	Phosphate buffered saline
PKCθ	Protein kinase C isoform θ
PPC	Population patch clamp
Pt	Platinum



q-PCR	Quantitative polymerase chain reaction
Q-TOF	Quadrupole time of flight
S1P	Sphingosine-1-phosphate
S1R	Sigma-1 receptor
SAR	Structure activity relationships
SD	Standard deviation
SDS-PAGE	Sodium dodecyl sulfate–polyacrylamide gel electrophoresis
SE	Standard error
siRNA	small interfering RNA
SOCE	Store operated calcium entry
STAB	Sodium triacetoxyborohydride
TBTA	tris[(1-benzyl-1 <i>H</i> -1,2,3-triazol-4-yl)methyl]amine
TCEP	tris(2-carboxyethyl)phosphine hydrochloride
TdP	Torsades de Pointes
TFA	Trifluoroacetic acid
THF	Tetrahydrofuran
TMS	Tetramethylsilane
TRP	Transient receptor potential
TRPA	Transient receptor potential ankyrin
TRPC	Canonical transient receptor potential
TRPM	Transient receptor potential melastatin
TRPML	Transient receptor potential mucolipin
TRPN	Transient receptor potential nompC
TRPP	Transient receptor potential polycystic
TRPV	Transient receptor potential vanilloid
TZL	Tonantzitolone
WT	Wild type

# Chapter 1- Introduction

## 1.1 TRP Channels

Modulation of calcium ( $\text{Ca}^{2+}$ ) concentration is an important signalling mechanism in cells, controlling numerous cellular processes.<sup>1,2</sup>  $\text{Ca}^{2+}$  ions play important roles in short-term cellular responses, such as contraction and secretion; long-term responses can include cell growth, proliferation and cell death.<sup>3</sup> Regulation of intracellular calcium concentrations is imperative to the life or death of cells, where an excessive increase is associated with cytotoxicity.<sup>4</sup> Ion channels are important regulators of intracellular calcium levels. Given the importance of  $\text{Ca}^{2+}$  signalling, it is not surprising that dysregulation of ion channels and thus  $\text{Ca}^{2+}$  signalling, is involved in the pathogenesis of several diseases.

TRP channels are a family of non-selective cation channels, with permeability to  $\text{Ca}^{2+}$ ,  $\text{Na}^+$  and  $\text{K}^+$ .<sup>5</sup> The name TRP originates from the *Drosophila* mutant *trp* (transient receptor potential) that showed a transient response to light causing impaired visual adaptation. This was caused by the lack of a specific  $\text{Ca}^{2+}$  entry pathway into photoreceptors.<sup>6</sup> TRP channels are widely expressed in mammalian tissue.<sup>1</sup> There are 28 genes encoding for mammalian homologues of the *Drosophila* TRP channel, however many more channels exist due to heteromerization. On the basis of amino acid sequence homology, the TRP family can be divided into six subfamilies. The family that closely resembles the original *Drosophila* TRP channel was named the 'canonical' or 'classical' TRP channel (TRPC) which will be the focus of this work. The other five TRP families are TRP ankyrin (TRPA), TRP melastatin (TRPM), TRP mucolipin (TRPML), TRP polycystic (TRPP) and TRP vanilloid (TRPV). TRP nompC (TRPN) is an additional TRP family which has been identified in fruit flies, but there are no mammalian homologues.<sup>7</sup>

TRP channels are promiscuous in modes of activation and ion selectivity; being gated by a variety of chemical and physical stimuli. This promiscuity in gating combined with the ubiquitous expression of TRP channels in mammalian tissues produces a wide range of physiological functions.<sup>8</sup>

## 1.2 TRPC Channels

The first mammalian TRP family reported was the canonical TRPC family.<sup>9</sup> All TRPC channels are considered to be permeable to both sodium ( $\text{Na}^+$ ) and  $\text{Ca}^{2+}$ .  $\text{Na}^+$  may contribute to depolarisation of the membrane and indirectly elevate intracellular  $\text{Ca}^{2+}$  levels *via*  $\text{Na}^+$ - $\text{Ca}^{2+}$  exchange.<sup>10</sup> TRPC channels have been found in a plethora of cell types including in the brain,<sup>11</sup> kidney,<sup>12</sup> skeletal muscle<sup>13</sup> and vascular smooth muscle cells amongst others.<sup>3</sup> On the basis of sequence homology and functional similarities the TRPC family can be further divided into two main subfamilies, one consisting of TRPC3, TRPC6 and TRPC7 and the other of TRPC1, TRPC4 and TRPC5.<sup>1</sup> TRPC2 is not expressed in humans; it is encoded by a pseudogene,<sup>14</sup> but it is thought to form fully regulated channels in some other mammalian species.<sup>15</sup> TRPC appears to be the most promiscuous within the TRP family in the formation of heteromeric channels. Additionally, TRPC1 is unique amongst the TRPC family, because it can interact promiscuously within the TRPC family, and interacts with other TRP proteins.<sup>16,17</sup> Furthermore, TRPC1 has been reported to interact with other proteins, including Orai<sup>18</sup> and STIM1<sup>19</sup> in cell lines. It is widely believed that TRPC1 is unlikely to form functional homomeric structures. Clapham and co-workers reported that when TRPC1 was expressed alone, there was a lack of current evoked by the TRPC activator carbachol (Cch).<sup>20</sup> However, when TRPC1 was co-transfected with TRPC5, application of Cch evoked an increase in current; these currents were significantly different to those generated from homomeric TRPC4 and TRPC5 channels. Furthermore, in recent years there has been additional evidence that TRPC1 plays an important role in heteromers of TRPC4 and TRPC5.<sup>21,22,23,24,25</sup> TRPC4 and TRPC5 are capable of forming homomeric channels, yet TRPC1 is widely expressed and therefore physiologically these channels presumably exist as heteromers with TRPC1. It is noteworthy that it remains a difficult challenge to determine the exact composition and contribution of heteromeric or homomeric channels with certainty. However, understanding the heteromerization of TRPC channels has important implications in drug discovery, because it is crucial to understand the subunit composition of the channels endogenously to appropriately target them.<sup>26</sup>

As with other TRP channels, TRPC channels have versatility in their modes of activation. TRPC channels are modulated both by physiological factors and exogenous chemicals. Modulators of these channels include  $\omega$ -3 fatty acids,<sup>24</sup> redox factors such as hydrogen peroxide,<sup>27</sup> stimulation of phospholipase C,<sup>28</sup> and metal ions.<sup>29</sup> The modulation of TRPC1/4/5 channels by exogenous chemicals will be discussed in more detail in *Section 1.3*.

Initially the structure of TRP channels was predicted based on similarities to voltage-gated potassium ( $K_v$ ) channels; the structure was thought to consist of four identical or similar subunits with each subunit consisting of six transmembrane spanning domains, with the ion pore forming between the fifth and sixth domain (*Figure 1*).<sup>1</sup> Recent advances in cryo-electron microscopy (cryo-EM) have facilitated the determination of TRPC structures, which are analogous to the earlier predicted structure. TRPC structures are discussed in more detail in *Section 1.5*.

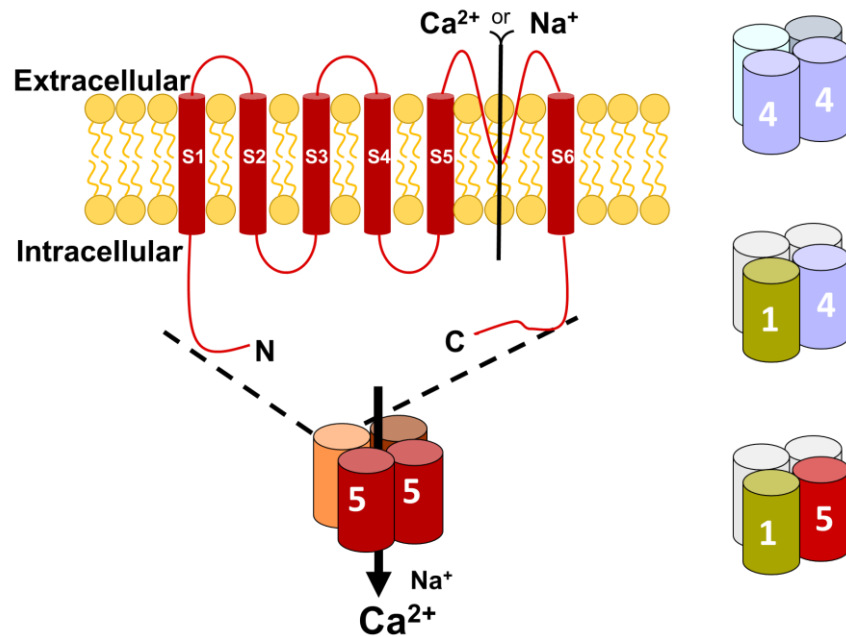


**Figure 1: Proposed composition of a TRPC channel**, showing one subunit with six transmembrane spanning domains and the ion pore between the fifth and sixth domain, with four subunits forming a functional channel. Possible homomeric TRPC5:C5 and TRPC4:C4, and heteromeric TRPC5:C1 and TRPC4:C1 channels are shown.

## 1.3 Pharmacology of TRPC1/4/5 Channels

TRPC1/4/5 channels are modulated by a variety of physical and chemical stimuli and in recent years a number of reviews have been published outlining modulators of TRPC channels.<sup>5,30,31,32</sup> Over the past 10 years there has been a rapid increase in the number of TRPC1/4/5 channel modulators identified. Although a distinct binding site is yet to be identified on a TRPC channel, the rapid increase in more potent and selective modulators of TRPC1/4/5 has yielded important information regarding the modes of action of these modulators.

### 1.3.1 Pharmacology 1: Activators

Traditionally, TRPC1/4/5 channels were activated by lanthanide ions, e.g. gadolinium ( $Gd^{3+}$ ),<sup>29</sup> G-protein-coupled receptor (GPCR) agonists e.g. carbachol<sup>33</sup> or the small molecule rosiglitazone.<sup>34</sup> Although these compounds were widely used to study TRPC1/4/5 channels, their lack of efficacy and potency was a disadvantage. However, in recent years several compounds have emerged as potent, specific and efficacious agonists of TRPC1/4/5 channels (*Figure 2*).

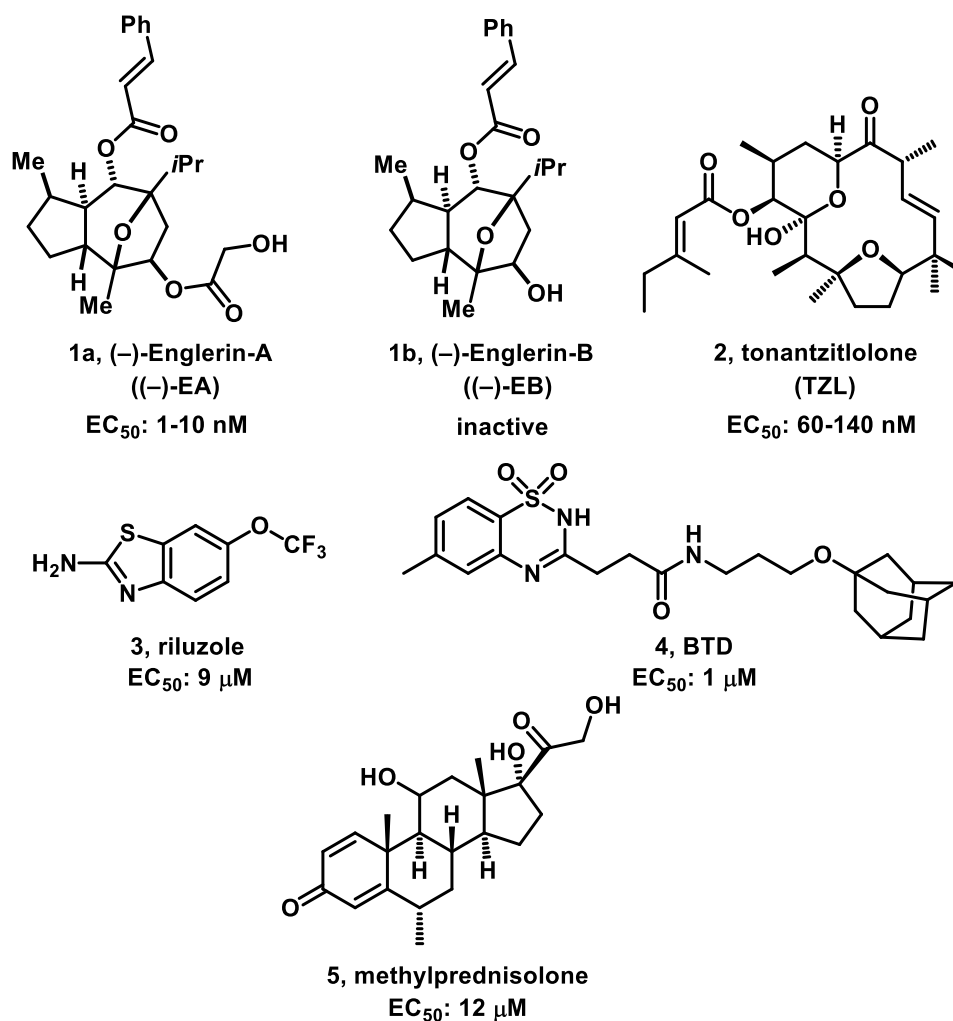


**Figure 2: Chemical structures of TRPC1/4/5 Channel activators:** (-)-Englerin A ((-)-EA, (-)-Englerin B ((-)-EB), tonantzitlolone (TZL), riluzole, BTD and methylprednisolone. All EC<sub>50</sub> values taken from calcium recording assays.

### 1.3.1.1 (-)-Englerin A

A screen of extracts of the East African plant *Phyllanthus engleri* against 60 different cancer cell lines and identification of the bioactive fragments, identified the sesquiterpene (-)-Englerin A ((-)-EA), (1a, Figure 2) as a very potent and selective inhibitor of renal cancer cell growth. Initial attempts to identify the cellular target by chemical proteomics were unsuccessful.<sup>21</sup> However a report linking TRPC4 to renal cell carcinoma<sup>21</sup> led to the identification of (-)-EA as a TRPC4 activator, with a half maximal effective concentration (EC<sub>50</sub>) of 11 nM. Independent target identification studies carried out by Akbulut *et al.*<sup>21</sup> and Carson *et al.*<sup>35</sup> identified TRPC4:C1 heteromeric channels as the target of (-)-EA in A498 cells with an EC<sub>50</sub> value of 10 nM. (-)-EA was then tested against other TRP channels and found to have a similarly high potency against TRPC4's closest homologue, TRPC5 (70% sequence identity from BLAST search<sup>36</sup>), with an EC<sub>50</sub> of 7.6 nM. There was no response of

TRPC6, TRPM2 or TRPV4, 10 other ion channels, and 59 GPCRs on application of (-)-EA, suggesting (-)-EA is highly selective towards TRPC1/4/5 channels.<sup>21,35</sup> (-)-EA has been reported to activate protein kinase C isoform  $\theta$  (PKC $\theta$ ), however this was at micromolar concentrations.<sup>37</sup>

The molecular mechanism of action of (-)-EA remains unclear; however, it shows clear activation of TRPC1/4/5 channels in outside-out patches. This suggests a direct mechanism, possibly by an extracellular site on the channel.<sup>21</sup> Furthermore, an (-)-EA analogue, A54 (*Section 1.3.2.1*), has recently been identified as a competitive antagonist of (-)-EA. A54 does not inhibit Gd<sup>3+</sup>-induced activation of TRPC4/5 channels. This suggests that (-)-EA has a well-defined binding site on TRPC4/5 channels.

Nonetheless, Carson *et al.* found (-)-EA to be unstable in plasma from rats and mice; (-)-EA converts to the inactive form (-)-Englerin B ((-)-EB), (**1b**, *Figure 2*) over time. Additionally it was identified that (-)-EA was toxic *in vivo* and lethal to rats if concentrations in the systemic circulation reached approximately 100 nM.<sup>35</sup> Cheung *et al.* recently identified that the toxic effect of (-)-EA was on target and *via* a similar mechanism to that of (-)-EA induced cancer cell death.<sup>38</sup>

### 1.3.1.2 Tonantzitolone

Tonantzitolone (TZL), (**2**, *Figure 2*) is a natural product found in plants, including *Stillingia sanguinolenta*.<sup>39,40</sup> TZL was identified in a cytotoxicity screen of 60 types of human cancer cells and showed selectivity towards subtypes of cancer cells.<sup>41</sup> Although chemically distinct to (-)-EA, TZL displayed striking similarities in selectivity. Following the identification of (-)-EA as a potent and specific activator of heteromeric TRPC1/4/5 channels; Beech and co-workers investigated the effects of TZL on these channels.<sup>42</sup> Primarily, TZL was shown to cause similar activation of Ca<sup>2+</sup> entry in A498 cells, which contain endogenous TRPC4:C1 heteromeric channels. TZL was found to be a nanomolar activator of TRPC1/4/5 channels, with an EC<sub>50</sub> of 141 nM for TRPC4:C1 heteromeric channels and an EC<sub>50</sub> of 123 nM for TRPC4:C4 homomeric channels. TZL appeared to be more potent towards TRPC5 containing channels with an EC<sub>50</sub> of 83 nM and 62 nM for homomeric TRPC5:C5 and heteromeric TRPC5:C1 channels respectively.<sup>42</sup> TZL activates TRPC5 when applied to outside-out membrane patches, but by contrast failed to activate TRPC5 when bath-applied to inside-out membrane patches. This suggests that TZL acts directly or at least *via* a mechanism

which does not require the intracellular environment and is acting *via* a site accessible from the extracellular side of the membrane.

### 1.3.1.3 Riluzole

Riluzole (**3**, *Figure 2*), was identified by Richter *et al.* as a novel activator of TRPC5, with an EC<sub>50</sub> of 9 μM.<sup>43</sup> Riluzole is an approved drug that delays the progression of amyotrophic lateral sclerosis (ALS),<sup>44</sup> having anti-depressant properties.<sup>45</sup> The effect of riluzole on neuronal activity is thought to be a result of its effect on several ion channels; for a review see Bellingham *et al.* 2011.<sup>46</sup> Richter *et al.* demonstrated that riluzole activates both heterologously expressed TRPC5 in human embryonic kidney (HEK) cells, and endogenous TRPC5 in U-87 glioblastoma cell line.<sup>43</sup> The mechanism of action was shown to be independent of G protein signalling and PLC activity, with riluzole activating TRPC5 in inside-out and cell-attached patches, indicating a direct effect on TRPC5.

### 1.3.1.4 BTD

A screen of a ChemBioNet compound library highlighted two compounds as novel TRPC5 inhibitors, the glucocorticoid methylprednisolone, (**5**, *Figure 2*) and N-[3-(adamantan-2-yloxy)propyl]-3-(6-methyl-1,1-dioxo-2H16,2,4-benzothiadiazin-3-yl)propenamide (BTD), (**4**, *Figure 2*) with EC<sub>50</sub> values of 12 μM and 1.4 μM, respectively.<sup>47</sup> The activation of TRPC5 by these compounds is long-lasting, reversible and sensitive to clemizole,<sup>47</sup> a published TRPC5 inhibitor.<sup>48</sup> Schaefer and co-workers focussed their attention on BTD, because methylprednisolone has a lower potency than the previously established riluzole.<sup>43</sup> BTD had no effect on closely related TRPC channels, such as TRPC3, TRPC6 and TRPC7. Most interestingly, there was no effect on TRPC4, the most closely related analogue to TRPC5, in whole cell patch recordings. Other related TRPC channels that were not activated by BTD include; TRPA1, TRPV1, TRPV2, TRPV3, TRPV4, TRPM2 and TRPM3. BTD activated all studied channel complexes containing TRPC5 subunits, however cells that co-expressed TRPC1 and TRPC4 were not activated. BTD reversibly activates TRPC5 in excised inside-out patches, suggesting a direct stimulatory effect. Although (–)-EA is far more potent (EC<sub>50</sub> 8-20 nM)<sup>21</sup>, (–)-EA also activates the closely related analogue TRPC4.



### 1.3.2 Pharmacology 2: Inhibitors

By definition, an agonist is a compound that binds to a receptor to evoke a response. An antagonist is defined as a molecule that blocks or decreases the effect of an agonist. Typically, an inhibitor is a substance that decreases or prevents the activity of a particular reactant, catalyst or enzyme. In contrast, an inverse agonist is a compound that binds to the same receptor as the agonist; however, it induces the opposite effect of the agonist. Throughout the literature antagonist and inhibitor appear to be used interchangeably with regards to compounds decreasing the response of activated TRPC1/4/5 channels. In this thesis the term inhibitor will be used as a general term which encompasses antagonists.

Traditionally, TRPC1/4/5 channel inhibitors included 2-aminoethoxydiphenyl borate (2-APB, **6**), which was originally identified as a general inhibitor of IP<sub>3</sub> receptors, store-operated calcium entry (SOCE) and TRPC and TRPM channels.<sup>49,50,51</sup> The phenylethylimidazole, SKF96365 is a non-specific inhibitor of Ca<sup>2+</sup> channels<sup>52</sup> and has been used previously as a small molecule antagonist of TRPC1/4/5 channels. However, SKF96365 is a more potent inhibitor of voltage-gated Ca<sup>2+</sup> channels than TRPC channels.<sup>53</sup> Nevertheless, in recent years there has been significant advancements in the development of potent and specific inhibitors of TRPC1/4/5 channels (*Figure 3*).

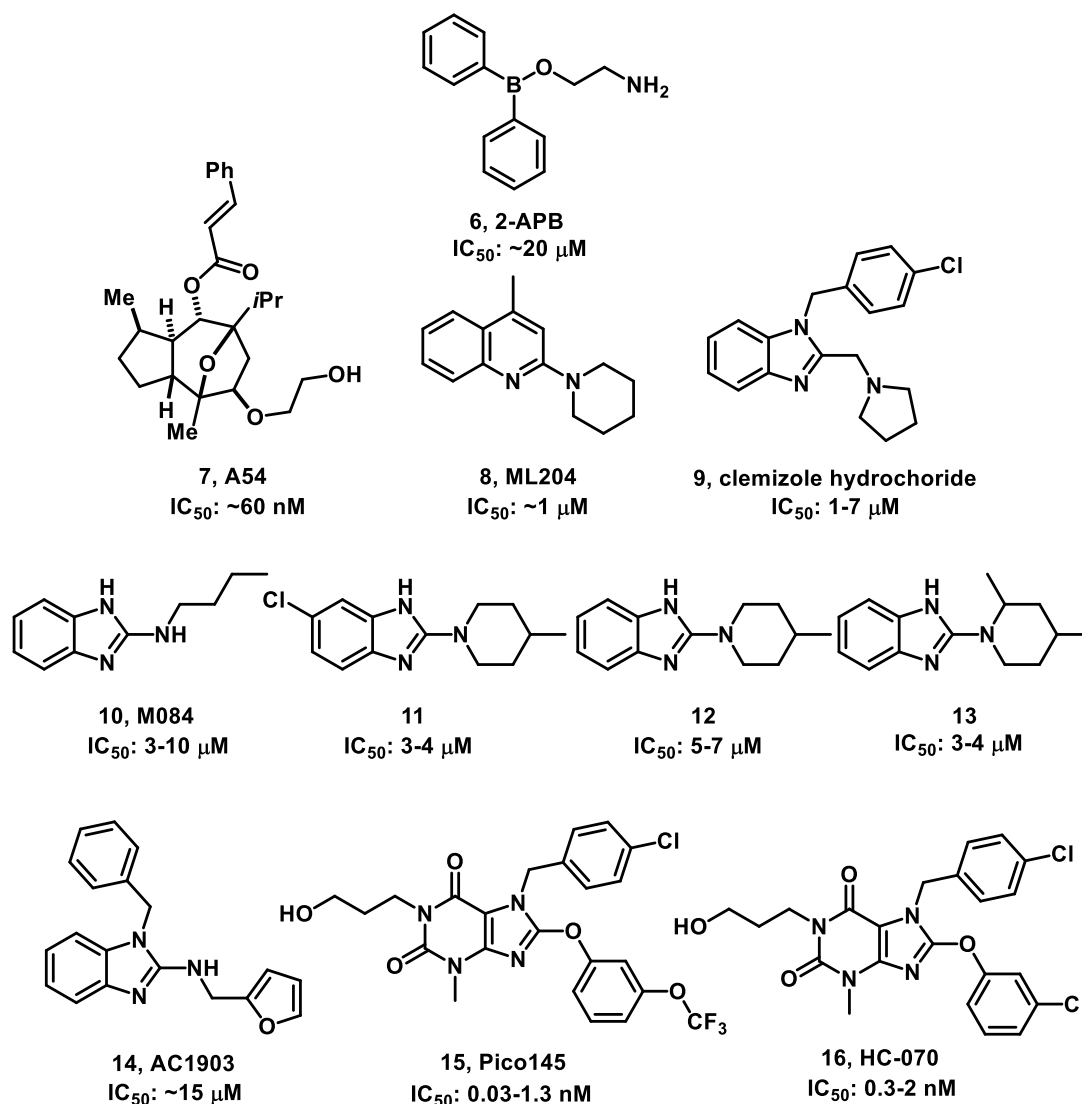


**Figure 3: Chemical structures of selected TRPC1/4/5 channel inhibitors;** A54, ML204, clemizole hydrochloride, M084 and its analogues, 9, 13, and 28, AC1903, Pico145 and HC-070. All IC<sub>50</sub> values taken from calcium recording assays, except 2-APB and AC1903 (taken from whole cell patch clamp recordings).

### 1.3.2.1 A54

Structure activity relationships (SAR) of the cytotoxic effect of (–)-EA have been extensively explored.<sup>54,55,56</sup> From this SAR, Beech and co-workers identified a novel analogue of (–)-EA which is a competitive antagonist of (–)-EA at TRPC1/4/5 channels.<sup>57</sup> A54 (7, Figure 3) abolished the (–)-EA response in A498 cells, which express endogenous TRPC4:C1 heteromeric channels,<sup>21,22</sup> causing 50% inhibition at 62 nM.<sup>57</sup> A54 eradicated the (–)-EA response in TRPC5 expressing HEK-293 cells and caused inhibition of the (–)-EA-evoked TRPC5 current in whole cell patch clamp. However, this effect was (–)-EA dependent; A54 further agonised responses from

Gd<sup>3+</sup>-activated TRPC5. A54 appears to be selective for TRPC1/4/5 channels, lacking effect on 13 other ion channels investigated including TRPC3.<sup>57</sup>

### 1.3.2.2 ML204

Miller *et al.* reported the identification of ML204<sup>58</sup> (**8**, *Figure 3*) as a TRPC4/5 channel inhibitor with an IC<sub>50</sub> of 1 μM against TRPC4 and 65% inhibition of TRPC5 activated through application of μ-opioid receptor agonist [D-Ala2 , N-MePhe4 , Gly-ol]-enkephalin (DAMGO). ML204 has subsequently been used extensively for studying TRPC1/4/5 channels. More recent studies have reported ML204 as a weaker inhibitor of heteromeric channels, at least when channels are activated by (-)-EA.<sup>59,23</sup> This is particularly important for functional studies using ML204, because it is hypothesised that most native channels are heteromeric channels.

### 1.3.2.3 Benzimidazoles

A number of derivatives of benzimidazoles and 2-aminobenzimidazoles have been reported as inhibitors of TRPC1/4/5 channels. Clemizole hydrochloride (**9**, *Figure 3*) was originally developed as a histamine H<sub>1</sub>-receptor agonist.<sup>60</sup> However Richter *et al.* identified it as a novel blocker of TRPC5 channels, with a half maximal inhibitory concentration (IC<sub>50</sub>) of 1 μM.<sup>48</sup> TRPC4β is also inhibited by clemizole with an IC<sub>50</sub> of 6 μM. Clemizole also inhibits TRPC3, TRPC6 and TRPC7, but has greater than 10-fold selectivity for TRPC5. Whole cell patch clamp recordings were used to confirm the inhibition of heteromeric TRPC1:TRPC5 channels when 10 μM clemizole was applied. However, it was identified that at 10 μM clemizole also blocks the human ether-a-go-go related gene (hERG) channels, (data obtained from <https://pubchem.ncbi.nlm.nih.gov/>) which is best known for its contribution to the electrical activity responsible for the heart beating.<sup>61</sup>

M084 (**10**, *Figure 3*) was identified in a cell-based high throughput screen,<sup>62</sup> alongside ML204,<sup>58,5</sup> as a TRPC4 and TRPC5 inhibitor.<sup>5</sup> Although M084 is not as potent as ML204,<sup>58</sup> M084 has improved stability and kinetics for inhibiting TRPC4/5 channels.<sup>63</sup> M084 inhibits TRPC4β with an IC<sub>50</sub> of 3.7 μM and TRPC1:C4 heteromeric channels with an IC<sub>50</sub> of 8.3 μM. In whole-cell voltage clamp recordings, TRPC4-mediated currents immediately decreased on addition of M084, however currents recovered only moderately and slowly on washout. 8 μM M084 rapidly inhibited whole-cell currents in cells expressing TRPC5. M084 had a clear but weak inhibition of TRPC3, with an IC<sub>50</sub> ~50 μM.

A series of compounds was generated based on the 2-aminobenzimidazoles scaffold. Through SAR studies, it appeared that the addition of an *n*-butyl or the joining of the amine by four or five carbons to form a pyrrolidine or piperidine, respectively, was essential for inhibition of TRPC4. The requirement of a heterocyclic aliphatic amine is similar to the SAR profile of ML204, suggesting that the two series share a similar mechanism of action.<sup>62</sup> These SAR studies generated three analogues (compounds, 9, 13 & 28, *Figure 3*) which had slightly improved potency compared to M084 (IC<sub>50</sub> values between 3.1 and 6.6 μM). At 30 μM, M084 and analogues, 9, 13 & 28, showed no agonistic or antagonistic effects on TRPA1, TRPM8, TRPV1 and TRPV3 channels in Ca<sup>2+</sup> fluorescence assays. Additionally, the compounds inhibited TRPC4-evoked currents when applied from the extracellular side, and the inhibition was not dependent on the mode of activation.

A recent publication on the use of small molecule inhibitors of TRPC5 to treat progressive kidney disease identified AC1903 (**14**, *Figure 3*) as a TRPC5 inhibitor.<sup>64</sup> AC1903 is structurally similar to clemizole and M084 and is equipotent to ML204 in inhibition of the riluzole-activated TRPC5 channel with an IC<sub>50</sub> of 14 μM (*cf.* ML204 IC<sub>50</sub>: 13 μM). AC1903 showed selectivity towards TRPC5, with no inhibition seen against TRPC4 or TRPC6, and no off-targets detected in a standard kinase profiling assay panel. It was not reported what the effect of AC1903 was on heteromeric TRPC1/4/5 channels.

#### 1.3.2.4 Xanthines

Pico145 (**15**, *Figure 4*) has recently emerged from an international patent by Hydra Biosciences identifying TRPC5 inhibitors for the treatment of CNS disorders.<sup>65</sup> More than 600 substituted xanthines were initially screened for their ability to block both inward and outward currents through the TRPC5 channel, *via* whole-cell patch clamp recordings. Compounds were tested at 5 μM and 500 nM, with compounds showing no block at 5 μM being categorised as IC<sub>50</sub> > 10 μM. Compounds showing some block of the current were then tested to get a rough estimate of the IC<sub>50</sub> value, then categorised into groups; IC<sub>50</sub> < 100 nM, 100-500 nM, 500-1000 nM, 1-2 μM and 2-10 μM. A high throughput assay was also performed on the xanthine library, detecting intracellular Ca<sup>2+</sup> (Ca<sup>2+</sup><sub>i</sub>) concentration, using fluorescent Ca<sup>2+</sup> indicator fluo-4. Compounds inhibiting the fluorescence response by at least 40% were considered hits for further investigation and IC<sub>50</sub> values were determined. The compounds were yet again categorised into the above groups depending on IC<sub>50</sub> values. Subsequently, four 'hit' compounds (*Figure 4*) from the above *in vitro* assays were tested in *in vivo*

studies for anxiolytic and 'anti-depressive' effects. Mice treated with these compounds showed depressed stress-evoked behaviour, as well as anti-anxiolytic characteristics.

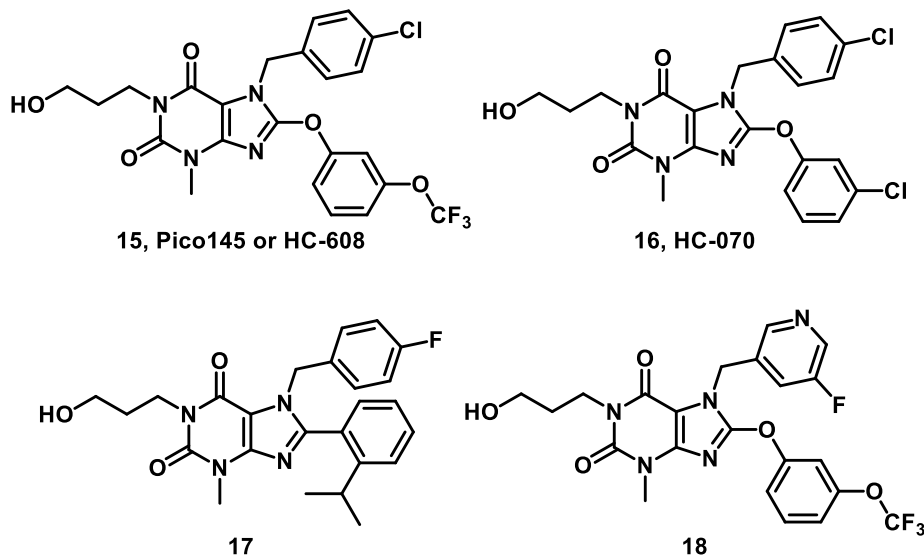


**Figure 4: The chemical structure of 'hit' compounds including Pico145/HC-608 and HC-070 which were tested in *in vivo* models for anti-depressive and anxiolytic effects.<sup>65</sup>**

Beech and co-workers confirmed Pico145 (later called HC-608 by Hydra Biosciences) as a high quality, potent and selective inhibitor of TRPC1/4/5 channels in a recent publication.<sup>59</sup> Pico145 can be synthesised in three steps from commercially available starting materials, making it readily available. Pico145 is a remarkably potent inhibitor of TRPC4 and TRPC5, with  $IC_{50}$  values of 63  $\mu$ M and 1.3 nM respectively. Nonetheless, it is even more potent against the TRPC1 containing concatemeric channels, with  $IC_{50}$  values of 33  $\mu$ M and 199  $\mu$ M for TRPC4-C1 and TRPC5-C1 respectively. Additionally, Pico145 is profoundly selective, with subtype specificity for the heteromeric channels of over two orders of magnitude concentration range.<sup>59</sup> Pico145 is also potent against endogenous (-)-EA-evoked  $Ca^{2+}$  entry into A498 cells, with an  $IC_{50}$  of 49  $\mu$ M.

The mechanism of action of Pico145 remains unclear; however, the excised membrane patch clamp data suggests it has a direct effect *via* the extracellular surface. The effect of Pico145 has not been seen to be rapid enough to suggest a plug of the ion pore. Furthermore, the voltage dependence in the presence of Pico145 is mild, also suggesting that it doesn't block the ion pore.

HC-070 (**16**, Figure 3) was developed in the same patent as Pico145 and has very similar *in vitro* properties. HC-070 has comparable potency against TRPC4 and TRPC5 channels, with  $IC_{50}$  values of 9.3 nM and 46 nM respectively. HC-070 also shares the potent inhibition of TRPC1 containing heteromeric channels; with  $IC_{50}$

values of 1.3 nM and 1.4 nM against TRPC1:C4 and TRPC5:C1, respectively. HC-070 and Pico145 were tested (at 1-2  $\mu$ M) against a variety of other ion channels including TRP channels and a set of potassium/calcium/sodium voltage-gated channels, receptors, enzymes, kinases and transporters; proving HC-070 to be 400 fold selective for human TRPC4 and TRPC5-containing channels.<sup>66</sup> Just *et al.* show that HC-070 is a potent and selective blocker of TRPC4/5 channels and a modulator of neuronal activity and anxious behaviour.<sup>66</sup>

Both Pico145 and HC-070 have suitable pharmacokinetic profiles for functional studies of TRPC1/4/5 channels in cells and animals, including suitability for oral dosing. Pico145 and HC-070 have excellent potency and specificity, in particular demonstrating subtype specificity; indicating that the development of multimer specific modulators of TRPC1/4/5 may be an attainable goal.

### 1.3.3 Comparison of TRPC1/4/5 channel modulators

Examples of recently published agonists of TRPC1/4/5 channels are summarised in *Table 1*. (-)-EA is a highly potent and specific TRPC1/4/5 activator making it a powerful tool for studying the channels. However, its toxicity and instability in rodents mean it is not suitable for *in vivo* studies. BTD shows selectivity towards TRPC5-containing channels over TRPC4, however it is significantly less potent than (-)-EA.

**Table 1:** Summary of TRPC1/4/5 Channel activators

Modulator	Target	Potency (EC <sub>50</sub> )	Potential off-targets	Comments
(-)-EA	TRPC1/4/5	1-10nM	PKC $\theta$ ( $\mu$ M concentrations)	Highly specific and potent. Unstable in plasma in rodents
Tonantzitolone	TRPC1/4/5	60-140 nM	PKC $\theta$ ( $\mu$ M concentrations)	Acts directly and <i>via</i> an extracellular mechanism
BTB	TRPC5:C5 TRPC5:C1 TRPC4:C5	1 $\mu$ M	TRPM8 (EC <sub>50</sub> = 20.6 $\mu$ M)	Distinguishes between TRPC4 and TRPC5 Apparent direct action
Riluzole	TRPC5:C5 TRPC5:C1	9.2 $\mu$ M	Not known	Apparent direct action

TRPC1/4/5 channel inhibitors are summarised in *Table 2*. Pico145 and HC-070 are currently the most promising inhibitors of TRPC1/4/5 channels, with high selectivity and potency. Pico145 and HC-070 have been demonstrated to be suitable for *in vivo* studies. The benzimidazole, AC1903 is a promising inhibitor as it can distinguish between TRPC4 and TRPC5 channels.

**Table 2:** Summary of TRPC1/4/5 channel inhibitors

Modulator	Target	Potency (IC <sub>50</sub> )	Potential off-targets	Comments
<b>A54</b>	TRPC1/4/5	~60 nM	Not known	(-)-EA dependent inhibition
<b>Clemizole Hydrochloride</b>	TRPC5:C5 TRPC4:C4 TRPC5:C1	1-7 μM	TRPC3, TRPC6, TRPC7, hERG	Apparent direct action
<b>Benzimidazoles</b>	TRPC1/4/5 channels	~5-15 μM	TRPC3	AC1903 appears selective to TRPC5:C5 over TRPC4:C4
<b>Pico145</b>	TRPC1/4/5	0.03-1.3 nM	Not known	Selective and suitable for use <i>in vivo</i> Acts directly and <i>via</i> an extracellular mechanism
<b>HC-070</b>	TRPC5:C5 TRPC5:C1 TRPC4:C5	0.3-2 nM	Not known	Selective and suitable for use <i>in vivo</i>

## 1.4 Disease relation of TRPC1/4/5 channels

This section gives an overview of selected studies that demonstrate the use of small molecules to probe the role of TRPC1/4/5 channels in disease. The relationship between Ca<sup>2+</sup> signalling dysregulation and cancer is well established. The roles of TRPC4 and TRPC5 channels in proliferation and migration of cancer cells, angiogenesis and (-)-EA induced renal cancer cell death have been reviewed by Gaunt *et al.*<sup>10</sup> (-)-EA is currently the most potent and specific agonist of TRPC1/4/5 channels and was initially identified as an inhibitor of renal cancer cell growth by Ratnayake *et al.*<sup>67</sup> The cytotoxic effect of (-)-EA was investigated on several types of cancer cells and initially thought to be caused by a Ca<sup>2+</sup> overload in the cell. However, it became apparent that it was Na<sup>+</sup> permeability of the cell that causes this effect. It has been shown that Na<sup>+</sup>/K<sup>+</sup>-ATPase protects cancer cells against Na<sup>+</sup> influx evoked by (-)-EA (two cell lines investigated: A498 renal cell carcinoma cells and Hs578T triple negative breast carcinoma cells).<sup>22</sup>

Subsequently, Muraki *et al.* investigated this Na<sup>+</sup> entry induced cell death in synovial sarcoma cells (SW982 cells). Evaluations of gene expression by quantitative polymerase chain reaction (q-PCR) detected levels of TRPC4 and TRPC1 mRNA, but not TRPC5 in this cell line. The (-)-EA induced cytotoxicity was resistant to TRPC4 inhibitor ML204 (*Section 1.3.2.2*);<sup>58</sup> which has been reported as a weak inhibitor of heteromeric channels activated by (-)-EA.<sup>59</sup> However, the (-)-EA induced cytotoxicity

was completely inhibited by the TRPC4:C1 inhibitor Pico145 (*Section 1.3.2.4*). This suggests that TRPC4:C1 heteromeric channels are responsible for this cytotoxic effect and that these channels are the target of (-)-EA.<sup>23</sup> These findings were further supported by knockdown experiments; cells depleted in TRPC1 showed (-)-EA induced a differently shaped I-V trace (chair shape typical of homomeric TRPC4 channels). In contrast, cells depleted in TRPC4 showed no activation by (-)-EA; further suggesting the importance of TRPC4:C1 heteromeric channels in the (-)-EA-induced cell death. Additionally, SW982 cells were protected against (-)-EA-induced cell death by knockdown of TRPC4; further implicating TRPC4:C1 heteromeric channels in the phenotypic effect of (-)-EA.

Several TRP channels are proposed to play roles in cardiovascular disease.<sup>68,3,69</sup> To date there has been limited use of small molecule modulators to unravel the role of TRPC1/4/5 channels in cardiovascular disease. Londoño *et al.* reported that TRPC1/4 proteins regulate a background Ca<sup>2+</sup> entry pathway that fine-tunes Ca<sup>2+</sup> cycling in cardiomyocytes.<sup>70</sup> TRPC1/4 suppression through double knockout protects against pathological cardiac remodelling, without altering normal cardiac functions. Alzoubi *et al.* reported that TRPC4 knockdown correlates with a survival benefit in rats with severe pulmonary hypertension.<sup>71</sup> Furthermore, TRPC4 has been reported to contribute to pulmonary arterial hypertension<sup>72</sup> and stenosis.<sup>73</sup>

Anxiety and depression is one of the most widely studied diseases in relation to TRPC1/4/5 channels. The pathologies of anxiety and depression disorders have been studied using both genetic manipulation and small molecule modulators. TRPC4 and TRPC5 channels are widely expressed in the brain and have been linked to innate fear. TRPC5 knockdown mice showed reduced fear in behavioural tests, and it was hypothesised that this effect was a result of a reduction in potentiation of TRPC5 by G-protein phospholipase C-coupled receptors.<sup>74</sup> A similar decreased anxiolytic behaviour was observed in mutant mice lacking the TRPC4 subunit.<sup>75</sup>

The TRPC4/5 inhibitor M084 (*Section 1.3.2.3*) was reported to have antidepressant and anxiolytic like effects in mice.<sup>63</sup> However it is unclear from this study if the phenotypic effect of M084 is due to inhibition of homomeric or heteromeric channels. The recent patent published by Hydra Biosciences focused on identifying novel inhibitors of TRPC5 for the treatment of neuropsychiatric and neurodegenerative diseases.<sup>65</sup> Following this, the authors published a compound reported in the patent, HC-070 (*Section 1.3.2.4*) for the treatment of anxiety and depression.<sup>66</sup> HC-070 reduced currents evoked by cholecystokinin tetrapeptide



(CCK-4) recorded from basolateral amygdala neurons, and demonstrated anxiolytic and anti-depressant effects in mouse behavioural studies.

There is conflicting literature with regards to the role of TRPC1/4/5 channels in the development of kidney disease. TRPC5 was found to modulate GTPase Rac1 activity, which regulates cell migration downstream of angiotensin stimulation, in kidney podocytes.<sup>76</sup> Kidney podocytes are cells which form the kidney filter. Greka and co-workers observed that TRPC5 knockout mice were protected against lipopolysaccharides (LPS) induced albuminuria and thus kidney filter barrier damage. Greka and co-workers were able to reproduce this result using wild type (WT) mice and the TRPC4/5 inhibitor ML204.<sup>77</sup> A second paper from the same group investigates the role of TRPC5 in the development of focal segmental glomerulosclerosis (FSGS), which results in progressive kidney disease. In this study Zhou *et al.* use transgenic rats with podocyte-specific over-expression of the angiotensin type 1 receptor (AT1R) with progressive kidney disease.<sup>64</sup> The use of TRPC4/5 inhibitor ML204 attenuated proteinuria caused by kidney damage. Additionally, Zhou *et al.* reported a novel TRPC5 inhibitor, AC1903 (Section 1.3.2.3), which replicated the reduction of proteinuria seen with ML204.

However a recent report published does not support the role of TRPC5 in progressive kidney disease.<sup>78</sup> Wang *et al.* observed no reduction in LPS-induced filtration barrier damage in transgenic mice over-expressing dominant-negative TRPC5 or with the use of ML204. No adverse effects of proteinuria in mice were observed upon treatment with TRPC4/5 agonist (-)-EA.

The differences observed in these reports could be a result of the tool compounds used to study the TRPC5 channels. Wang *et al.* observed no effect when using (-)-EA in mice; however, it has been previously reported that (-)-EA displays poor stability in rodents,<sup>35</sup> and thus it is debatable whether (-)-EA would reach a sufficient concentration to activate TRPC5 channels in the kidney. Furthermore, Van der Wijst and Bindels comment on the differing doses of ML204 used in both reports (Zhou *et al.* used twice daily injections of 25 mg/kg vs. three doses of 2 mg/kg used in the study by Wang *et al.*).<sup>79</sup> Additionally the composition of the subunits of the TRPC5 channels in podocytes and the contribution of heteromers involving TRPC1 is currently unknown. ML204 is a relatively weak inhibitor of heteromeric (-)-EA-activated TRPC5:C1 channels,<sup>59</sup> and deletion of TRPC5 in knockout mice may lead to changes in the formation of tetrameric channels by unaffected proteins e.g. TRPC1, and therefore may not lead to the desired phenotype.

## 1.5 Composition and recent structural studies of TRPC1/4/5 Channels

The ability to rationally design drugs based on protein structure enables structure-based drug design to be an integral part of many drug development projects.<sup>80</sup> Until recently the most common experimental methods to determine structures of proteins were X-ray crystallography and NMR, with over 140,000 available in the public domain (128,359 X-ray structures and 12,323 NMR structures, as of August 2018), and possibly many more in the private sector. Many structures remain undetermined by X-ray crystallography or NMR studies, perhaps due to flexibility, complexity and molecular size.<sup>81</sup> Furthermore, structures determined by X-ray crystallography display a fixed conformation of the protein, disregarding information on flexibility, and this is potentially not the most common conformation in a cellular context. Obtaining crystal structures of membrane proteins can be particularly difficult, especially those of the mammalian origin. TRP channels respond to diverse stimuli, both chemical and physical, thus are believed to be conformationally dynamic;<sup>82</sup> therefore it can be more difficult to encourage these proteins to form well-ordered crystal structures. Over the past 5 years cryo-EM has emerged as a technique to determine protein structures at the near-atomic level.<sup>83,84,85</sup> Utilising cryo-EM, larger and more complex biological systems can be studied, and multiple conformations can be determined.<sup>86</sup> This can provide insights into more biologically relevant states.<sup>87</sup>

This recent revolution in cryo-EM has afforded the emergence of a number of TRP channel structures, covering each TRP sub family. To begin with, Liao *et al.* reported a cryo-EM structure of the rat TRPV1 channel.<sup>82</sup> Liao *et al.* identified a tetrameric architecture, where subunits are arranged around a central ion pore as predicted from the crystal structure of Kv1.2 potassium channels.<sup>88</sup> This structure confirms the hypothesis that there are six transmembrane domains, with the ion pore located between the fifth and sixth domains. Over the subsequent five years an exponential number of TRP channel structures have emerged, many published in both apo and ligand-bound confirmations, including; TRPA1,<sup>89</sup> TRPV2,<sup>90,91,92</sup> TRPV4,<sup>93</sup> TRPV5,<sup>94</sup> TRPV6,<sup>95,96</sup> TRPP2,<sup>83</sup> TRPML1,<sup>97</sup> TRPML3<sup>98</sup> and TRPM4.<sup>84,99</sup>

Several TRPC structures have also emerged in the last year. The structures of human TRPC3:C3 and TRPC6:C6 were recently published.<sup>100,101</sup> TRPC3 and TRPC6 share approximately 40 % sequence homology to human TRPC5 (BLAST search<sup>36</sup>). The TRPC3 structure was determined in an inactive state at 3.3 Å (*Figure 5a*) and two lipid-like densities were identified within the structure. Fan *et al.* identified

an unusually long S3 helix extracellular domain in the structure of TRPC3, with a cavity which may act as a binding site for small molecules (*Figure 5b*).<sup>100</sup> It is noteworthy that the TRPC6 channel structure determined by Tang *et al.* was stabilised in the closed state using the inhibitor BTDM. The binding site identified for BTDM, a position between the voltage sensor-like domain of one subunit and the pore-forming region of another, was in a similar position to the binding sites of resiniferatoxin and capsaicin in TRPV1 structures (*Figure 5d*).<sup>102,103</sup>

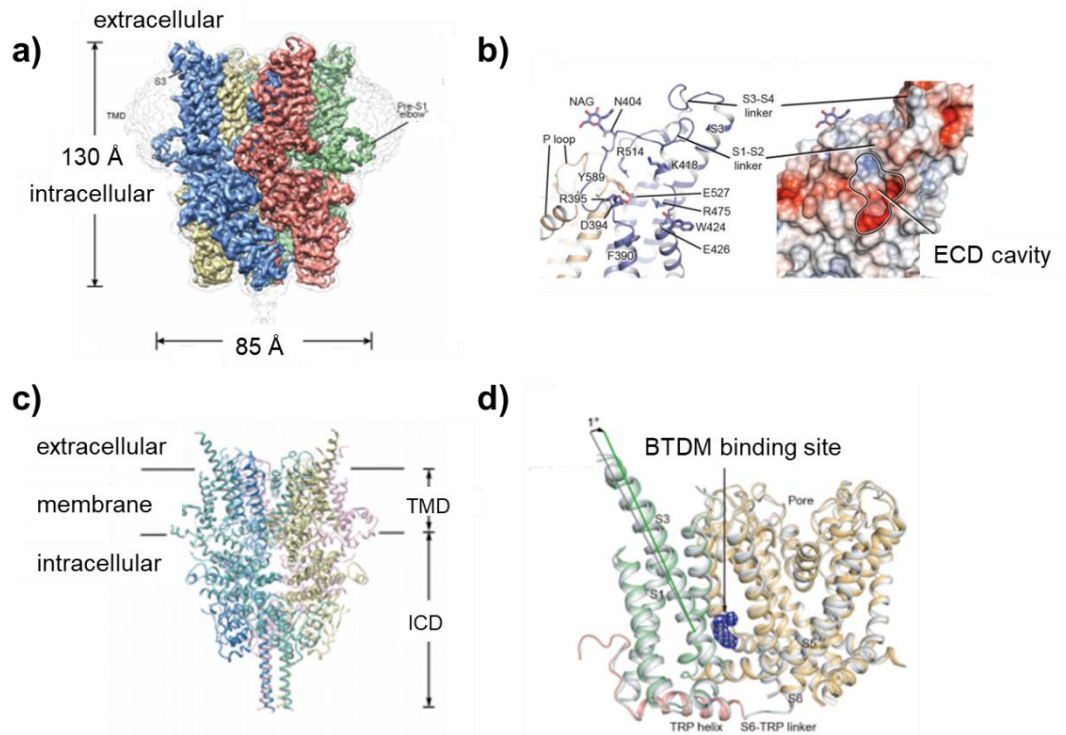


**Figure 5: Structures of human TRPC3 and TRPC6 channels.** **a)** Three-dimensional reconstruction of human TRPC3 viewed parallel to the membrane. Figure copied from Fan *et al.*<sup>100</sup> **b)** Structure of the extracellular domain of hTRPC3 in ribbon (left) and surface representation (right), highlighting the cavity. Figure copied from Fan *et al.*<sup>100</sup> **c)** hTRPC6 model shown from side view. Figure copied from Tang *et al.*<sup>101</sup> **d)** hTRPC6 in allosterically inhibited state with the BTDM density shown in blue. Figure copied from Tang *et al.*<sup>101</sup>

Two TRPC4 structures have recently been reported; the zebrafish<sup>104</sup> and mouse<sup>105</sup> structures (*Figure 6*). mTRPC4 shares 97% sequence identity with hTRPC4, whereas DRTRPC4 shares 79% sequence identity to mTRPC4 (*Table 3*). Both mouse and zebrafish analogues share ~ 70% sequence identity to hTRPC5 and 48% sequence identity to hTRPC1. The disulfide bond (Cys 549A and Cys 554A numbered according to the mouse gene) previously noted by Beech and co-workers to be essential in gating of TRPC5,<sup>106</sup> was identified in the mTRPC4 structure. Duan *et al.*<sup>105</sup> reported that mutation of one of the cysteine residues on TRPC4 would substantially alter the architecture of the poor loop and thus channel activity would be altered. Both TRPC4 structures were solved in their ligand unbound and closed

states, therefore there is a need for further structural studies. Furthermore, there are currently only four structures of heteromeric ion channels,<sup>107,108,109,110</sup> and thus far no structures of heteromeric TRP channels have been reported.

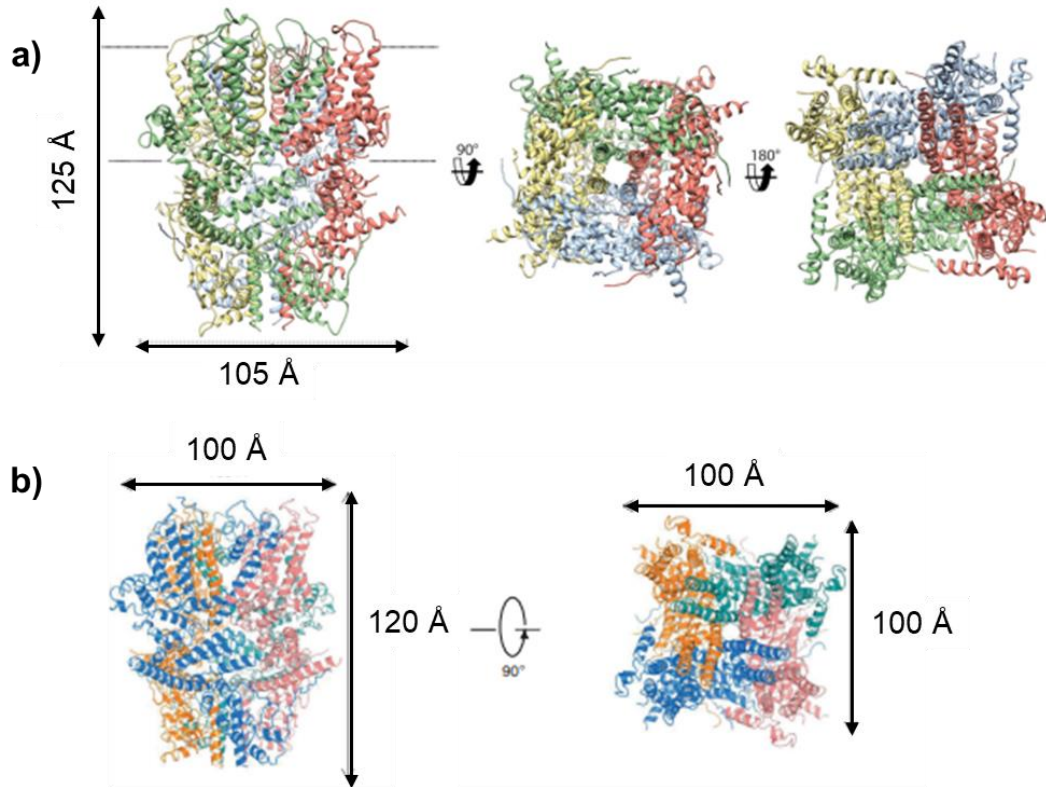


**Figure 6: Structures of zebrafish and mouse TRPC4 channels** a) Ribbon representation of the atomic model of zebrafish TRPC4 with each protomer coloured differently and shown as side, bottom and bottom view. Figure copied from Vinayagam et al.<sup>104</sup> b) Ribbon map of mTRPC4, side and top views at 3.3 Å overall resolution. Each monomer is represented in different colours with channel dimensions indicated. Figure copied from Duan et al.<sup>105</sup>

A summary of recently published TRPC structures is given in Table 3 along with comparisons of the sequence identity to human analogues of TRPC1/4/5 channels.

**Table 3: Cryo-EM structures of TRPC channels**, with details of the resolution, species, state, sequence identity to TRPC1/4/5 channels and the percentage of the sequence modelled.

Channel	Open/closed	Apo/ligand bound	Resolution	Species	% sequence identity vs.			% modelled de novo
					hTRPC5	hTRPC4	hTRPC1	
TRPC1	<i>No structure</i>							
TRPC3	closed	lipid-occupied	3.3 Å	human	39	40	35	83
TRPC4	closed	apo	3.28 Å	mouse	70	97	48	72
TRPC4	closed	apo	3.6 Å	zebrafish	75	79	48	70
TRPC5	<i>No structure</i>							
TRPC6	closed	BTDM bound	3.8 Å	human	37	40	35	72

## 1.6 Ligand-directed labelling in target- and binding-site identification

Over recent years biological and technical advances have facilitated an increase in the use of cell-based assays for phenotypic screening to discover biologically active small molecules. It is often presumed that a direct interaction occurs between the small molecule and the target protein to yield the phenotypic effect; however, this is not always the case. Additionally, the phenotypic effect observed may be from the small molecule binding to one target alone, or it may be the accumulation of effects on multiple targets.<sup>111</sup> Identification of the possible range of targets of a drug candidate is essential to maximise therapeutic potential (e.g. potency and selectivity), minimise toxicity and aid regulatory approval. Once a potential target has been identified, or if it was previously hypothesised, then validation of target engagement can be used to confirm a direct interaction between a small molecule and its target protein. Subsequently, the mode of action and binding site can be investigated, however this can be very challenging as well. There are three typical approaches to target identification or engagement experiments: biochemical approaches,<sup>112,113,114</sup> genetic manipulation methods<sup>115,116</sup> and computational approaches.<sup>117,118,119</sup> However many approaches to target identification and mechanism of action studies often proceed through a combination of these methods.

To date, (–)-EA and Pico145 are the most potent and selective activator and inhibitor of TRPC1/4/5 channels respectively. (–)-EA and Pico145 both show modulation of TRPC1/4/5 channels in excised outside-out membrane patch clamp experiments, suggesting a direct mechanism, possibly by an extracellular site on the channel (*Section 1.3*).<sup>21</sup> Thus this project will focus on target engagement and binding site identification experiments for modulators of TRPC1/4/5 channels.

Structural approaches could be applied to identify the binding site of modulators on TRPC1/4/5 channels. However, obtaining crystal structures of membrane proteins can be particularly difficult (*Section 1.5*). There are currently a few TRPC channel structures determined, however only the structure of TRPC6 has been reported with a ligand bound, with TRPC6 having approximately 40 % sequence identity with TRPC1/4/5 channels. Genetic methods and biochemical approaches are frequently used for confirmation of an interaction between a small molecule and a protein, as well as in binding site identification studies.

### 1.6.1 Genetic manipulation methods

Genetic modifications can be used to 'silence' a specific protein to unravel its role in the phenotypic effect observed in cell-based assays. If genetic knockdown of a protein shares the phenotypic effect of a small molecule inhibitor, or abolishes the effect of an activator, it suggests that this protein is the target.<sup>120</sup> The heteromerization of TRPC channels makes this approach more complicated. The formation and disassembly of protein complexes are under spatial and temporal regulation and thus cannot be fully understood solely on the basis of deletion of one protein.<sup>121</sup> Genetic perturbation of TRPC channels may lead to alterations of native channel stoichiometries, with proteins being capable of overcompensating with the deletion of one protein. This could result in the role of the channels being underestimated.<sup>122</sup>

Once the target of a small molecule has been confirmed, a more direct set of oligonucleotide primers could be used to identify mutations that alter the effects of small molecules. By implementing mutations in hypothesised binding sites, a reduced effect by a small molecule would indicate that mutations have been made in the binding site (*Figure 7*). However, it is difficult to separate effects of ligand binding from effects of conformational changes, for example related to channel function or gating, caused by the mutagenesis.<sup>123</sup> Additionally, both mutated and wild type receptors have to be transfected separately into different batches of cells, thus the transfection efficiency may affect the phenotype observed.<sup>123</sup>

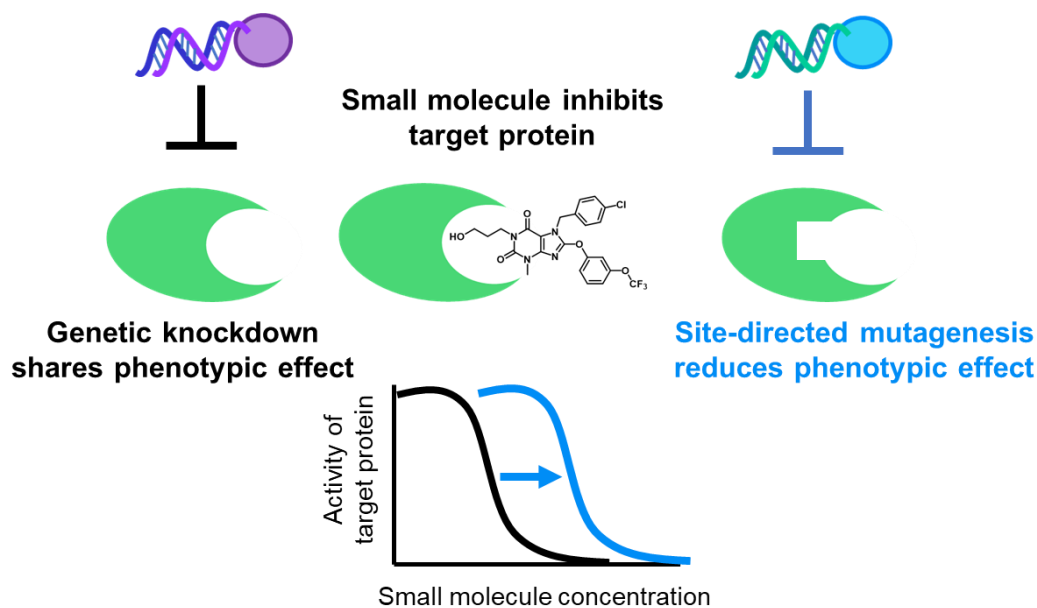


**Figure 7: Genetic manipulation approaches to target engagement and binding site identification.** When genetic knockdown of a protein has the same phenotypic effect of a ligand (inhibitor) binding, it is indicative that this protein is the target for the small molecule. To identify a binding site on the protein, site-directed mutagenesis in the hypothesised binding site can disrupt ligand binding and decrease the phenotypic effect.

## 1.6.2 Biochemical approaches

Biochemical approaches for target engagement and binding site identification include affinity labelling methods. Affinity labelling methods employ a ligand that drives selectivity towards a protein of interest and facilitates targeted labelling. The generation of a covalent ligand-protein complex enables the use of analytical techniques such as sodium dodecyl sulfate–polyacrylamide gel electrophoresis (SDS-PAGE) and mass-spectrometry (MS) to study interactions which would typically dissociate under these harsh conditions.<sup>124</sup>

In many protocols, cells or cell lysates are treated with an affinity labelling probe and sufficient time is allowed for the ligand to associate to the target protein. A reactive group forms a covalent bond to the target protein (irradiation at a specific wavelength is used for photoaffinity probes). If performed on live cells, cells can be lysed and biorthogonal click chemistry performed to incorporate a reporter tag. Labelled and tagged proteins may be identified *via* separation by SDS-PAGE and analysis with a fluorescent dye for a fluorescence gel scan, or a partner for a binding interaction, e.g. biotin-avidin for western blot analysis. Alternatively, MS may allow identification of labelled and tagged proteins, and the specific amino acids modified in the binding pocket (*Figure 8c*).



An affinity labelling approach requires a chemical or photoaffinity probe that frequently consists of 3 parts; the ligand which binds to the target protein, a reactive group, affording permanent attachment to targets, and a reporter group that enables detection or isolation (*Figure 8a,b*). This affinity labelling probe should mimic the activity of the parent compound to the target protein. Achieving incorporation of a reactive group and reporter group to the ligand, whilst retaining equivalent activity towards the target protein can be challenging. An affinity labelling probe often benefits from a small reactive group, minimalising the change in structure from the parent compound. Many reporter groups such as fluorescent dyes and affinity tags are large and thus can affect both activity towards the target protein and cell permeability. An alkyne is frequently used as the reporter group and following cell lysis, biorthogonal click chemistry can be utilised to chemoselectively attach a reporter tag. Bioorthogonal click chemistry utilises chemical reactions which do not interact or interfere with biological systems.<sup>125</sup>

Affinity labelling experiments can be performed with reversibly binding ligands, however there is a degree of reliance on the affinity of the ligand. If the affinity of the probe is low, then the likelihood that nonspecific interactions are also detected increases, driven for example by the hydrophobic effect.<sup>126</sup> Non-specific labelling can be an obstacle in affinity labelling methods, with crosslinking frequently occurring to highly abundant or 'sticky' proteins. Several control experiments can be employed to distinguish between background labelling and specific binding, e.g. competition for binding with the parent compound.

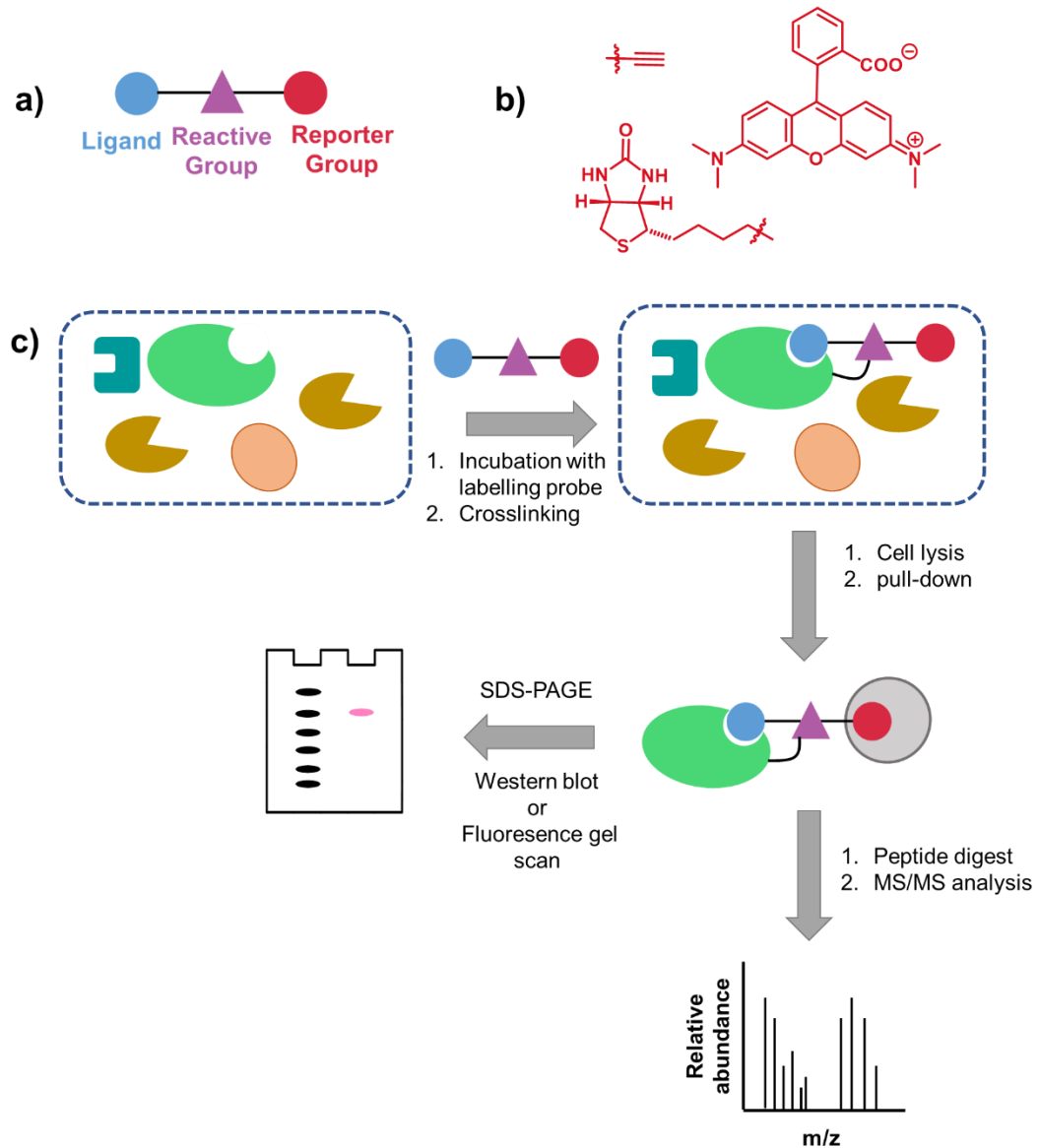


**Figure 8: Affinity labelling approach.** *a)* An affinity labelling probe, consisting of a ligand, reactive group and reporter group; *b)* Chemical structures of reporter groups including an alkyne, fluorescent dye (TAMRA) and biotin; *c)* General schematic of a ligand-directed labelling approach, including crosslinking of the probe to the target protein, cell lysis and purification by pull-down or immunoprecipitation and analysis of target engagement by western blot analysis or a fluorescence gel scan. Identification of peptides in the binding pocket can be achieved through MS/MS analysis.

### 1.6.3 Target engagement studies of membrane protein modulators

Photoaffinity labelling (PAL) and click chemistry are being increasingly used to validate ligand-protein interactions for membrane proteins and ion channels. Gregory *et al.* developed three novel clickable photoaffinity probes for the G protein-coupled receptor (GPCR) Metabotropic Glutamate Receptor 5 (mGlu<sub>5</sub>)<sup>127</sup> (**19**, **20** and **21**, *Figure 9*). These photoaffinity probes enabled Gregory *et al.* to confirm target

engagement of a negative allosteric modulator to mGlu<sub>5</sub> utilising a fluorescent dye. This was the first report of tandem photoaffinity labelling and bioorthogonal click chemistry on a G protein-coupled receptor. Gregory *et al.* demonstrated the irreversible attachment of these probes to mGlu<sub>5</sub> using photoaffinity labelling and bioorthogonal conjugation. The photoaffinity probes were incubated with membrane preparations from HEK-293 cells stably expressing high levels of mGlu<sub>5</sub> and UV irradiation was used to form a covalent bond between mGlu<sub>5</sub> and the probe. Then click chemistry was performed to incorporate a fluorophore and the labelled proteins were separated using SDS-PAGE. A high degree of non-specific interactions were observed, therefore to confirm the direct interaction of the photoaffinity probes to mGlu<sub>5</sub>, mGlu<sub>5</sub> was purified before click chemistry was carried out.<sup>127</sup>

It is noteworthy that photoaffinity labelling has been performed on a TRPC protein. Mori and co-workers used photoaffinity labelling to identify TRPC3 as the target of a pyrazole compound (Pyr3) (**22**, *Figure 9*).<sup>52</sup> A bifunctional probe (Pyr-PP) (**23**, *Figure 9*) was designed containing a functional group for selective modification by aldehyde/keto reactive biotin derivative (ARP) and a photoreactive group (diazirine) for photoaffinity labelling, which retained activity against TRPC3. Cells expressing GFP-tagged TRPC3 were incubated with Pyr-PP, irradiated and Pyr-PP was modified with biotin. Pyr-PP was incorporated into a ~130 kDa protein band (TRPC3-GFP) and importantly this interaction was inhibited by Pyr3. Mori and co-workers were able to pull down photolabelled proteins using Avidin and perform Western blot analysis to GFP to show direct binding of Pyr-PP to TRPC3. Additionally, immunoprecipitation of GFP tagged TRPC3 and western blot analysis for biotin further confirmed the direct interaction between Pyr-PP and TRPC3.

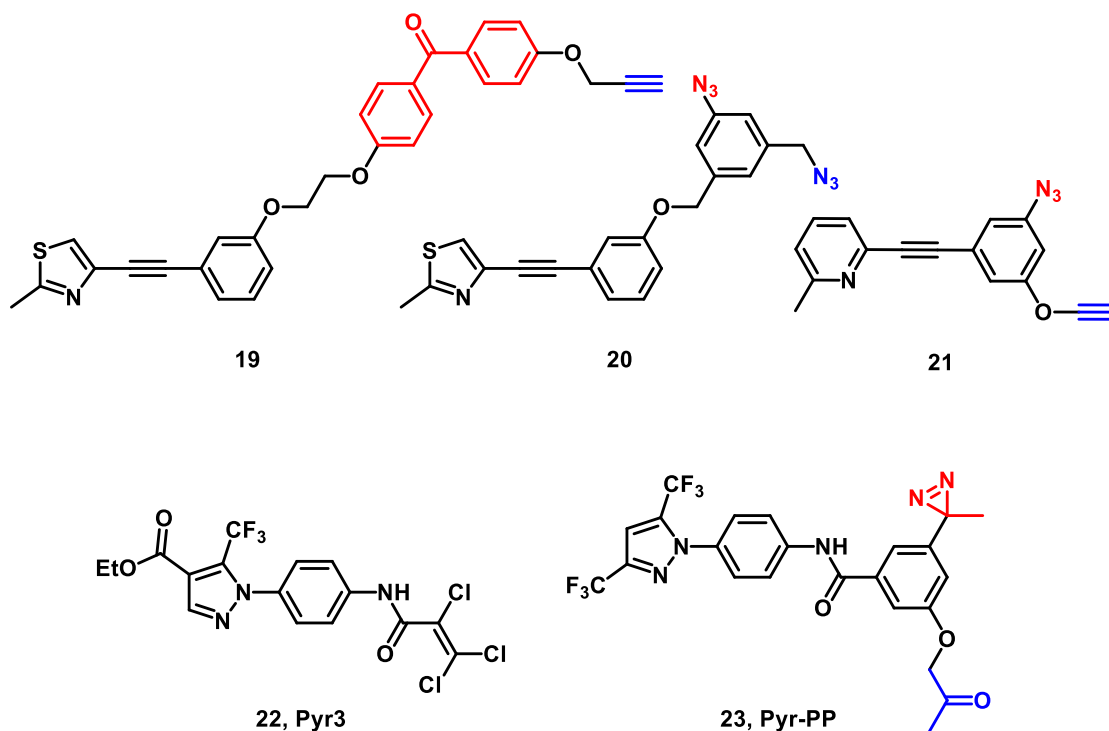


**Figure 9: Clickable photoaffinity probes where photoreactive groups are shown in red and reporter groups are shown in blue. Top: 19, 20 and 21 are photoaffinity probes for the Metabotropic Glutamate Receptor 5. Bottom: Pyr3, 22, a TRPC3 inhibitor and its corresponding photoaffinity probe Pyr-PP, 23.**

#### 1.6.4 Binding site identification of ion channel modulators

Furthermore, photoaffinity labelling has been used by Franks and co-workers to identify the binding site of propofol, (**24**, Figure 10) on a ligand gated ion channel.<sup>128</sup> Propofol is the world's most widely used anaesthetic, where the ligand-gated ion channel, GABA<sub>A</sub> receptor was thought to be the target protein. Franks and co-workers were able to identify a single modified peptide by the photoaffinity label. Franks and co-workers synthesised four different propofol photoaffinity probes incorporating a trifluoromethyl diazirine in the *ortho*-**25**, *meta*-**26** or *para*-**27** and **28** positions (Figure 10). However only one of these was an effective photolabel (*ortho*-propofol diazirine, **25**), with both high efficiency for crosslinking to ethanol (percentage incorporation into ethanol) and with similar activity to the parent compound *in vitro*. The other compounds (**26**, **27** and **28**) were either inefficient photolabelling probes or inactive towards GABA<sub>A</sub> receptors. For binding site identification, membranes were incubated with *ortho*-propofol diazirine, irradiated (>320 nm, 3 minutes), lysed and purified by affinity chromatography. The purified GABA receptors were digested using multiple-timed chymotryptic digestions. LC/MS analysis of protein digests provided unambiguous identification of 96% of amino acids in the  $\beta_3$  subunit and 95% of amino acids in the  $\alpha_1$  subunit. Previous work by Evers and co-workers details the

optimisation of the peptide mapping of GABA<sub>A</sub>,<sup>129</sup> where several previously described peptide digest methods were incorporated into one workflow to enable a high level of sequence coverage, with only small amounts of membrane proteins required. Evers and co-workers used multiple proteases to obtain overlapping peptides, which covered both hydrophilic and transmembrane domain portions of the protein.<sup>129</sup> Franks and co-workers were able to identify a single peptide as being labelled with GABA receptors, whether  $\alpha_1\beta_3$  heteromers or  $\beta_3$  homomers.

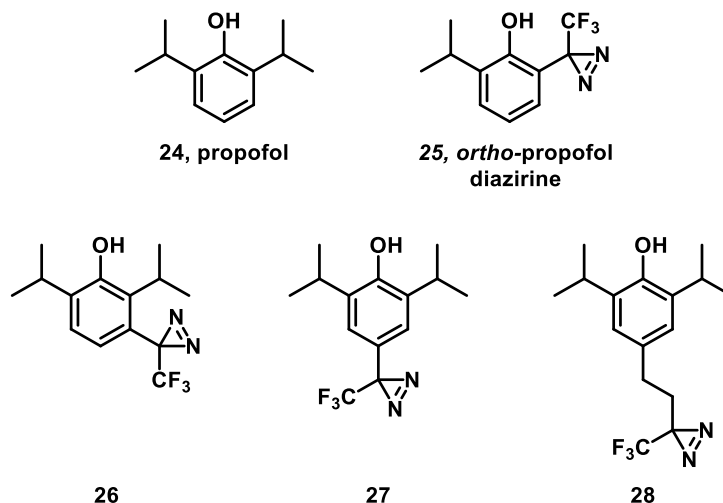


**Figure 10: The chemical structures of propofol, 24 and propofol diazirine derivatives: ortho-propofol diazirine, 25 (the effective photolabel), 26, 27 and 28.**

Additionally, Woll *et al.* managed to determine the binding sites of the anaesthetic, sevoflurane, on the K<sub>V</sub>1.2 channel.<sup>130</sup> Sevoflurane is a widely used anaesthetic, however its mode of action remained unclear. It is noteworthy that TRP channels are thought to have structural and functional similarities to the K<sub>V</sub> channel family.<sup>131</sup> MS analysis resulted in 74% coverage, covering most of the ion channel pore region, and sections of the voltage sensing transmembrane domains. This was sufficient coverage to identify labelling of a leucine residue in the linker which connects the pore region with the voltage sensing transmembrane domains. Woll *et al.* carried out competition assays using Sevoflurane, 29, and Azisevoflurane, 30, to confirm that labelling is occurring in a mutually occupied binding site. For these experiments they utilised a large excess of Sevoflurane to Azisevoflurane (25:1) to account for the non-equilibrium binding conditions, i.e. reversible binding of Sevoflurane compared to irreversible binding of Azisevoflurane (due to labelling). For these experiments a mutant of K<sub>V</sub>1.2 (K<sub>V</sub>1.2 Gly329Thr) was used, which had previously been reported to enhance modulation of K<sub>V</sub>1.2 by sevoflurane.<sup>132</sup> Three modifications were identified in the absence of Sevoflurane, with two of these no longer present in the competition experiments. The sequence coverage of the mutant K<sub>V</sub>1.2 was higher than that of the

wild type (WT) (mutant: ~86%, WT: 74%), therefore it is difficult to confirm whether the labelled residue which has not been competed away by Sevoflurane is a site that is present in the WT channels. It is hypothesised that the residue labelled in both experiments is a nonspecific or lower affinity binding site. Nonetheless, Woll *et al.* identified two distinct binding sites which were competitive with Sevoflurane, in regions thought to be vital to the gating of the channel.<sup>130</sup> One of the binding sites was further confirmed by mutagenesis, where a leucine residue was mutated to alanine, significantly reducing the sevoflurane modulation of K<sub>v</sub>1.2.

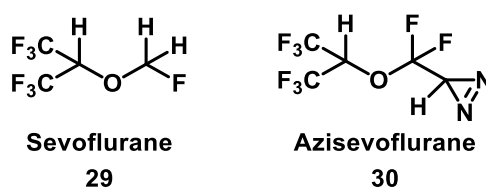


**Figure 11:** Chemical structure of Sevoflurane, **29**, and its photoaffinity labelling derivative Azisevoflurane, **30**.

### 1.6.5 Considerations for photoaffinity labelling experiments

There are many considerations when designing a photoaffinity probe. Firstly, the photoaffinity probe must resemble the parent compound closely so that it binds in exactly the same location. Furthermore, the photoaffinity probe must preferentially partake in intermolecular crosslinking, as opposed to intramolecular rearrangement after photoactivation, to achieve successful labelling of the target protein.<sup>128</sup> This can be difficult to accomplish, in particular for simple aromatic structures. Importantly, the photoaffinity probe must retain activity against the target protein, Franks and co-workers noted this to be particularly difficult. Proof of target engagement can be achieved with a photoaffinity probe, for example using photolabelling, followed by copper(I)-catalyzed azide-alkyne cycloaddition (CuAAC) and functionalisation with a fluorescent dye. However, a high degree of nonspecific labelling is not uncommon for photoaffinity probes in this method.<sup>133,134</sup> A photoaffinity probe can be a direct method of identifying a binding site on a protein of interest. However it is more challenging with regards to membrane proteins, usually due to the small quantities of membrane protein available, and difficulty digesting both hydrophilic and transmembrane portions of the protein.<sup>129</sup> Furthermore, the low efficiency of crosslinking can mean there is very small quantities of modified peptides to detect, thus it is essential the sequence coverage of the protein is high to identify a modification and confirm there is only a single peptide modified.

### 1.6.6 Photo-induced crosslinking chemistries

PAL is increasingly used in drug discovery to covalently bind a chemical probe to its target protein, identifying molecular interactions.<sup>126</sup> PAL requires the addition of a photoreactive group to a reversibly binding ligand, which upon UV irradiation with a specific wavelength of light generates a reactive intermediate that rapidly reacts with a proximal molecule. A successful photoaffinity probe must form a highly reactive intermediate rapidly at wavelengths that do minimal damage to biological molecules, whilst reacting with many bond types and remaining stable in the dark at a range of pH values.<sup>135</sup> The activation energy of the photoreactive group should be greater than the absorption wavelength of proteins. Excess absorbance of UV light can degrade proteins; UV light is absorbed at 280 nm due to aromatic amino acids, tryptophan, tyrosine and phenylalanine, while peptide bonds absorb at 200 nm. Optimising all of these features can be a challenging task.<sup>126</sup> In a PAL probe, the photoreactive moiety can be incorporated into the ligand structure, or attached *via* a linker, however the length of the linker is very important. The length, rigidity and orientation of the linker can be critical in reducing the possibility that the photoreactive group may crosslink with itself. Additionally, the photoreactive group should be at an optimal distance to create efficient crosslinking to the protein of interest, in particular crosslinking should preferentially occur in the binding pocket for binding site identification experiments.

Some of the most widely utilised photoreactive groups are aryl azides, benzophenones and diazirines. Upon irradiation with specific wavelengths these form a nitrene, a diradical and a carbene, respectively (*Figure 12*).

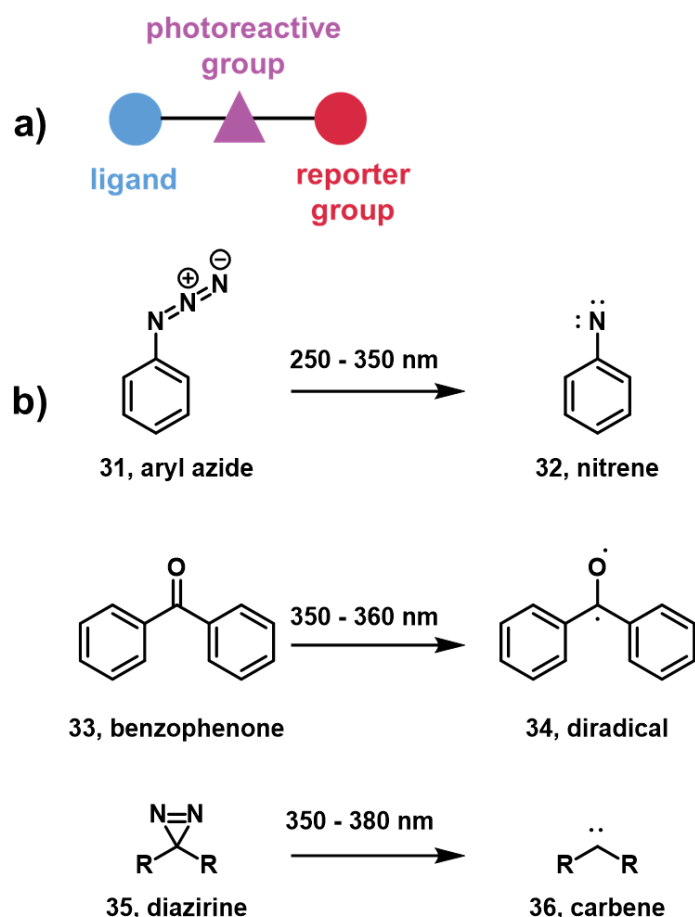


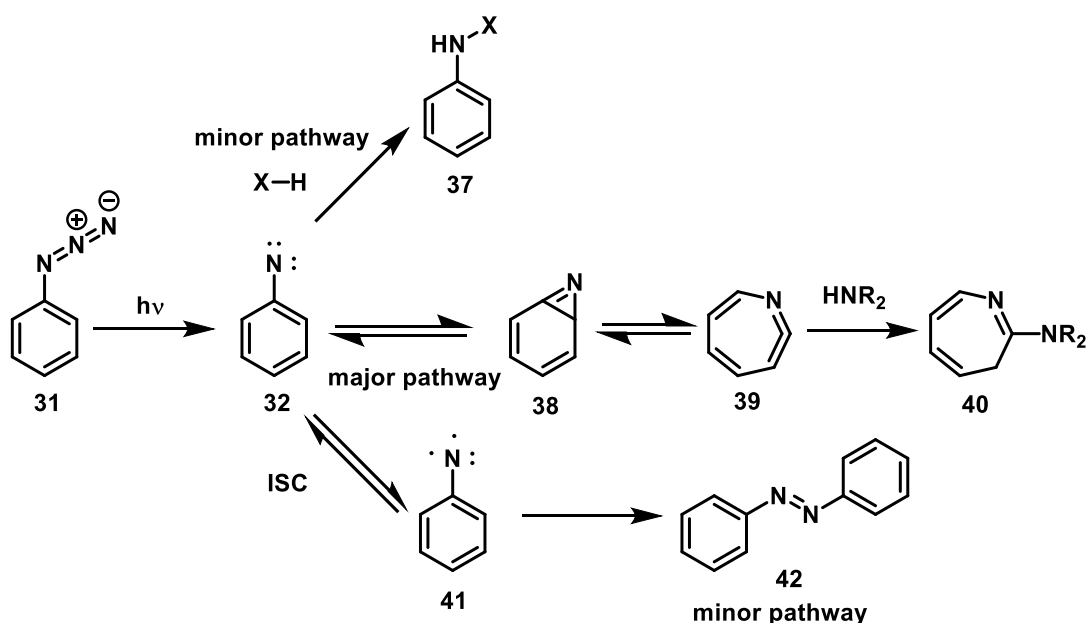
**Figure 12:** a) General structure of a photoaffinity labelling probe. b) Chemical structure of photoreactive groups and their photolysis products.<sup>126</sup>

### 1.6.6.1 Aryl azides

Aryl azides were initially thought to be ideal for photoaffinity labelling, because they are more chemically stable than their alkyl and acyl counterparts and react indiscriminately with protein functional groups. They are utilised widely as they are readily synthesised and are available commercially. Nevertheless, the shorter wavelengths (250-350 nm) required to generate the reactive species can be detrimental to biological molecules. Upon irradiation of aryl azides, the loss of molecular nitrogen results in generation of a singlet state nitrene, which can insert into X-H bonds of proteins.<sup>136,137</sup> It has been reported that the singlet state nitrenes can rearrange through ring expansion to form less reactive isomers, benzazirines and ketenimines, as undesired side products,<sup>138</sup> limiting their use in many biochemical experiments (*Scheme 1, major pathway*). Nevertheless, substituted aryl azides have been reported to minimise this rearrangement. However, substituents at the *ortho* position are avoided due to intramolecular cyclisation following photolysis.<sup>139</sup> A second electronic structure is thought to be generated upon irradiation of aryl azides;



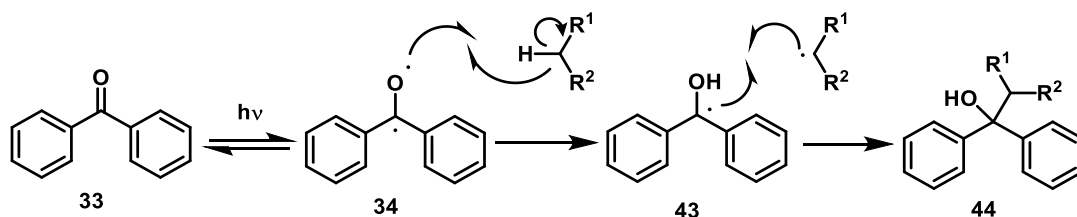
however it is proposed that only the singlet state can be accessed from the azide and that the triplet state is formed by relaxation of the singlet state (*Scheme 1, bottom minor pathway*).<sup>140</sup> Both states are thought to have different reactive properties; the singlet state having electrophilic character, whereas the triplet state behaves as a diradical.<sup>141</sup> Dubinsky *et al.* reported that nitrenes have lower photoaffinity yields in comparison to that of a carbene.<sup>142</sup>



**Scheme 1: Photolysis of an aryl azide and the reaction pathway of the singlet nitrene photolysis product.**

### 1.6.6.2 Benzophenones

Benzophenone was first introduced as a photoaffinity labelling group by Galardy *et al.* who showed benzophenone to crosslink to the  $\alpha$ -carbon of glycine.<sup>143</sup> Benzophenone is a promising photolabel because it can be readily synthesised and is relatively inert in solvents. Benzophenone was proposed to be superior to simple aryl ketones due to the longer wavelength ( $\geq 320$  nm) required for activation, minimising the potential to damage biomolecules.<sup>143</sup> The benzophenone chromophore absorbs at 350 nm and promotes a non-bonding electron on the carbonyl oxygen into the carbonyl  $\pi^*$  orbital; this is singlet to triplet intersystem crossing. It is this reactive intermediate which reacts with protein functional groups *via* an abstraction-recombination mechanism (*Scheme 2*).<sup>141</sup> The electron deficient ketyl oxygen can abstract a hydrogen. This hydrogen abstraction can occur with weak C-H  $\sigma$ -bonds. Additionally, reactions with N-H bonds can occur *via* electron transfer followed by proton abstraction. It is noteworthy that if this abstraction of a hydrogen does not occur, the excitation is reversible, and the benzophenone can return to the ground state.

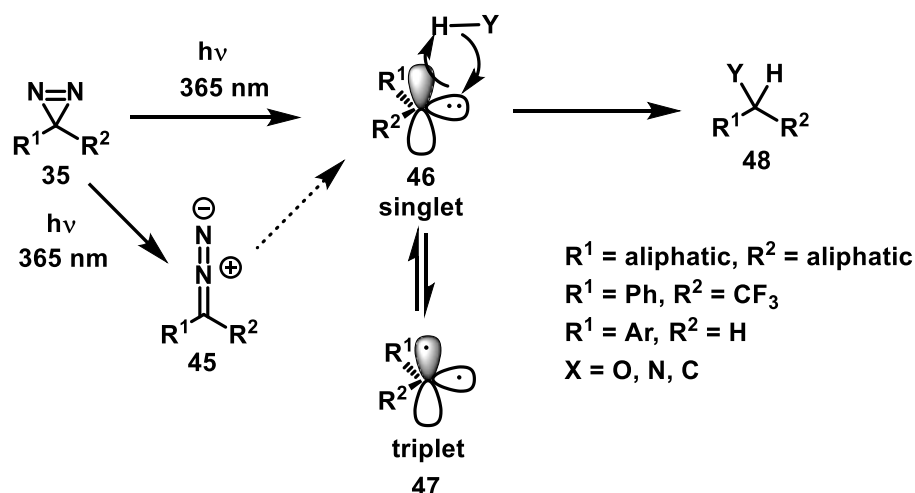


**Scheme 2:** The photolysis pathway of benzophenone, crosslinking occurring via a sequential abstraction-recombination mechanism.<sup>141</sup>

Nevertheless, long irradiation times can be required for activation of the benzophenone, which can increase non-specific labelling.<sup>144</sup> Additionally benzophenone is a bulky photolabel, which can affect the interaction of the probe to the target protein, and this steric hindrance can also cause non-specific labelling.<sup>145</sup> It has been proposed that benzophenone may not be chemically inert in the dark; the carbonyl is available for imine formation with biological amines. Schultz and co-workers observed the addition of benzophenone to a lysine residue on HIV protease.<sup>146</sup>

### 1.6.6.3 Diazirines

Diazirines are advantageous photolabelling compounds due to their small size and the longer wavelength at which they are activated to the reactive species, minimizing potential damage of biomolecules. Upon irradiation at ~ 365 nm the diazirine extrudes molecular nitrogen, to generate the carbene. As the two  $\sigma$ -bonds between the carbon atom and the azo group are broken the bonding electrons are redistributed between the newly formed divalent carbon atom and molecular nitrogen. The carbene generated upon irradiation is in the singlet state. However it is proposed that the triplet state can also be accessed through interconversion of the singlet state.<sup>147</sup> Carbenes can undergo a range of reactions depending on their electronic state;<sup>148</sup> importantly the singlet state can insert into C-H and heteroatom-H bonds *via* a concerted mechanism (*Scheme 3*).<sup>149</sup>



**Scheme 3:** The photolysis of a diazine. The diazine is converted mostly to a reactive singlet carbene upon irradiation which insert into C-H, N-H or O-H. A minor pathway in the photolysis of a diazine, generates the largely unreactive diazoisomer.

Upon photolysis of the diazine a diazo species can be generated as an undesired side product.<sup>150</sup> Irradiation at 365 nm can convert approximately 30% of the diazine to a diazo compound. This diazo compound can generate the singlet-state carbene, yet the conversion is relatively slow.<sup>126</sup> These undesired diazo isomers tend to form diazonium ions, by formation of the carbocation *via* protonation at carbon, followed by loss of N<sub>2</sub>, thus leading to unwanted crosslinking products.<sup>150</sup> Although it is not possible to completely avoid formation of the diazoisomer;<sup>150</sup> Richards and co-workers demonstrated that the combination of a trifluoromethyl and aromatic substituents improves chemical stability whilst maintaining the photochemical properties of the diazine ring.<sup>141,151</sup>

It is noteworthy that the high reactivity of the carbene generated means that it is often quenched by water. Although this is a disadvantage in terms of labelling efficiency, this is also an advantage with regards to minimalizing non-specific labelling. Furthermore, the trifluoromethyl-3-aryldiazirine is a promising photolabelling compound because it is highly resistant to several factors; e.g. temperature, acidic and basic conditions, nucleophiles and oxidising and reducing agents.<sup>126</sup>

#### 1.6.6.4 Summary of photoaffinity labelling functional groups

The information on photo-reactive groups for photoaffinity labelling, discussed in Section 1.6.6 is summarised in Table 4.

**Table 4:** Summary of the most common photo-reactive groups used for photoaffinity labelling.

Photo-reactive group	Advantages	Limitations
<b>Aryl azides</b>	<ul style="list-style-type: none"> <li>• Easily synthesised or commercially available.</li> <li>• Nitro substituted azides can be activated by longer wavelengths (~350 nm).</li> </ul>	<ul style="list-style-type: none"> <li>• Unsubstituted aryl azides require activation at ~ 250 nm which can be damaging to biological molecules.</li> <li>• Ring expansion can occur to form less reactive isomers.</li> </ul>
<b>Benzophenone</b>	<ul style="list-style-type: none"> <li>• Longer wavelengths are required to form the reactive species</li> <li>• Relatively inert in solvents</li> <li>• The formation of the diradical is reversible, thus there is a high labelling efficiency</li> </ul>	<ul style="list-style-type: none"> <li>• Sterically bulky</li> <li>• There is not indiscriminate reactivity</li> <li>• Longer irradiation times are necessary which can be damaging to biological samples</li> </ul>
<b>Diazirines</b>	<ul style="list-style-type: none"> <li>• A highly reactive and indiscriminate carbene is generated</li> <li>• Small size</li> <li>• Reduced non specific labelling</li> <li>• Highly resistant to a variety of conditions</li> <li>• Activation at longer wavelengths (~365 nm)</li> </ul>	<ul style="list-style-type: none"> <li>• Undesired diazoisomer formation upon irradiation</li> <li>• Low labelling efficiency</li> </ul>

### 1.6.7 Traceless affinity labelling chemistries

Another method of protein labelling is ligand-directed traceless chemical labelling. This approach is based on the 'proximity effect'. The reactive group is brought near to the ligand binding pocket thereby increasing the effective local concentration of the amino acid and reactive group, and only amino acid residues in the binding pocket are modified.<sup>152</sup> Upon covalent labelling using a traditional affinity labelling approach the ligand moiety permanently sits in the ligand binding pocket rendering the protein inactive.<sup>153</sup> The group of Hamachi describe two types of traceless affinity labelling that avoid this problem: an exchange/cleavage reaction (*Figure 13a*) and a catalyst tethering reaction (*Figure 13b*). Both methods proceed *via* a general approach: recognition of the ligand, activation of the catalyst and/or covalent attachment to the target protein and finally concurrent cleavage or subsequent exchange of the ligand.<sup>152</sup> In the case of the ligand-directed exchange/cleavage approaches, the labelling reagent consists of a ligand and reporter group which are connected by a cleavable electrophilic moiety. The ligand binds to the protein of interest, facilitating the transfer of the functional group onto a nucleophilic amino acid in the ligand binding site *via* covalent bond formation.<sup>154</sup>

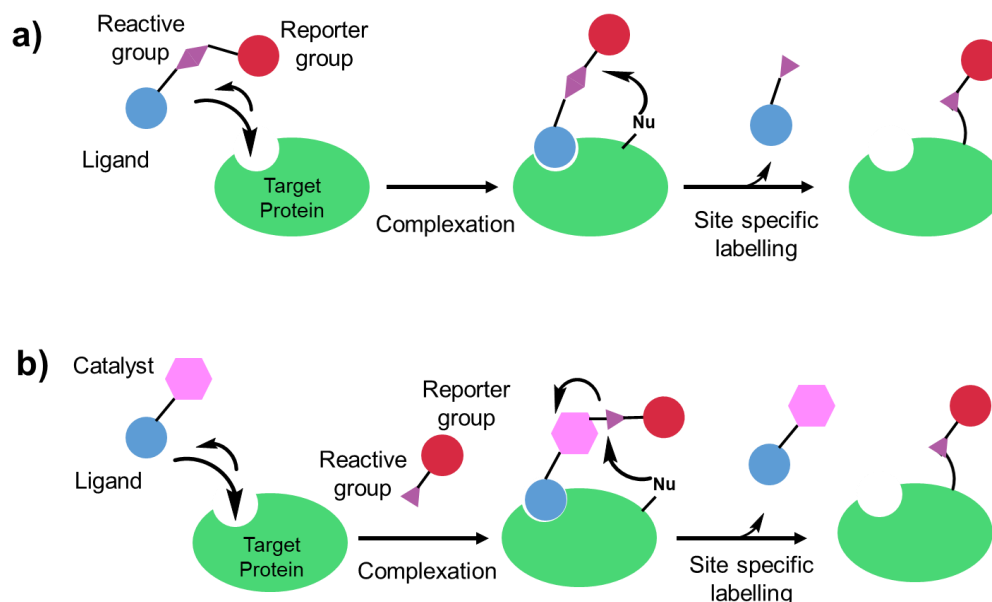


**Figure 13: Traceless affinity labelling techniques.** *a)* The mechanism for an exchange/cleavage type labelling reaction (includes LDT, LDAI, LDBB, LDSP and LDNASA); *b)* The mechanism for a catalyst tethering type labelling reaction (includes AGD and AGOX).

Thus far, nine different traceless affinity labelling techniques have been developed, however the first two methods<sup>155,156</sup> developed were only suitable for *in vitro* protein labelling. The subsequent seven techniques were applicable to cell

lysates and whole cell protein labelling studies. Ligand-directed methods (exchange/cleavage) were developed based on the following reactive moieties; tosyl (LDT),<sup>157,158,159</sup> acyl imidazole (LDAI),<sup>160,161,162,163</sup> (di)bromophenyl benzoate (LDBB),<sup>164</sup> *N*-sulfonyl pyridine (LDSP),<sup>165</sup> and *N*-acyl-*N*-alkyl sulfonamide (LDNASA).<sup>154</sup> In addition, catalyst tethering techniques include affinity guided DMAP (AGD) catalysis,<sup>166,167,168</sup> and affinity guided oxime (AGOX) chemistry (Figure 14).<sup>169</sup>

The first generation of traceless affinity labelling to be successful *in vivo* was LDT chemistry. LDT labelling proceeds *via* an S<sub>N</sub>2 type reaction between the tosylate ester moiety and a nucleophilic amino acid residue. Hamachi and co-workers demonstrated the application of LDT chemistry in living cells, tissues and mice.<sup>157</sup> However, LDT chemistry is typically very slow; usually incubations of over 12 hours are required, and labelling efficiency is frequently low, thus intracellular protein labelling remained challenging.<sup>159,170</sup> Subsequently LDAI chemistry was developed, with a faster labelling rate than LDT. Nonetheless, LDAI chemistry was limited by the labile carbonate bond formed which could undergo hydrolysis.<sup>161</sup> Additionally LDAI chemistry has thus far been restricted to cell surface labelling.<sup>160</sup> Subsequently Hamachi *et al.* described LDBB chemistry,<sup>164</sup> which is based on a ligand-directed phenyl ester (LDPE) method reported by Fenical *et al.*<sup>171</sup> LDBB has a labelling rate seven-fold faster than that of LDAI.<sup>164</sup> However, the reactive moiety is particularly bulky and hydrophobic, thus an LDBB probe may drastically alter the activity of the ligand. LDSP was established with the aim to overcome some of shortfalls of previous methods. LDSP chemistry utilised 2-pyridone as the reactive moiety for protein sulfonylation.<sup>165</sup> The labelling rate for LDSP was accelerated in comparison to LDT and LDAI chemistries under the same conditions, with partial labelling identified after 1 hour. Nonetheless 100% labelling efficiency was only observed after 12 hour incubation times. Despite this LDSP proved a successful intracellular labelling method in mammalian cells, labelling both carbonic anhydrase 2 (CA2) (intracellular) and carbonic anhydrase 12 (CA12) (cell surface) in MCF7 human breast cancer cells. LDNASA is the most recent traceless affinity labelling method developed by Hamachi and co-workers. LDNASA has the fastest labelling rate of all the above techniques, with a reaction rate of  $\sim 10^4 \text{ M}^{-1} \text{ s}^{-1}$ , which is comparable to the fastest bioorthogonal protein bioconjugations.<sup>154</sup> Additionally, LDNASA demonstrated labelling to both endogenous intracellular and membrane proteins. LDNASA is in the early stages of development, however it is currently limited to the labelling of lysine residues.

Hamachi and co-workers exploited the ability of DMAP to catalyse acyl transfer reactions for traceless affinity labelling.<sup>166</sup> AGD chemistry allows lower

concentrations of reagents due to its catalytic nature. Nevertheless, AGD chemistry had several limitations, including the requirement of basic pH conditions (pH > 8). Additionally, AGD chemistry can result in two undesired pathways; acylation can occur with nontarget proteins due to the high electrophilicity of the thioester acyl donors, resulting in non-specific labelling. Furthermore, the thioester acyl donor is readily decomposed by esterases, thus high concentrations of reagents are required.<sup>169</sup> Subsequently AGOX chemistry was developed which resulted in more efficient labelling than DMAP chemistry, because the  $pK_a$  of the ligand-conjugated pyridinium oxime (PyOx) is lower (PyOx: 7-8.5 *cf.* DMAP: 9.6).<sup>169</sup> To date AGOX chemistry has not been applied to intracellular proteins.

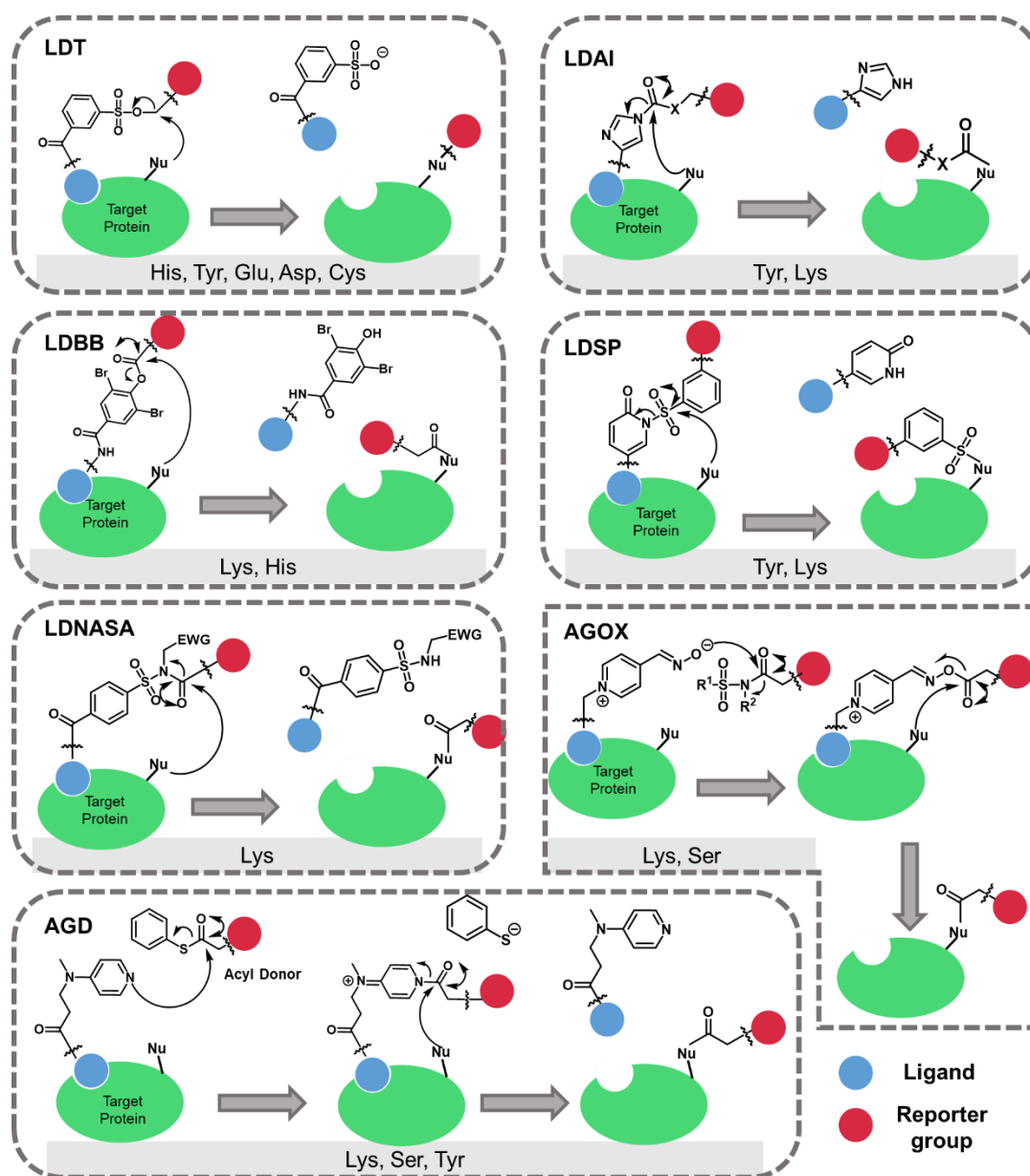


**Figure 14: Ligand-directed traceless affinity labelling techniques;** including ligand-directed tosyl (LDT) chemistry, ligand-directed acyl imidazole (LDAI), ligand-directed (di)bromophenyl benzoate (LDBB), ligand-directed N-sulfonyl pyridine (LDSP), ligand-directed N-acyl-N-alkyl sulfonamide (LDNASA), affinity guided oxime (AGOX) chemistry and affinity guided DMAP (AGD) catalysis. (Where X=O,N). Reported Amino acid residues labelled using each method indicated in the grey box. (Histidine (His), Tyrosine (Tyr), Glutamic acid (Glu), Aspartic acid (Asp), Lysine (Lys) and Serine (Ser)).

Despite the advances in traceless affinity labelling, there are still some limitations. There are currently no traceless affinity labelling methods which can indiscriminately label amino acid residues for *in vivo* studies. Additionally, the reaction rate is still significantly slower than other labelling techniques, e.g. photoaffinity labelling (hours or days *cf.* minutes).



## 1.7 Project aims

TRPC1/4/5 channels are linked to a variety of diseases and in recent years there has been a rapid increase in the number of TRPC1/4/5 modulators published, with the emergence of (–)-EA and Pico145 as a particularly potent and specific activator and inhibitor respectively. Despite the recent progress with modulators of TRPC1/4/5 channels and progressions in cryo-EM technologies that have resulted in the determination of a number of TRPC channel structures; there is limited knowledge of how these compounds modulate TRPC1/4/5 channels. Unravelling the mode of action of modulators of TRPC1/4/5 could lead to the design of potent multimer specific modulators.

The mode of action of modulators of ion channels can be unravelled in a number of ways: through calcium recording assays, electrophysiology and photoaffinity labelling techniques. Electrophysiology experiments can indicate a direct effect of modulators on TRPC1/4/5 channels and can suggest an intracellular or extracellular mechanism of action. Photoaffinity labelling is a more challenging yet more accurate technique to determine a direct mode of action of modulators on TRPC1/4/5 channels. Furthermore, the use of a photoaffinity labelling approach could facilitate the identification of peptides in the binding pocket.

The work described in this thesis aims to unravel the modes of action of novel modulators of TRPC1/4/5 channels, in addition to determining target engagement and binding sites of a published TRPC1/4/5 inhibitor, Pico145. A variety of techniques have been used to unravel the modes of action of TRPC1/4/5 channel modulators; some specialist techniques are described in *Chapter 2*. *Chapter 3* of this thesis details the development of novel flavonol-based TRPC1/4/5 inhibitors and the work towards probing their mode of action through calcium recording assays, patch clamp recordings and electrochemical assays. *Chapter 4* of this thesis includes the development of two novel photoaffinity probes based on the TRPC1/4/5 inhibitor Pico145 and their use in unravelling proof of a direct interaction with TRPC1/4/5 channels. *Chapter 4* also highlights the work towards binding site identification of the photoaffinity probes on TRPC5 channels. *Chapter 5* describes the development of a novel series of TRPC5 inhibitors, based on previous work within the Bon group.

## Chapter 2 - Techniques and Methods

This Chapter gives a brief introduction to some of the techniques used throughout this thesis, including a brief overview of experimental protocols and how the data is presented. For detailed experimental protocols see *Experimental section*.

### 2.1 Intracellular calcium measurements

The FlexStation scanning fluorimeter can be used to measure changes in the free intracellular  $\text{Ca}^{2+}$  levels, using a calcium indicator dye. Fluo-4 (**49**, *Figure 15a*) and fura-2 (**50**, *Figure 15b*) are common  $\text{Ca}^{2+}$  indicator dyes that can be used for cell-based calcium assays. Fluo-4 and fura-2 are used as their acetoxymethyl ester (AM) derivatives which are membrane permeant. Once inside the cell, cellular esterases cleave the AM groups trapping the dyes inside the cell, and generating the active form which is able to bind  $\text{Ca}^{2+}$ .<sup>172</sup> Fluo-4 is a non-ratiometric  $\text{Ca}^{2+}$  indicator that is excited at 488 nm<sup>172</sup> and emits light at 506 nm. Upon binding of  $\text{Ca}^{2+}$  the intensity of light emitted increases, thus indicating the levels of free intracellular  $\text{Ca}^{2+}$ . Fura-2 is a ratiometric dye which is considered the standard for intracellular  $\text{Ca}^{2+}$  measurements and has been used to a greater extent in this project. Fura-2 is excited at 340 nm and 380 nm with emission at 510 nm. Upon  $\text{Ca}^{2+}$  binding the excitation spectrum shifts, resulting in an increase in fluorescence emission at excitation 340 nm and a decrease in fluorescence emission at excitation 380 nm (*Figure 15c*). Intracellular calcium is measured based upon the 340/380 emission ratio, which minimises effects of differences in local concentrations and cell thickness which could lead to artefacts.<sup>173</sup>

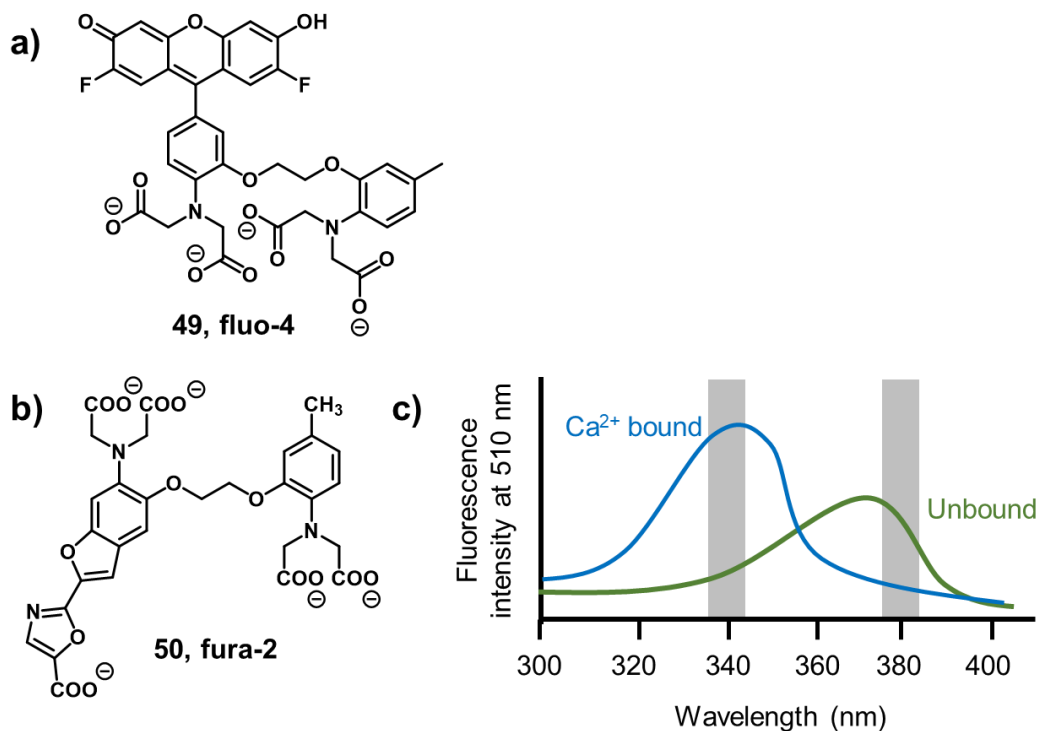


**Figure 15: Calcium indicators.** **a)** Chemical structure of fluo-4; **b)** chemical structure of Fura-2; **c)** Excitation spectra of fura-2, showing the fluorescence intensity at 510 nm of fura-2  $\text{Ca}^{2+}$  bound in blue and unbound in green.

#### Experimental protocol

HEK-293 T-REx cells are seeded onto 96-well plates and channel expression is induced by the addition of tetracycline 18 hours before experimentation (tet+), or no addition of tetracycline constitutes a negative control experiment (tet-) (Figure 16). Subsequently, calcium indicator dye is loaded and cells are incubated at 37 °C for one hour.

#### Agonist mode

To investigate the agonistic effects of compounds, cells are subsequently incubated with standard bath solution (SBS) for half an hour. Basal  $\text{Ca}^{2+}$  levels are recorded and then the agonist is added and the increase in intracellular  $\text{Ca}^{2+}$  is recorded as a level of fluorescence (Figure 16).

#### Antagonist mode

To investigate antagonist effects, cells are incubated with a calcium indicator dye, and then preincubated with antagonist compounds for 30 minutes at room temperature. The agonist can subsequently be transferred to the assay plate in the FlexStation and

fluorescence levels recorded (Figure 16), to determine the degree of inhibition of the TRP channels.

### Interpretation of data

The fluorescence is recorded over time and traces show basal  $Ca^{2+}$  entry for 60 seconds at the start. The application of the channel activator is shown by a black line at the top of the graph, normally applied at 60 seconds (Figure 16), and the ion channel investigated is indicated in the top left corner of each graph. Where  $IC_{50}$  data are generated at least three independent repeats have been performed and are typically reported as a percentage of the control.

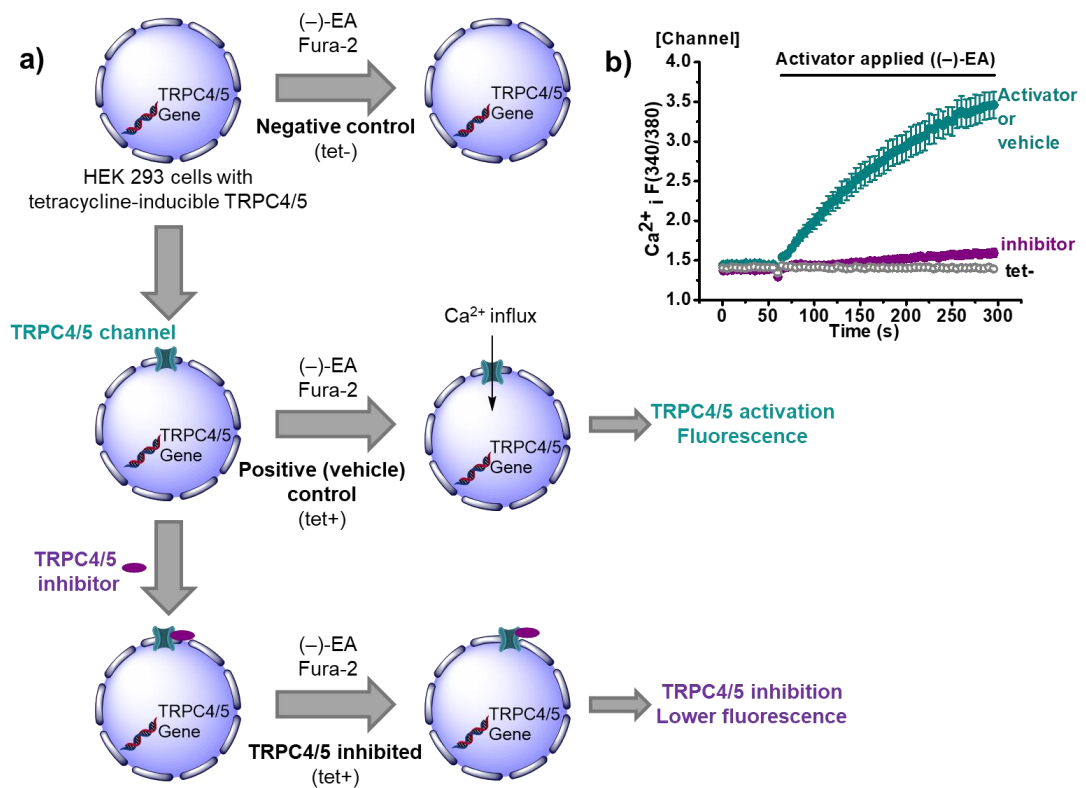


**Figure 16: Calcium recording assays using a FlexStation.** **a)** Schematic of the workflow of the calcium recording assays; **b)** Example data from a single 96-well plate, showing basal  $Ca^{2+}$  entry (0-60 secs) before an activator (e.g. (-)-EA) is added to induce channel expression. The changes in intracellular  $Ca^{2+}$  are measured using a calcium indicator dye. Cells lacking channel induction (negative control) are labelled tet-. The presence of an inhibitor shows a reduction in  $Ca^{2+}$  entry.

## 2.2 Manual electrophysiology

Electrophysiology allows the measurement of voltage changes or electric currents across the cell membrane. Biological electrical activity results from the movement of charged particles, e.g.  $\text{Na}^+$ ,  $\text{K}^+$  and  $\text{Ca}^{2+}$ .<sup>174</sup> Patch clamp is one of the most widely used electrophysiology techniques and can be used to resolve the current contributions of ion channels in the membrane.<sup>175</sup> Manual patch clamp techniques have been discussed in the introduction of this thesis and are used in *Section 3.3.5*. In this technique a glass microelectrode is pressed against the cell membrane and an electrical seal is formed with resistance in the order of gigaohms.<sup>176</sup> This high resistance allows currents from a small patch of membrane to flow into the pipette. There are a number of different patch clamp configurations: cell-attached, inside-out, whole-cell and outside-out patch (*Figure 17*).

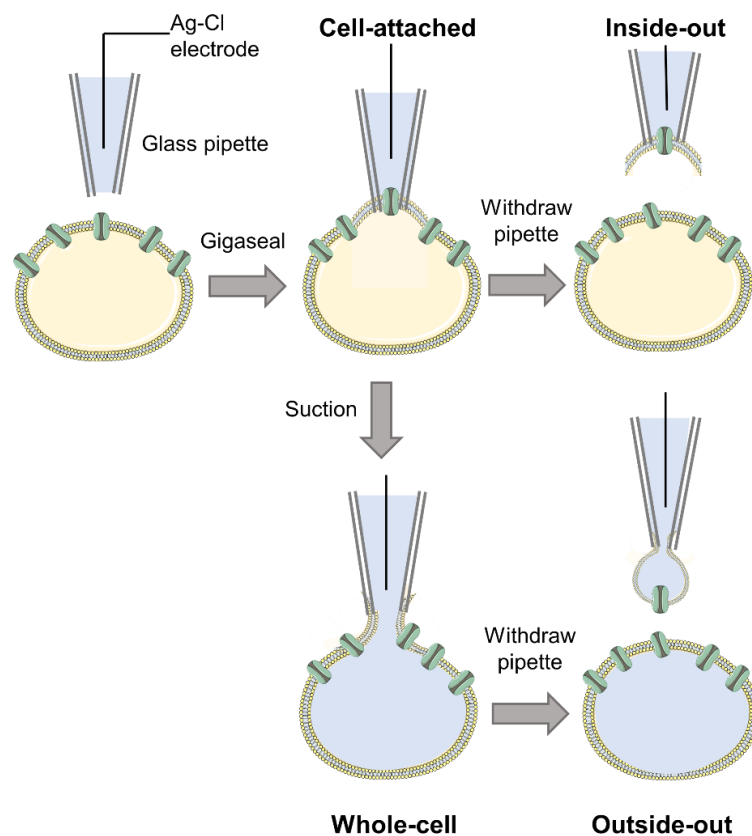


**Figure 17: Schematic diagram of patch clamp configurations.**

### *Cell-attached*

In cell-attached configurations, the pipette is placed on the cell membrane and the cell remains intact. The current is recorded through single or a few ion channels in the patch of membrane captured by the pipette. In the cell-attached configuration the

intracellular mechanisms are able to function as they would physiologically. For the investigation of ligand-gated ion channels, ligands can be applied in the pipette. However, it is not usually possible to change the concentration of the ligand, once applied. Therefore, to achieve a dose-response experiment multiple patches and cells are needed.

#### *Inside-out*

As in the cell-attached method, the pipette is placed on the cell membrane, forming a seal. The pipette is then retracted to break off a patch of membrane. In inside-out configurations, external solutions can be applied to the intracellular/cytosolic surface of the membrane.

#### *Whole-cell*

During the whole-cell configuration currents are recorded through multiple channels simultaneously over the membrane of the entire cell. The pipette is attached to the cell membrane as in the cell-attached method. However, more suction is applied to rupture the membrane, allowing access to the intracellular environment. Access to the interior *via* the pipette facilitates rapid loading of the cells with ligands. However, this means the intracellular environment is disturbed and signalling cascades may be disrupted.<sup>177</sup> Alternatively, compounds may be bath-applied to the extracellular face of the membrane in the whole-cell attached configuration. Applying compounds to the bath solution means multiple concentrations of compounds can be tested on the same cell by changing the bath solution.

#### *Outside-out*

The outside-out configuration is similar to the inside-out method, but in this case the external surface of the cell membrane is on the outside of the patch of membrane. The outside-out method can be accessed *via* the whole-cell configuration. After the seal has been achieved, the pipette can be slowly pulled away from the membrane, allowing a bulb of the membrane to form around the end of the electrode. This results in the original outside of the membrane facing outwards from the electrode.<sup>178</sup> Solutions may be bath applied to the external surface of the cell membrane. This allows the ion channels to be investigated isolated from the intracellular environment and exposed to solutions at the extracellular surface. Dose-response relationships can be investigated in the outside-out configuration by applying the same patch to different solutions.<sup>174</sup>

### Example data

Example data from a patch clamp experiment is shown in *Figure 18*, where the currents are obtained during ramp changes in voltage from  $-100$  to  $+100$  mV every 10s. The double trace shown represents the inward ( $-100$  mV) and outward flux ( $+100$  mV) of ions. The application of an activator shows an increase in the flux of ions across the membrane; followed by application of an inhibitor which shows a decrease in the flux of ions. In the trace displayed the current is recovered upon washout of the inhibitor.

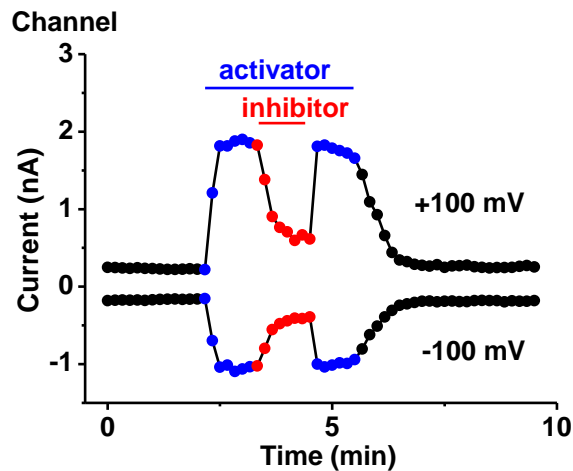


**Figure 18:** Example data from a manual patch clamp experiment, with the application of activator shown in blue and inhibitor shown in red.

## 2.3 Automated electrophysiology

In ‘manual’ or ‘conventional’ patch clamping, a single cell at a time is patched with a glass microelectrode. Due to the one cell setup this process is very low throughput and it is also technically challenging. To circumvent this problem, many companies use automated platforms for performing electrophysiology studies. The low-throughput of manual patch clamp recordings is improved in automated setups based on a planar array system; where multi-well configurations in a plate-based format are used to enable multiple recordings in parallel.<sup>179</sup> The IonWorks HT system (Molecular Devices) was the first of the screening systems that became widely available for use.<sup>180</sup> In this system, a single cell settles on a hole at the bottom of a well separating two aqueous compartments. The buffer acting as the interior of the cell contains an antibiotic which is used to perforate the cell to allow recording of currents mediated by ion channels in the cell membrane.<sup>180</sup> Perforated patch clamp is similar to the whole-cell patch configuration (*Section 2.2*). In whole-cell recordings suction is used

to rupture the membrane; in the perforated configuration an antibiotic is applied which diffuses into the membrane and forms small holes, providing electrical access to the interior of the cell.<sup>181</sup> One model of IonWorks technology affords simultaneous recordings of 64 cells per well, termed the population patch clamp (PPC) technique, averaging the response from each cell, improving the well-to-well variability observed from a single-hole approach.<sup>182</sup>

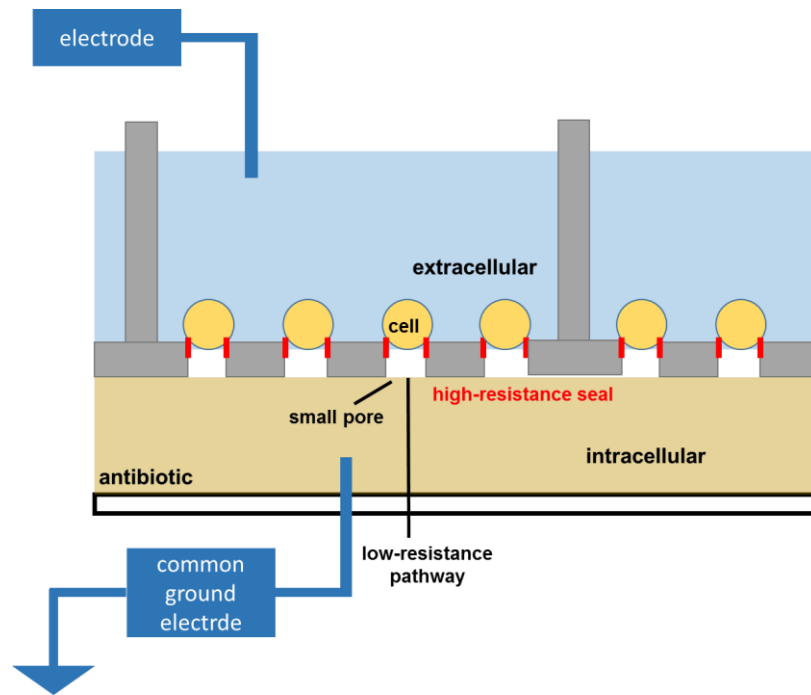


**Figure 19: Schematic of the population patch clamp (PPC) technique, whereby multiple cells seal onto an array of holes at the bottom of the well, and the response is averaged from each of these cells.**

### 2.3.1 Cardiac safety

Automated patch clamp recordings have been performed in this thesis on a set of cardiac ion channels, which are routinely used in cardiac safety screening. These ion channels have been used to investigate the selectivity and potential for unwanted off-target effects of TRPC1/4/5 modulators. Ion channels are critical for rhythmicity and contractility in cardiac function.<sup>183</sup> Sodium voltage-gated channels (Nav1.5) and potassium voltage-gated channels (Kv11.1 aka hERG/I<sub>Kr</sub>, Kv7.1 aka I<sub>Ks</sub> and Kv4.3 and Kv1.4 aka I<sub>to</sub>) are expressed in the heart and vasculature and together contribute towards the ventricular action potential which controls contraction and relaxation of the heart (*Figure 20*).

In the 1990s a significant number of drugs were withdrawn from the market due to association with a potentially fatal cardiac arrhythmia called Torsades de



Pointes (TdP).<sup>61</sup> Specifically, TdP is the prolongation of the repolarisation phase of the ventricular myocyte action potentials. This prolongation can be quantitatively assessed by measuring the time between the Q (depolarisation) and T (repolarisation) waves of the ventricular action potential. A drug-induced prolongation of the action potential is often a result of the complex interplay of multiple ion channels, thus evaluating the risk of a drug candidate is difficult (Figure 20).<sup>184</sup>

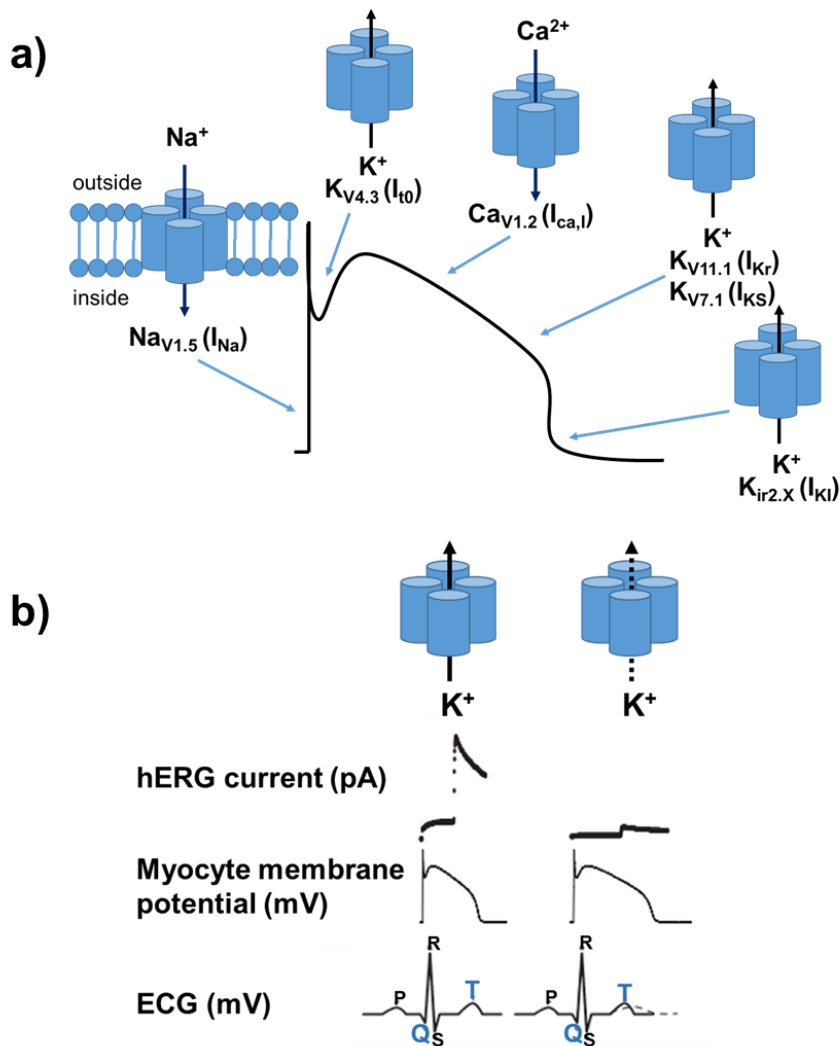


**Figure 20: Six ion channels that regulate the ventricular action potential which controls contraction and relaxation of the heart; a) the phases of depolarisation and repolarisation of the ventricular action potential, with the contribution of six key ion channels indicated; b) The hERG current with (right) and without (left) a hERG blocker, showing the prolongation of the myocyte action potential and thus the prolongation of the interval between the Q and T waves in the electrocardiogram (ECG).**

The ion channels related to QT interval prolongation are voltage-gated ion channels. Therefore, to investigate these channels using perforated patch clamp; a potential difference is applied over the cell membrane, which causes a conformational change in these ion channels. This conformational change results in activation or

opening of the channel to allow the flow of ions according to the electro-chemical gradient across the membrane.<sup>185</sup> This movement of ions generates an electric current which depolarises the cell membrane. Following activation, voltage-gated ion channels go to an inactivated state in which the channel is non-conducting and unable to open (*Figure 21*). Subsequently the channel transitions to the closed state, where it is available for activation. The ability to control the voltage of the cellular membrane for voltage-gated channels means the 'ligand' for these channels can be precisely controlled.<sup>186</sup> Compounds may block a voltage-gated ion channel in its open, closed or inactivated state.<sup>187</sup> Therefore to investigate the potency of compounds against voltage-gated ion channels a voltage step pattern of stimulation can be applied, to access each conformational state of the channel.

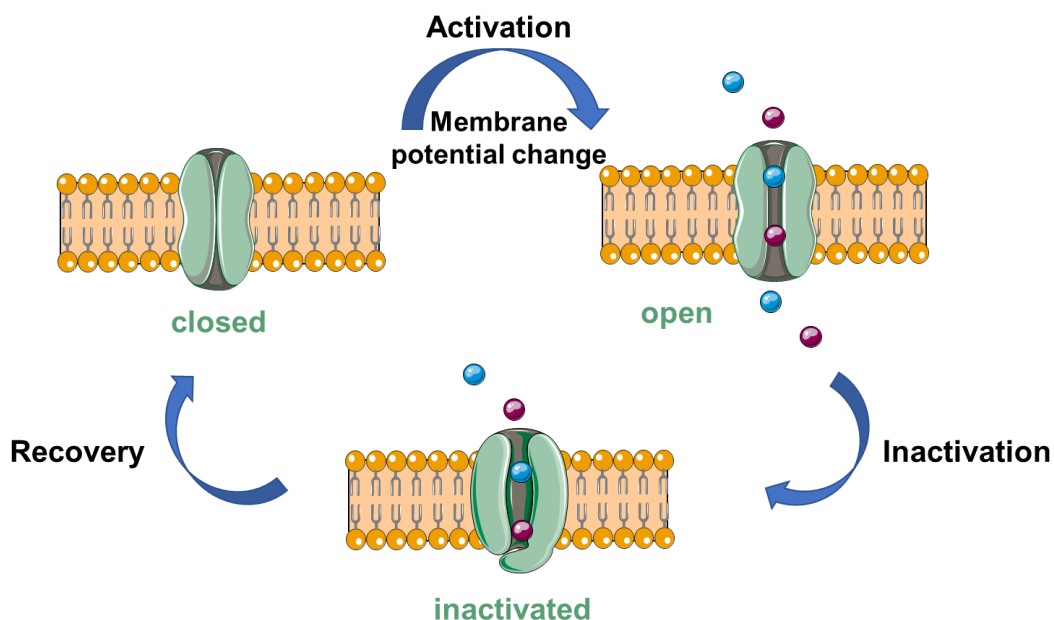


**Figure 21: Schematic of the states of a voltage-gated ion channel;** which transitions between activated, inactivated and closed states upon changes in membrane potential.

### 2.3.2 Experimental protocols

Whole-cell recordings are taken from CHO cells stably expressing Nav1.5, Kv11.1 (hERG), Kv7.1 ( $I_{KS}$ ) and Kv4.3 ( $I_{to}$ ), using Amphotericin B as an antibiotic to perforate the membrane. Currents are obtained for the pre-compound control, by applying a voltage step protocol (example of hERG protocol shown in *Figure 22*). Subsequently, the compounds are incubated for three minutes and then recordings are measured using the same voltage protocol to determine the current post-compound (*Figure 22*). Concentration-response data were collected and  $IC_{50}$  values were reported as a percentage of a pre-compound activity. Reference compounds were included in each

experiment as a control; hERG: cisapride **51**, Na<sub>v</sub>1.5 and I<sub>to</sub>: flecainide, **52**, and I<sub>Ks</sub>: XE-991, **53** (Figure 23).

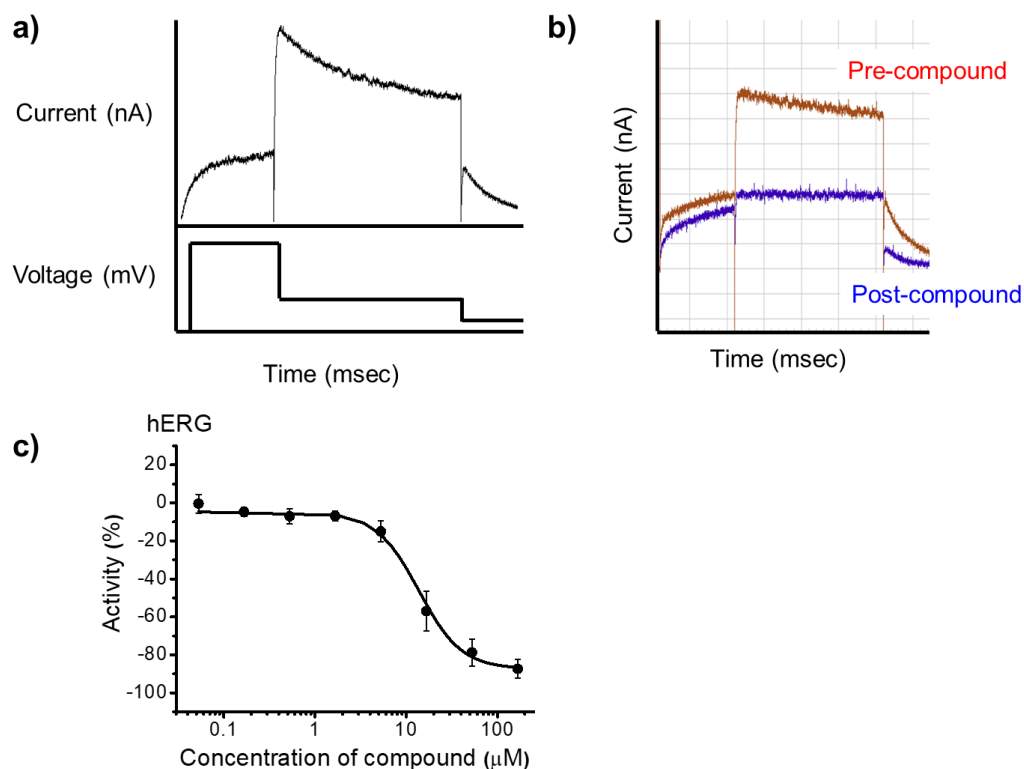


**Figure 22: Voltage protocol and measurement of the hERG current metric; a)** hERG current (top) is evoked by a single voltage pulse (bottom) consisting of a 1 s step to +40 mV, a 2 s step to -30 mV and finally 500 ms step to -70 mV; **b)** example data of the hERG current recorded pre-compound addition (red) and post addition of a hERG blocker (blue); **c)** example trace data from a dose-response experiment using this protocol, where the activity of a compound is plotted as a percentage of the pre-compound activity.

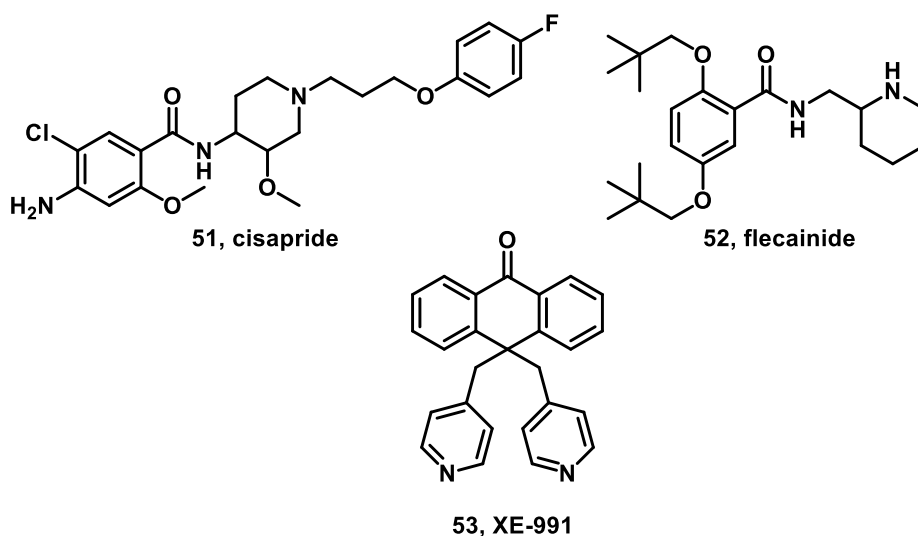


**Figure 23: Chemical structures of reference compounds: hERG - cisapride, Na<sub>v</sub>1.5 and I<sub>to</sub> - flecainide, I<sub>Ks</sub> - XE-991.**

## 2.4 Electrochemical biosensor assays

The interactions of molecules with a biomembrane can be investigated using a phospholipid monolayer deposited on a microfabricated electrode to constitute a biosensor device. When an electric potential is applied to a phospholipid monolayer, e.g. dioleoyl phosphatidylcholine (DOPC) it undergoes two potential induced phase transitions.<sup>188</sup> These transitions can be characterised by two sharp capacitance current peaks at potentials  $\sim -0.94$  V and  $\sim -1.0$  V; changes in these peaks correlate to an increase in the ion permeability of the monolayer and the subsequent reorganisation of the monolayer. By monitoring these transitions through rapid cyclic voltammetry, the level of disruption of the monolayer can be determined.

The biosensor device comprises a mercury (Hg) layer bound to a platinum (Pt) contact. The DOPC monolayer is deposited onto this electrode. Firstly, rapid cyclic voltammetry is used to determine the electrochemical properties of the monolayer alone. Subsequently, compounds can be flowed over the surface of the monolayer and disruption of the monolayer can be monitored by detecting changes to the two indicative capacitance peaks in the voltammograms (*Figure 24*).<sup>189</sup>

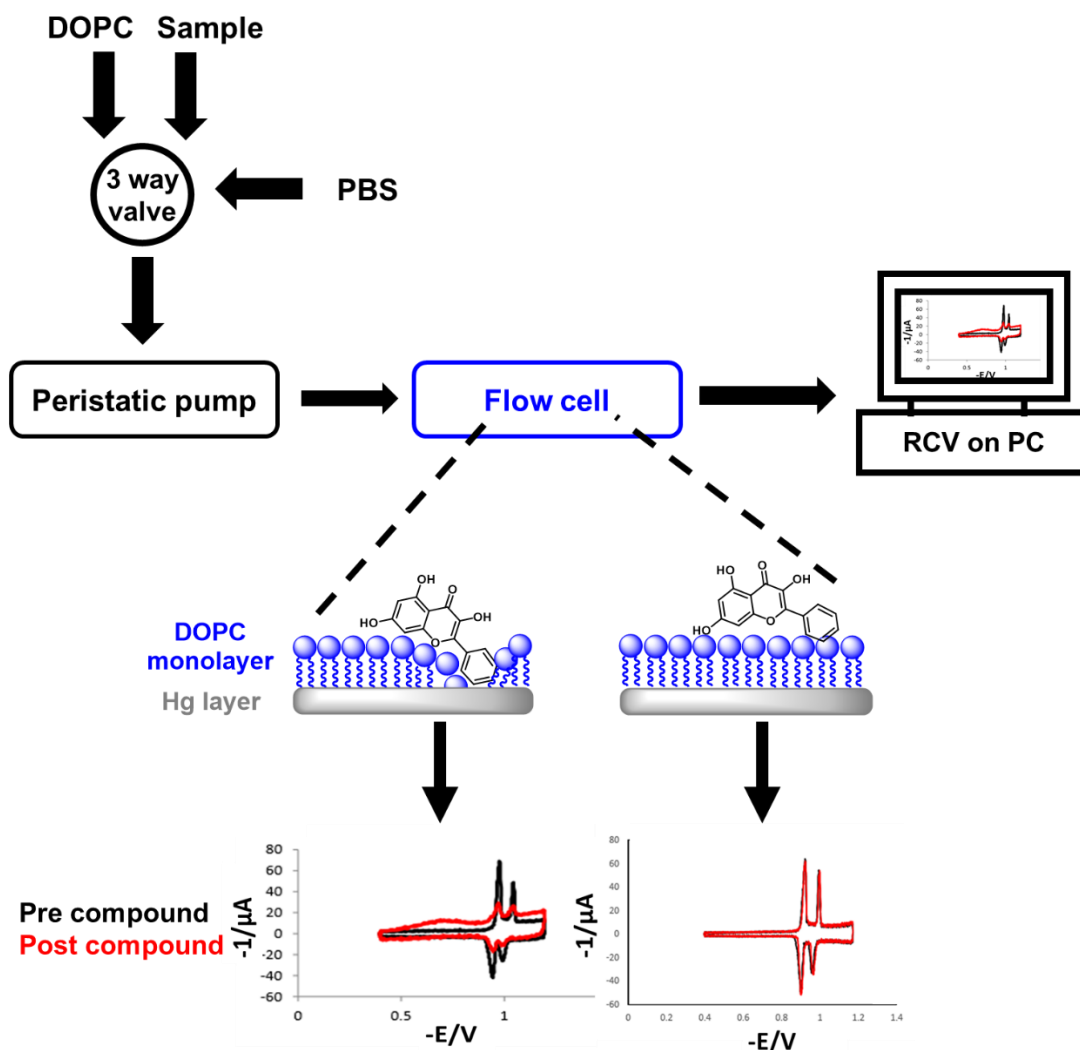


**Figure 24: Schematic showing the biosensor device used for indicating an interaction between compounds and a phospholipid monolayer.** Example traces are shown which indicate the cyclic voltammogram which would be observed from a compound disrupting the monolayer (left) and the monolayer remaining intact (right).

## 2.5 Photoaffinity labelling experiments

An affinity labelling approach (*Section 1.6*) may be used in the investigation of target engagement and binding site identification. Firstly, HEK-293 cells over-expressing TRPC5 are plated 24 hr prior to experimentation and channel expression is induced with tetracycline. Subsequently, cells are incubated with a photoaffinity probe for 5 minutes, followed by irradiation for 25 minutes at 365 nm to covalently link the probe to the target protein. Cells are lysed and click chemistry performed on the cell lysates. Proteins are subsequently precipitated using acetone and resuspended for SDS-PAGE analysis. Fluorescently labelled proteins can be identified using a fluorescent

gel scan; identifying which proteins have a direct interaction with the photoaffinity probe (*Figure 25*).

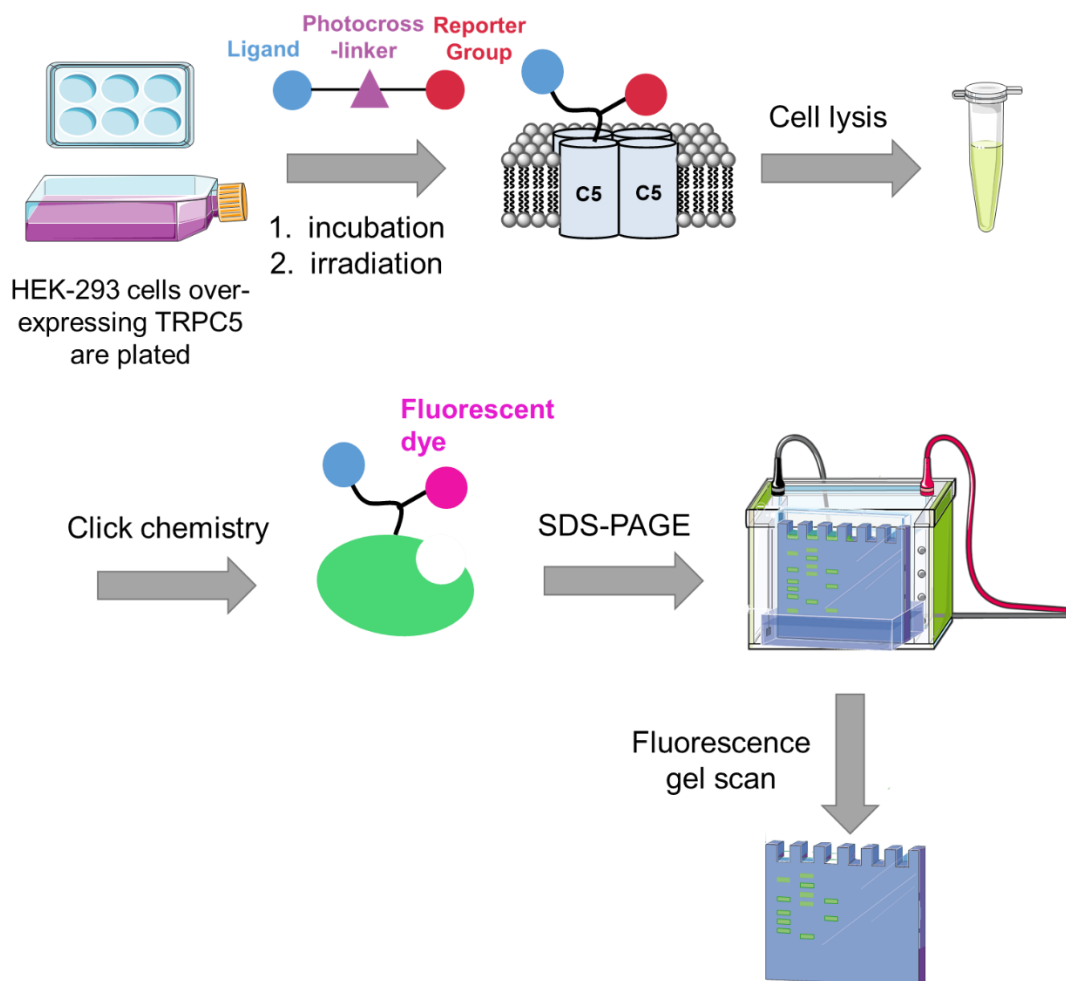


**Figure 25: Photoaffinity labelling workflow.** HEK-293 cells over-expressing TRPC5 are incubated with a photoaffinity probe and irradiated (365 nm, 25 minutes). Cells are subsequently lysed and click chemistry is performed to incorporate a fluorescent dye onto the target protein. Fluorescently labelled proteins are identified by SDS-PAGE and a fluorescent gel scan. Servier Medical Art was used in the generation of this figure.

Photoaffinity probes in this thesis have been designed with an alkyne as the reporter group to enable the attachment of either a fluorescent dye or biotin post cell lysis. This attachment occurs using CuAAC 'click' chemistry. To initiate the click chemistry reaction the alkyne coordinates to a copper(I) centre of an active catalyst (*Figure 26*). The concentration of copper(I) ions must be maintained at a high level for the click reaction to be successful. Frequently the copper(I) ion is generated from a copper(II) source using a reducing agent in large excess. The use of a reducing agent decreases the susceptibility of the click reaction to oxygen.<sup>190</sup> Tris(2-carboxyethyl)phosphine (TCEP) is an example of a water-soluble reducing agent and is particularly useful in biological systems, because it protects cysteine residues from oxidative coupling.<sup>191</sup> Additionally a ligand is used to prevent reoxidation of copper (I)

to copper (II) by air and protect copper (I) against disproportionation to copper (0) and copper (II).<sup>190</sup> Tris(benzyltriazolylmethyl)amine (TBTA) is an example of a ligand which is commonly used to stabilise the copper (II) ions.

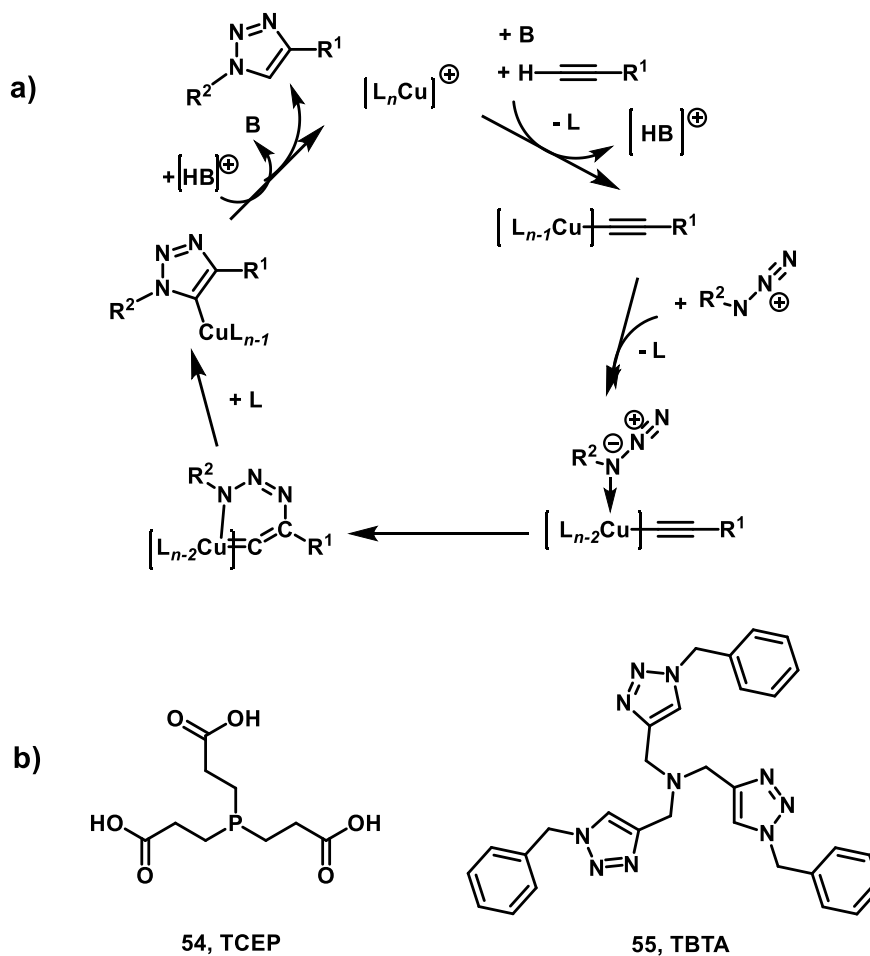


**Figure 26: Click chemistry mechanistic proposal by Sharpless;<sup>192</sup> a) click chemistry mechanism where L represents a ligand (e.g. Tris(benzyltriazolylmethyl)amine (TBTA)) b) chemical structures of a reducing agent: Tris(2-carboxyethyl)phosphine (TCEP) and ligand: TBTA**

## Chapter 3 - Modulation of TRPC5 using natural and synthetic flavonols

### 3.1 Introduction

TRP channels are modulated by chemicals, including plant-based natural products. This has led to the suggestion that TRPC channels may be integrators of animal biology with the external environment. TRPC5 can be modulated by numerous dietary substances, such as  $\omega$ -3 fatty acids and antioxidant chemicals, including vitamin C, gallic acid and the polyphenol resveratrol.<sup>193,24</sup> These antioxidants are components of some fruits, vegetables, and beverages, including green tea and red wine.<sup>194</sup>

Flavonoids are formed in plants from aromatic amino acids, e.g. phenylalanine and tyrosine, as well as malonate, and have antioxidant properties. The basic flavonoid structure consists of the flavan core; two aromatic rings connected by a pyran group, the rings are labelled A, B, and C, (*Figure 27*).<sup>195</sup> Flavonoids can be divided into subclasses based on their level of oxidation and pattern of substitution on the C ring (*Figure 27*).<sup>195</sup> Flavonoids generally occur in plants as glycosylated derivatives and are predominant in a variety of fruits, vegetables, seeds, nuts, grains, spices and different medicinal plants. In particular, the flavones apigenin **61** and luteolin **62** are abundant in cereal grains and aromatic herbs (*Figure 28*). The basic backbone structure of flavones consists of a 2-phenylchromen-4-one, **59** and various hydroxyl groups distributed on both rings A and B (*Figure 27*).<sup>196</sup> Flavonols quercetin **63** and kaempferol **64** are more commonly found in vegetables and fruits (*Figure 2828*).<sup>195</sup> Flavonols contain the 3-hydroxybenzopyran core, **60**, with a phenolic group in the 3-position (*Figure 27*).



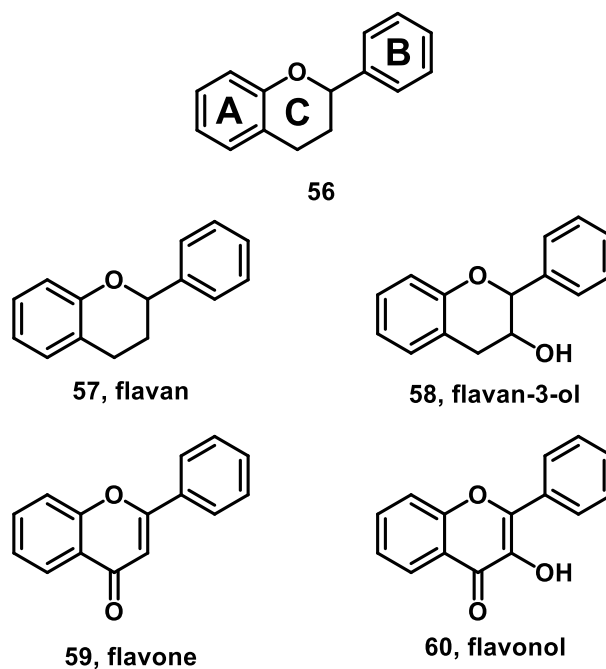


**Figure 27: The flavonoid family;** a) Basic flavonoid structure, **56**; and the basic structures of b) flavans, **57** c) flavan-3-ols, **58** d) flavones, **59** and e) flavonols, **60**.

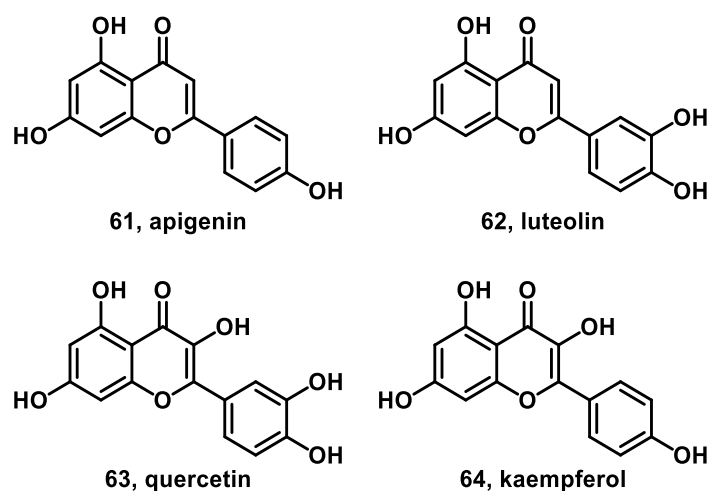


**Figure 28: Structures of flavones; apigenin 61 and luteolin 62, and flavonols; quercetin 63 and kaempferol 64.**

Following evidence of modulation of TRPC5 by oxidised phospholipids,<sup>197</sup> the polyphenol resveratrol<sup>193</sup>, and  $\omega$ -3 fatty acids;<sup>24</sup> the effect of dietary chemicals on TRPC5 was investigated (experiments performed by Jacqueline Naylor). Initially, a set of diverse natural products from traditional Chinese medicines were tested in cells over-expressing TRPC5 within the Beech group. Through this screen a number of flavonoids were identified to inhibit the  $Gd^{3+}$ -evoked  $Ca^{2+}$  entry. Subsequently, several other flavonoids were tested, which demonstrated that apigenin **61** and luteolin **62** were inactive against TRPC5, whilst quercetin **63** and kaempferol **64** had  $IC_{50}$  values

of 6.5 and 3.9  $\mu\text{M}$  respectively.<sup>198</sup> These results indicated that activity against TRPC5 was dependent on the hydroxyl group present in flavonols on the C ring (Figure 27).

Galangin, **65** was identified in the flavonoid screening assays to be the most potent TRPC5 inhibitor in the flavonol series with an  $\text{IC}_{50}$  of 0.45  $\mu\text{M}$  (Figure 29). Galangin is present in high concentrations in honey and *Alpinia officinarum*, a plant which has been used as a herbal medicine for a variety of ailments in Asia for centuries.<sup>199</sup> Galangin is involved in a variety of biological activities, including; anti-mutagenic,<sup>200</sup> anticlastogenic,<sup>201</sup> anti-oxidative and radical scavenging.<sup>202,203</sup> Au and co-workers describe how galangin's anticlastogenic properties arise from its flavonol type structure, specifically the importance of having the 2,3 double bond and the 3,5,7-hydroxyl groups.<sup>201</sup> The 2,3 double bond provides  $\pi$ -conjugation throughout the molecule, favouring near planarity between the two rings.

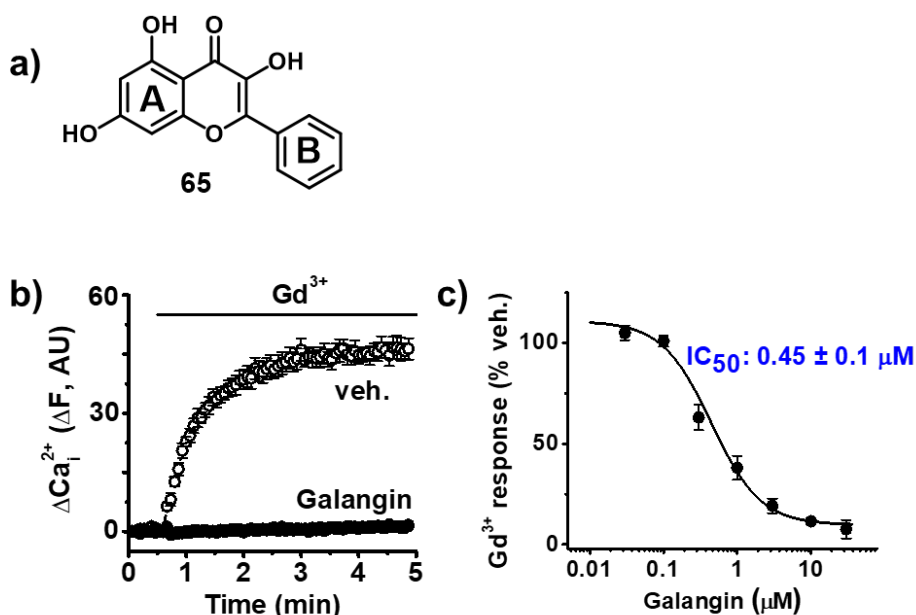
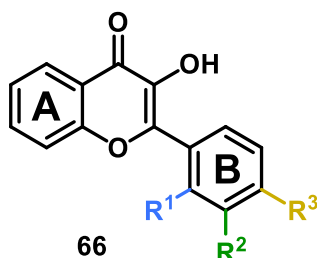


**Figure 29: Galangin, 65, inhibits TRPC5.** Recordings were from TRPC5-expressing (*tet+*) HEK-293 cells and extracellular  $\text{Ca}^{2+}$  was present at 1.5 mM. **a)** Structure of galangin **b)** Free intracellular calcium ( $\text{Ca}_i^{2+}$ ) concentration shown by fluo-4 fluorescence intensity ( $F$ ) in arbitrary units (AU). Cells were incubated with 10  $\mu\text{M}$  galangin or ethanol vehicle control (veh.) for 30 min before 50  $\mu\text{M}$   $\text{Gd}^{3+}$  was applied **c)** concentration-response data for **b)**, showing an  $\text{IC}_{50}$  of the fitted Hill equation of  $0.45 \pm 0.1 \mu\text{M}$  ( $n/N=3/12$ ) (Mean  $\pm$  SE of mean).<sup>198</sup> (Experiments were performed by Jacqueline Naylor).

The structure activity relationships (SAR) of these flavonols was subsequently investigated. A library of 41 mono-substituted flavonols (synthesis performed by Dr Marco Migliore) were tested by the group of Prof. David Beech at a concentration of 10  $\mu\text{M}$  against  $\text{Gd}^{3+}$ -evoked  $\text{Ca}^{2+}$  entry in TRPC5-over-expressing HEK-293 cells. The right-hand phenyl ring (B) was mono-substituted using different groups including; H, F, Cl, Br,  $\text{CH}_3$ ,  $\text{CF}_3$ , OH, OMe,  $\text{NO}_2$ , 2-thienyl and 2-furyl. The screening showed that

most compounds that caused over 50% inhibition (at 10  $\mu$ M) were *ortho*- ( $R^1$ ) substituted flavonols, with Me and Br having the greatest inhibitory effect, while *meta*- ( $R^2$ ) and *para*- ( $R^3$ ) substituents showed decreasing inhibitory effect. (Figure 30) *Note: the hydroxyl groups on the A ring were not present in these flavonols.*



**SAR synthetic flavonols**

+  $R^1$  substituents: **CH**<sub>3</sub>, F, Cl, **Br**, OH

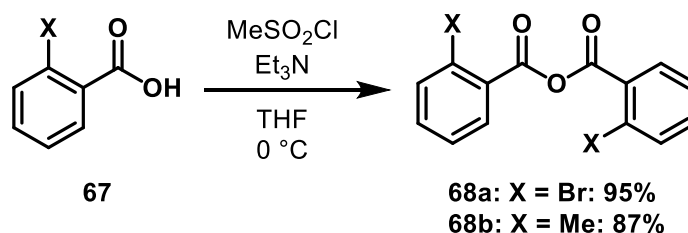
-  $R^2$  or  $R^3$  substituents

**Figure 30:** SAR of the synthetic, mono-substituted flavonols.

*Ortho*-substitution of the B ring was seen to be most promising for inhibition of TRPC5, particularly with halogen substitution. Therefore, substitution at the *ortho*-position, combined with hydroxyl groups on the A ring was investigated for novel flavonol-based TRPC5 inhibitors.

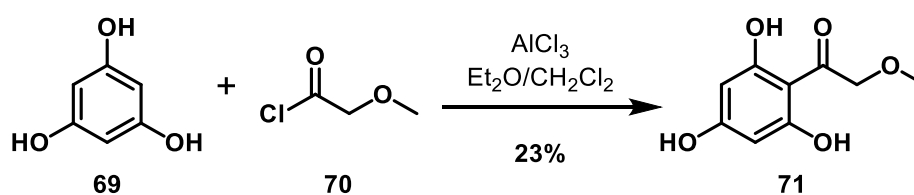
### 3.2 Synthesis of galangin analogues AM12 and AM13

The synthesis of two *ortho*-substituted galangin derivatives was achieved by utilising a combination of literature procedures. Firstly, *ortho*-substituted benzoic anhydrides **68**, were synthesised following the literature procedure described by Daskiewicz *et al.*<sup>204</sup> (*Scheme 4*), where **67** was mixed with methanesulfonylchloride at 0 °C to yield the acid chloride, which was converted to the benzoic anhydrides **68**.



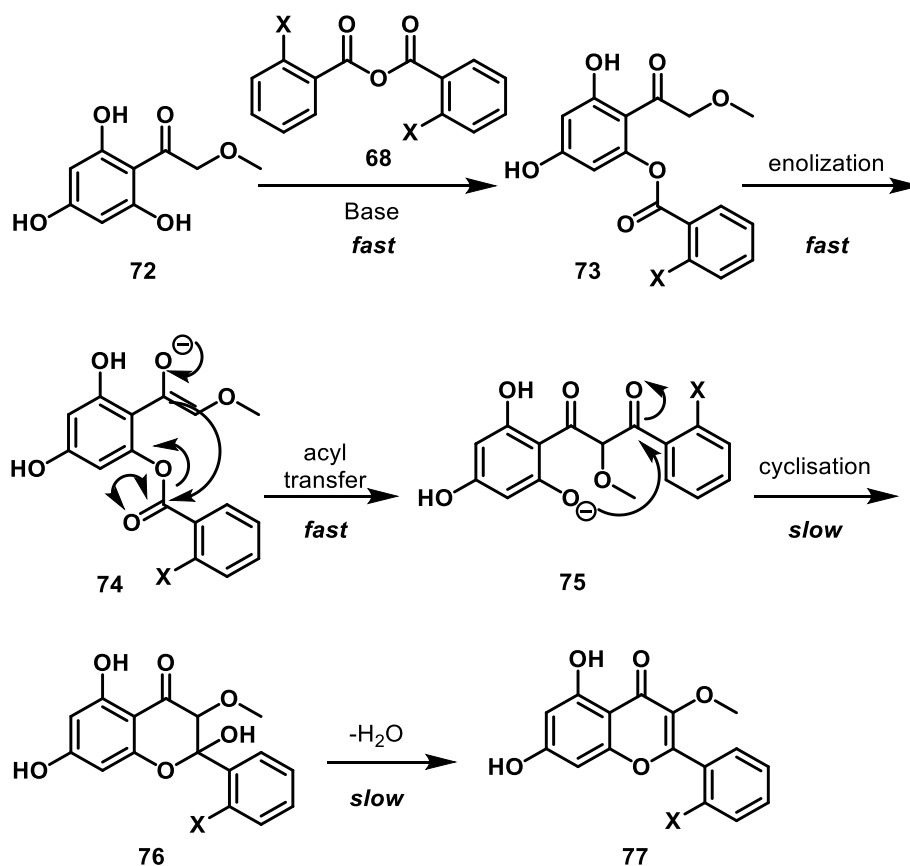
**Scheme 4:** Synthesis of *ortho*-substituted benzoic anhydrides **68**. THF: Tetrahydrofuran.

The synthesis of methoxyphloroacetophenone **71** followed a combination of literature procedures by Carola *et al.*<sup>205</sup> and Gerrad *et al.*<sup>206</sup> The Friedel-Crafts acylation reaction was successful with a 23% yield. (*Scheme 5*). In this reaction, Rochelle's salt was used to break up the emulsion formed, and the aqueous layer was then extracted with ether. However, the use of Rochelle's salt did not fully separate the aqueous and organic layers, thereby making the extraction difficult. The yield reported by Gerard *et al.* for this step was 58%, however the 23% yield obtained equated to 0.92 g of product and therefore this was sufficient for the following steps.



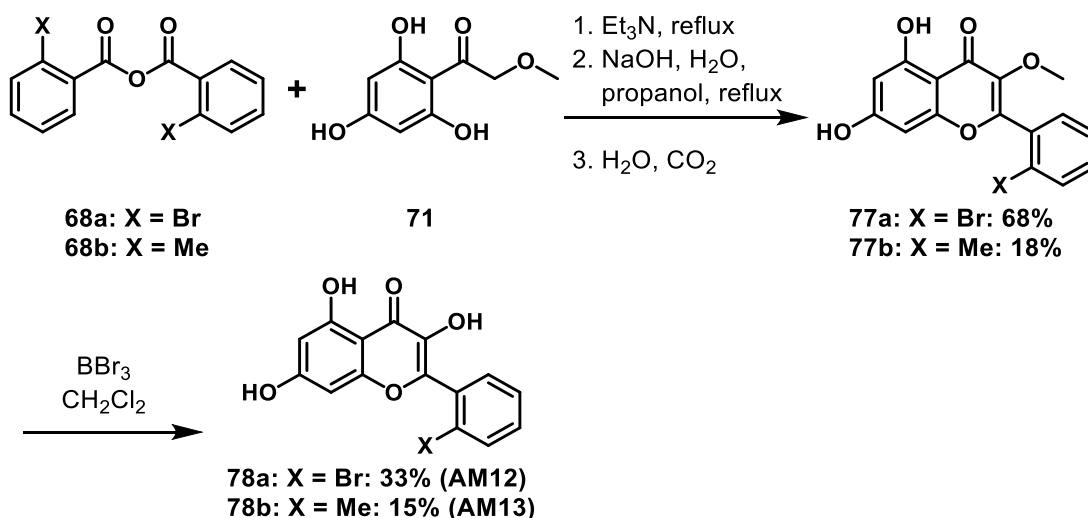
**Scheme 5:** Friedel-Crafts acylation of phloroglucinol **69** with acyl chloride **70** gave methoxyphloroacetophenone **71**.

The synthesis of the methyl-protected galangin derivatives **77** proceeded via the Kostanecki-Robinson reaction.<sup>207</sup> This reaction allowed the conversion of a hydroxyl ketone **71** and an aromatic acid anhydride **68** to form a flavonol.<sup>208</sup> The mechanism is shown in *Scheme 6*.<sup>209</sup> The yield was significantly lower for the methyl derivative of **77**; this is due to an excess of ethanol being added to break up a precipitate that formed. Thus, upon addition of a solid CO<sub>2</sub> to the reaction mixture there was reduced precipitation of the product, **77**.



**Scheme 6:** Flavone/flavonol formation proceeds via the Kostanecki-Robinson mechanism.<sup>210</sup>

The methyl deprotection of **77** was the final step in the formation of the B ring *ortho*-substituted galangin derivatives **78**. This step was originally attempted using a method described by Forbes *et al.*<sup>211</sup> This procedure used HBr and acetic acid under reflux conditions; however, no product or starting material could be seen by <sup>1</sup>H NMR after approximately 16 hrs. It was concluded that these conditions were too harsh, and therefore a milder deprotection method was sought. Methyl deprotection using BBr<sub>3</sub> was investigated, because this reaction does not require high temperatures. The synthesis was completed following the literature procedure by Carola *et al.*<sup>205</sup> The purification of both the bromine and methyl derivatives proved difficult. Purification for both derivatives was attempted using column chromatography, which was successful for the bromo-derivative **78a** (named AM12), however the methyl derivative **78b** (named AM13) co-eluted with an impurity and thus preparative TLC was used to obtain the pure product.



**Scheme 7: Synthesis of galangin derivatives AM12 and AM13.** Benzoic anhydride **68** and intermediate **71** were combined to yield methyl-protected galangin derivatives **77a** and **77b** in a Kostanecki-Robinson reaction, followed by boron tribromide-mediated demethylation, which afforded **78a** (AM12) and **78b** (AM13).

### 3.3 Identification of AM12 and AM13 as synthetic flavonols that selectively inhibit TRPC5

#### 3.3.1 Comparison of AM12 and AM13 to a known TRPC5 inhibitor, 2-APB

Initially, intracellular calcium measurements were performed to compare the ortho-substituted galangin derivatives AM12, **78a** and AM13, **78b** (Scheme 7) to the known TRPC4/5 inhibitor 2-aminoethoxydiphenyl borate (2-APB).<sup>50</sup> Although 2-APB has been widely used experimentally, it lacks specificity and efficacy.<sup>50</sup> Cells over-expressing TRPC5 upon induction with tetracycline, were pre-treated with AM12, AM13 or 2-APB for 30 minutes prior to intracellular calcium recordings. The treatment with AM12 and AM13 caused decreased levels of Ca<sup>2+</sup> entry in the presence of Gd<sup>3+</sup> in alignment with 2-APB, with greater than 95% inhibition of TRPC5 (Figure 31). In marked contrast the vehicle, Gd<sup>3+</sup> with DMSO control, showed the activation of TRPC5 channels by 100 μM Gd<sup>3+</sup> causing an increase in the fluorescence recorded. These results gave an initial indication that AM12 and AM13 were relatively potent TRPC5 inhibitors.

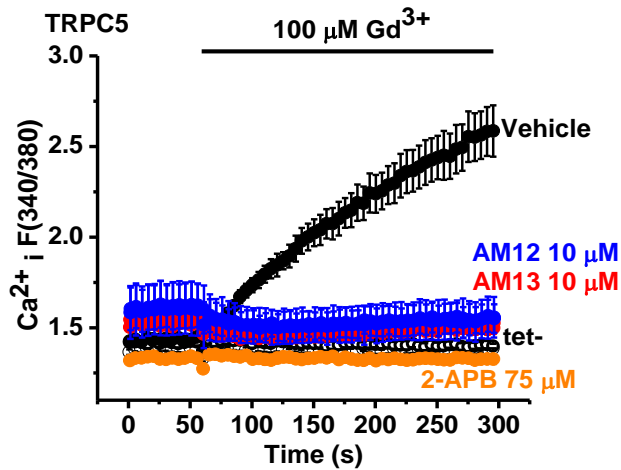


**Figure 31: Galangin derivatives AM12 and AM13 inhibit TRPC5 at 10  $\mu\text{M}$ .** Intracellular  $\text{Ca}^{2+}$  was measured using fura-2 and recordings were from TRPC5-expressing (*tet+*) HEK-293 cells or control non-induced (*tet-*) cells. Example data from a 96-well plate showing basal  $\text{Ca}^{2+}$  and then 100  $\mu\text{M}$   $\text{Gd}^{3+}$ -evoked  $\text{Ca}^{2+}$  entry in the presence of vehicle (DMSO), 75  $\mu\text{M}$  2-APB, 10  $\mu\text{M}$  AM12 and 10  $\mu\text{M}$  AM13. ( $n/N=2/12$ )

### 3.3.2 Evaluation of the potency of AM12 and AM13 on TRPC5

Concentration dependence effects were investigated to determine the potency of AM12 and AM13 as TRPC5 channel inhibitors. A dose-dependent increase in intracellular calcium was detected with 10  $\mu\text{M}$ , 1  $\mu\text{M}$ , 0.3  $\mu\text{M}$  and 0.1  $\mu\text{M}$ . With extracellular application of 0.03  $\mu\text{M}$  AM12 and AM13 only a slight decrease in intracellular calcium was observed (Figure 32). Analysis of the concentration dependent inhibitory effects indicated an  $\text{IC}_{50}$  of 0.28  $\mu\text{M}$  and 0.49  $\mu\text{M}$ , for AM12 and AM13, respectively. Therefore, these data suggest that AM12 and AM13 are similar in potency to the natural product galangin as inhibitors of TRPC5 (Figure 32).

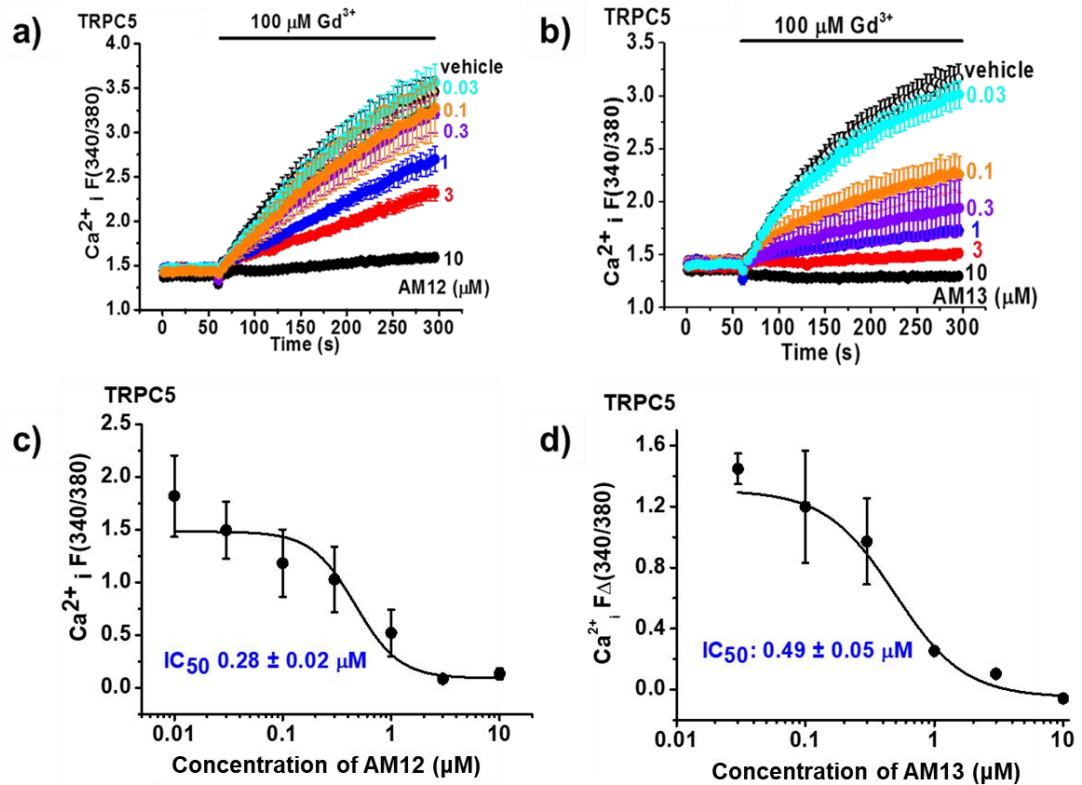


**Figure 32: AM12 and AM13 act as potent TRPC5 inhibitors.** Recordings were taken from TRPC5-expressing (tet+) HEK-293 cells. Intracellular Ca<sup>2+</sup> was measured using fura-2; **a,b**) Example data from a 96-well plate showing basal Ca<sup>2+</sup> and then 100 μM Gd<sup>3+</sup>-evoked Ca<sup>2+</sup> entry in the presence of vehicle, and 10, 1, 0.3, 0.1, 0.03 and 0.01 μM for a) AM12 b) AM13; **c**) Summarized concentration-response data for experiments of the type shown in a) for Gd<sup>3+</sup>-evoked Ca<sup>2+</sup> entry (IC<sub>50</sub> 0.28 ± 0.02 μM, n/N = 5/30); **d**) Summarized concentration-response data for experiments of the type shown in b) for Gd<sup>3+</sup>-evoked Ca<sup>2+</sup> entry (IC<sub>50</sub> 0.49 ± 0.05 μM, n/N = 3/48). (mean ± SE of mean)

### 3.3.3 Evaluation of the activity of AM12 on TRPC5 in the presence of alternative activators

TRPC5 channels are strongly stimulated by lanthanide ions (Gd<sup>3+</sup> or La<sup>3+</sup>), but they can also be stimulated by other externally-applied factors, such as sphingosine-1-phosphate (S1P).<sup>29,212</sup> Lanthanides appear to act as direct activators of the TRPC channels or facilitators of channel opening, whereas S1P acts indirectly via G protein signalling.<sup>29,213</sup> Subsequently, the potency of AM12 against S1P-evoked Ca<sup>2+</sup> entry was tested in HEK-293 cells over-expressing TRPC5. Unexpectedly, AM12 stimulated rather than inhibited the S1P-evoked Ca<sup>2+</sup> entry. S1P is an endogenous activator of TRPC5, therefore it is hypothesised that the stimulatory effects observed are due to stimulation of endogenous Ca<sup>2+</sup> entry. Hui *et al.* have previously described Ca<sup>2+</sup>-mediated facilitation of TRPC5 in the same TRPC5 (tet+) cells.<sup>214</sup> These data suggest that stimulator as well as inhibitor actions can exist in the same molecule, and this can be dependent on the mode of activation of the TRPC5 channel.



Furthermore, the lack of stimulation previously seen by galangin when applied to S1P-activated TRPC5 containing cells,<sup>198</sup> indicates that a very small change in the chemical structure of flavonols can alter the activity and possibly the mechanism of action towards TRPC5.

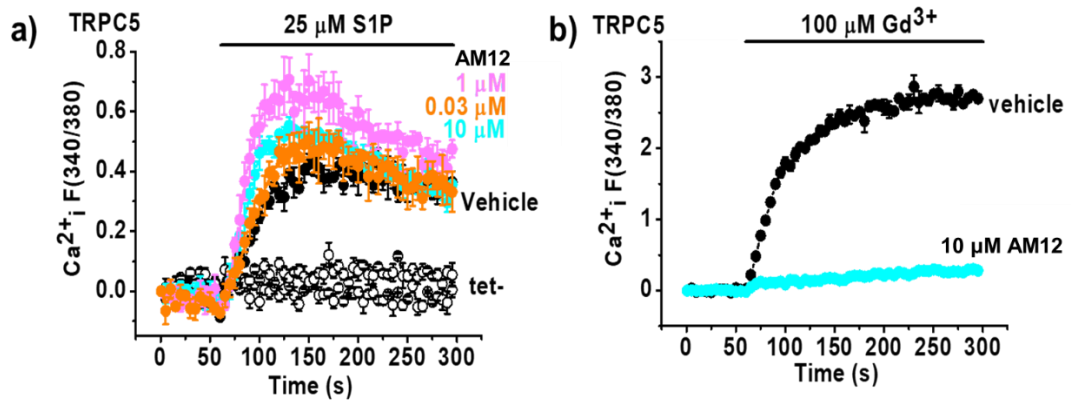


**Figure 33: Stimulatory effects of AM12 on TRPC5.** Intracellular Ca<sup>2+</sup> was measured using fura-2 and recordings were from TRPC5-expressing (tet+) HEK-293 cells or control non-induced (tet-) cells. Example data from a 96-well plate showing basal Ca<sup>2+</sup> and then: **a)** 25 μM S1P-evoked Ca<sup>2+</sup> entry in the presence of vehicle, and 10, 1 and 0.03 μM AM12; **b)** 100 μM Gd<sup>3+</sup>-evoked Ca<sup>2+</sup> entry in the presence of vehicle and 10 μM AM12 as a control.

### 3.3.4 AM12 inhibits TRPC1/4/5 channels relatively directly

To investigate if AM12 has a direct effect on TRPC5 channels, outside-out patch clamp recordings were used, with AM12 bath-applied to the extracellular face of the membrane (experiments were carried out by Prof. Katsuhiko Muraki). Additionally, to address the possibility that the effect of AM12 is specific to Gd<sup>3+</sup>-activated channel activity, a newly described agonist was used, (-)-Englerin A ((-)-EA).<sup>21</sup> (-)-EA is considerably more potent and efficacious than Gd<sup>3+</sup>. Firstly, application of 100 nM (-)-EA evoked clear activation of the TRPC5 current, subsequently AM12 caused prompt inhibition of both the inward and outward (-)-EA evoked-TRPC5 currents. This suggests that AM12 may have a direct interaction with the TRPC5 channel. Additionally, there was fast recovery on washout (*Figure 34a,b*), suggesting that AM12 is a reversible binder. The average inhibition at 5 μM AM12 was ~65%. Outside-out patch clamp recordings were also taken from cells over-expressing TRPC4 homomeric channels, which are the most closely related to TRPC5 channels with 70% sequence identity (BLAST search<sup>36</sup>) (*Figure 34c,d*). AM12 promptly inhibited TRPC4 where the average inhibition was ~ 80 % at 5 μM AM12.

TRPC4 and TRPC5 proteins have been shown to readily form heteromers with TRPC1.<sup>20,21</sup> These heteromeric channels have distinct characteristics,<sup>5</sup> and are thought to be of more physiological relevance. TRPC4 and TRPC5 are capable of forming homomeric channels, yet TRPC1 is widely expressed and therefore physiologically these channels presumably exist as heteromers with TRPC1.<sup>10</sup> TRPC1-TRPC5 heteromeric channels were also investigated (experiments performed by Katsuhiko Muraki); this was done in whole-cell recordings because of difficulty in obtaining outside-out patches of TRPC1-expressing cells. AM12 inhibited current through TRPC1-TRPC5 heteromeric channels, however this was relatively weak in comparison with the inhibition seen against TRPC5 homomeric channels (*Figure 34a cf. Figure 34e*). These data suggest that AM12 inhibits TRPC5 and TRPC4 *via* a site accessible from the extracellular face of the membrane, acting either directly on the channel or on a site closely associated with it. It is also noteworthy that AM12 inhibits TRPC1-TRPC5 heteromeric channels which are hypothesised to be more relevant physiologically.

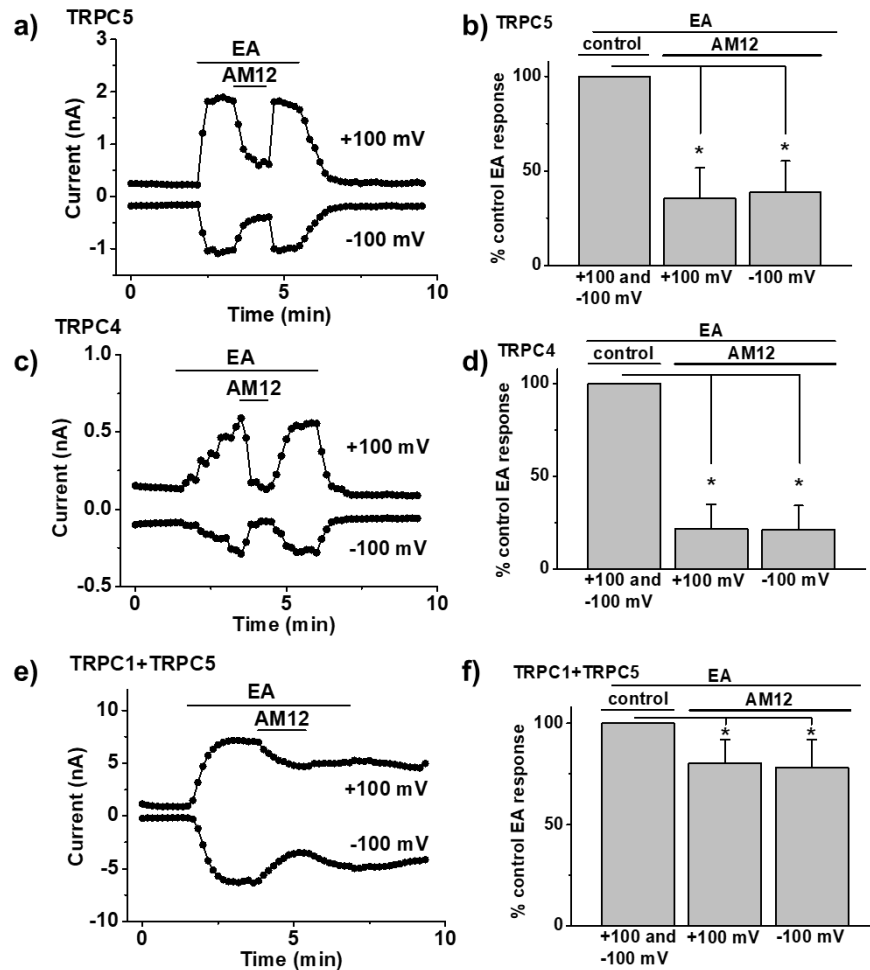


**Figure 34: Inhibitory effect of AM12 on TRPC1/4/5 channels stimulated by (-)-Englerin A ((-)-EA).** Recordings were made from outside-out membrane patches from HEK-293 cells over-expressing **a,b** TRPC5 or **c,d** TRPC4 upon induction with tetracycline (tet+) or **e,f** from whole-cells expressing SYFP2-TRPC1 and mTurquoise2-TRPC5. **a**) Example TRPC5 outside-out patch currents during ramp changes in voltage from -100 to +100 mV every 10 s and application of 100 nM (-)-EA and 5  $\mu$ M AM12; **b**) Mean normalized data for TRPC5 outside-out patch currents evoked by 100 nM (-)-EA and 5  $\mu$ M AM12 (n=5); **c**) Example TRPC4 outside-out patch currents during ramp changes in voltage from -100 to +100 mV every 10 s and application of 100 nM (-)-EA and 5  $\mu$ M AM12. **d**) Mean normalized data for TRPC4 outside-out patch currents evoked by 100 nM (-)-EA and 5  $\mu$ M AM12 (n=5). **e**) Example TRPC1-TRPC5 whole-cell currents obtained during ramp changes in voltage from -100 to +100 mV every 10 s and during application of 100 nM (-)-EA and 5  $\mu$ M AM12; **f**) Mean normalized data for TRPC1-TRPC5 whole cell currents evoked by 100 nM (-)-EA and 5  $\mu$ M AM12 (n=5); (Experiments performed by Prof. Katsuhiko Muraki)

### 3.3.5 Investigation into the effect of AM12 on other TRP channels

Further experiments were carried out to identify the specificity of AM12 to TRPC4 and TRPC5 (experiments were performed by Hannah Gaunt). Intracellular calcium measurements were performed on HEK-293 cells over-expressing TRPC3 and TRPM2, and CHO cells stably expressing human TRPV4. At 10  $\mu$ M, AM12 had no

significant inhibitory effect against TRPC3 channels or TRPM2 channels (*Figure 35a,b*). AM12 caused a stimulatory effect on  $\text{Ca}^{2+}$  entry through TRPV4 channels, but no effect was observed on TRPM2 channels (*Figure 35b,c*).<sup>198</sup> These data suggest that AM12 appears to have a degree of selectivity towards TRPC1/4/5 channels amongst other TRP channels.

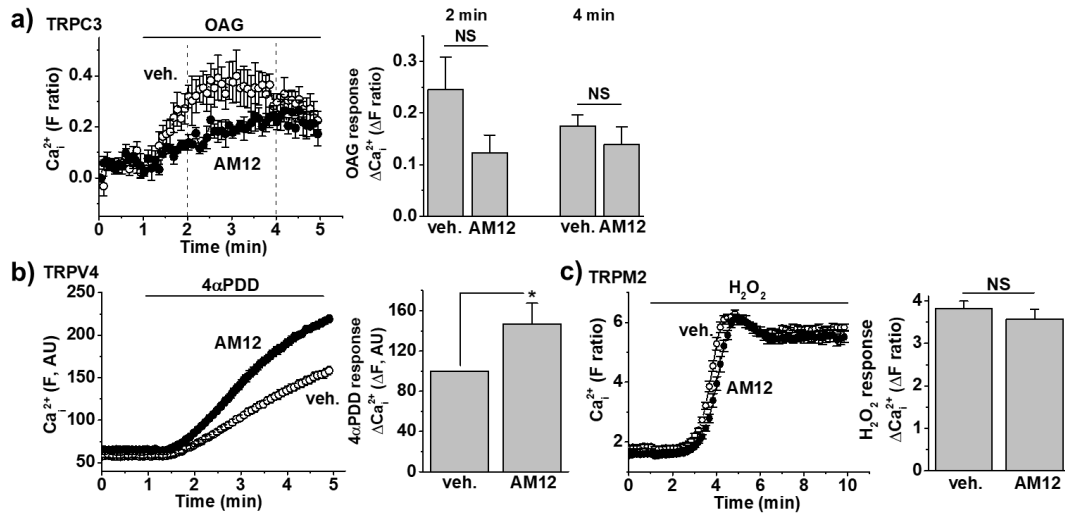


**Figure 35: AM12 has little or no effect on TRPC3 channels, TRPV4 channels and TRPM2 channels.**<sup>198</sup> Intracellular  $\text{Ca}^{2+}$  was measured using **a,b** fura-2 or **c** fluo-4. **a-c**) Left: example data is shown from a single 96-well plate; right: mean data for multiple plates of this type; **a**) Cells were stably over-expressing TRPC3 and 1-oleoyl-2-acetyl glycerol (OAG, 50  $\mu\text{M}$ ) was used to activate the TRPC3 channels in the presence of vehicle control (veh.) or 10  $\mu\text{M}$  AM12 ( $n/N = 5/26$ ); **b**) Cells were over-expressing TRPV4 and hydrogen peroxide ( $\text{H}_2\text{O}_2$ , 1 mM) was used to activate the channels in the presence of veh. or 10  $\mu\text{M}$  AM12 ( $n/N=5/24$ ); **c**) Cells were stably over-expressing TRPM2 and 4 $\alpha$ -phorbol-didecanoate (4 $\alpha$ -PDD, 1  $\mu\text{M}$ ) was used to activate the TRPV4 channels in the presence of the veh. or 10  $\mu\text{M}$  AM12. ( $n/N=3/24$ ).<sup>198</sup> (Experiments performed by Hannah Gaunt)

### 3.4 Effect of AM12 and AM13 on a series of cardiac ion channels

Limited selectivity experiments identified AM12 to be relatively selective towards TRPC4/5 channels amongst a number of other TRP channels tested (*Chapter 3.3.5*). To further investigate the selectivity of AM12 and AM13 and identify potential off-targets; AM12 and AM13 were tested against a set of cardiac ion channels. Ion channels are critical for rhythmicity and contractility in cardiac function, and off-target interactions can result in unwanted side-effects.<sup>183</sup> Sodium voltage-gated channels (Nav1.5) and potassium voltage-gated channels (Kv11.1 aka hERG/ $I_{Kr}$ , Kv7.1 aka  $I_{Ks}$  and Kv4.3 and Kv1.4 aka  $I_{to}$ ) are expressed in heart and vasculature and together

contribute towards the ventricular action potential which controls contraction and relaxation of the heart (*Section 2.3.1*). Thus, the effects of AM12 and AM13 on cardiac channels: hERG, Nav1.5,  $I_{KS}$  and  $I_{to}$ , were investigated by automated whole cell patch clamp recordings (experiments performed at AstraZeneca in collaboration with Ann Woods) (*Section 2.3*). CHO cells stably expressing Nav1.5, Kv11.1, Kv7.1 and Kv4.3 were preincubated and then maintained in the presence of AM12 or AM13 for three minutes prior to current recordings. Concentration-response data were collected for AM12 and AM13 between 167  $\mu$ M and 0.05  $\mu$ M and  $IC_{50}$  values are summarised in (*Table 5*). (For  $IC_{50}$  graphs, see *Appendix I*)

The degree of inhibition of cardiac channels necessary to induce QT interval prolongation and therefore induce cardiac arrhythmias is much debated. In 2005, guidelines were issued for evaluating the risk of QT interval prolongation.<sup>215</sup> However the complex interplay of multiple ion channels relating to QT interval prolongation makes evaluating the risk of a drug candidate difficult,<sup>184</sup> and approaches to cardiac safety testing differ from company to company.<sup>216</sup> At AstraZeneca compounds are declared active where inhibition of ion channel current is > 20% at the top test concentration. AM12, AM13 and galangin are all above this threshold for one or more of the cardiac ion channels. Interestingly, these are the same compounds which are the most potent against TRPC5, suggesting there may be a common mechanism of action on multiple ion channels.

A publication by GSK<sup>217</sup> reports that drug candidates should have an activity against hERG over 30  $\mu$ M or greater that 1000-fold selectivity for the target. Following these guidelines AM12 and galangin would be regarded as unsuitable drug candidates. Additionally, AM12, AM13 and galangin have relatively poor selectivity towards TRPC5, in comparison with the cardiac ion channels tested (*Table 5*).

**Table 5: Summary of the selectivity of AM12, AM13 and natural flavonols for a number of cardiac ion channels relative to TRPC5. IC<sub>50</sub> values for AM12, galangin, kaempferol and quercetin from Naylor et al.<sup>198</sup>**

Compound	IC <sub>50</sub> (μM)					Selectivity
	hERG	I <sub>KS</sub>	I <sub>t0</sub>	Na <sub>V1.5</sub>	TRPC5	
AM12	8 ± 4.4	53.4 ± 8.6	> 167 uM	28.5 ± 50.0	0.28	>100
AM13	33.8 ± 8.0	25.1 ± 6.0	23.9	7.1 ± 8.2	0.49	>14
Galangin	52.7	21.4	> 166.7	> 166.7	0.45	>~50
Apigenin	> 166.7	> 166.7	> 166.7	> 166.7	>10	>15
Luteolin	> 166.7	> 166.7	> 166.7	> 166.7	>10	>15
Kaempferol	140	> 166.7	> 166.7	> 166.7	3.9	>35
Myricetin	> 166.7	> 166.7	> 166.7	153.2	>10	>15
Quercetin	> 166.7	> 166.7	75.0	> 166.7	6.5	>10
Reference	8.2	0.5	15	3.5	-	-

### 3.5 Electrochemical biosensor assays

Phenolic phytochemicals modulate numerous unrelated proteins; however, their modes of action remain poorly understood. Anderson and co-workers<sup>218</sup> highlighted that a protein may be modulated in a synergistic manner by seemingly unrelated polyphenols, which suggests a common mechanism of action. All membrane proteins are embedded in a lipid bilayer. This common feature could be the link to the many diverse effects of polyphenols on membrane proteins. Due to the amphiphilic character of polyphenols, they can adsorb to lipid bilayer/solution interfaces, thus altering membrane protein function.<sup>219,220</sup> Anderson and co-workers propose that the mechanism of action of some polyphenols is by physical alteration of membrane protein properties, rather than by a discrete binding site.<sup>218</sup>

The natural flavonol quercetin, **63**, was found to be a TRPC5 inhibitor in the original flavonol screen (*Section 3.1*). Trouillas and co-workers used molecular dynamic simulations to identify that quercetin and its metabolites localise to the membrane/solution interface, enhancing their local concentrations and thereby their antioxidant effects on nearby membrane proteins.<sup>221</sup> Additionally, the membrane penetration and thus antioxidant effect has also been correlated with the polarity of substituents.<sup>221</sup> TRPC5 has been suggested to be sensitive to the biophysical properties of the lipid bilayer, indicated by TRPC5 channel activity correlating to lipid chain length.<sup>222,223</sup> Therefore, it is a plausible hypothesis that the mechanism of action of flavonols on TRPC4/5 channels is *via* local perturbation of the bilayer.

The flavonols tested against TRPC5 all have a predicted pK<sub>a1</sub> (first deprotonation) of ~6.4, which means that at physiological pH, their amphiphilic mono-anions are the most prevalent species (predicted using Marvin Beans; downloaded from ChemAxon: <http://www.chemaxon.com>).<sup>198</sup> In addition, the predicted octanol/water partition coefficients (cLogP) of galangin and AM12 (2.76 and 3.53 respectively) are in the same range as those of other polyphenol phytochemicals predicted to localise to the membrane/solution interface.<sup>198,218</sup>

To test this hypothesis, AM12, AM13 and natural flavonols, apigenin **61**, kaempferol **64**, luteolin **62**, myricetin **79** and quercetin **63** (*Figure 28* and *Figure 36*) were tested using a membrane-based sensing device (*Section 2.4*). This membrane-sensing device uses dioleoyl phosphatidylcholine (DOPC) which forms a phospholipid monolayer on a mercury (Hg) electrode and performs a role analogous to the outer leaflet of a phospholipid bilayer.<sup>224</sup>

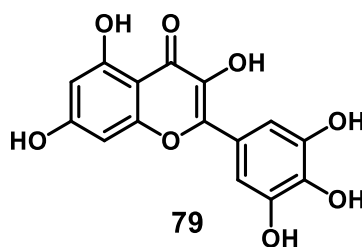


**Figure 36:** Structure of myricetin 79

The flavonols were tested in this biosensor which measures the current against the electrical potential (experiments performed in collaboration with Dr Shahrzad Mohamadi). The monolayer undergoes two potential induced phase transitions, which can be characterised by two sharp capacitance current peaks. The two peaks represent entry of electrolytes into the layer and reorganisation of the layer (Figure 37). These experiments showed that there was a clear distinction between natural flavonols tested (Figure 37) and the two synthetic flavonols, AM12 and AM13 (Figure 38) in regards to perturbation of the phospholipid monolayer.

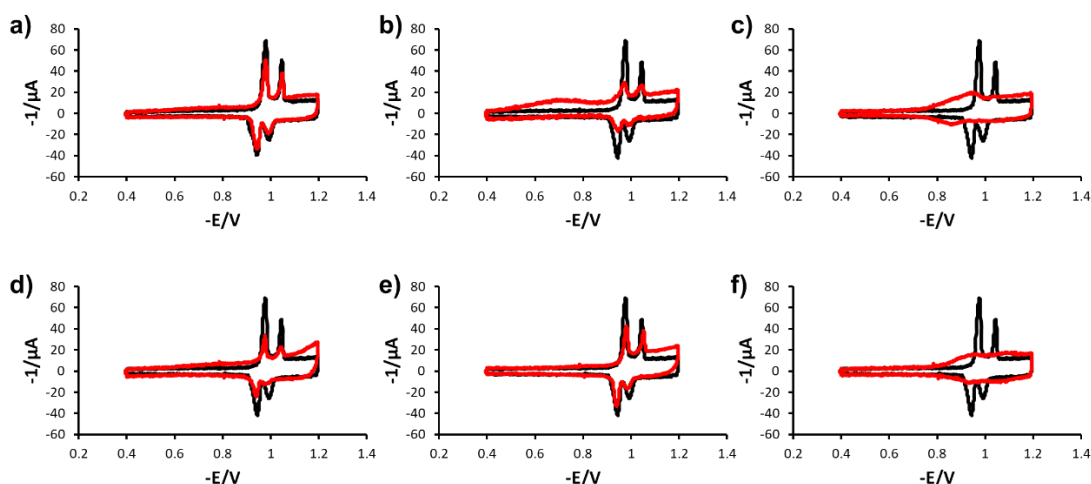


**Figure 37:** RCVs recorded at  $40 \text{ V s}^{-1}$  of a DOPC coated Pt/Hg electrode (black line) in the presence of (red line); a) apigenin, b) galangin, c) kaempferol, d) luteolin, e) myricetin, f) quercetin, at  $8 \mu\text{M}$ .

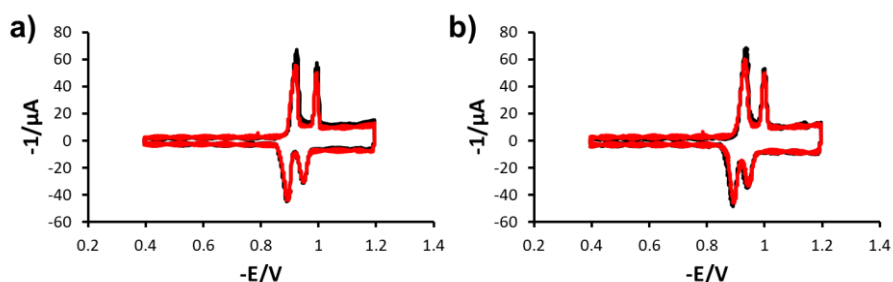


**Figure 38:** RCVs recorded at  $40 \text{ V s}^{-1}$  of a DOPC coated Pt/Hg electrode (black line) in the presence of (red line) a) AM12 and b) AM13 at  $8 \mu\text{M}$ .



These results show that there is not necessarily a direct correlation between TRPC5 inhibition and monolayer perturbation. Galangin, which was the most potent natural flavonol, perturbs the monolayer (Figure 37b), whereas the synthetic flavonols, AM12 and AM13, which have a similar potency towards TRPC5, do not perturb the monolayer (Figure 38). It is possible that the *ortho*-substitution of flavonols reduces membrane perturbation, meaning there may be a conformational effect of the *ortho*-substitution. Additionally, this further suggests that there is a distinct flavonol binding site on the TRPC4/5 channels, or the effect is dependent on other lipids or the presence of a bilayer.

### 3.6 Summary and Conclusions

In summary, a screen of natural products from Chinese herbal medicines led to the identification of galangin as a TRPC5 inhibitor. AM12 and AM13 were designed based on SAR of synthetic and natural flavonols. A series of techniques were used to identify the mode of action of AM12 and AM13 on TRPC5. AM12 inhibited TRPC5 in manual outside-out patch clamp recordings, suggesting that AM12 has a direct effect on TRPC5; because its effect is independent of cellular constituents, other Ca<sup>2+</sup> handling mechanisms or membrane potential (*Section 3.3.4*). AM12 was tested against other TRP channels and appeared to be selective towards TRPC4 and TRPC5 channels (*Section 3.3.5*). This was further explored using automated patch clamp to identify the selectivity of AM12 and AM13 with respect to a selection of cardiac ion channels. AM12 and AM13 showed poor selectivity towards TRPC5 over the cardiac ion channels investigated. Furthermore, there appears to be a correlation between potency against TRPC5 and the activity against other cardiac channels. This suggests there may be a common mode of action of flavonol compounds towards membrane proteins.

There has been literature precedent to suggest that phenolic phytochemicals can modulate the function of membrane proteins by localising to the lipid bilayer-solution interface. Therefore, both natural and synthetic flavonols were tested using an electrochemical biosensor assay (*Chapter 3.5*) which identified that the natural flavonols perturbed a DOPC monolayer. However, the two synthetic flavonols AM12 and AM13 appeared to have no effect on this monolayer, suggesting a conformational effect (as a result of the *ortho*-substitution) on membrane interaction. Alongside the ability of AM12 to inhibit TRPC5 in excised outside-out membrane patch recordings, the electrochemical biosensor data suggest that AM12 and AM13 may interact with TRPC5 through a distinct binding site. To understand the relationship between TRPC5 inhibition and membrane perturbation, published TRPC5 inhibitors (e.g. Pico145) could be tested in the biosensor device. Furthermore, synthesis of additional compounds could be used to explore different conformational and electronic properties in relation to membrane perturbation. A methyl or bromo substituent could be placed in the *meta*- or *para*-position to explore conformational changes without changing the hydrophilicity (cLogP) of the compounds.

## Chapter 4 - Pico145 based photoaffinity probes to elucidate the mechanism of action of Pico145

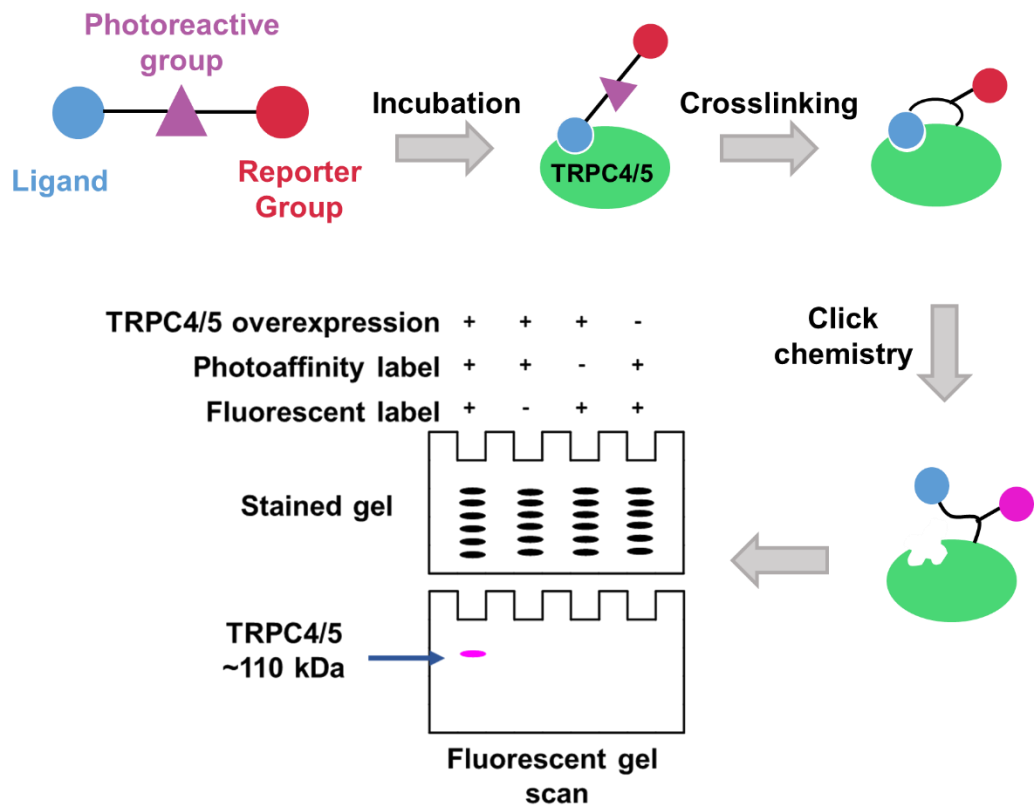
### 4.1 Introduction

A key constraint on the study of TRPC1/4/5 channels has been the lack of potent and specific inhibitors and activators of the channels. In 2015, (-)-EA (*Section 1.3.1.1*) was reported as an efficacious, potent and specific activator of TRPC1/4/5 channels, both homomers and heteromers.<sup>21,35,22</sup> Until recently, the most widely used and characterised inhibitor of the channels was ML204 (*Section 1.3.2.2*).<sup>58</sup> ML204 was originally identified as a TRPC4 inhibitor with an IC<sub>50</sub> of 1 µM, and caused about 65% inhibition of TRPC5 at 10 µM.<sup>58</sup> Although ML204 was found to be relatively selective towards TRPC1/4/5, it is not particularly potent and it was later found that ML204 may be less potent on TRPC1-containing channels. Rubaiy *et al.* found ML204 active against TRPC4-C1 concatemers (activated by (-)-EA) at relatively high concentrations, with an IC<sub>50</sub> of 58 µM.<sup>59</sup>

Pico145 (*Section 1.3.2.4*) was originally specified in an international patent as a TRPC5 inhibitor with an IC<sub>50</sub> < 100 nM.<sup>65</sup> Pico145 was further characterised by Beech and co-workers as a potent and specific inhibitor of TRPC1/4/5 channels, particularly the heteromeric channels.<sup>59</sup> The detailed mechanism of action of Pico145 remains to be understood, however from excised outside-out membrane patch recordings, Pico145 shows dose dependent inhibition of TRPC4 and is reversible on washout. This suggests Pico145 has a direct effect on the channel, because its effect is independent of cellular constituents, other Ca<sup>2+</sup> handling mechanisms or membrane potential. The effect of Pico145 is not thought to be rapid enough for a compound that blocks the ion pore.<sup>59</sup>

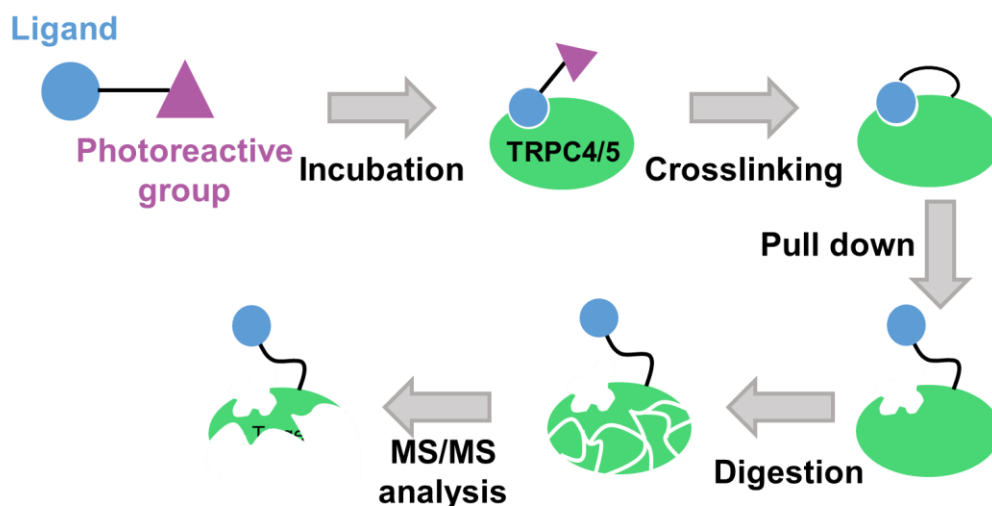
The efficacy, potency and selectivity of Pico145, alongside the evidence to suggest it acts directly on the channel make it an ideal compound to identify a small-molecule binding site in TRPC1/4/5 channels. The identification of such a binding site in TRPC1/4/5 channels will contribute alongside mutagenesis and progress in structural determinations of TRPC channels, to allow rational structure-based design of modulators with enhanced characteristics e.g. *in vivo* stability and the ability to differentiate amongst TRPC1/4/5 channels.

Photoaffinity labelling is commonly used in conjunction with biorthogonal click chemistry to determine ligand-receptor contacts, particularly for enzymes and ion channels as described in *Section 1.6*.<sup>126,225</sup> The direct action of Pico145 on TRPC1/4/5 channels could be confirmed using this approach. This could be achieved using a photoaffinity probe with an alkyne handle; to afford the addition of a fluorescent dye by click chemistry post photolabelling (*Scheme 8*) (*Section 1.6*). Fluorescently labelled proteins could then be identified using SDS-PAGE and a fluorescent gel scan.



**Scheme 8: Photoaffinity labelling for target engagement studies.** A photoreactive probe, consisting of a ligand, photoreactive moiety and a reporter group, is incubated with the target protein. Irradiation causes covalent bond formation to the interacting protein. Following this click chemistry is utilised to incorporate a reporter group, e.g. fluorescent dye. The sample can be separated by SDS-PAGE, to identify a fluorescent band with the molecular weight of the interacting protein.

Following proof of engagement of Pico145 to TRPC1/4/5 channels, identification of the location of a binding site could be achieved using a similar photoaffinity probe. Following photoaffinity labelling and purification, the sites of modification may be identified using peptide digest and liquid chromatography–MS/MS (LC-MS/MS) (*Scheme 9*) (*Section 1.6*).<sup>130</sup>



**Scheme 9: Binding site identification** A photoreactive probe, consisting of a ligand and a photoreactive moiety, is incubated with the target protein. Upon irradiation a reactive chemical species is generated, which inserts into a bond on a proximal amino acid. This protein of interest is digested, and the modified peptide is detected by MS/MS analysis.

## 4.2 Design and synthesis of photo-reactive Pico145 derivatives

### 4.2.1 Design

Pico145 was identified in an international patent by Hydra Biosciences investigating TRPC5 inhibitors for the treatment of CNS disorders (*Section 1.3.2.4*). The patent detailed the structures of > 600 substituted xanthines. Through analysing the SAR of the library of xanthines, based on the semi-quantitative  $IC_{50}$  values given, it was identified that  $R^1$  could mostly tolerate benzyl groups with substitution in the para position.  $R^1$  could also tolerate pyridines and unsubstituted thiazoles; however, alkyl chains and oxazoles in this position resulted in loss of activity against TRPC5 (*Figure 39*). The  $R^2$  position allowed many different substituents whilst retaining activity against TRPC5; alkyl, heterocycle and aromatic substituents were tolerated. However, the length of  $R^2$  seemed to be crucial to preserve activity.  $R^3$  and  $R^4$  were intolerant to most deviations from the structure of 'compound 31', for example  $R^4$  could only tolerate a methyl or ethyl substituent.

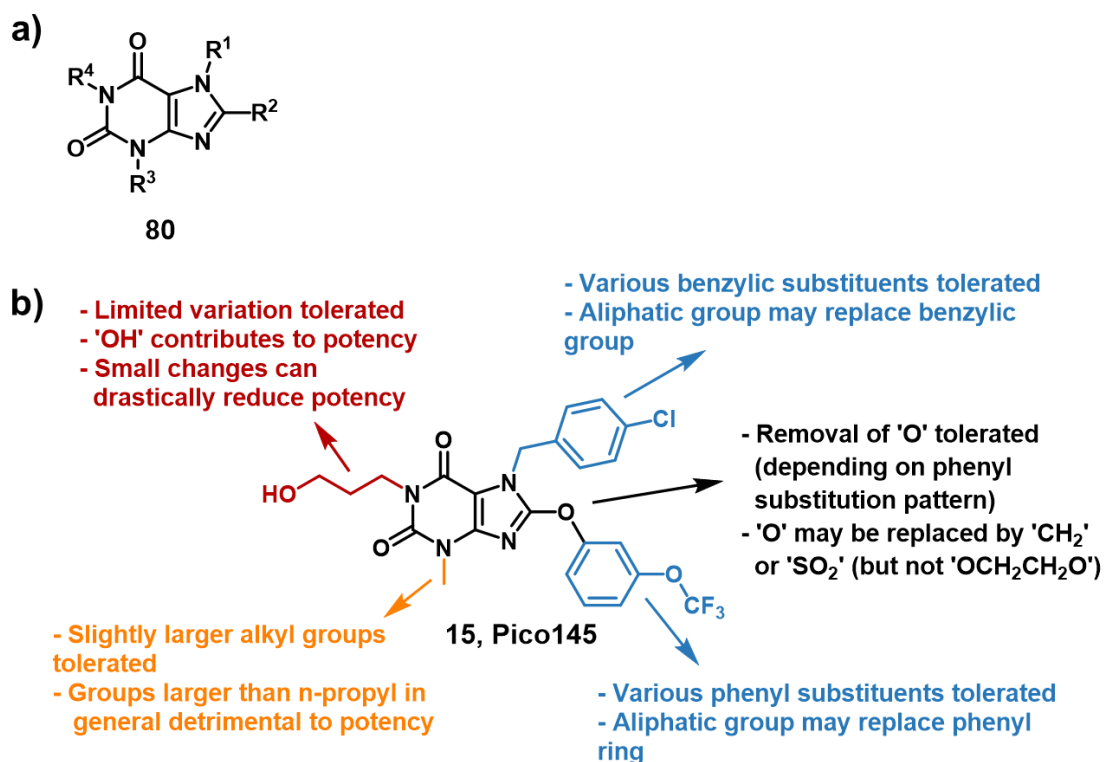


**Figure 39: Structure activity relationships of substituted xanthines from a patent by Hydra Biosciences.** a) Chemical structure of substituted xanthines, b) details of SAR with regards to a 'hit' compound, compound 31 or later called Pico145, 15.

Based on the above SAR, two photoaffinity probes were designed. These were designed based on the similarity to Pico145, replacing the oxygen in R<sup>2</sup> with a diazirine to afford minimal changes to the structure (Figure 39 cf. Figure 40). In addition to this, there is synthetic precedent for making trifluoromethyl-aryldiazirine based compounds.<sup>226,227,228,151</sup> It has been proposed that the combination of a trifluoromethyl and aromatic substituents induces chemical stability whilst maintaining the photochemical properties of the diazirine ring.<sup>141,151</sup> Pico145-DA, (**81**, Figure 40) differs only in the diazirine moiety from Pico145, with the intention that it should bind in exactly the same location on TRPC5. Furthermore, the addition of large bulky groups e.g. reporter tags was avoided, with the aim to reduce complication of MS/MS spectra due to fragmentation of the label. Moreover, in one photoaffinity probe, Pico145-DAAIk, (**82**, Figure 40) incorporation of an alkyne into R<sup>2</sup> in place of the *para*-chloro benzyl group would allow click chemistry to be utilised to attach a reporter group (fluorescent dye or biotin) for target engagement studies. The R<sup>2</sup> position was chosen due to its acceptance of other substituents of a similar size, and the alkyne having similar electron rich characteristics to the benzyl substituent.<sup>229</sup>

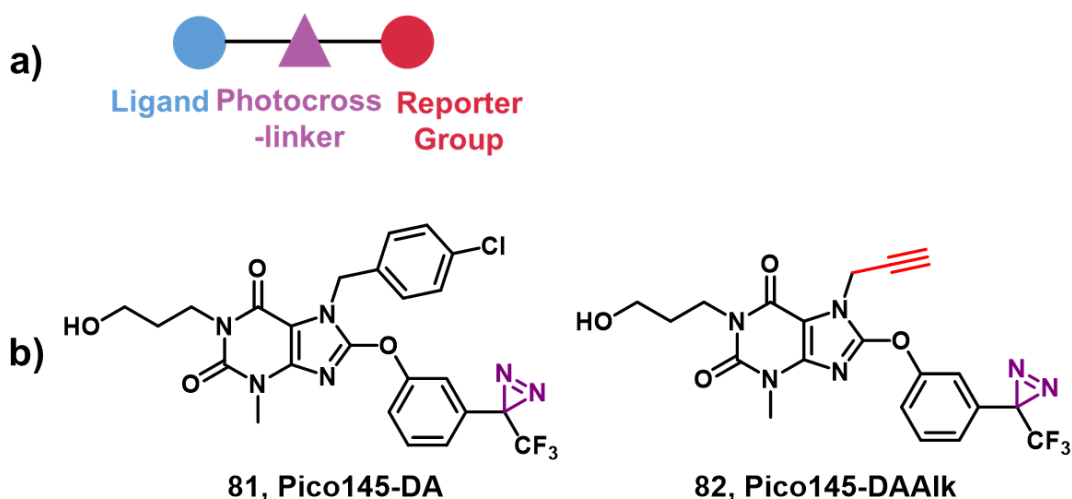
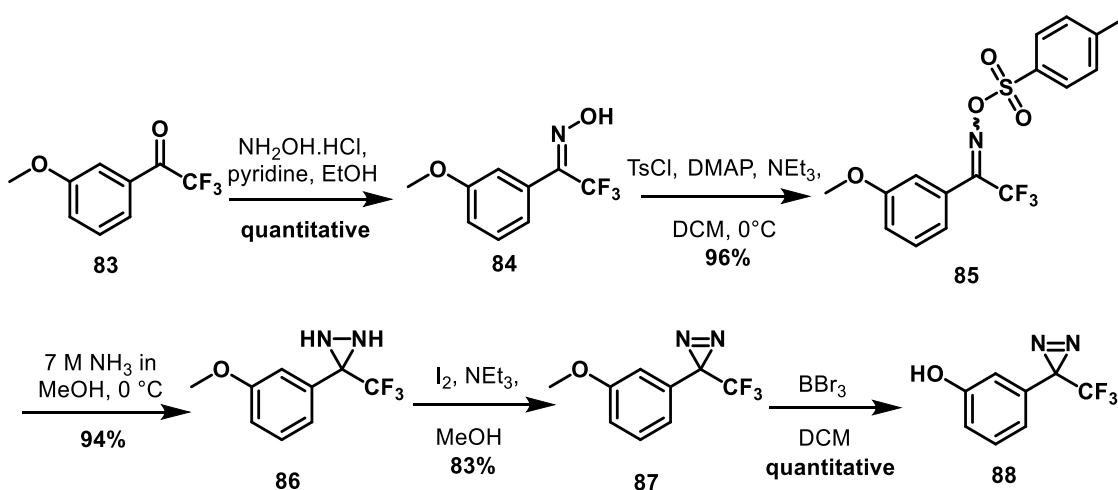


**Figure 40: Pico145 photoaffinity probes** a) General structure of a photoaffinity probe; b) Chemical structure of photoaffinity probes Pico145-DA, **81** and Pico145-DAAIk, **82**, which contains an alkyne reporter group.

## 4.2.2 Synthesis

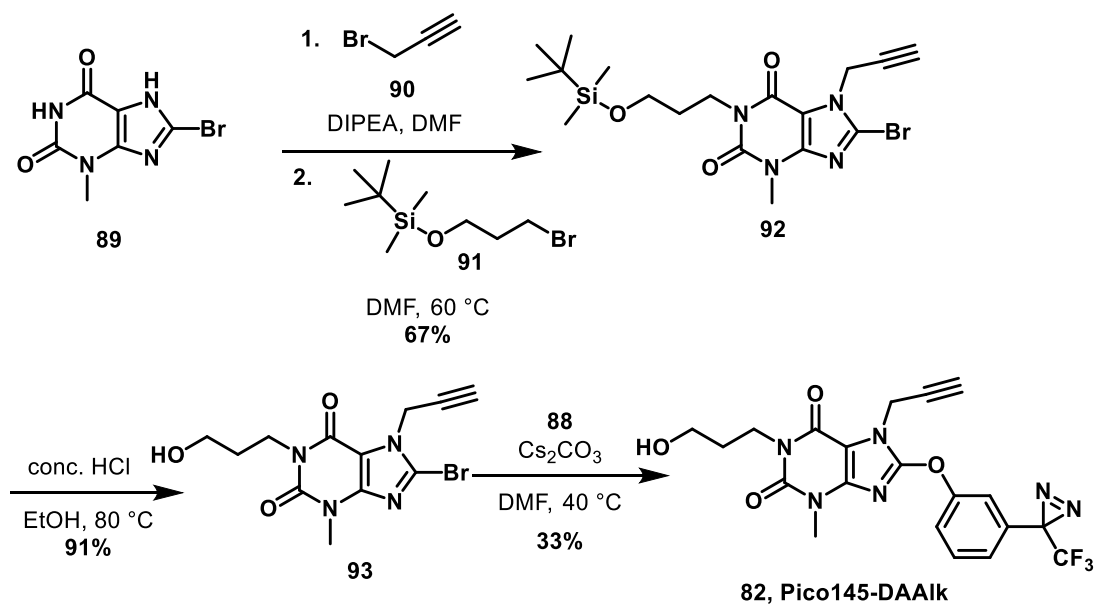
The photoaffinity probes were synthesised in two parts, the initial part being the synthesis of a phenol diazirine, **88**. The synthesis of the diazirine moiety was achieved through a combination of published procedures (*Scheme 10*).<sup>226,230,231</sup> The tosyl oxime, **85**, was prepared following a procedure described by Fishwick *et al.*<sup>226</sup> for a comparable trifluoromethyl-aryldiazirine. Tosyl oxime **85** was prepared *via* oxime formation from ketone **83** and tosylation of the resulting oxime, **84**, to yield **85**. Fishwick *et al.* synthesised the diazirine using excess ammonia at -78 °C, however a method described by Bond *et al.*<sup>230</sup> was chosen due to the more detailed protocol, in addition to minimizing the need for specialist equipment. The procedure described by Bond *et al.* utilised a solution of 7 M ammonia in methanol reacting with the tosyl oxime, **85**, under an ammonia atmosphere. The work-up was adapted from this procedure, by the addition of sodium bicarbonate solution to precipitate the tosylate group as the sodium salt and filtration to yield diaziridine **86**. Diaziridine **86** was oxidised using iodine to yield diazirine **87**.<sup>230</sup> The demethylation of diazirine **87** was achieved following a procedure by Ghiassian *et al.* using BBr<sub>3</sub> to give the phenol diazirine, **88**.



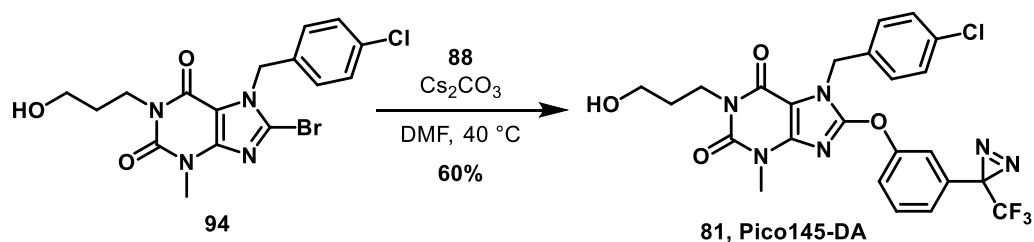
**Scheme 10:** Synthetic route to diazirine moiety **88** via procedures described by Fishwick et al.<sup>226</sup> Bond et al.<sup>230</sup> and Ghiassian et al.<sup>231</sup>

Xanthine building block **93** was synthesised from xanthine **89**, via propargylation and addition of 3-(bromopropoxy)-*tert*-butyldimethylsilane to yield **92**. Subsequent deprotection using conc. HCl to afford **93** (**93** synthesised in collaboration with Dr Robin Bon) (*Scheme 11*). The photoaffinity probes were prepared by a nucleophilic aromatic substitution reaction between phenol diazirine **88** and xanthines **93** and **94** (**94** synthesised by Dr Robin Bon)<sup>59</sup> (*Scheme 12*). This procedure was modified from the synthesis of Pico145 described in the patent published by Hydra Biosciences,<sup>65</sup> by substituting Cs<sub>2</sub>CO<sub>3</sub> for the weaker base K<sub>2</sub>CO<sub>3</sub>. Additionally, the temperature of the reaction mixture was lowered from 60 °C to 40 °C, to reduce the possibility of degradation of the diazirine upon heating.





**Scheme 11: Synthesis of photoaffinity probes Pico145-DA and Pico145-DAAIk.** Building block **93** was synthesised via propargylation and addition of 3-(bromopropoxy)-tert-butyldimethylsilane, subsequent deprotection to yield **93**. A nucleophilic aromatic substitution reaction between **93** and the phenol diazirine **88** afforded Pico145-DAAIk, **82**.



**Scheme 12: Synthesis of photoaffinity probe Pico145-DA, 81,** adapting the procedure for synthesis of Pico145 described by Hydra Biosciences.<sup>65</sup>

### **4.3 Evaluation of the activity of Pico145 photoaffinity probes**

#### **4.3.1 Investigations into the activity of Pico145-DA and Pico145-DAAIk against TRPC5**

Pico145-DA and Pico145-DAAIk were initially investigated for their ability to inhibit TRPC5-SYFP2 in HEK-293 T-REx cells, compared to Pico145. Calcium measurements initially showed inhibition of the (-)-EA-evoked activation of TRPC5 (*Figure 41a,b*). However, cells treated with Pico145-DA or Pico145-DAAIk exhibited higher than normal basal calcium levels (*Figure 41a*). A tetracycline inducible system to over-express TRPC5 with an SYFP2 tag was utilised in these experiments. Within the Beech lab TRPC5 and TRPC4 with an SYFP2 tag were stably-incorporated into HEK-293 T-REx cells for tetracycline inducible expression (cloning was performed by Dr Melanie Ludlow, constructs and stable cell lines generated by Dr Eulashini Chuntharpursat), the SYFP2 can afford purification of the protein by immunoprecipitation using GFP-trap beads. The TRPC4/5-SYFP2 stable cell lines were used for all further studies examining the activity of photoaffinity probes on the TRPC5 channel, unless otherwise stated, and will enable purification of TRPC5 for MS experiments.

Fluorescence experiments were performed to exclude the possibility that the diazirine containing compounds, Pico145-DA and Pico145-DAAIk, were causing this apparent increase in basal calcium by interference with the fluorescence readout. The compounds were plated into a 96-well plate and excited at both 340 nm and 380 nm and the fluorescence signal detected at a range of wavelengths. During calcium recording experiments using Fura-2, upon  $\text{Ca}^{2+}$  binding the excitation spectrum shifts, resulting in an increase in fluorescence emission at excitation 340 nm and a decrease in fluorescence emission at excitation 380 nm. Intracellular calcium is measured based upon the 340/380 ratio (*Section 2.1*). Fura-2 emits light at 510 nm, therefore the emission was recorded with close attention to 510 nm (*Figure 41c,d*). The diazirine photoaffinity probes Pico145-DA and Pico145-DAAIk showed no difference in fluorescence detected in comparison with both the DMSO control and Pico145 (*Figure 41c,d*). This result indicates that the photoaffinity probes alone are not causing any increased fluorescence that would affect the Fura-2 ratio, which would then be misinterpreted as an increase in intracellular calcium.

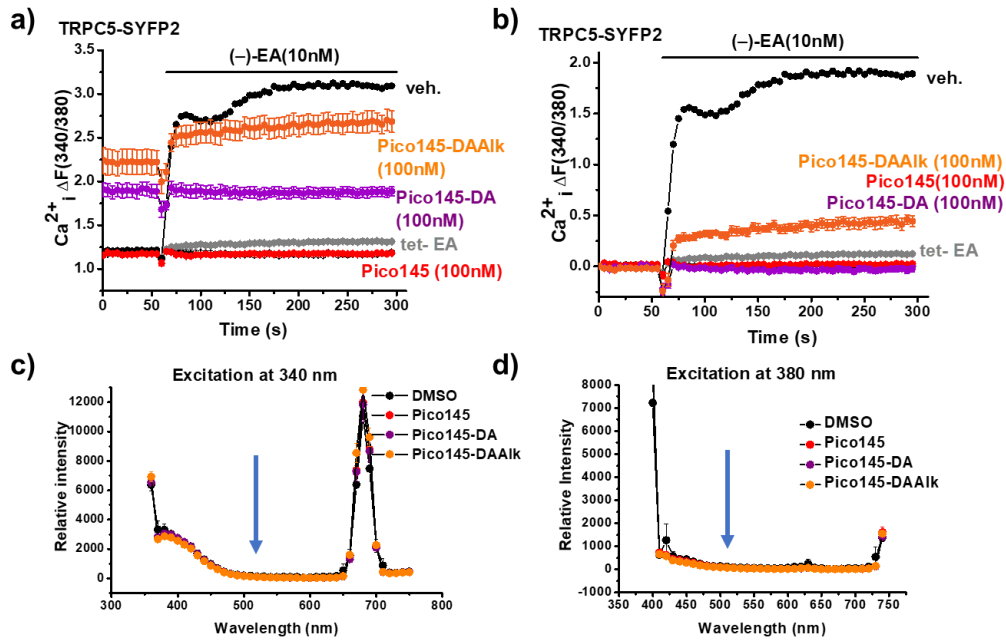


**Figure 41: Photoaffinity probes cause high levels of basal  $Ca^{2+}$  entry prior to application of (-)-Englerin A** *a,b*) Recordings were from TRPC5-SYFP2-expressing (*tet+*) HEK-293 T-REx cells, or no channel induction (*tet-*) and extracellular  $Ca^{2+}$  was present at 1.5mM. Intracellular  $Ca^{2+}$  was measured using fura-2. Cells were incubated with 100 nM Pico145, Pico145-DA and Pico145-DAAIk or DMSO vehicle control (veh.) for 30 min before 10 nM (-)-EA was applied; *a*) Pico145-DA and Pico145-DAAIk inhibit the (-)-EA activated TRPC5 response, however increased basal levels of  $Ca^{2+}$  entry were observed *b*) Pico145DA and Pico145DAAIk appear to potentially inhibit the (-)-EA response when basal  $Ca^{2+}$  levels are corrected to zero. *c,d*) 100nM Pico145, Pico145-DA and Pico145-DAAIk or DMSO vehicle control excited at *c*) 340nm and *d*) 380 nm and the emission recorded 350-750 nm. Blue arrow indicates 510 nm, the emission wavelength of Fura-2. (*n/N*=1/6)

It was hypothesised that the increased basal calcium levels seen in antagonist mode of Pico145-DA and Pico145-DAAIk was a result of activation of the TRPC5 channel during pre-incubation of the compounds. Consequently, Pico145-DA and Pico145-DAAIk were tested in agonist mode against TRPC5. Application of Pico145-DA and Pico145-DAAIk to HEK-293 T-REx cells over-expressing TRPC5-SYFP2 evoked a rapid and sustained increase in intracellular calcium. In contrast, no calcium entry was seen upon application of Pico145 or the DMSO vehicle control (*Figure 42a*). This was initially a surprising result, given the very small change in structure between Pico145, Pico145-DA and Pico145-DAAIk (*Figure 39 cf. Figure 40*). To confirm that the increase in intracellular calcium was *via* the TRPC5 channel, Pico145-DA and Pico145-DAAIk were applied to HEK-293 T-REx cells without over-expression of the TRPC5 channel (*tet-*). There was no increase in intracellular calcium observed with the application of Pico145-DA and Pico145-DAAIk to *tet-* cells (*Figure 42b*). This result suggests that the increase in intracellular calcium is a result of activation of the TRPC5 channel.

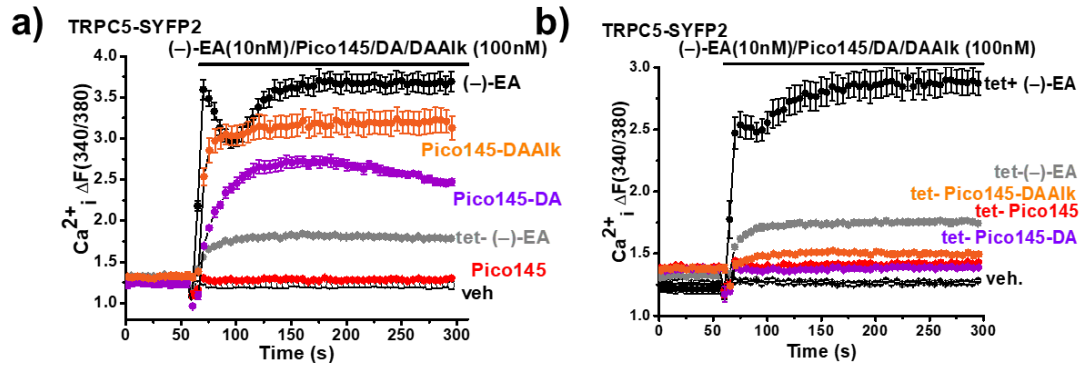


**Figure 42: Pico145-DA and Pico145-DAAIk activate TRPC5 in TRPC5-expressing (tet+) cells; a) Calcium measurement traces of the free intracellular calcium concentration indicated as a fura-2 fluorescence (F) ratio in HEK-293 T-REx TRPC5-expressing (tet+) cells with extracellular application of (-)-EA (10 nM), Pico145 (100 nM), Pico145-DA (100 nM), Pico145-DAAIk (100 nM), or DMSO vehicle control (veh.) (n/N = 3/ 18); b) Calcium measurement traces of the extracellular application of (-)-EA (10 nM), Pico145 (100 nM), Pico145-DA (100 nM), Pico145-DAAIk (100 nM), or DMSO control (veh.) on HEK-293 T-REx cells lacking channel induction (tet-), with a positive control trace for channel induction (tet+) with (-)-EA (10nM) activation. (n/N= 2/12)**

#### 4.3.2 Investigation of Pico145-DA and Pico145-DAAIk on calcium elevation mechanisms

Further investigations were required to determine the mode by which calcium levels are increased upon application of the photoaffinity probes. The increase in calcium levels recorded could be a result of calcium entering the cells or a release of calcium from intracellular stores. To investigate whether the increase in calcium recorded upon application of the photoaffinity probes is due to calcium entering the cells, cells were pre-treated with 0 mM extracellular calcium SBS (0 Ca<sup>2+</sup><sub>e</sub>) or 1.5 mM Ca<sup>2+</sup><sub>e</sub> for 10 minutes, before extracellular application of Pico145-DAAIk. An increase in intracellular calcium was observed under normal experimental conditions; however, no activation was recorded in the 0 mM Ca<sup>2+</sup><sub>e</sub> experiments (Figure 43). This indicates that the increase in calcium observed is extracellular calcium entering the cell, seemingly through the TRPC5 channel.

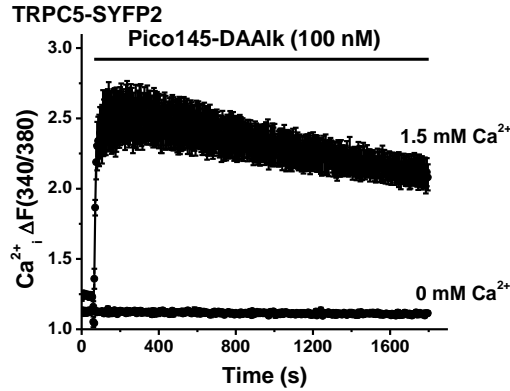


**Figure 43: Pico-DAAIk activates TRPC5 causing an increase of intracellular calcium only when  $\text{Ca}^{2+}$  is present in the extracellular buffer (SBS).** Representative calcium measurement trace of the free intracellular calcium ion ( $\text{Ca}^{2+}_i$ ) concentration indicated as a fura-2 fluorescence ( $F$ ) ratio. HEK-293 T-REx cells induced with tetracycline to over-express TRPC5-SYFP2 were pre-treated with 0 mM extracellular calcium SBS ( $0 \text{ Ca}^{2+}_e$ ) or 1.5 mM  $\text{Ca}^{2+}_e$  for 10 minutes, followed by application of 100 nM Pico145-DAAIk to the extracellular solution at 60 seconds. ( $n/N= 1/6$ )

### 4.3.3 Evaluation of the potency of Pico145-DA and Pico145-DAAIk on TRPC5

The potency of Pico145-DA and Pico145-DAAIk on TRPC5 was next examined in two cell lines. The potency was compared in the cells with a tetracycline inducible system to over-express TRPC5 or TRPC5 with an SYFP2 tag. Calcium measurements showed that application of 300 nM and 100 nM Pico145-DA (Figure 44a,c) and Pico145-DAAIk (Figure 45a,c) exhibited maximum response in both cell lines; detected by a rapid and sustained increase in intracellular calcium ( $\text{Ca}^{2+}_i$ ). Concentrations of 30 nM, 10 nM and 3 nM showed activation in a dose-dependent manner for Pico145-DAAIk in both cell lines and Pico145-DA against TRPC5-SYFP2. 10 nM and 3 nM Pico145-DA resulted in no activation of TRPC5. Whilst for concentrations of 1 nM, 0.3 nM and 0.1 nM Pico145-DA and Pico145-DAAIk in both cell lines, no response was observed (Figure 44a,c, Figure 45a,c). Investigation into the concentration-dependence of the response of Pico145-DA indicated a  $\text{EC}_{50}$  of 9.1 nM and 73 nM for TRPC5-SYFP2 and TRPC5 respectively (Figure 44b,d). For Pico145-DAAIk the  $\text{EC}_{50}$  was calculated at 22 nM and 37 nM for TRPC5-SYFP2 and TRPC5 respectively (Figure 45b,d). The  $\text{EC}_{50}$  values for TRPC5-SYFP2 and TRPC5 are in a comparable range for both Pico145-DA and Pico145-DAAIk suggesting that TRPC5-SYFP2 is a suitable alternative for TRPC5 in these experiments (Pico145-DA – TRPC5-SYFP2: 9 nM *cf.* TRPC5: 73 nM, Pico145-DAAIk – TRPC5-SYFP2: 22 nM *cf.* 37 nM).

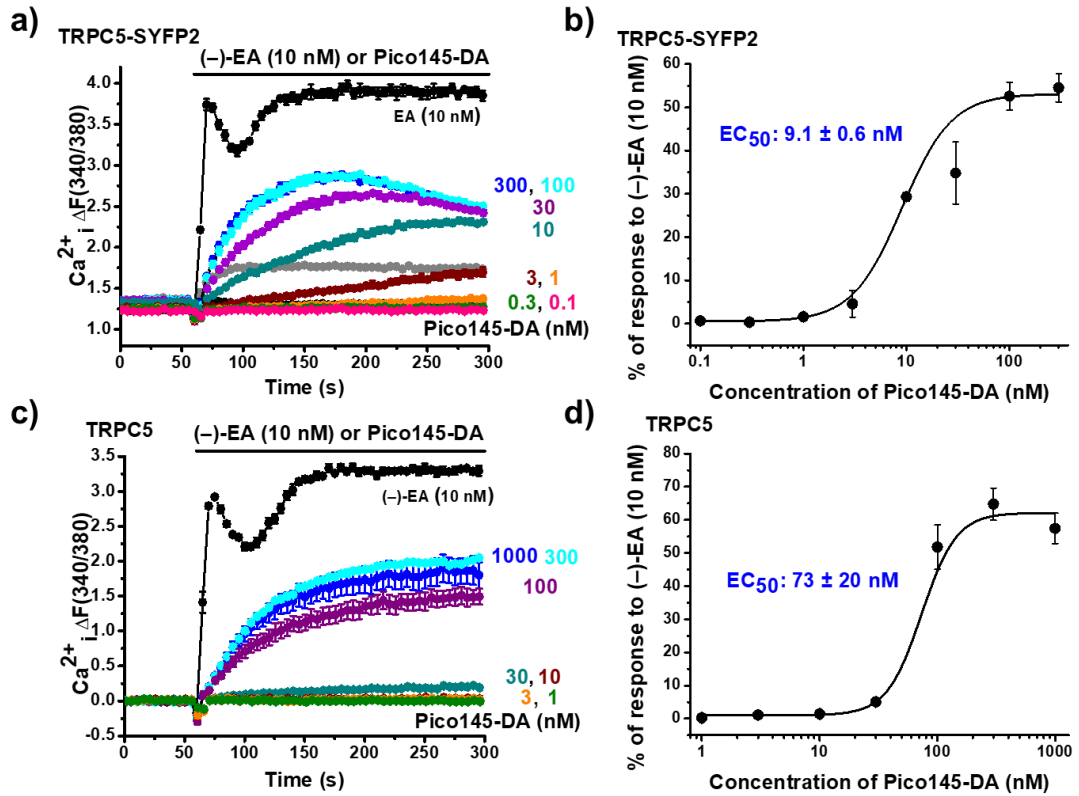


**Figure 44: Pico145-DA activates TRPC5-SYFP2 and TRPC5.** Concentration-response data on HEK-293 T-REx cells over-expressing **a,b** TRPC5-SYFP2 and **c,d** TRPC5. **a,c**) Representative calcium measurement trace of the free intracellular calcium ion (Ca<sup>2+</sup><sub>i</sub>) concentration indicated as a fura-2 fluorescence (F) ratio with extracellular application of (-)-EA (10nM) or Pico145-DA (1000 nM) 300 nM, 100 nM, 30 nM, 10 nM, 3 nM, 1 nM, 0.3 nM and 0.1 nM. **b**) Concentration-response data for Pico145-DA on TRPC5-SYFP2 (n/N = 3/18). The fitted curve is a Hill equation with a half-maximal concentration (EC<sub>50</sub>) of 9.1 ± 0.6 nM. **d**) Concentration-response data for Pico145-DA on TRPC5 (n/N = 3/18). The fitted curve is a Hill equation with a half-maximal concentration (EC<sub>50</sub>) of 73 ± 20 nM. (mean ± SE of mean)

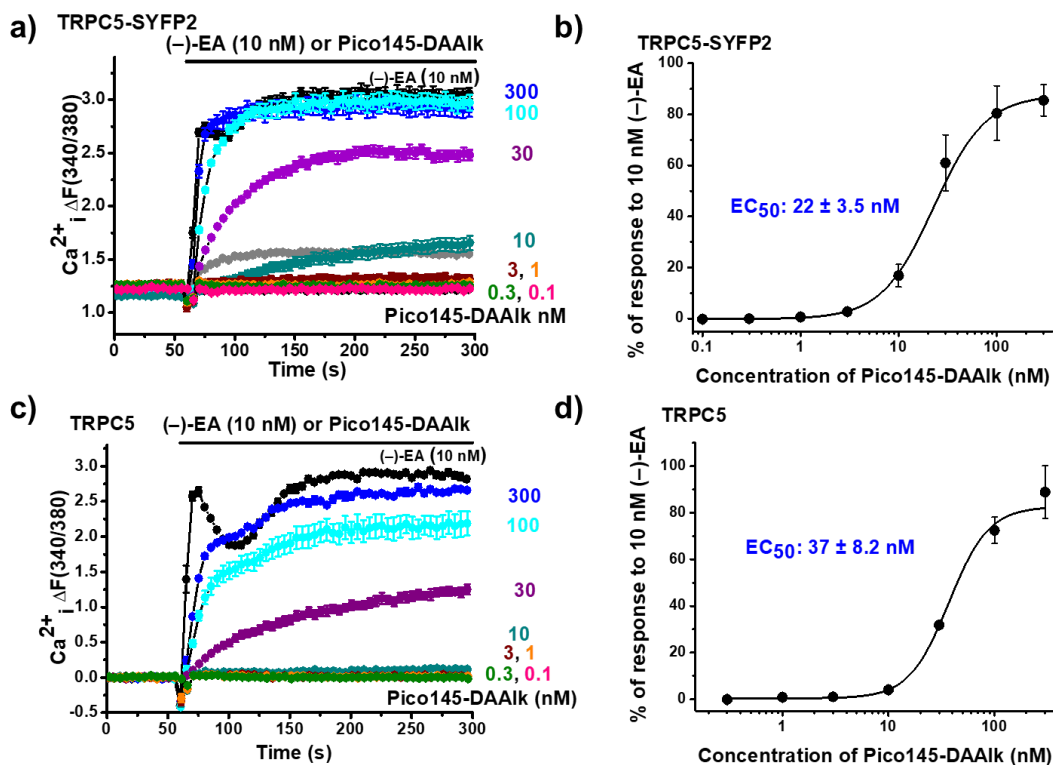


**Figure 45: Pico145-DAAIk activates TRPC5-SYFP2 and TRPC5.** Concentration-response data on HEK-293 T-REx cells over-expressing **a,b** TRPC5-SYFP2 and **c,d** TRPC5. **a,c**) Representative calcium measurement traces of the free intracellular calcium ion ( $Ca^{2+}_i$ ) concentration indicated as a fura-2 fluorescence ( $F$ ) ratio with extracellular application of (-)-EA (10nM) or Pico145-DAAIk 300 nM, 100 nM, 30 nM, 10 nM, 3 nM, 1 nM, 0.3 nM and 0.1 nM. **b**) Concentration-response data for Pico145-DAAIk on TRPC5-SYFP2 ( $n/N = 3/18$ ). The fitted curve is a Hill equation with a half-maximal effective concentration ( $EC_{50}$ ) of  $22 \pm 3.5$  nM. **d**) Concentration-response data for Pico145-DAAIk on TRPC5 ( $n/N = 3/18$ ). The fitted curve is a Hill equation with a half-maximal effective concentration ( $EC_{50}$ ) of  $37 \pm 8.2$  nM. (mean  $\pm$  SE of mean)

#### 4.3.4 Inhibition of the Pico145-DA and Pico145-DAAIk activated calcium entry via TRPC5 with Pico145

It was hypothesised that the designed photoaffinity probes, Pico145-DA and Pico145-DAAIk, would maintain the same binding site on TRPC5 as Pico145, owing to the similarity in structure of all three compounds. To further investigate the relationship of the photoaffinity probes to Pico145 with respect to TRPC5; the Pico145 inhibition of the Pico145-DA- and Pico145-DAAIk-evoked TRPC5 activity was measured. Cells over-expressing TRPC5-SYFP2 were pre-incubated with Pico145 at varying concentrations for 30 minutes prior to extracellular application of either Pico145-DA (Figure 46a,b) or Pico145-DAAIk (Figure 46c,d). Calcium measurements showed a dose-dependent inhibition of Pico145-DA- and Pico145-DAAIk-evoked TRPC5 activity. Investigation into the concentration-dependent inhibition by Pico145 indicated

an  $IC_{50}$  of 0.9 nM and 1.7 nM for Pico145-DA and Pico145-DAAIk activation of TRPC5 respectively (*Figure 46*). This shows that although the activity of the compounds has been altered upon addition of the diazirine it is plausible that they are still interacting with TRPC5 by a similar mechanism to Pico145 and the binding site may be the same.

However, these data are not sufficient evidence to confirm two compounds are occupying the same binding site. A dose-dependent inhibition can be seen from an activator and an inhibitor which occupy different sites, possibly even different targets. Investigation into the target of these compounds is described in *Section 4.6*. Indication of a direct effect on TRPC1/4/5 channels could be examined through excised membrane patch recordings, either outside-out or inside-out (*Section 2.2*). To further investigate if the photoaffinity probes have the same binding as Pico145, Schild regression analysis<sup>232</sup> could have been performed, which would indicate competitive antagonism. Obtaining concentration-dependence data for the antagonist (Pico145) with increasing concentrations of the agonist (photoaffinity probes) would identify competitive antagonism in a Schild plot, if these concentration-response curves displayed parallel shifts to the right.<sup>233</sup> Competitive antagonism gives an indication of competition for the same binding site, or an allosteric site on the same receptor.



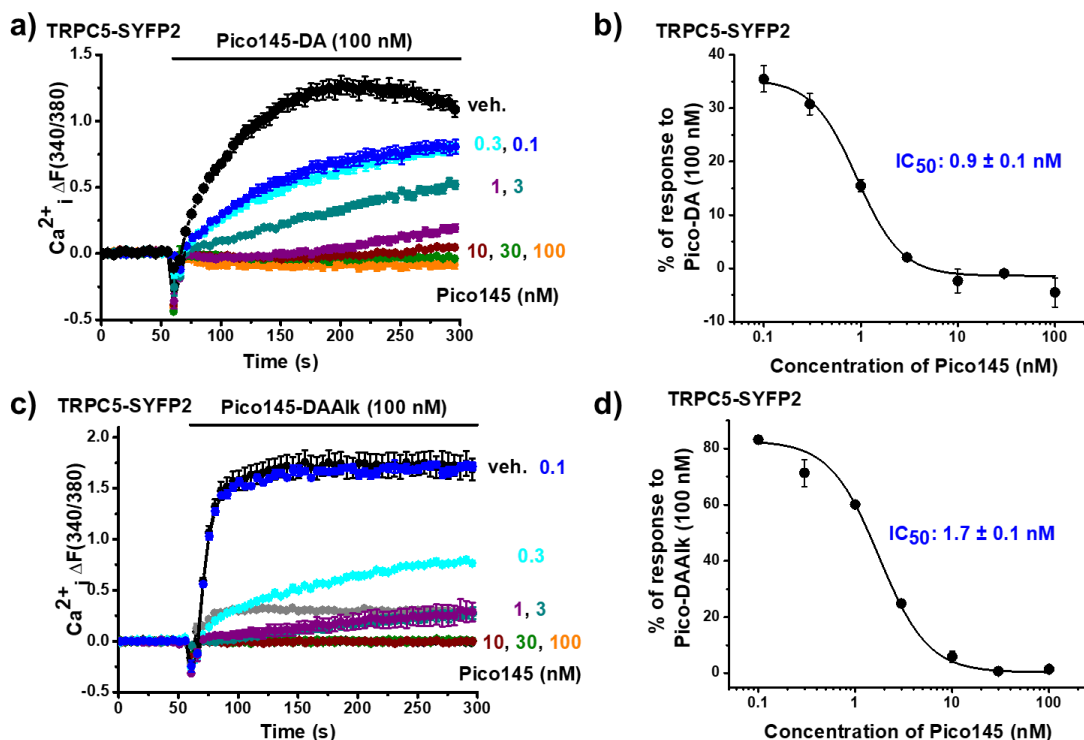


**Figure 46: Pico145 inhibits the Pico145-DA and Pico145-DAAIk evoked TRPC5 activity.** Concentration-response data on HEK-293 T-REx cells over-expressing TRPC5-SYFP2. **a,c**) Representative calcium measurement traces of the free intracellular calcium ion ( $Ca^{2+}_i$ ) concentration indicated as a fura-2 fluorescence (F) ratio with pre-incubation for 30 minutes of Pico145 at 100 nM, 30 nM, 10 nM, 3 nM, 1 nM, 0.3 nM and 0.1 nM, or DMSO vehicle (veh.) followed by extracellular application of **a**) Pico145-DA (100nM) and **c**) Pico145-DAAIk (100 nM) at 60 seconds. **b**) Concentration-response data for Pico145 on TRPC5-SYFP2 as a percentage of the Pico145-DA (100 nM) activation ( $n/N = 3/18$ ). The fitted curve is a Hill equation with a half-maximal inhibitory concentration ( $IC_{50}$ ) of  $0.9 \pm 0.1$  nM. **d**) Concentration-response data for Pico145 on TRPC5-SYFP2 as a percentage of the Pico145-DAAIk (100 nM) activation ( $n/N = 3/18$ ). The fitted curve is a Hill equation with a half-maximal inhibitory concentration ( $IC_{50}$ ) of  $1.7 \pm 0.1$  nM. (mean  $\pm$  SE of mean).

#### 4.3.5 Inhibition of the Pico145-DA and Pico145-DAAIk activated calcium entry via TRPC5 with ML204

Until recently, ML204<sup>58</sup> was the most thoroughly characterised inhibitor of TRPC5 channels (Section 1.3.2.2) and it inhibits TRPC5 with a low micromolar  $IC_{50}$ .<sup>58</sup> Therefore, the ML204 inhibitory effect on the Pico145-DAAIk-evoked TRPC5 channel activity was investigated. Calcium measurements showed that preincubation with 30  $\mu$ M and 10  $\mu$ M ML204 results in partial inhibition; no inhibition was observed with preincubation of 3  $\mu$ M, 1  $\mu$ M and 0.3  $\mu$ M ML204 (Figure 47). Although ML204 inhibits the Pico145-DAAIk evoked TRPC5 channel activity in a dose-dependent manner, ML204 is chemically distinct from Pico145-DA and Pico145-DAAIk, therefore it is less likely that it shares the same binding site. However, this would need to be further

confirmed, for example through binding site identification experiments for Pico145 and ML204.

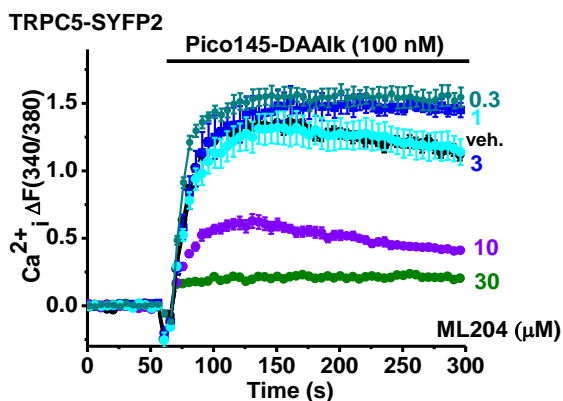


**Figure 47: ML204 inhibits the Pico145-DAAIk evoked TRPC5 activity.** Intracellular calcium measured using fura-2 in HEK-293 T-REx cells over-expressing TRPC5-SYFP2. Showing the Pico145-DAAIk evoked  $Ca^{2+}$  entry in the presence of vehicle (veh.) or 0.3  $\mu$ M, 1  $\mu$ M, 3  $\mu$ M, 10  $\mu$ M and 30  $\mu$ M ML204. (n/N= 1/6)

#### 4.3.6 Evaluation of the potency of the photoaffinity probes against TRPC4

TRPC4 is the most closely related protein to TRPC5 with 70% sequence identity (BLAST search<sup>36</sup>). Pico145 inhibits TRPC4 more potently than TRPC5,<sup>59</sup> therefore the effect of Pico145-DA and Pico145-DAAIk was subsequently investigated using HEK-293 T-REx cells over-expressing TRPC4-SYFP2. 30 nM (-)-EA was used to activate the TRPC4 channel, as opposed to 10 nM (-)-EA used for TRPC5, to maximise the size and clarity of the calcium recordings against which the effect of the photoaffinity probes could be tested (*Appendix II*). Cells were preincubated and then maintained in the presence of Pico145-DA or Pico145-DAAIk for 30 minutes prior to experimentation, then (-)-EA was applied extracellularly. There was no observed increase in basal calcium levels prior to application of (-)-EA, confirming that the photoaffinity probes cause no activation of the TRPC4 channel alone. Concentration-response data were collected for Pico145-DA (*Figure 48a*) and Pico145-DAAIk (*Figure 48c*); concentrations of 300 nM, 100 nM for Pico145-DAAIk and Pico145-DA failed to show response to (-)-EA. Concentrations of 30 nM, 10 nM, 3 nM and 1 nM showed inhibition in a dose dependent manner, whilst 0.3 nM and 0.1 nM showed almost full (-)-EA response. Investigation into the concentration-dependence of the inhibition of the (-)-EA-evoked  $Ca^{2+}$  entry by Pico145-DA and Pico145-DAAIk indicated an  $IC_{50}$  of 39 nM (*Figure 48b*) and 51 nM (*Figure 48d*) respectively. There are currently few known modulators which can distinguish between TRPC4 and TRPC5 channels, therefore the activation of TRPC5 (*Chapter 4.3.3*) and inhibition of

TRPC4 by Pico145-DA and Pico145-DAAIk suggests these photoaffinity probes could be promising tool compounds for studying TRPC1/4/5 channels. BTD (Section 1.3.1.4) has been reported by Beckmann *et al.* to selectively activate TRPC5:C5 and TRPC5:C1 channels, where no activation is reported for TRPC4:C4 or TRPC4:C1 channels, however BTD is less potent with an  $EC_{50}$  of 1.4  $\mu\text{M}$ .<sup>47</sup>

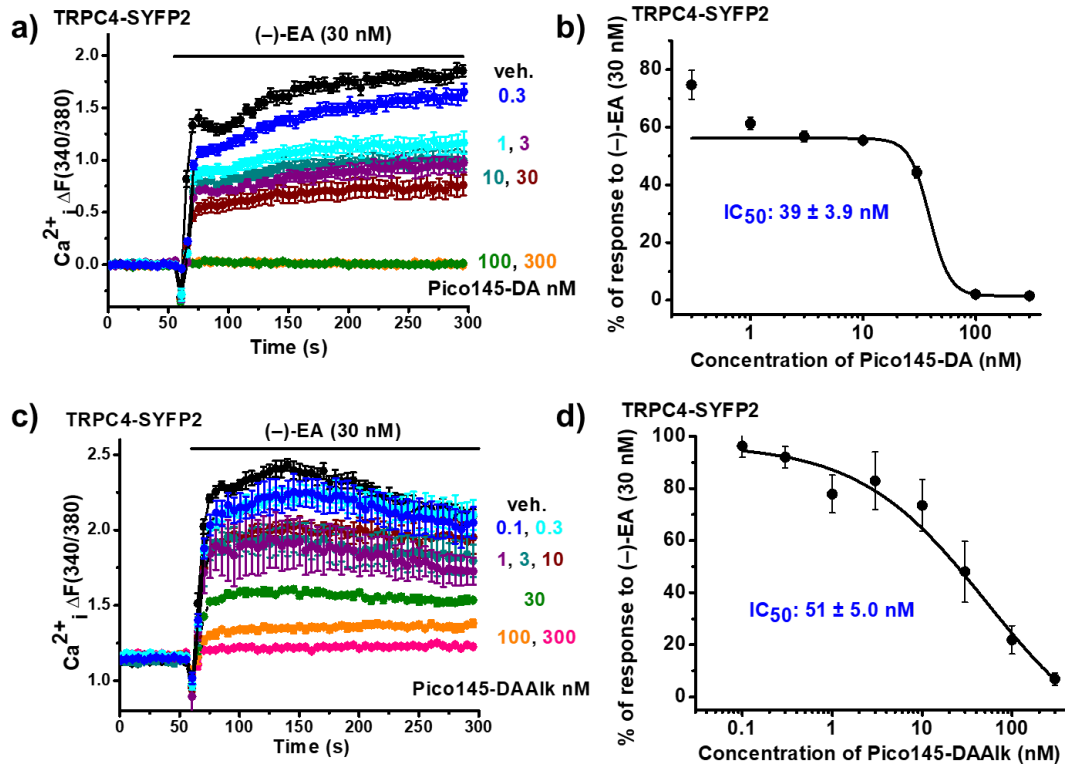


**Figure 48: Pico145-DA and Pico145-DAAIk inhibit TRPC4.** Concentration-response data on HEK-293 T-REx cells over-expressing TRPC4-SYFP2. **a,c)** Representative calcium measurement traces of the free intracellular calcium ion ( $\text{Ca}^{2+}_i$ ) concentration indicated as a fura-2 fluorescence (F) ratio with pre-incubation for 30 minutes of DMSO vehicle (veh.) or **a)** Pico145-DA or **c)** Pico145-DAAIk at 300 nM, 100 nM, 30 nM, 10 nM, 3 nM, 1 nM, 0.3 nM and 0.1 nM followed by extracellular application of (-)-EA (30 nM) at 60 seconds. **b)** Concentration-response data for Pico145-DA on TRPC4-SYFP2 as a percentage of the (-)-EA (30 nM) activation ( $n/N = 3/18$ ). The fitted curve is a Hill equation with a half-maximal inhibitory concentration ( $IC_{50}$ ) of  $39 \pm 3.9$  nM. **d)** Concentration-response data for Pico145-DAAIk on TRPC4-SYFP2 as a percentage of the (-)-EA (30 nM) activation ( $n/N = 3/18$ ). The fitted curve is a Hill equation with a half-maximal inhibitory concentration ( $IC_{50}$ ) of  $51 \pm 5.0$  nM. (mean  $\pm$  SE of mean)

#### 4.3.7 Evaluation of the potency of the photoaffinity probes against heteromeric channels TRPC5:C1 and TRPC4:C1

TRPC4 and TRPC5 proteins may form heteromeric channels with distinct characteristics,<sup>5</sup> and have been shown to readily form heteromers with TRPC1.<sup>20,21</sup> These heteromers are thought to be of more physiological relevance. TRPC4 and TRPC5 are capable of forming homomeric channels, yet TRPC1 is highly widely expressed and therefore physiologically these channels presumably exist as heteromers with TRPC1.<sup>10</sup> Akbulut *et al.* identified that the intracellular  $Ca^{2+}$  elevation seen by application of (-)-EA in native A498 cells was a result of the activation of the heteromeric TRPC4:C1 channel.<sup>21</sup> Ludlow *et al.* confirmed that the cytotoxic effect of (-)-EA was *via* the heteromeric TRPC4:C1 channel.<sup>22</sup> Due to the importance of heteromers containing TRPC1; concatemers were generated of TRPC4 with TRPC1 (TRPC4-C1) and TRPC5 with TRPC1 (TRPC5-C1), stably incorporating them in HEK-293 T-REx cells for tetracycline inducible expression (generated by Katie Musialowski and Nicola Blythe respectively).<sup>59</sup> Concatemers involve multiple sequences of DNA strung together in tandem,<sup>234</sup> thus meaning the DNA sequence for TRPC1 is connected to TRPC4/5 to force heteromeric channel formation. Pico145 was shown to inhibit the concatemeric channels more potently than homomeric TRPC4 and TRPC5 channels.<sup>59</sup> The activity of Pico145-DA (*Figure 49*) and Pico145-DAAIk (*Figure 50*) on TRPC4-C1 and TRPC5-C1 concatemers was investigated (experiments performed by Dr Claudia Bauer). The signals were small relative to those of homomers because TRPC1 suppresses  $Ca^{2+}$  permeability.<sup>235</sup> Thus the concentration of (-)-EA used to activate  $Ca^{2+}$  entry was increased to maximise the size and clarity of the  $Ca^{2+}$  entry recordings. Pico145-DA and Pico145-DAAIk inhibited both TRPC5-C1 and TRPC4-C1 heteromeric channels at concentrations in the nanomolar range. Pico145-DA inhibited TRPC5-C1 and TRPC4-C1 with an  $IC_{50}$  of  $5.5 \pm 2.4$  nM and  $1.4 \pm 0.1$  nM respectively (*Figure 49b,d*). Pico145-DAAIk inhibited TRPC5-C1 and TRPC4-C1 with an  $IC_{50}$  of  $206 \pm 17$  nM and  $114 \pm 15$  nM respectively (*Figure 50b,d*). The photoaffinity probes potently inhibit the heteromeric channels, and therefore could be sufficiently potent for target engagement and binding site identification studies of the heteromeric channels in addition to TRPC4 and TRPC5 homomeric channels. There is currently no evidence to confirm a binding site on TRPC heteromeric channels.

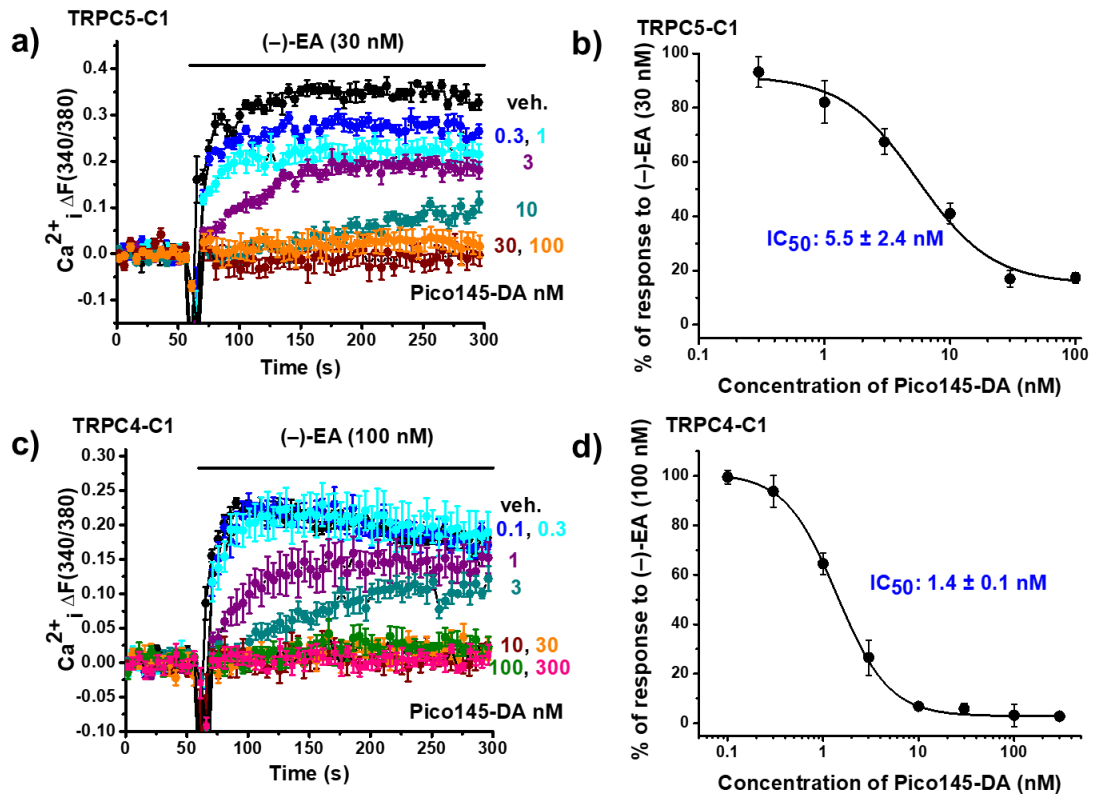


**Figure 49: Pico145-DA inhibits TRPC5-C1 and TRPC4-C1 heteromeric channels.** (Experiments performed by Dr Claudia Bauer). Concentration-response data on HEK-293 cells over-expressing **a)** TRPC5-C1 **c)** TRPC4-C1. **a,c)** Representative calcium measurement traces of the free intracellular calcium ion ( $Ca^{2+}_i$ ) concentration indicated as a fura-2 fluorescence (F) ratio with pre-incubation for 30 minutes of DMSO vehicle (veh.) or Pico145-DA at 300 nM, 100 nM, 30 nM, 10 nM, 3 nM, 1 nM, 0.3 nM and 0.1 nM followed by extracellular application of **a)** (-)-EA (30nM) or **c)** (-)-EA (100nM) at 60 seconds. **b)** Concentration-response data for Pico145-DA on TRPC5-C1 as a percentage of the (-)-EA (30 nM) activation ( $n/N = 3/18$ ). The fitted curve is a Hill equation with an  $IC_{50}$  of  $5.5 \pm 2.4 \text{ nM}$ . **d)** Concentration-response data for Pico145-DA on TRPC5-C1 as a percentage of the (-)-EA (100 nM) activation ( $n/N = 3/18$ ). The fitted curve is a Hill equation with and  $IC_{50}$  of  $1.4 \pm 0.1 \text{ nM}$ . (mean  $\pm$  SE of mean)

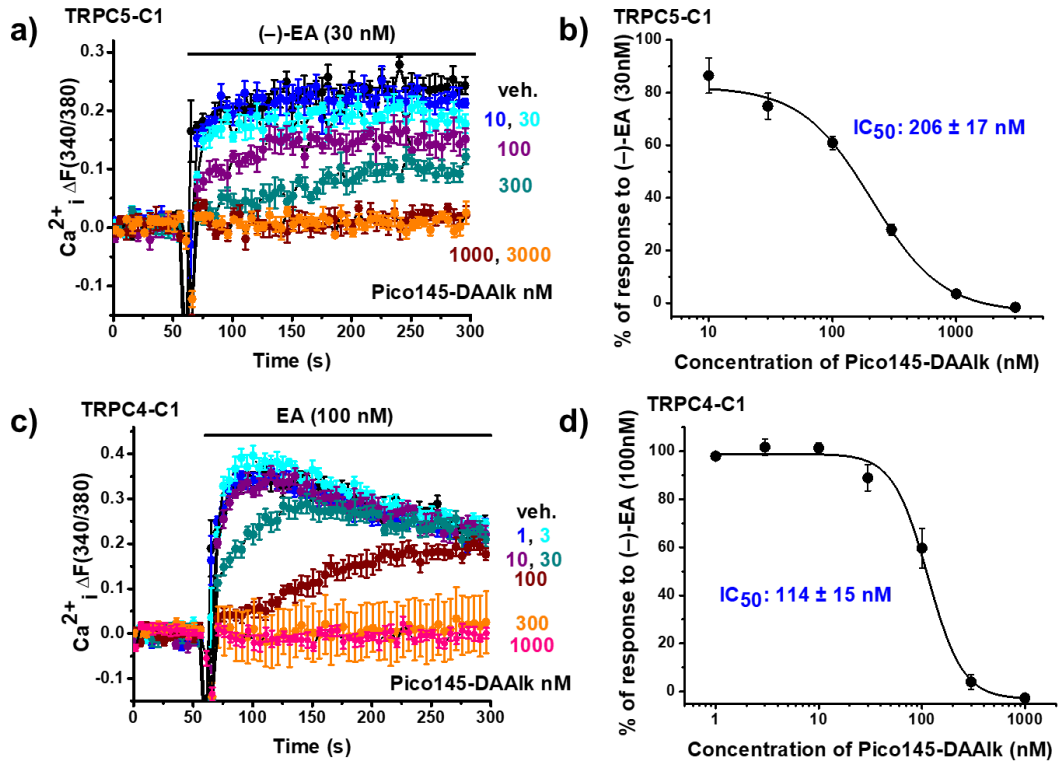


**Figure 50: Pico145-DAAIk inhibits TRPC5-C1 and TRPC4-C1 heteromeric channels.** (Experiments performed by Dr Claudia Bauer). Concentration-response data on HEK-293 cells over-expressing **a)** TRPC5-C1 **c)** TRPC4-C1. **a,c)** Representative calcium measurement traces of the free intracellular calcium ion ( $Ca^{2+}_i$ ) concentration indicated as a fura-2 fluorescence (F) ratio with pre-incubation for 30 minutes of DMSO vehicle (veh.) or Pico145-DAAIk at 3000 nM, 1000 nM, 300 nM, 100 nM, 30 nM, 10 nM, 3 nM and 1 nM, followed by extracellular application of **a)** (-)-EA (30nM) or **c)** (-)-EA (100nM) at 60 seconds. **b)** Concentration-response data for Pico145-DA on TRPC5-C1 as a percentage of the (-)-EA (30 nM) activation ( $n/N = 3/18$ ). The fitted curve is a Hill equation with an  $IC_{50}$  of  $206 \pm 17 \text{ nM}$ . **d)** Concentration-response data for Pico145-DAAIk on TRPC5-C1 as a percentage of the (-)-EA (100 nM) activation ( $n/N = 3/18$ ). The fitted curve is a Hill equation with and  $IC_{50}$  of  $114 \pm 15 \text{ nM}$ . (mean  $\pm$  SE of mean)

## 4.4 Characterisation of a TRPC5 agonist

Substituted xanthines appear to stabilise both the open and closed states of the TRPC5 channel (*Chapter 4.3.1*). This is consistent with data reported in the patent published by Hydra Biosciences.<sup>65</sup> This patent that identified Pico145 as a TRPC5 inhibitor contains other substituted xanthines described as agonists of TRPC5. In the whole-cell patch clamp recordings and calcium recording assays several compounds were rated 'F' correlating to an agonist of TRPC5 (*Figure 51*). Investigation of a TRPC5 agonist described in the patent in comparison with Pico145-DA and Pico145-DAAIk would verify the role that the diazine plays in stabilising the open state of the channel. Of the described agonists, the compound with most similarity in structure to Pico145, **98** was synthesised and named AM237 (*Figure 51*).

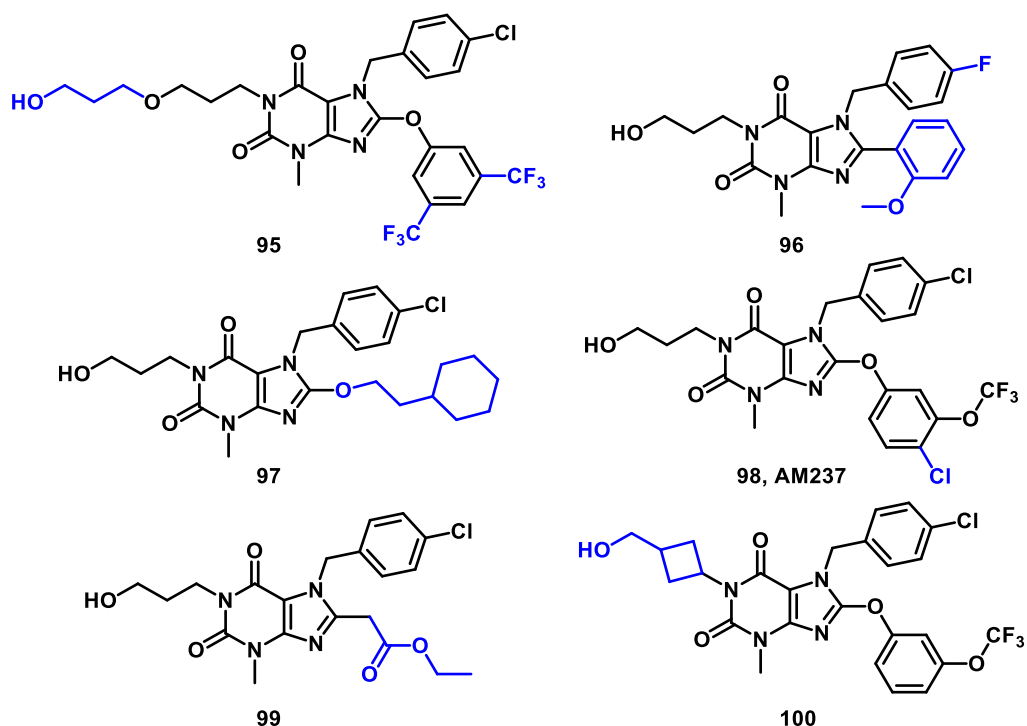


**Figure 51: A selection of compounds described as agonists of TRPC5 by Hydra Biosciences.** Parts of the structure which are chemically distinct from Pico145 are shown in blue.

The synthesis of AM237 was as described in the patent, a nucleophilic aromatic substitution reaction between **94** and 4-chloro-3-(trifluoromethyl)phenol afforded **AM237**.

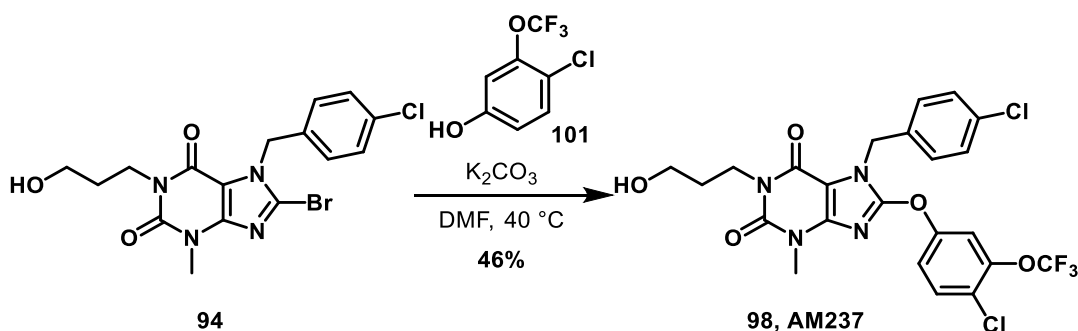


**Figure 52: Synthesis of AM237** by a nucleophilic aromatic substitution reaction, as described by Hydra biosciences.<sup>65</sup>

#### 4.4.1 Evaluation of the potency of AM237 on TRPC5

The potency of AM237 TRPC5 activation was examined on HEK-293 T-REx cells over-expressing TRPC5-SYFP2 or TRPC5. Calcium measurements for cells containing TRPC5-SYFP2 revealed that the maximum response was observed with application of 300 nM, 100 nM and 30 nM AM237, with a rapid and sustained increase in free intracellular calcium measured (*Figure 53a*). For TRPC5 the maximum response was observed with application of 300 nM (*Figure 53c*). Application of 100 nM to 1 nM AM237 caused an increase in intracellular calcium in a dose dependent manner, whilst application of 0.3 nM AM237 resulted in no response. Investigation into the concentration-dependence of the response of AM237 indicated a  $EC_{50}$  of 10 nM and 22 nM for TRPC5-SYFP2 and TRPC5 respectively (*Figure 53b,d*). The similarity between AM237 and photoaffinity probes with regards to TRPC5 activation (*Figure 44* and *Figure 45 cf. Figure 53*) validates that the diazine moiety is not essential for the unexpected activation of TRPC5. Evidently, small changes to the structure of Pico145 and related xanthines can cause significant changes to the modulation of TRPC5, further indicating the importance of the binding site of Pico145.



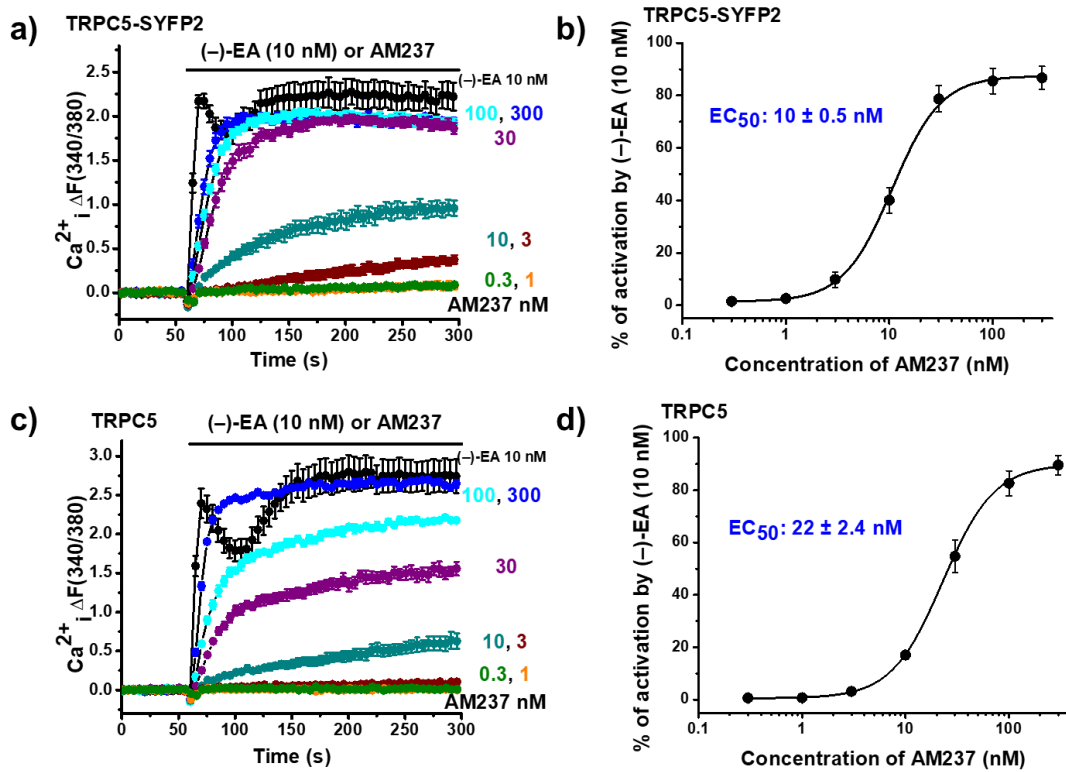


**Figure 53: AM237 activates TRPC5-SYFP2 and TRPC5.** Concentration-response data on HEK-293 cells over-expressing **a,b** TRPC5-SYFP2 and **c,d** TRPC5. **a,c** Representative calcium measurement trace of the free intracellular calcium ion (Ca<sup>2+</sup><sub>i</sub>) concentration indicated as a fura-2 fluorescence (F) ratio with extracellular application of (-)-EA (10nM) or AM237 300 nM, 100 nM, 30 nM, 10 nM, 3 nM, 1 nM and 0.3 nM. **b** Concentration-response data for AM237 on TRPC5-SYFP2 (n/N = 3/18). The fitted curve is a Hill equation with an EC<sub>50</sub> of 10 ± 0.5 nM. **d** Concentration-response data for AM237 on TRPC5 (n/N = 3/18). The fitted curve is a Hill equation with an EC<sub>50</sub> of 22 ± 2.4 nM (mean ± SE of mean)

#### 4.4.2 Evaluation of the potency of AM237 on TRPC4

The effect of AM237 was subsequently investigated using HEK-293 T-REx cells over-expressing TRPC4. 30 nM (-)-EA was used to activate the TRPC4 channel, as opposed to 10 nM (-)-EA used for TRPC5, to maximise the size and clarity of the calcium response against which the effect of the photoaffinity probes could be tested (*Appendix I*). Cells were preincubated with AM237 for 30 minutes prior to experimentation, then 30 nM (-)-EA was applied extracellularly. Concentration-response data were collected for AM237 (*Figure 54*) and the maximum response was observed with application of 100 nM AM237. Concentrations of 30 nM, 10 nM and 3 nM showed inhibition in a dose dependent manner, whilst 1 nM, 0.3 nM and 0.1 nM showed full (-)-EA response. Investigation into the concentration-dependence of the inhibition of the (-)-EA-evoked Ca<sup>2+</sup> entry by AM237 indicated an IC<sub>50</sub> of 33 nM (*Figure 54*). The potency of AM237 is significantly lower than Pico145 (IC<sub>50</sub> 0.4 nM against TRPC4), however 10 nM (-)-EA was used for IC<sub>50</sub> determination of Pico145,<sup>59</sup> compared to 30 nM (-)-EA used in these experiments. Beech *et al.* found the potency

of Pico145 to be decreased with increasing concentrations of (-)-EA.<sup>59</sup> The potency of AM237 at differing concentrations of (-)-EA would need to be investigated to compare AM237 and Pico145 as TRPC4 inhibitors. AM237 replicates the activity of the photoaffinity probes (*Figure 48 cf. Figure 54*), it activates TRPC5 and inhibits the (-)-EA-evoked Ca<sup>2+</sup> entry in HEK-293 T-REx cells over-expressing TRPC4, distinguishing between the two closely related channels. The hypothesised improvement in stability of this compound, due to the lack of photoreactive moiety, in comparison with the photoaffinity probes makes it a superior tool compound for studying TRPC1/4/5 channels.

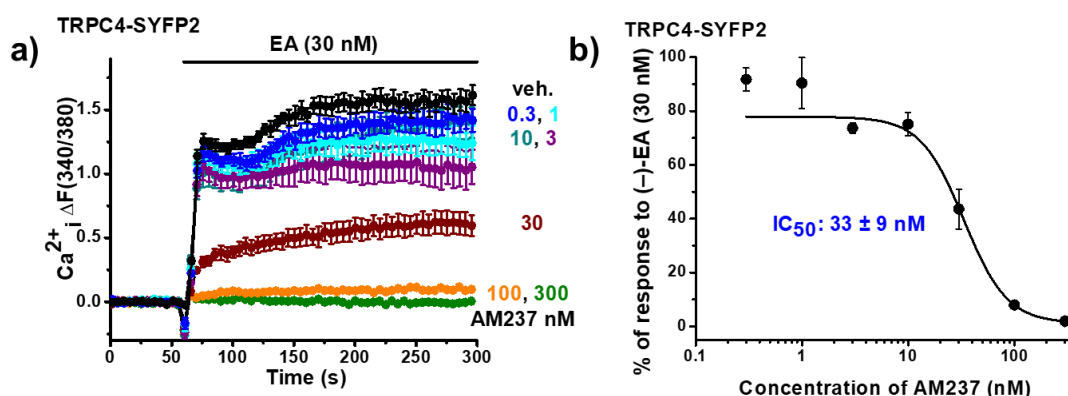


**Figure 54: AM237 inhibits TRPC4-SYFP2.** Concentration-response data on HEK-293 T-REx cells over-expressing TRPC4-SYFP2. **a)** Representative calcium measurement traces of the free intracellular calcium ion (Ca<sup>2+</sup><sub>i</sub>) concentration indicated as a fura-2 fluorescence (F) ratio with pre-incubation for 30 minutes of AM237 300 nM, 100 nM, 30 nM, 10 nM, 3 nM, 1 nM and 0.3 nM or DMSO vehicle (veh.) followed by extracellular application of (-)-EA (30nM) at 60 seconds. **b)** Concentration-response data for AM237 on TRPC4-SYFP2 as a percentage of the (-)-EA (30 nM) activation (n/N = 3/18). The fitted curve is a Hill equation with a half-maximal inhibitory concentration (IC<sub>50</sub>) of 33 ± 9 nM. (mean ± SE of mean)

#### 4.4.3 Evaluation of the potency of AM237 against heteromeric channels TRPC5-C1 and TRPC4-C1

Due to the importance of the heteromeric channels endogenously, the potency of AM237 in HEK-293 cells over-expressing TRPC5-C1 and TRPC4-C1 concatemers was investigated (experiments performed by Dr Claudia Bauer). AM237 was a potent inhibitor of the heteromeric channels with low nanomolar IC<sub>50</sub> values, 2.5 nM and 3.9 nM against TRPC5-C1 and TRPC4-C1 respectively (*Figure 55*). This data indicates AM237 to be a potent tool compound to study TRPC1/4/5 channels; it has high potency against concatemeric channels containing TRPC1, which are of physiological relevance. Additionally, AM237 has different activities towards TRPC5 homomeric channels, compared to TRPC4 homomeric, and TRPC5-C1 and TRPC4-C1 concatemeric channels, indicating AM237 could isolate the role of TRPC5 channels.

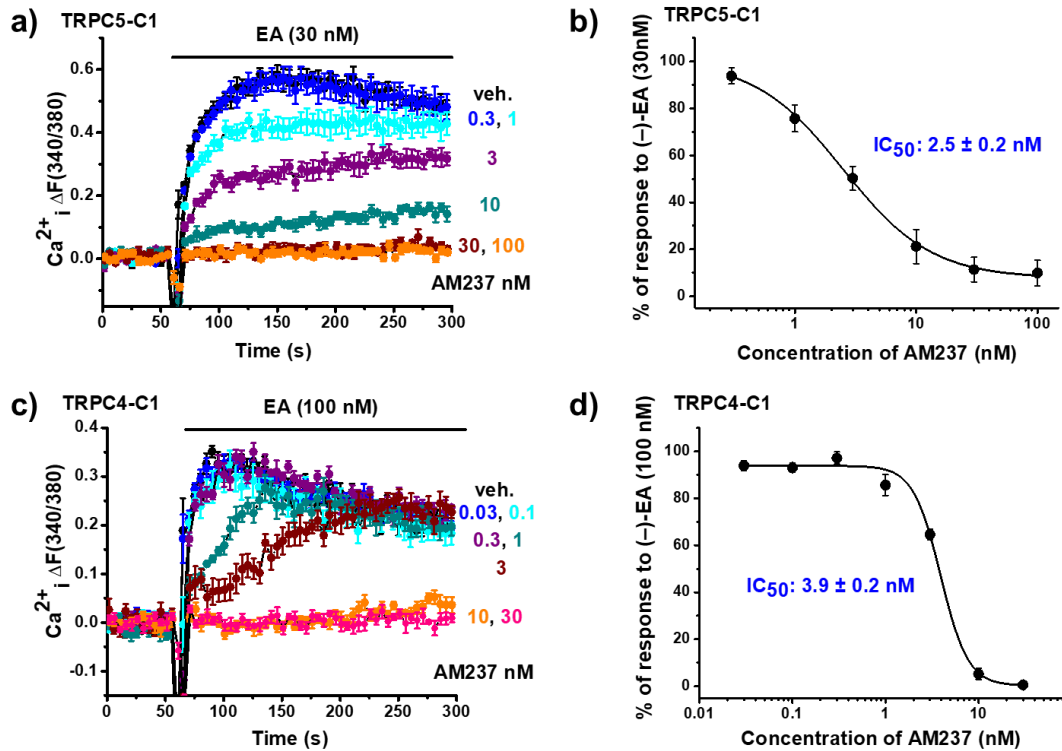
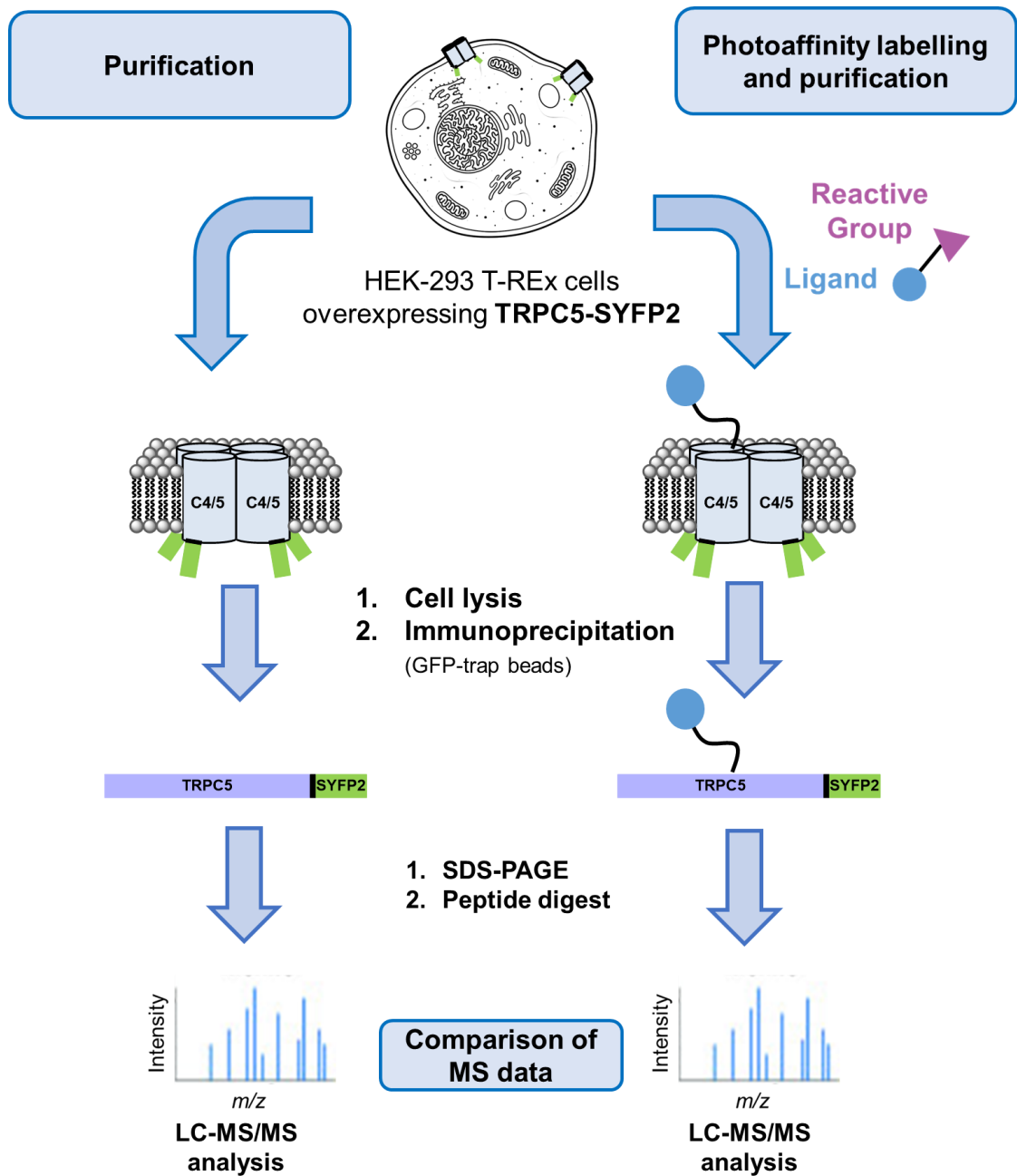


**Figure 55: AM237 inhibits heteromeric TRPC5-C1 and TRPC4-C1 channels.** Concentration-response data on HEK-293 cells over-expressing **a,b** TRPC5-C1 and **c,d** TRPC4-C1. **a,c**) Representative calcium measurement trace of the free intracellular calcium ion (Ca<sup>2+</sup>) concentration indicated as a fura-2 fluorescence (F) ratio with extracellular application of **a**) (-)-EA (30nM) or **c**) (-)-EA (100nM) and AM237 100 nM, 30 nM, 10 nM, 3 nM, 1 nM, 0.3 nM, 0.1 nM and 0.03 nM or DMSO vehicle (veh.) **b**) Concentration-response data for AM237 on TRPC5-C1 (n/N = 3/18). The fitted curve is a Hill equation with IC<sub>50</sub> of 2.5 ± 0.2 nM. **d**) Concentration-response data for AM237 on TRPC4-C1 (n/N = 3/18). The fitted curve is a Hill equation with an IC<sub>50</sub> of 3.9 ± 0.2nM. (mean ± SE of mean)

## 4.5 Sequence mapping of TRPC5 protein

Pico145-DA could be used to label an amino acid in the binding pocket on the TRPC1/4/5 channel, as described in *Section 1.6*. Identification of the binding site of Pico145 in TRPC1/4/5 channels requires purification of TRPC1/4/5 proteins and high sequence coverage by tandem mass spectrometry (MS). To investigate the binding site of Pico145-DA on TRPC5; Pico145-DA would be incubated with TRPC5-SYFP2 cells, UV irradiation applied to the cells, followed by cell lysis and immunoprecipitation. The purified TRPC5 protein could be cleaved from the GFP-trap beads, followed by SDS-PAGE, in-gel digestion and MS/MS analysis with the aim to identify the peptide modified by Pico145-DA (*Scheme 13*). The MS analysis of the peptides and the detection of the modified peptide can be quite difficult, the modification can often be in very small amounts in comparison to the unmodified peptides. Acquiring optimal digestion conditions to yield high sequence coverage of the protein before photolabelling, can make it easier to detect the modification after photolabeling (*Scheme 13*).



**Scheme 13: Proposed photoaffinity labelling and binding site identification workflow using Pico145-DA.** Right side: A photoreactive probe, consisting of a ligand and a photoreactive moiety, is incubated in HEK-293 T-REx cells over-expressing TRPC5 with an SYFP2 tag attached. When cells are irradiated, a reactive chemical species is generated, which inserts into a bond of a proximal amino acid residue on the TRPC1/4/5 channel. Both right and left: HEK-293 T-REx cells over-expressing TRPC5 with an SYFP2 tag cells are lysed, TRPC5 is purified by immunoprecipitation using GFP-trap beads. SDS-PAGE is performed, followed by in-gel digestion, and finally MS analysis of the peptides. By comparing the unmodified peptide mapping of TRPC5 with the modified proteins, it may be possible to identify the labelled peptides.

#### **4.5.1 Identification of TRPC4/5 protein *via* immunoprecipitation and mass spectrometry**

Before commencing photocrosslinking experiments it was necessary to validate the approach by showing that TRPC5 protein could be identified from cells using immunoprecipitation targeted against the SYFP2. SYFP2 is a variant of the GFP protein and therefore it could be possible to utilise GFP trap beads to purify TRPC5-SYFP2. Initially, T-REx cells over-expressing TRPC5-SYFP2 were lysed with NP-40 lysis buffer and immunoprecipitation was carried out with GFP-trap beads. SDS-PAGE was performed on samples, and the over-expression and purification of TRPC5-SYFP2 was shown using an InstantBlue Coomassie stain (*Figure 56a*). The Instant Blue Coomassie stain was used because it is a MS-compatible stain, as opposed to Coomassie Brilliant Blue (CBB) which would provide a stronger signal. In-gel proteolytic digestion using chymotrypsin and trypsin resulted in peptide fragments which were analysed using reverse-phase high performance liquid chromatography (HPLC) and quadrupole time-of-flight (Q-TOF) MS/MS (digestion and HPLC-MS/MS incl. data analysis performed by Dr Rachel George). Peptide analysis and mapping confirmed TRPC5 as the protein purified and resulted in 66% peptide coverage (*Figure 56b*) (*Appendix IV*). Enhancing the sequence coverage of TRPC5 was essential before endeavouring to identify a modified peptide. Enhanced sequence coverage would increase the chance of detecting the modification and confirm that there has only been one modification made on the protein. The purification of TRPC4-SYFP2 by immunoprecipitation utilising GFP-trap beads was also confirmed by Western blot analysis (*Appendix III*).

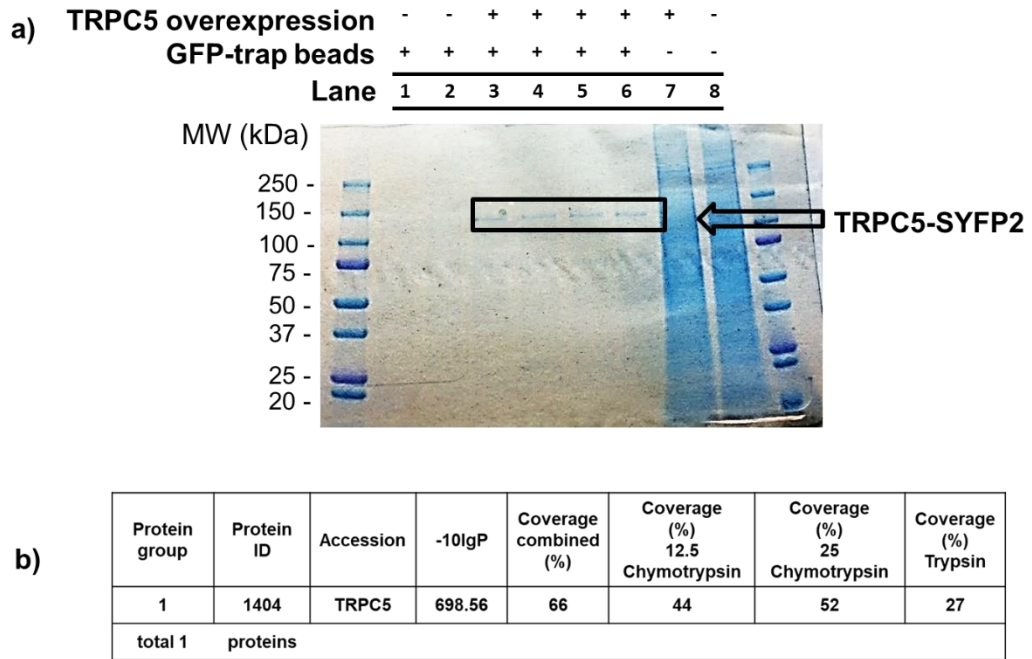


**Figure 56: Purification and identification of TRPC5-SYFP2 construct.** **a)** Lysates from HEK-293 T-REx cells over-expressing TRPC5-SYFP2, purified using immunoprecipitation and SDS-PAGE, then stained with InstantBlue Coomassie stain; **b)** In-gel proteolytic digestion of purified TRPC5-SYFP2 bands seen in a) using chymotrypsin and trypsin proteases to identify TRPC5 sequencing with 66% peptide coverage (from all digests combined) (Appendix IV).

#### 4.5.2 Sequence coverage optimisation

Initial proteolytic digestions were performed using a combination of trypsin and chymotrypsin, resulting in 66% sequence coverage (Appendix IV) (digestion and HPLC-MS/MS incl. data analysis performed by Dr Rachel George). ProteaseMAX surfactant was then incorporated to enhance digestion. ProteaseMAX solubilizes membrane proteins and enhances protein digestion by providing a denaturing environment prior to protease addition. The use of ProteaseMAX resulted in 48% coverage using trypsin, 34% using chymotrypsin and 54% combined coverage (Appendix IV). The quality of peptides improved with the use of ProteaseMAX, however there were still key regions of the protein which were inaccessible (e.g. the extracellular loop regions). On-bead tryptic digestion has previously been shown to provide sufficient coverage of a post-translational modification from a whole proteome.<sup>236,237</sup> Therefore an on-bead digest was initially tried using pepsin as the protease, resulting in 65% coverage, followed by digestion combining chymotrypsin, trypsin and Glu-C yielding a sequence coverage of 65% (Table 6) (Appendix IV). By combining the peptide mapping from all on-bead digestions, the sequence coverage is 82% (Figure 57). (Purification done in collaboration with Dr David Wright, digestion and mass spectrometry analysis performed by Dr Rachel George). A number of

TRPC1/4/5 modulators have been reported to modulate the channel extracellularly, as indicated by modulation in excised outside-out membrane patch recordings.<sup>59,29,21</sup> Beech and co-workers have previously reported the importance of a disulfide bridge in the predicted extracellular loop adjacent to the ion pore.<sup>106</sup> The evidence for this region being an important potential binding site has been strengthened since Tang *et al.* reported the small molecule inhibitor, BTDM, binding to TRPC6 in a similar region.<sup>101</sup> These extracellular loops have been the focus of the peptide mapping experiments as they are thought to be crucial to the gating of the ion channel and thus are a speculated binding site for Pico145. The sequence coverage obtained using an on-bead digestion protocol with chymotrypsin, trypsin, Glu-C and pepsin combined gave a coverage of 82% and the extracellular loop region (534-603) was mostly sequenced. Therefore this coverage may be sufficient to identify a site of modification by photoaffinity labelling, as demonstrated by Woll *et al.*<sup>130</sup> who identified a labelled leucine residue on the K<sub>v</sub>1.2 channel with 74% sequence coverage. However, higher sequence coverage may be required to verify that there is only one site of modification on the protein.

**Table 6: Proteolytic digestion conditions and the corresponding sequence coverage of TRPC5-SYFP2.**

<b>Digestion proteases</b>	<b>Digestion protocol</b>	<b>Coverage (%)</b>
Trypsin + Chymotrypsin	In gel	66
Trypsin + Chymotrypsin with ProteaseMAX	In gel	54
pepsin	On-bead	65
chymotrypsin and trypsin + Glu-C	On-bead	65
chymotrypsin and trypsin + Glu-C + pepsin	On-bead	82



10	20	30	40	50
<u>MAQLYKQV</u>	<u>YSPYDRIP</u>	<u>QIVRAETEL</u>	<u>AEEKAFINAV</u>	<u>EKGDIATVKQ</u>
60	70	80	90	100
<u>ALQEAIEIYN</u>	<u>VNINCMDPLG</u>	<u>RSALLIAIEN</u>	<u>ENLEIMELLL</u>	<u>NHSVYVGDAL</u>
110	120	130	140	150
<u>LYAIRKEVVG</u>	<u>AVELLLSYRR</u>	<u>PSGEKQVPTL</u>	<u>MMDTQFSEFT</u>	<u>PDITPIMLAA</u>
160	170	180	190	200
<u>HTNNYEIIKL</u>	<u>LVQKRVTIPR</u>	<u>PHQIRCNCVE</u>	<u>CVSSSEVDSL</u>	<u>RHSRSLNIY</u>
210	220	230	240	250
<u>KALASPSLIA</u>	<u>LSSDPILTA</u>	<u>FRLGWELKEL</u>	<u>SKVENEFKAE</u>	<u>YEELSQQCKL</u>
260	270	280	290	300
<u>FAKDLDQAR</u>	<u>SSRELEIILN</u>	<u>HRDDHSEELD</u>	<u>PQKYHDLAKL</u>	<u>KVAIKYHQKE</u>
310	320	330	340	350
<u>FVAQPNQQOL</u>	<u>LATLWYDGF</u>	<u>GWRRKHVVVK</u>	<u>LLTCMTIGFL</u>	<u>FPMLSIAYLI</u>
360	370	380	390	400
<u>SPRSNLGLFI</u>	<u>KKPFIKFICH</u>	<u>TASYLTFLFM</u>	<u>LLASQHIVR</u>	<u>TDLHVQGPPP</u>
410	420	430	440	450
<u>TVVEWMILPW</u>	<u>VLGFIWGEIK</u>	<u>EMWDGGFTEY</u>	<u>IHDWNLMDF</u>	<u>AMNSLYLATI</u>
460	470	480	490	500
<u>SLKIVAVVKY</u>	<u>NGSRPREEWE</u>	<u>MWHPTLIAEA</u>	<u>LFAISNILSS</u>	<u>LRLISLFTAN</u>
510	520	530	540	550
<u>SHLGPLQISL</u>	<u>GRMLLDILKF</u>	<u>LFIYCLVLLA</u>	<u>FANGLNQLYF</u>	<u>YYETRAIDEP</u>
560	570	580	590	600
<u>NNCKGIRCEK</u>	<u>QNAFSTLFE</u>	<u>TLQSLFWSVF</u>	<u>GLLNLYVTNV</u>	<u>KARHEFTEFV</u>
610	620	630	640	650
<u>GATMFGTYNV</u>	<u>ISLVVLLNML</u>	<u>IAMMNSYQL</u>	<u>IADHADIEWK</u>	<u>FARTKLWMSY</u>
660	670	680	690	700
<u>FDEGGTLPPP</u>	<u>FNIIPSPKSF</u>	<u>LYLGNWFNNT</u>	<u>FCPKRDPDGR</u>	<u>RRRRNLSRFT</u>
710	720	730	740	750
<u>ERNADSLIQN</u>	<u>QHYQEVIRNL</u>	<u>VKRYVAAMIR</u>	<u>NSKTHEGLTE</u>	<u>ENFKELKQDI</u>
760	770	780	790	800
<u>SSFYEVLDL</u>	<u>LGNRKPRSF</u>	<u>STSSTELSQR</u>	<u>DDNNDGSGGA</u>	<u>RAKSKSVSN</u>
810	820	830	840	850
<u>LGCKKKTCHG</u>	<u>PPLIRTMPRS</u>	<u>SGAQGKSKAE</u>	<u>SSSKRSFMGP</u>	<u>SLKKLGLLFS</u>
860	870	880	890	900
<u>KFNHGMSEPS</u>	<u>SEPMYTISDG</u>	<u>IVQQHCMQD</u>	<u>IRYSQMEK GK</u>	<u>AEACSQSEIN</u>
910	920	930	940	950
<u>LSEVELGEVQ</u>	<u>GAAQSSECPL</u>	<u>ACSSSLHCAS</u>	<u>SICSSNSKLL</u>	<u>DSEDFVETW</u>
960	970			
<u>GEACDLLMHK</u>	<u>WGDQEEQVT</u>	<u>TRL</u>		

**Figure 57: MS-based peptide mapping of TRPC5-SYFP2.** The TRPC5 sequence shown is colour coded to indicate cytoplasmic domains (red), transmembrane domains (black with grey highlight) and extracellular domains (blue), as predicted from comparison to the mTRPC4:C4 structure.<sup>104</sup> Limited proteolysis with combinations of trypsin, chymotrypsin, Glu-C and pepsin has resulted in 82% peptide mapping of TRPC5 (bold and underlined).

## 4.6 The use of photoaffinity probes to confirm target engagement with TRPC5

### 4.6.1 Irradiation of photoaffinity probes and mass spectrometric analysis

To utilise Pico145-DA and Pico145-DAAIk successfully in photolabelling experiments, the photochemical properties need to be characterised. The most convincing evidence that a reagent is responding correctly to irradiation is the appearance of photolysis products. To evaluate the interactions of the diazirines with UV light, Pico145-DAAIk was dissolved in H<sub>2</sub>O at 1  $\mu$ M and methanol (MeOH) at 300 nM (diluted from 10 mM DMSO stock solutions) and irradiated at 365 nm for varying amounts of time (0, 5, 10, 15, 20, 25 and 30 minutes). Using high resolution mass spectrometry (HRMS), the irradiated samples were analysed for solvent adducts. In H<sub>2</sub>O two products were observed (*Figure 58*), a H<sub>2</sub>O adduct **102** and a hydrate of a trifluoromethyl ketone **103**. Kanoh *et al.* identified both of these products and rationalised the formation of a trifluoromethyl ketone as an oxidation product of the carbene by dissolved oxygen.<sup>238</sup> The parent ketone was expected to be hydrated<sup>239</sup> and therefore not appreciably abundant. The irradiation in MeOH predominately resulted in one product **104**, from insertion into MeOH (*Figure 59*). In both cases there appears to be a significant amount of diazirine starting material (Pico145-DAAIk) remaining after 30 minutes of irradiation. Preston *et al.* report that upon irradiation the diazirine groups are consumed to generate a carbene and a diazo isomer; the former reacts further, whereas the latter is considered to be relatively inert (*Section 1.6.6.3*).<sup>150</sup> This has been previously described by Hashimoto and Hatanaka, where no decrease in the diazo isomer was observed upon prolonged irradiation over 30 minutes.<sup>240</sup> This diazo species has the same mass as the starting material and therefore this is difficult to determine by MS experiments. However, to confirm the presence of the diazo species, <sup>19</sup>F NMR could be used to monitor the appearance of a characteristic signal of the diazo species over time and the disappearance of the <sup>19</sup>F NMR peak for the diazirine.<sup>240</sup>

These results were generated using the total ion count, which can be an unreliable method without an internal calibrant present. However, it does demonstrate that Pico145-DAAIk shows photoactivation upon irradiation at 365 nm and generates sufficient carbene to yield notable amounts of solvent adducts. Therefore Pico145-DAAIk was used for future photolabelling experiments.

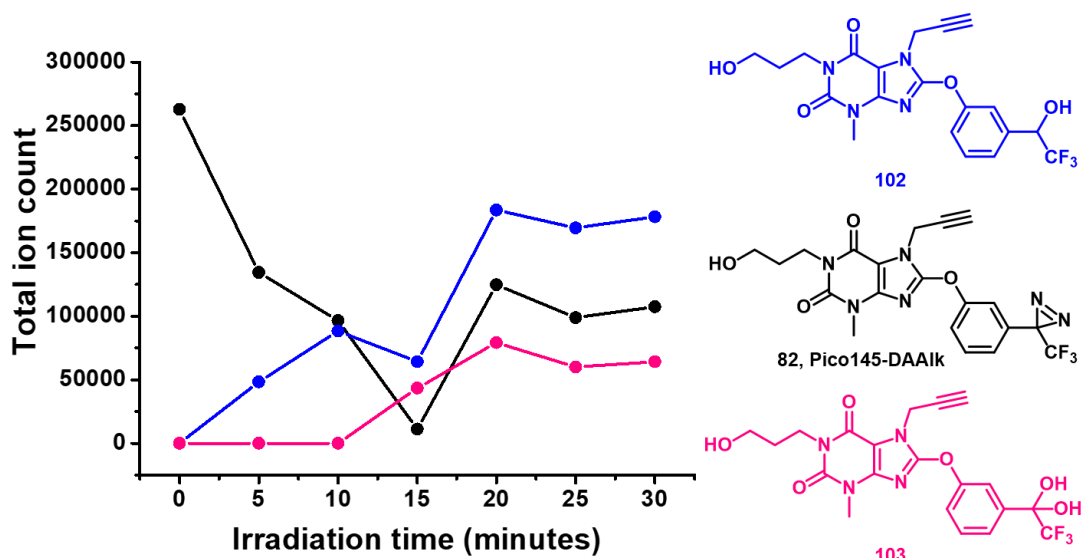


**Figure 58: Irradiation of Pico145-DAAIk in H<sub>2</sub>O at 365 nm.** Total ion count for solvent adducts and Pico145-DAAIk at different irradiation times. Pico145-DAAIk ([M+H]<sup>+</sup> 463.1336) shown in black, a H<sub>2</sub>O adduct ([M+H]<sup>+</sup> 453.1380) shown in blue, and a hydration product ([M+H]<sup>+</sup> 469.1329) shown in pink. MS data shown in appendix V.

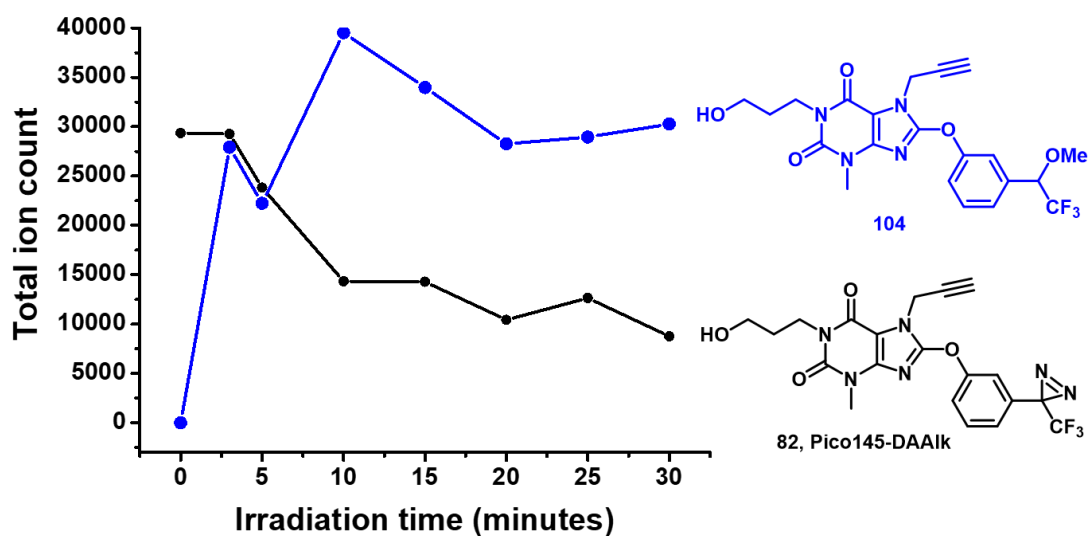


**Figure 59: Irradiation of Pico145-DAAIk in methanol at 365 nm.** Total ion count for solvent adducts and Pico145-DAAIk at different irradiation times. Pico145-DAAIk ([M+H]<sup>+</sup> 463.1336) shown in black and MeOH adduct ([M+H]<sup>+</sup> 467.1537) shown in blue. MS data shown in appendix V.

#### 4.6.2 Click chemistry using alkyne tagged protein lysates

As a proof of principle experiment, fatty acid analogues functionalised with an alkyne (YnMyr) were incubated in *L. donovani* promastigotes and incorporated by cellular machinery into lipidated proteins (performed by Dr Megan Wright).<sup>241</sup> Utilising these lysates, it was possible to determine that CuAAC click chemistry to incorporate a

fluorescent dye would be successful on proteins functionalised with an alkyne. Click reagents were added; Azide-Fluor-545 (100  $\mu$ M) (*Figure 60b*),  $\text{CuSO}_4$  (1 mM), tris(2-carboxyethyl)phosphine hydrochloride (TCEP) (1 mM), tris[(1-benzyl-1H-1,2,3-triazol-4-yl)methyl]amine (TBTA) (100  $\mu$ M) from a 'master mix', to 50  $\mu$ g of lysates, and proteins were precipitated with acetone. Resuspended proteins were separated by SDS-PAGE and functionalisation with Azide-Fluor-545, **105**, was observed in the YnMyr samples (*Figure 60*).

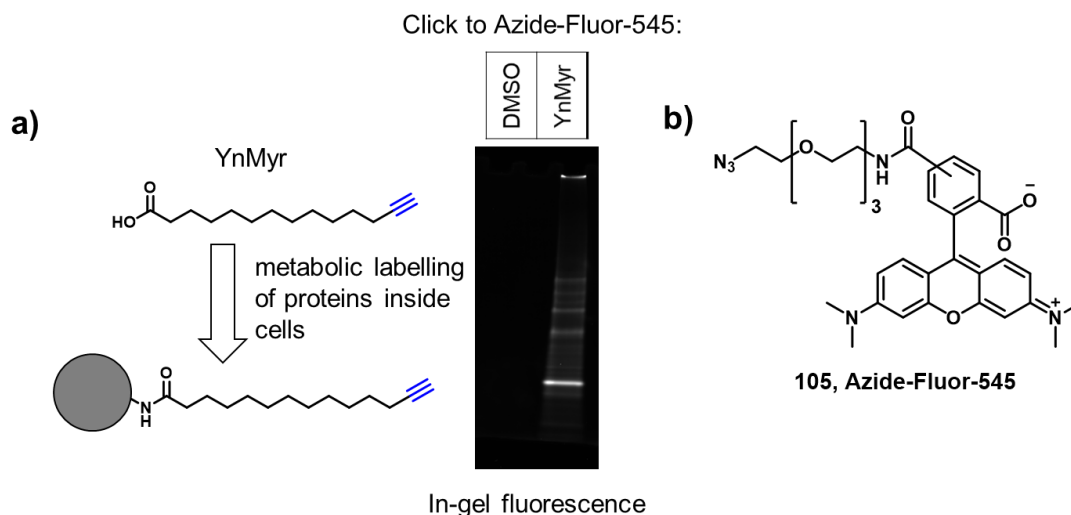


**Figure 60: Tagged proteins confirm CuAAC click chemistry with Azide-Fluor-545.** *a)* Metabolic tagging of proteins with YnMyr (performed by Dr Megan Wright) and subsequent analysis by CuAAC labelling, samples were precipitated with acetone. *b)* Structure of Azide-Fluor-545.

### 4.6.3 Photoaffinity labelling followed by click chemistry with Azide-fluor-545 for target engagement studies

Photoaffinity labelling combined with CuAAC click chemistry could be used to validate the possible direct action of Pico145 on TRPC1/4/5 channels, as suggested by the inhibition in excised outside-out membrane patch recordings<sup>59</sup> (*Section 1.3.2.4*). HEK-293 T-REx cells over-expressing TRPC5-SYFP2 were incubated with Pico145-DAAlk (300 nM) and irradiated for 25 minutes at 365 nm. For previous mass spectrometry studies (*Section 4.5*) cells were lysed using NP-40 lysis buffer, however the lysis buffer was changed for all click chemistry experiments. NP-40 lysis buffer contains Ethylenediaminetetraacetic acid (EDTA) which can chelate to copper,<sup>242</sup> thus the click reaction would be unsuccessful. Two new lysis buffers were explored, a Triton X-100 (lanes 1, 3, 4, and 5, *Figure 61b*) and a DDM-CHS lysis buffer (lanes 2 and 6, *Figure 61b*), both compatible with click reagents. Following cell lysis, CuAAC was performed as described above (*Chapter 4.6.2*). Resuspended proteins were separated by SDS-

PAGE and labelling could be seen where Pico145-DAAIk and click reagents were present (lanes 1 and 2, *Figure 61b*). In the absence of Pico145-DAAIk (lane 3, *Figure 61b*) or click reagents (lane 4, *Figure 61b*) no photolabelling was observed. A high degree of nonspecific labelling was observed. This is not unusual when using photoreactive ligands<sup>133,134</sup> and has been reported by Lapinsky and co-workers when using photoaffinity labelling for identification of binding to a GPCR.<sup>127</sup> An additional band can be seen at ~140 kDa in HEK-293 T-REx cells over-expressing TRPC5-SYFP2 (lanes 1 and 2, *Figure 61*), in comparison with WT HEK-293 cells (lanes 5 and 6, *Figure 61b,c*). Furthermore, the band is slightly more intense in lane 1 than in lane 2, suggesting that Triton-X100 was better at solubilising TRPC5-SYFP2 than the milder detergents DDM-CHS (*Figure 61*). This alone is not strong enough evidence to confirm a direct interaction between the photoaffinity probes and TRPC5, as the additional band seen in the TRPC5 containing cells may be observed due to additional non-specific labelling and the increased quantity of TRPC5 protein. The use of an alternative photoreactive group could indicate the role of the photoreactive group in non-specific labelling, i.e. if a different photoreactive group demonstrates a different labelling pattern this could indicate the reactive group rather than the ligand is responsible for the non-specific interactions, e.g. benzophenone *cf.* diazirine.<sup>127</sup>

To confirm photolabelling to TRPC5-SYFP2, enrichment of the TRPC5 protein could be used in conjunction with photoaffinity labelling and CuAAC chemistry. Purification of the TRPC5 protein and identification of a direct binding event could be achieved *via* two possible routes. Firstly, purification of TRPC5-SYFP2 by immunoprecipitation with GFP-trap beads and on-bead click using Azide-Fluor-545. A fluorescently labelled band at ~140 kDa would indicate direct binding of the photoaffinity probe to TRPC5. Alternatively, following photoaffinity labelling, biotin azide could be incorporated through click chemistry, subsequent pull down using Neutravidin beads and then western blotting for TRPC5-SYFP2 would also suggest a direct interaction between the photoaffinity probes and TRPC5. Although these experiments would identify a direct interaction, this would not confirm if the interaction occurs at the hypothesised binding site, the site thought to be responsible for gating of the channel. To investigate if the binding site of Pico145-DAAIk identified was the same binding site as Pico145 or an allosteric site, and therefore likely an important site on the channel due to the potency of Pico145, competition assays could be performed. If there is no fluorescent labelling or a reduction in labelling when Pico145 and Pico145-DAAIk are applied concomitantly, this indicates that there is competition, and thus the photoaffinity probe is binding to a potentially crucial site on the channel.

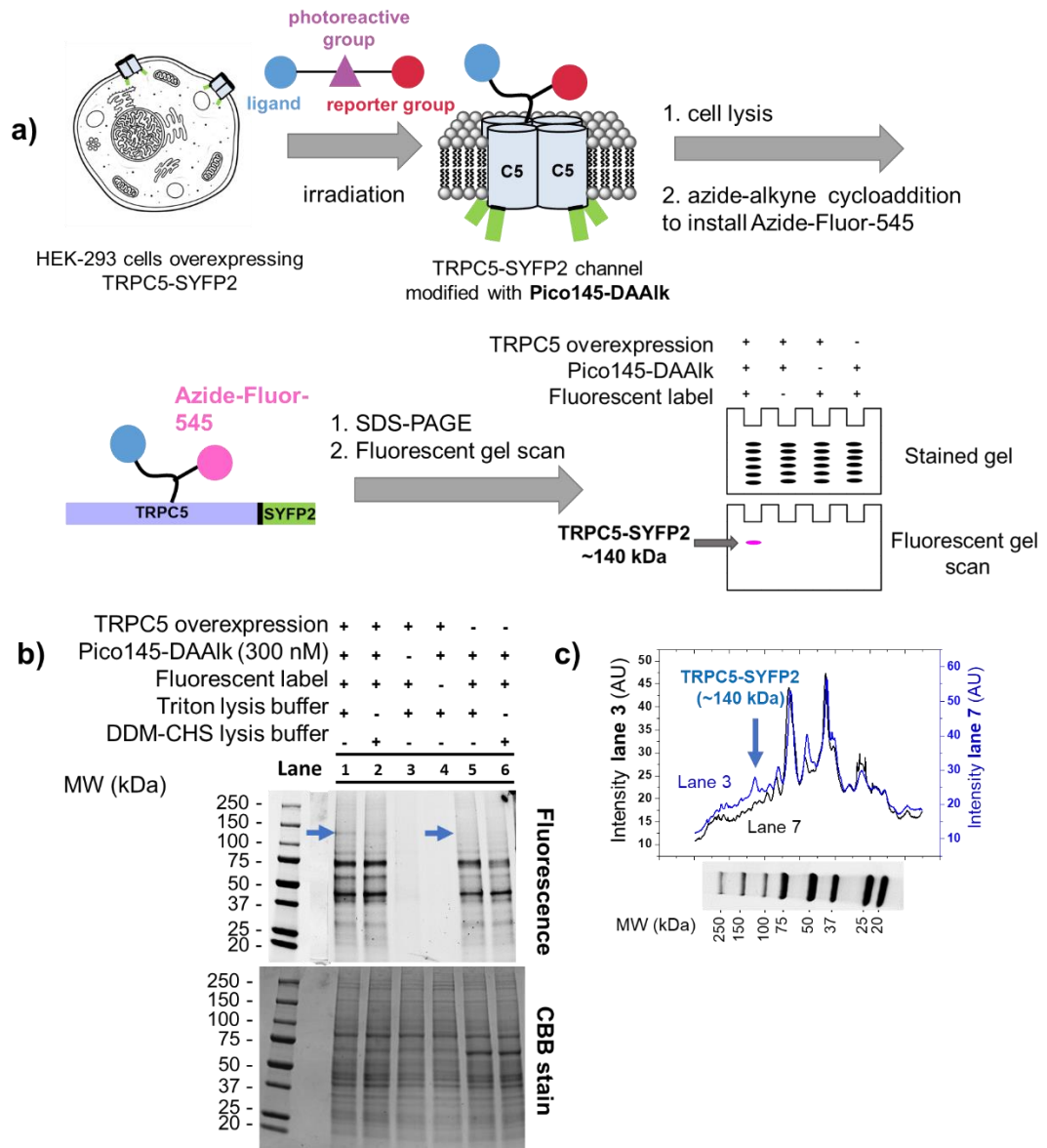


**Figure 61: Labelling of TRPC5-SYFP2 with Azide-Fluor-545.** **a)** Schematic representation of labelling reaction; **b)** Fluorescence image and Coomassie Brilliant Blue (CBB) stained SDS-PAGE gels; fluorescence image shows Pico145-DAAIk (300 nM) labelling in HEK-293 T-REx cells with 25 minutes irradiation (365 nm) at 0 °C and click chemistry utilising Azide-Fluor-545 (100 µM), CuSO<sub>4</sub> (1 mM), tris(2-carboxyethyl)phosphine hydrochloride (TCEP) (1 mM), tris[(1-benzyl-1H-1,2,3-triazol-4-yl)methyl]amine (TBTA) (100 µM) was performed (lanes 1,2,5 and 6, compared to control lanes 3 and 4). The faint band at ~140 kDa indicated by the blue arrow was only present in TRPC5-SYFP2-expressing cells (lanes 1 and 2 vs lanes 5 and 6), suggesting a direct interaction between Pico145-DAAIk and TRPC5-SYFP2. The band is slightly more intense in lane 1 than in lane 2, suggesting that Triton-X100 was better at solubilising TRPC5-SYFP2 than the milder detergents DDM/CHS.; **c)** Quantification of fluorescent bands in lanes 3 and 7 in the SDS-PAGE gel. ImageJ was used for densitometry analysis of lanes, and intensity profiles were plotted (normalised to most intense peaks) (Quantification performed by Dr Eulashini Chuntharpursat).

## 4.7 Conclusions

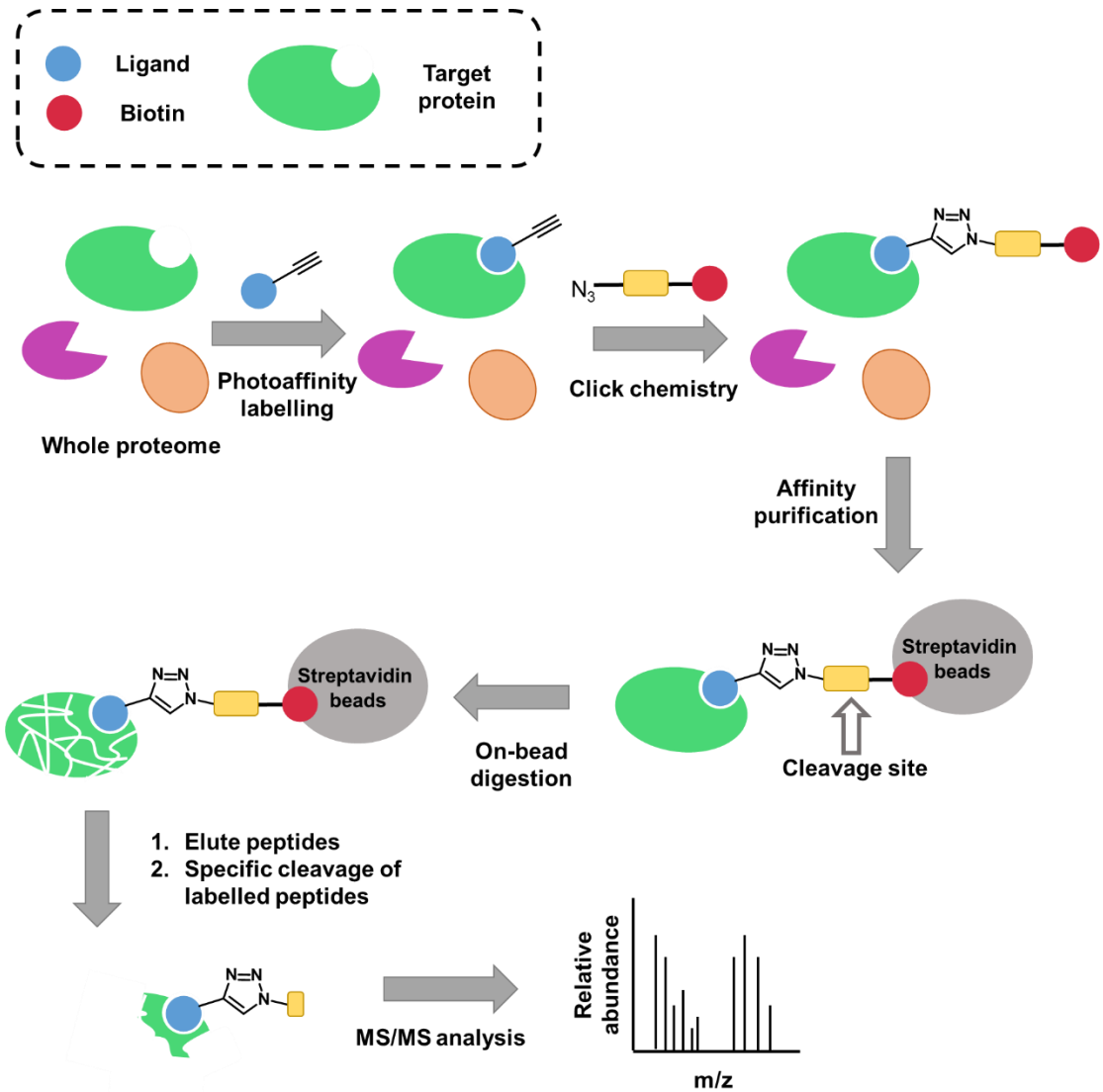
In summary, two novel photoaffinity probes for TRPC1/4/5 channels have been developed. Pico145-DA and Pico145-DAAIk were designed based on SAR of substituted xanthenes described in the international patent by Hydra Biosciences.<sup>65</sup> Following synthesis of these photoaffinity probes calcium recording assays were utilised to determine the similarity in activity towards TRPC1/4/5 channels to Pico145. Notably, Pico145-DA and Pico145-DAAIk were found to inhibit (-)-EA-evoked  $\text{Ca}^{2+}$  entry in cells over-expressing TRPC5 (*Figure 41a*), yet when applied alone these compounds activated TRPC5 (*Figure 41b*). The activation observed was dependent on the over-expression of TRPC5 and the presence of  $\text{Ca}^{2+}$  in the extracellular medium. Pico145-DA and Pico145-DAAIk activate TRPC5 and TRPC5-SYFP2 channels with  $\text{EC}_{50}$  in the low nanomolar range and Pico145 can inhibit this activation in a dose-dependent manner (*Figure 46*). Pico145-DA and Pico145-DAAIk were seen to inhibit TRPC4 channels, distinguishing between these two closely related channels. There are currently few known modulators which can potently distinguish between TRPC4 and TRPC5 channels. Furthermore, these photoaffinity probes maintain potent inhibition of heteromeric TRPC4:C1 and TRPC5:C1 channels (*Figure 49 and Figure 50*), based on concatemers generated within Leeds. Due to the small change in structure from Pico145 to the photoaffinity probes, their retention of activity and the requirement for TRPC5 channel induction for activation in calcium recording assays, it is hypothesised that these compounds will bind to the same location on TRPC1/4/5 channels as Pico145. Additionally, the characterisation of a TRPC5 agonist identified in the patent by Hydra Biosciences<sup>65</sup> has confirmed the similarity in activity to the photoaffinity probes, Pico145-DA and Pico145-DAAIk. AM237 could be a useful tool to study TRPC1/4/5 channels due to its expected increased stability over Pico145-DA and Pico145-DAAIk and the ability to potently distinguish between TRPC4 and TRPC5 channels.

Identification of the binding site of Pico145 on TRPC1/4/5 channels requires purification of TRPC1/4/5 and high sequence coverage by mass spectrometry. TRPC5-SYFP2 was successfully purified and digestion was attempted using several proteases. Limited proteolysis with combinations of trypsin, chymotrypsin, Glu-C and pepsin has resulted in 82% peptide mapping of TRPC5, in particular there was significant sequence coverage of the extracellular loops thought to be of importance in gating the ion channel. This level of sequence coverage may be sufficient to identify a site of modification by photoaffinity labelling. However, higher sequence coverage may be required to verify that there is only one site of modification on the protein.

Photoaffinity labelling and CuAAC click chemistry experiments showed photolabelling only occurred in samples containing both Pico145-DAAIk and click reagents, however a high degree of non-specific labelling was observed. To confirm direct action of Pico145-DAAIk on TRPC5, enrichment of the protein and subsequent functionalisation with a fluorophore would need to be achieved. TRPC5-SYFP2 could be purified using immunoprecipitation and then click chemistry performed on the GFP-nanobody, identifying the interaction using a fluorophore.<sup>243</sup> Furthermore, click chemistry could be utilised to incorporate a biotin, subsequent purification of TRPC5 using Neutravidin beads and identification of TRPC5-SYFP2 using a Western blot to confirm the hypothesis that Pico145 binds directly to TRPC1/4/5 channels. Additionally, competition experiments could be performed to identify competitive binding of Pico145 and Pico145-DAAIk, indicating they bind to the same or allosteric binding sites. A reduction or abolishment of fluorescence labelling when using Pico145 and Pico145-DAAIk concomitantly during photoaffinity labelling experiments would indicate competitive binding.

Additionally, the development of a cleavable linker for mass spectrometry experiments could allow the enrichment of peptides in the binding pocket (*Scheme 14*).<sup>244,245,246</sup> Target proteins are commonly isolated using affinity purification techniques, exploiting the strong and specific interaction of probe-biotin conjugates with avidin.<sup>247</sup> The strength of this interaction can be detrimental to mass spectrometry experiments, due to the harsh elution conditions and the high level of background from numerous proteins which bind to avidin, including naturally biotinylated proteins.<sup>248</sup> A cleavable linker approach facilitates selective release of labelled peptides, under mild conditions. The isolation and enrichment of peptides is particularly useful for low abundant proteins, e.g. membrane proteins. A generic workflow would include photoaffinity labelling, CuAAC to attach a cleavable tag, enrichment, on bead digest, and cleavage to release the labelled peptides. A variety of cleavable linkers have been reported in the literature, including protease cleavable linkers, e.g. TEV,<sup>249,246</sup> photochemically cleavable linkers, e.g. *ortho*-nitrobenzyl group,<sup>250,248</sup> and chemically cleavable linkers which cleave under acidic conditions (acylhydrazone<sup>251</sup>), nucleophilic conditions (nitrobenzenesulfonamide<sup>252</sup>) or dithionite treatment (azobenzene<sup>245,250,253,254</sup>). Chemically cleavable linkers have some advantages over protease linkers, including lower cost of reagents and reduced cleavage time. Other considerations for a cleavable linker include stability in a variety of digestion conditions, to enable sufficient digestion of the target protein followed by selective release of the labelled peptides.





**Scheme 14: Schematic of the workflow for selective elution of peptides using a cleavable linker.** Photoaffinity labelling followed by CuAAC enables the incorporation of a cleavable tag. Affinity purification, subsequent on-bead digestion and selective elution of the peptides can afford isolation of the peptides in the binding site.

## Chapter 5 - Synthesis of a library of novel TRPC5 inhibitors

### 5.1 Introduction

The sigma-1 receptor (S1R) is a membrane protein in the endoplasmic reticulum, which regulates Ca<sup>2+</sup> entry at intracellular compartments and the plasma membrane *via* receptors and ion channels.<sup>255</sup> There has been a lack of clarity about the biological function of the S1R and as a result there is uncertainty about substances that are agonists and antagonists of S1R. Beech *et al.* investigated the importance of S1R for Ca<sup>2+</sup> signalling in endothelial cells.<sup>256</sup> The S1R antagonists BD1047, **106**, and BD1063, **108**, and S1R agonist 4-IBP, **107** (*Figure 62*) inhibited histamine evoked Ca<sup>2+</sup> entry in endothelial cells, but not Ca<sup>2+</sup> release from intracellular stores. TRPC5 and TRPM2 have been implicated in mediating Ca<sup>2+</sup> entry in endothelial cells.<sup>257,258,259</sup> TRPM2 was not sensitive to the S1R ligands. However, the S1R ligands inhibited TRPC5- and TRPM3-evoked Ca<sup>2+</sup> entry in HEK-293 cells, independent of modes of TRP channel activation.<sup>256</sup> The inhibition of Ca<sup>2+</sup> entry by both antagonists and agonist of S1R suggested the mechanism of action was not mediated by S1R. Beech *et al.* confirmed the results were independent of S1R, because the inhibitory effects of S1R ligands were unaffected by S1R knockdown. BD1047, BD1063 and 4-IBP are structurally similar. BD1063 and 4-IBP consist of a core piperazine/piperidine connected to a halogenated aromatic ring *via* a two-atom linker. BD1047 could be considered a ring-opened analogue of BD1063. Based on these structural similarities a TRPC5 pharmacophore, **109** was proposed (*Figure 62*).<sup>256</sup>

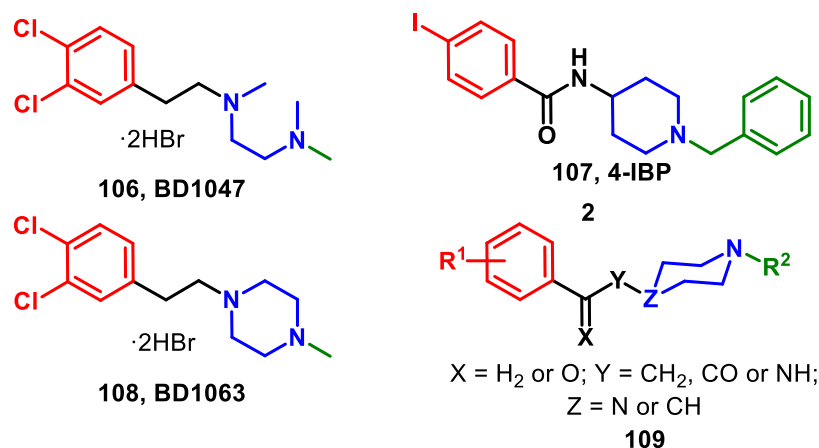


**Figure 62:** Structures of the Sigma-1-Receptor ligands and TRPC inhibitors **106-108** and proposed pharmacophore **109**.

Structure activity relationships (SAR) based on this pharmacophore were investigated by the Bon and Beech groups. For these studies, compounds were synthesised by Katherine Brodie, Dr James Holt-Martyn, Jason Gresly, Dr Dimitrios Poulcharidis and Anet Varghese, and assays were performed by Dr Paul Turner, Dr Xin Jin, Dr Mohamed Amer and Dr Zoe Jackson. SAR of the scaffold, linker and R<sup>1</sup> position were investigated, and the most pronounced effect on activity against TRPC5 was observed with variation of R<sup>1</sup>. Changes to the scaffold or linker had little effect on the potency against TRPC5. A 3,4-dichlorophenyl substituent in the R<sup>1</sup> position was present in the most potent compounds tested (*Figure 63*).

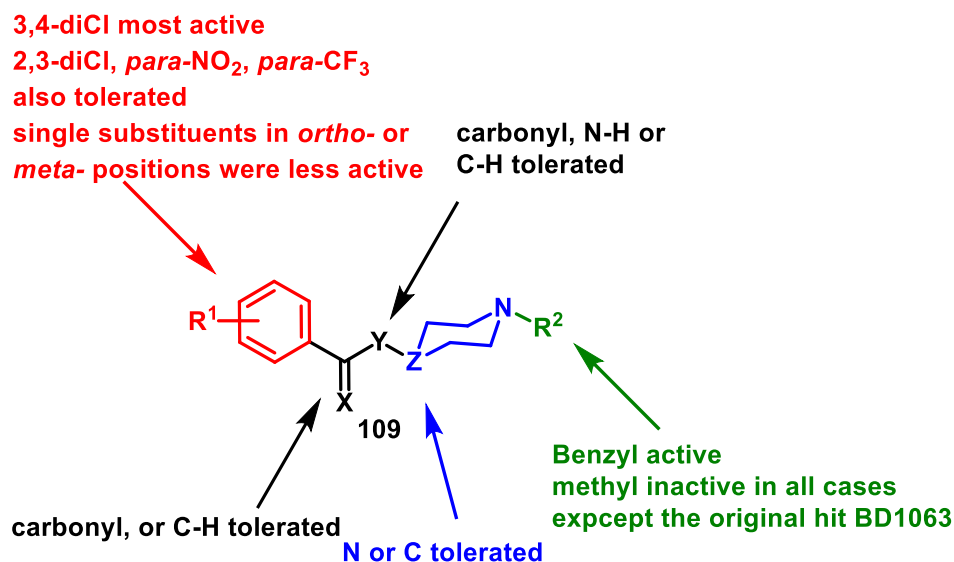
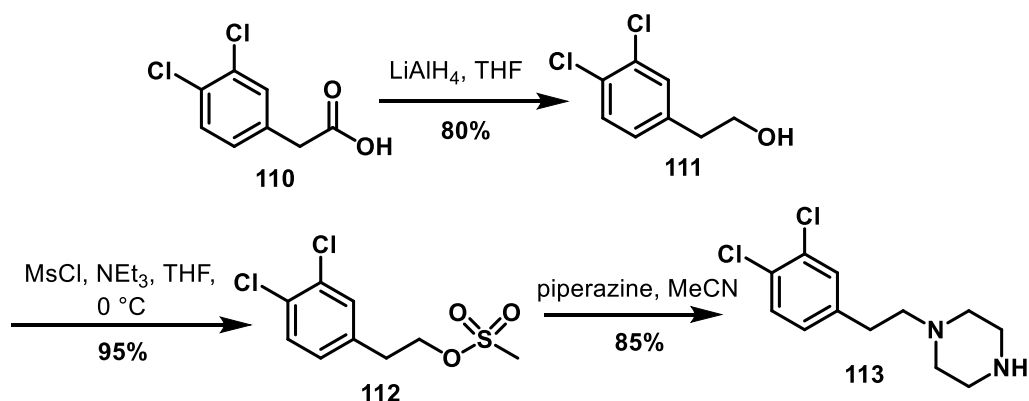


**Figure 63:** Previous SAR studies of the TRPC5 pharmacophore described by Beech *et al.*<sup>256</sup>

Subsequently a synthetic route to a 3,4-dichlorophenyl piperazine was designed by Dr Dimitrios Poulcharidis. The synthetic route was adapted from Lorschach *et al.* who reported the synthesis of 2,4-dichlorophenyl-ethyl piperazine.<sup>260</sup>

The piperazine building block, **113**, was synthesised by reduction of carboxylic acid, **110** to give dichlorophenylethyl alcohol, **111** and subsequent mesylation to afford **112**. Finally, a substitution reaction on mesylate **112** with piperazine, afforded building block **113**, (Scheme 15).



**Scheme 15:** Synthetic procedure for the a piperazine building block **113**.

## 5.2 Design and synthesis of a third series of piperazine inhibitors of TRPC5

The  $\text{R}^2$  position remained largely unexplored in previous SAR studies. Therefore, this was investigated whilst the core was kept as a piperazine group and a 3,4-dichlorophenyl moiety was kept in the  $\text{R}^1$  position. To test whether substitution of the  $\text{R}^2$  position would change the potency of piperazine-based TRPC5 inhibitors, a small library of compounds was made. Investigation into the electronics of the substituent began with an electron withdrawing (Cl) **114** and electron donating (OMe) **115** group placed in the *para*- position of the aromatic ring of  $\text{R}^2$  (Figure 64). Furthermore, compounds were designed with amide linkers in the *meta*- and *para*- positions, **116-119**, on the aromatic ring of  $\text{R}^2$  (Figure 64). Active compounds with such amide linkers could facilitate the addition of a photoreactive group to investigate the mechanism of action of these piperazine inhibitors on TRPC5.

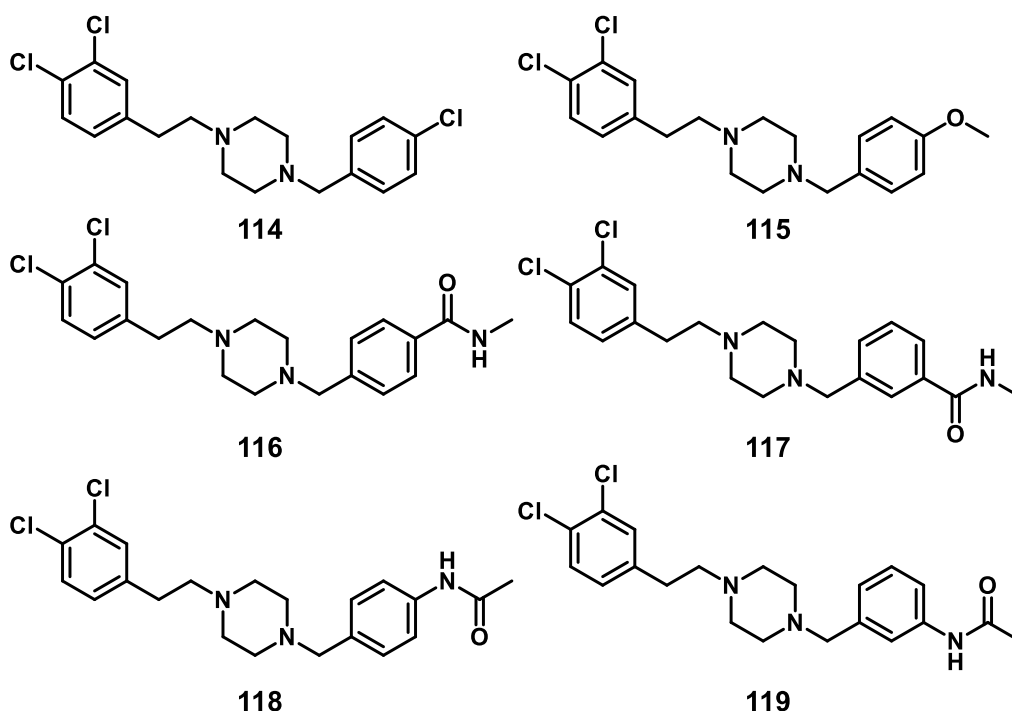
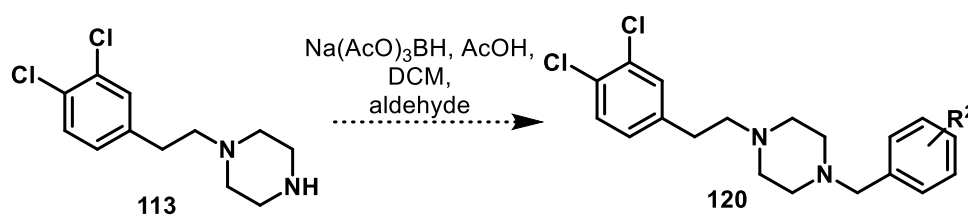


**Figure 64:** Proposed compounds to investigate the SAR of the  $R^2$  position of a TRPC5 pharmacophore proposed by Beech *et al.*<sup>256</sup>

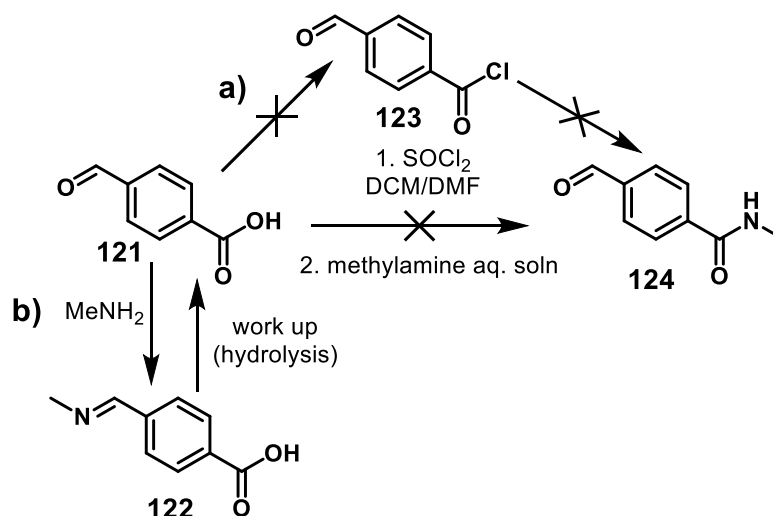
The piperazine building block previously described could be used to synthesise the speculated piperazine TRPC5 inhibitors **114-119**. The synthesis for the piperazine building block was scaled up and subsequent reductive amination reactions with the corresponding aldehydes were used in the synthesis of **114-119** (Scheme 16).



**Scheme 16:** Proposed reductive aminations to afford a small library of piperazine compounds.

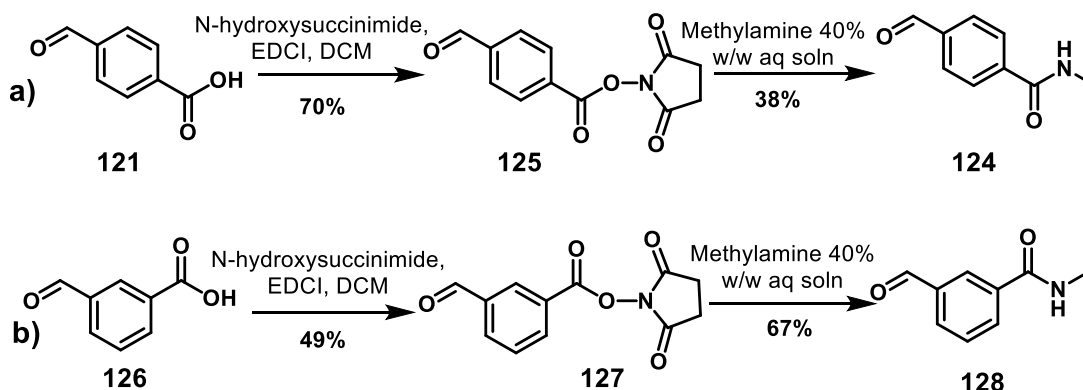
Corresponding aldehydes for compounds **114**, **115** and **118** were commercially available. However, compounds **116**, **117** and **119** required synthesis of aldehydes for reductive aminations. Firstly, the synthesis of **124** was attempted by the procedure described by Tanaka and co-workers.<sup>261</sup> Unfortunately the synthesis of **124** was not successful using this procedure. Analysis of the reaction mixture using LC-MS analysis showed the correct mass for compound **124**. However, following aqueous work up, <sup>1</sup>H NMR analysis confirmed isolation of the starting material. It was hypothesised that the amide was not synthesised *via* the acid chloride **123** (Scheme

17a), but the imine **122** was formed, which was then converted back to the acid **121** upon aqueous work up, (Scheme 17b).



**Scheme 17: Initial attempted synthesis of aldehyde **124**; a) predicted route via the acid chloride **123** b) hypothesized route via formation of imine, **122**, which is then hydrolysed upon an aqueous work up to afford the starting material, **121**.**

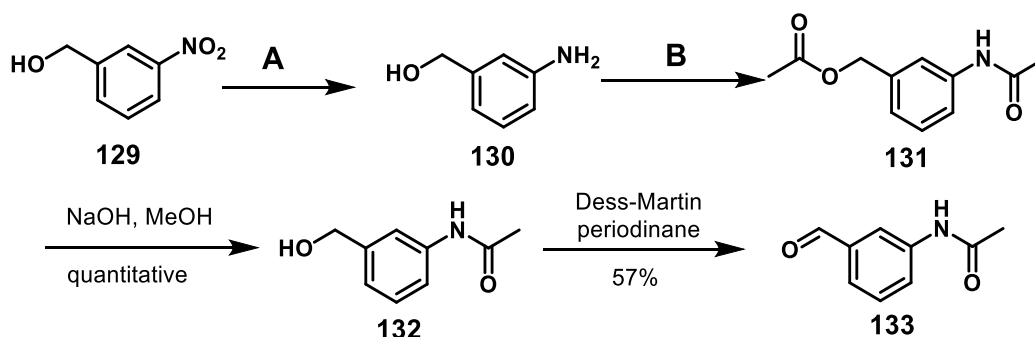
Subsequently, a procedure described by Tang *et al.*<sup>262</sup> was followed for the synthesis of aldehyde **124**, which proceeded via an NHS-ester intermediate **125** (Scheme 18). This synthetic route could also be applied to the *meta*-substituted amide, **128**, (Scheme 18) required for the synthesis of piperazine **117**. The NHS-ester in this procedure was used as an activating group for the carboxylic acid, by creating a good leaving group, which improved the reactivity with the methylamine solution.



**Scheme 18: Synthesis of aldehydes a) **124** and b) **128** via an NHS-intermediate**

The synthesis of piperazine **119** required an aldehyde with an amide in the *meta*-position with connection to the aromatic ring through the nitrogen. Initially, a procedure described by Storz *et al.*<sup>263</sup> was followed (Scheme 19). Synthesis of aldehyde **133** proceeded by reduction of the nitro substituted benzyl alcohol **129**. This was primarily attempted using iron powder and  $\text{NH}_4\text{Cl}$ , which obtained the desired

product **130** in a 28% yield. To optimise the yield of this reaction zinc was substituted for iron, as an alternative mild reducing agent, following a procedure described by McCutcheon *et al.*<sup>264</sup> which resulted in quantitative yield (*Table 7*). The procedure described by Storz *et al.* used acetyl chloride for the acetylation of **130**; analysis by LC-MS led to the identification of both mono- and di-acetylation products. Purification by column chromatography afforded the desired acetyl **139** with a 10% yield. Subsequently, a procedure described by Chaturvedula *et al.*<sup>265</sup> using acetic anhydride with a DMAP catalyst afforded the desired product in quantitative yield. Sodium hydroxide was used to hydrolyse the ester, followed by oxidation of the alcohol **132** to aldehyde **133** using Dess-Martin periodinane as described in the original procedure by Storz *et al.*<sup>263</sup> (*Table 7*).

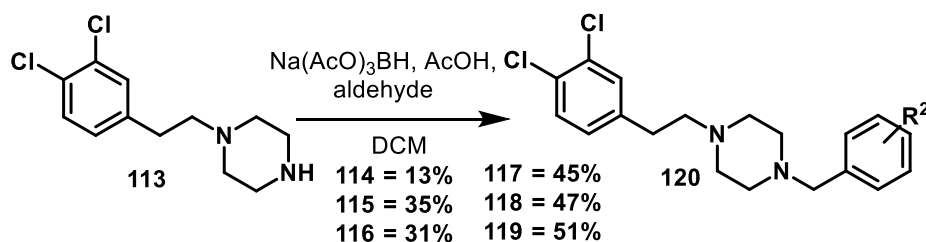


**Scheme 19:** Synthesis of aldehyde **133**, via reduction of nitro **129**, then acetylation of amine **130** to yield **132**, mono-deacetylation and finally oxidation to yield the desired aldehyde **133**.

**Table 7:** Optimization of conditions used for the synthesis of aldehyde **133**, adapted from the procedure described by Storz *et al.*<sup>263</sup> shown in Scheme 19.

Step	Reagents	Yield
A	Iron powder, NH <sub>4</sub> Cl, ethanol:water (10:1 v/v) <sup>263</sup>	28%
A	Zinc powder, NH <sub>4</sub> Cl, MeOH <sup>264</sup>	quantitative
B	acetyl chloride, triethylamine, DCM <sup>263</sup>	10%
B	acetic anhydride, DMAP, triethylamine, DCM <sup>265</sup>	quantitative

Following the synthesis of aldehydes **124**, **128** and **133**, compounds **114-119** were synthesised by reductive amination using sodium triacetoxyborohydride (STAB) as described by Dvorak *et al.*<sup>266</sup> (*Scheme 20*).



**Scheme 20:** Synthesis of piperazine predicted TRPC5 inhibitors **114-119** by reductive amination as described by Dvorak et al.<sup>266</sup>

As control compounds for the biological testing of **114-119**, compounds with no substitution at the R<sup>2</sup> position, 3,4-dichlorophenyl amidopiperazine, **136** and 3,4-dichlorophenyl piperidine **139**, were re-synthesised following procedures established by Katherine Brodie and Dr Dimitrios Poulcharidis respectively. Additionally, the 3,4-dichlorophenyl piperazine **141** was re-synthesised using the reductive amination procedure described for compounds **114-119**.

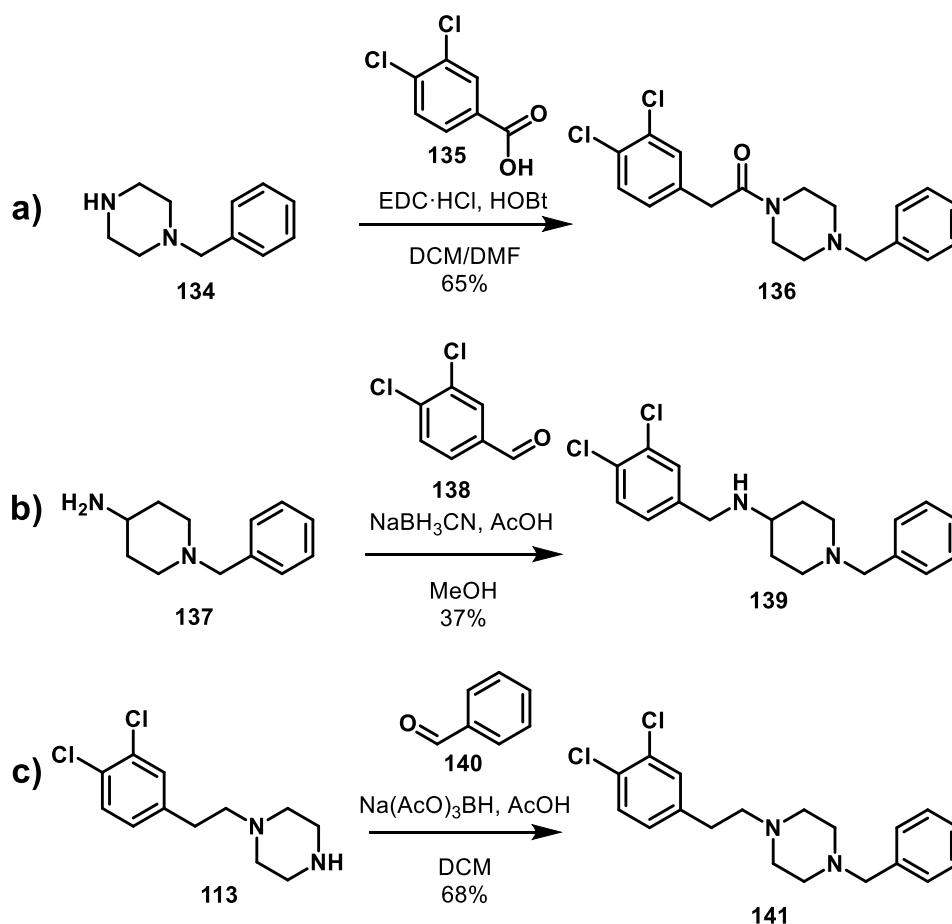


**Figure 65:** Synthesis of previously described piperazine and piperidine compounds with no substitution at the R<sup>2</sup> position, **136**, **139** and **141**.

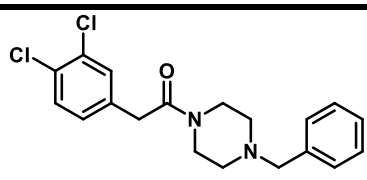
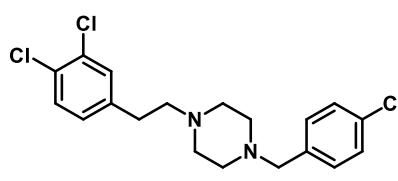
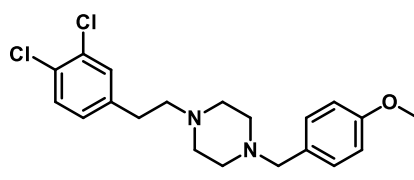
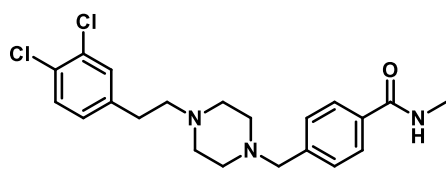
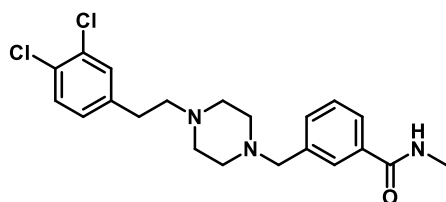
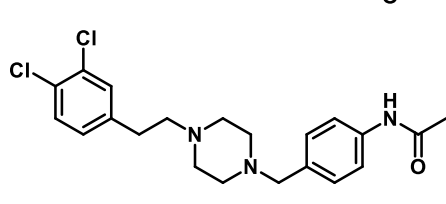
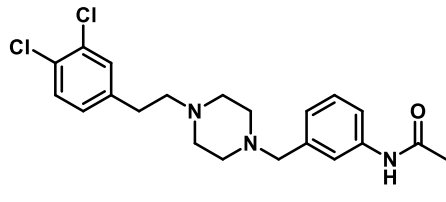


## 5.3 Evaluation of the potency of piperazine and piperidine inhibitors

### 5.3.1 Evaluation of potency of Gd<sup>3+</sup>-evoked TRPC5 activity

Compounds **114-119** were initially tested at 10  $\mu$ M for their ability to inhibit Gd<sup>3+</sup>-evoked Ca<sup>2+</sup> entry in HEK-293 cells with a tetracycline inducible system to over-express TRPC5 (experiments performed by Dr Hussein Rubaiy). The results are outlined in *Table 8*. The addition of either an electron withdrawing group (Cl), **114** or an electron donating group (OMe), **115** at the *para* position of R<sup>2</sup> resulted in almost complete abolishment of activity against TRPC5, with < 5% inhibition. Interestingly, an amide linker at the *para* position of R<sup>2</sup> gave more pronounced inhibition of TRPC5 than compounds with the corresponding *meta*-substituents (~60% inhibition *cf.* ~30% inhibition). The amide linker *para*-substituents on the R<sup>2</sup> position have comparable activity against Gd<sup>3+</sup>-evoked Ca<sup>2+</sup> entry to the 3,4- dichlorophenyl amidopiperazine **136**, identified in previous SAR experiments. These investigations of substituents on the R<sup>2</sup> position of the TRPC5 pharmacophore described by Beech *et al.* showed no clear improvement in potency against Gd<sup>3+</sup>-evoked TRPC5 activity. However, the amide linker *para*-substituents **116** and **118** did not show a decrease in activity compared to 3,4-dichlorophenyl amidopiperazine **136**, therefore these could be investigated further as a possible position to introduce a photoreactive group for target engagement and binding site studies.

**Table 8:** Percentage inhibition results of compounds **114-119** and **136** against  $Gd^{3+}$ -evoked TRPC5 activity in HEK-293 cells. Percentage inhibition results are given as the mean  $\pm$  SE of the mean,  $n/N = 5/20$ . (Experiments performed by Dr Hussein Rubaiy)

Compound No.	Structure	% inhibition (10 $\mu$ M)
136		52 $\pm$ 7.0
114		4.7 $\pm$ 9.8
115		1.4 $\pm$ 5.5
116		59 $\pm$ 11
117		36 $\pm$ 9.0
118		58 $\pm$ 3.6
119		25 $\pm$ 1.7

### 5.3.2 Evaluation of potency of (-)-EA-evoked TRPC5 activity

In 2015 (-)-Englerin-A ((-)-EA) emerged as a novel inhibitor of TRPC1/4/5 channels (Section 1.3.1.1). Due to its remarkable selectivity, efficacy and potency it is now widely used in *in vitro* experiments to study TRPC1/4/5 channels.<sup>267</sup> Therefore the effect of the piperazine and piperidine inhibitors described in Section 5.2 was next investigated against (-)-EA-evoked TRPC5 activity. The activity was investigated in HEK-293 cells stably over-expressing TRPC5 upon induction with tetracycline (tet+). Cells were preincubated with 10  $\mu$ M **114-119**, **136**, **139** or **141**, prior to application of 10 nM (-)-EA. Calcium measurements showed no inhibition of the (-)-EA-evoked  $\text{Ca}^{2+}$  entry for these compounds at 10  $\mu$ M. This suggests that the inhibition of TRPC5 by the piperazine/piperidine inhibitors is dependent on the mode of activation. Neither  $\text{Gd}^{3+}$  or (-)-EA are endogenous activators of TRPC5 and therefore it would be important to investigate the activity of these compounds against an endogenous activator, e.g. sphingosine-1-phosphate (S1P) to unravel the possible physiological role of this series of inhibitors.

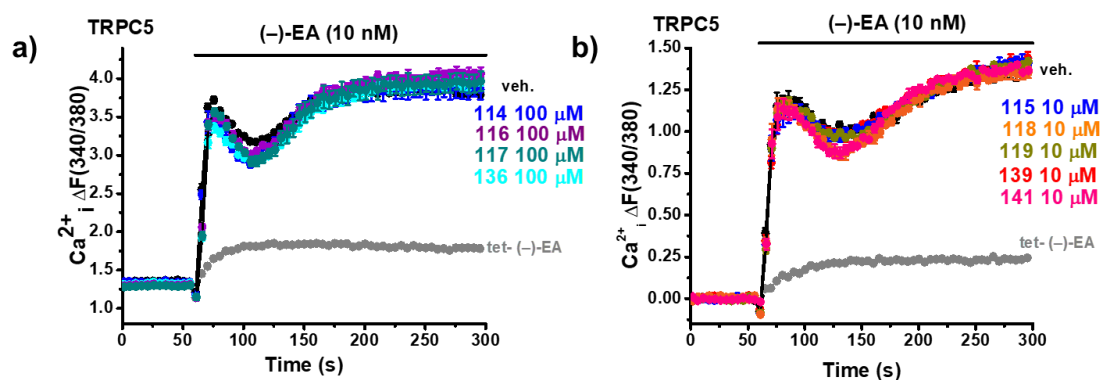


**Figure 66: Compounds 114-119, 136, 139 or 141 show no inhibition of the (-)-EA induced  $\text{Ca}^{2+}$  entry in HEK-293 cells over-expressing TRPC5.** Recordings were from TRPC5 expressing (tet+) HEK-293 cells or no induction (tet-), and extracellular  $\text{Ca}^{2+}$  was present at 1.5mM. Intracellular  $\text{Ca}^{2+}$  was measured using fura-2. Cells were incubated with 10  $\mu$ M **a) 114, 116, 117, 136** or DMSO vehicle control (veh.), **b) 115, 118, 119, 139, 141** or DMSO vehicle control (veh.), for 30 min before 10 nM (-)-EA was applied. Compounds **114-119, 136, 139 or 141** show no inhibition of the (-)-EA response.

## 5.4 Evaluation of the selectivity of piperazine and piperidine inhibitors

Limited selectivity studies have been performed on the piperazine and 4-aminopiperidine series of inhibitors. Compounds **6** and **31** showed no inhibition of the H<sub>2</sub>O<sub>2</sub>-evoked Ca<sup>2+</sup> entry in cells over-expressing TRPM2 (experiments performed by Dr Mohamed Amer). This indicates there may be selectivity amongst the TRP family, however more TRP channels would need to be investigated to confirm this. To further investigate the selectivity of this series and identify possible off-targets, compounds **114-119**, **136**, **139** and **141** were tested against a set of cardiac ion channels: hERG, Nav1.5, I<sub>KS</sub> and I<sub>to</sub> by automated whole cell patch clamp recordings (experiments performed at AstraZeneca in collaboration with Ann Woods). CHO cells stably expressing Nav1.5, Kv11.1, Kv7.1 and Kv4.3 were preincubated and then maintained in the presence of **114-119**, **136**, **139** and **141** for three minutes prior to current recordings. Concentration-response data were collected for compounds **114-119**, **136**, **139** and **141** between 167 µM and 0.05 µM and IC<sub>50</sub> values are summarised in *Table 9* (for IC<sub>50</sub> graphs see *Appendix I*).

In general, the piperazine and piperidine series of TRPC5 inhibitors showed poor selectivity towards TRPC5 over the cardiac channels investigated. Compounds **114-119**, **139** and **141** all had IC<sub>50</sub> values below 2 µM against hERG. Blockade of the hERG channel has become one of the most frequent reasons for drug withdrawal.<sup>268</sup> Furthermore, compounds **114**, **115**, **118**, **136**, **139** and **141** have IC<sub>50</sub> values in the low micromolar range for all of the cardiac ion channels tested. **116**, **117** and **119** showed little activity against the I<sub>KS</sub> channel, however they inhibited hERG, Nav1.5 and I<sub>to</sub> with low micromolar IC<sub>50</sub> values. Therefore, these compounds would be unsuitable drug candidates. Additionally, the lack of selectivity renders these compounds unsuitable for target engagement and binding site studies on TRPC5.

**Table 9: Summary of the selectivity of piperazine/piperidine TRPC5 inhibitors 114-119, 136, 139 and 141 for a number of cardiac ion channels. Where reference compounds are: hERG – cisapride,  $I_{KS}$  – XE-991,  $I_{t0}$  – flecainide, Nav1.5 – flecainide (Chapter 2). (For  $IC_{50}$  graphs see Appendix I)**

Compound No.	$IC_{50}$ ( $\mu$ M)				% inhibition
	hERG	$I_{KS}$	$I_{t0}$	Nav <sub>1.5</sub>	TRPC5
114	0.9 ± 0.1	2.8 ± 6.9	13 ± 2.0	8.0 ± 2.4	4.7 ± 9.8
115	0.2 ± 0.1	1.4 ± 4.1	11 ± 0.8	4.0 ± 0.4	1.4 ± 5.5
116	0.4 ± 0.1	>167	36 ± 7.2	3.8 ± 2.2	59 ± 11
117	1.7 ± 0.2	>167	58 ± 16	8.3 ± 6.0	36 ± 9.0
118	1.6 ± 0.1	1.2 ± 2.7	34 ± 4.8	9.0 ± 3.4	58 ± 3.6
119	0.8 ± 0.1	>167	33 ± 8.7	12 ± 2.6	25 ± 1.7
136	9.6 ± 2.3	14 ± 4.6	16 ± 2.4	9.1 ± 3.3	>52 ± 7.0
139	1.6 ± 0.2	8.1 ± 1.8	15 ± 1.4	3.3 ± 2.1	-
141	1.2 ± 0.1	23 ± 6.6	17 ± 2.8	13 ± 1.6	-
Reference	8.2 ± 1.6	0.5 ± 0.1	15 ± 1.6	3.5 ± 0.3	-

## 5.5 Future work and conclusions

In summary, six novel compounds were designed and synthesised based on a TRPC5 pharmacophore previously described by Beech *et al.*<sup>256</sup> and previous SAR performed within the Bon group. Compounds **114-119** and **136** were tested for their inhibition of the Gd<sup>3+</sup>-evoked Ca<sup>2+</sup> entry in HEK-293 cells over-expressing TRPC5. Piperazine compounds with amide linkers at the *para* position of R<sup>2</sup>, **116** and **118**, proved most promising; although percentage inhibition remained in a similar range to that of previously designed compounds with no substitution at the R<sup>2</sup> position. Subsequently, compounds **114-119**, **136**, **139** and **141** were tested for their inhibition of the (–)-EA-evoked Ca<sup>2+</sup> entry in HEK-293 cells over-expressing TRPC5. These results showed that compounds **114-119**, **136**, **139** and **141** did not inhibit Ca<sup>2+</sup> entry when tested at 10 µM, suggesting that the inhibition by piperazines/piperidine compounds is dependent on the mode of activation of TRPC5. However, neither Gd<sup>3+</sup> or (–)-EA are endogenous activators of TRPC5 and therefore it would be important to investigate the activity of these compounds against an endogenous activator, e.g. S1P to unravel the possible physiological role of this series of inhibitors.

The selectivity of piperazine/piperidine TRPC5 inhibitors was investigated against a set of cardiac channels. All piperazine/piperidine compounds tested showed a degree of activity against at least three out of four cardiac channels investigated. This demonstrates that the piperazine inhibitors have poor selectivity towards TRPC5. Additionally, compounds **114-119**, **139** and **141** inhibited the hERG channel with IC<sub>50</sub> values less than 2 µM. Therefore, this limits the therapeutic potential of these compounds. To proceed with the development of TRPC5 inhibitors using this pharmacophore, the dependence on mode of activation of TRPC5 would need to be explored, possibly with the endogenous activator, S1P. Additionally the selectivity of these compounds would need to be further investigated, and design of new compounds based on SAR could be used in efforts to reduce off-target effects. The emergence of Pico145 as a much more potent and selective TRPC1/4/5 channel inhibitor (see *Section 1.3*) shifted the focus of this PhD project.

## Chapter 6 - Thesis summary and future directions

This thesis describes a combination of approaches to investigate the mechanism of action of TRPC1/4/5 inhibitors. Calcium recordings and electrophysiology assays were used in *Chapter 3* to unravel the mode of action of novel flavonol-based TRPC5 inhibitors. Photoaffinity labelling was used in *Chapter 4* to determine the mode of action of a published TRPC1/4/5 inhibitor. Finally, the SAR of a previously described series of inhibitors was investigated in *Chapter 5*.

*Chapter 2* summarises some of the specialist techniques used throughout this thesis. *Chapter 3* describes the development of novel flavonol-based TRPC1/4/5 inhibitors. Manual outside-out patch clamp recordings showed inhibition of TRPC5 by AM12. This suggests that AM12 has a direct effect on TRPC5 because its effect is independent of cellular constituents, other Ca<sup>2+</sup> handling mechanisms or membrane potential. Subsequently, the selectivity of AM12 was investigated against other TRP channels, exhibiting no inhibition of TRPC3, TRPM2 or TRPV4. These data suggest AM12 has a degree of selectivity towards TRPC5 amongst other TRP channels. However, AM12 and AM13 showed poor selectivity towards TRPC5 when tested against a set of cardiac ion channels. There appeared to be a correlation between the inhibition of TRPC5 and cardiac ion channels, implying that there could be a common mechanism of action. Furthermore, there was literature precedent to suggest the mechanism of action of polyphenols was *via* alterations of membrane protein function by localising to the membrane/solution interface. Subsequently, membrane perturbation experiments highlighted a distinct difference between synthetic (AM12, AM13) and natural flavonols. Natural flavonols perturbed a DOPC monolayer, whereas synthetic flavonols had no effect. This suggests that there may be a conformational difference induced by *ortho*-substitution that means the synthetic flavonols can no longer interact with a phospholipid monolayer. Additionally, this suggests that AM12 and AM13 do not inhibit TRPC5 through perturbation of the membrane. Together with the inhibition in excised outside-out patch recordings; these results suggest AM12 and AM13 may have a distinct binding site on the TRPC5 channel.

Future efforts would focus on the design and synthesis of new flavonol-based compounds, firstly to investigate the conformational effect of *ortho*-substitution. This could be achieved by synthesising *meta*- and *para*-substituted flavonols, with the same hydrophilicity (cLogP) as AM12 and AM13 (*Figure 67*). Furthermore, these compounds would help to develop more SAR of galangin, which could be used for the

synthesis of photoaffinity probes to confirm a direct interaction with TRPC5. Additionally, the effect of known TRPC5 inhibitors e.g. Pico145 on a phospholipid monolayer could be tested to further investigate the relationship between TRPC5 activity and membrane perturbation.

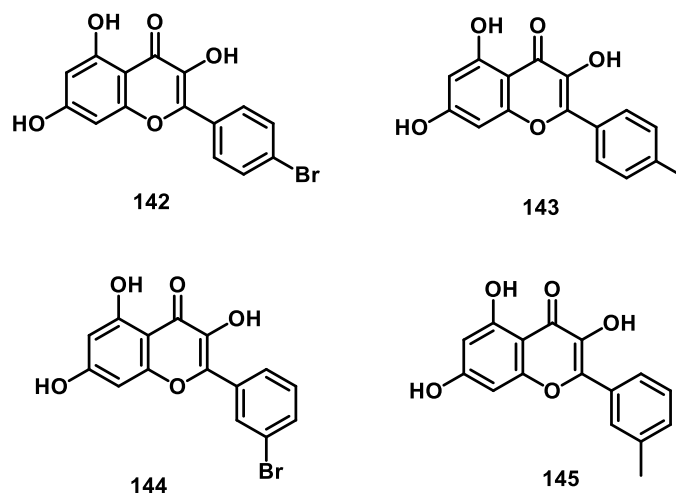


**Figure 67: Chemical structures of proposed galangin derivatives with meta- and para-substitution, to investigate conformational effects on membrane perturbation.**

Chapter 4 details the development of two novel photoaffinity probes based on the recently published TRPC1/4/5 inhibitor, Pico145. Pico145-DA and Pico145-DAAIk were found to inhibit (–)-EA-evoked  $\text{Ca}^{2+}$  entry in cells over-expressing TRPC5, yet when applied alone these compounds activated TRPC5. The activation observed was dependent on the over-expression of TRPC5 and  $\text{Ca}^{2+}$  present in the extracellular medium. This suggests that the increase in  $\text{Ca}^{2+}$  entry was through the TRPC5 channel. Pico145-DA and Pico145-DAAIk activate TRPC5 with an  $\text{EC}_{50}$  in the low nanomolar range and this activation was competitively inhibited by Pico145. Pico145-DA and Pico145-DAAIk were found to inhibit TRPC4 and concatemeric channels TRPC4:C1 and TRPC5:C1. There are currently few known modulators which can distinguish between TRPC4 and TRPC5 channels. Subsequently a compound described in the patent by Hydra Biosciences as an agonist of TRPC5 was investigated and later called AM237. AM237 displayed similar activity to Pico145-DA and Pico145-DAAIk, activating TRPC5 and inhibiting TRPC4, TRPC4:C1 and TRPC5:C1 channels. AM237 could be a useful tool to study TRPC1/4/5 channels due to its expected increased stability over Pico145-DA and Pico145-DAAIk and the ability to potently distinguish between TRPC4 and TRPC5 channels.

TRPC5 was purified and sequence coverage of 82% was achieved using a combination of trypsin, chymotrypsin, Glu-C and pepsin. Importantly, there was significant coverage of the extracellular loop which is thought to be essential in gating



of the ion channel. This coverage could be sufficient to identify a labelled residue on the TRPC5 protein and therefore the same protocol could be used in future studies following photoaffinity labelling. However, higher sequence coverage may be required to verify that there is only one site of modification on the protein. Photoaffinity labelling and click chemistry have confirmed a direct interaction between Pico145-DAAIk and TRPC5, however non-specific labelling also occurred. Purification of TRPC5 for click chemistry experiments would be necessary to validate this result. Furthermore, excess Pico145 could be used in these experiments to determine competitive binding between Pico145 and Pico145-DAAIk. A reduction or abolishment of fluorescence labelling when using Pico145 and Pico145-DAAIk concomitantly during photoaffinity labelling experiments would indicate competitive binding. Additionally, the development of a cleavable linker for mass spectrometry experiments could allow the enrichment of peptides in the binding pocket, as described in *Section 4.7*.

*Chapter 5* details the investigation of SAR of a known series of TRPC5 inhibitors. Six novel piperazine compounds were designed and synthesised. Two of these compounds showed similar activity against  $Gd^{3+}$ -evoked TRPC5 activity to a previously described amidopiperazine TRPC5 inhibitor. The novel piperazine compounds and previously described piperazine/piperidine TRPC5 inhibitors lacked inhibition of (-)-EA evoked TRPC5 activity. This suggests that the inhibition of this series of compounds is dependent on the mode of activation of TRPC5. To investigate the physiological relevance of these compounds it would be important to test the inhibition of TRPC5 activated by an endogenous activator, e.g. S1P. Furthermore, the piperazine/piperidine compounds were tested against a set of cardiac ion channels and showed poor selectivity for TRPC5. Therefore, this limits the therapeutic potential of these compounds. Further SAR studies would be needed to improve the selectivity towards TRPC5 and efforts made to reduce off-target effects.

## Experimental Section

### 7.1 Experimental section applying to all chapters

#### 7.1.1 General materials and methods for organic synthesis

All chemical reagents were purchased from commercial suppliers and used without further purification. When used as reaction solvents, THF, EtOH and CH<sub>2</sub>Cl<sub>2</sub> were dried and deoxygenated using an Innovative Technology Inc. PureSolv® solvent purification system. Other anhydrous solvents and liquid reagents were either purchased in Sure/Seal™ bottles or pyridine and triethylamine were prepared by distillation from KOH.

Flash column chromatography was carried out using silica (Merck Geduran silica gel, 35–70 μm particles). Thin layer chromatography was carried out on commercially available pre-coated aluminium plates (Merck silica 2 8 8 0 Kieselgel 60 F<sub>254</sub>). Analytical HPLC was performed on an Agilent 1290 Infinity Series equipped with a UV detector and a Hyperclone C<sub>18</sub> reverse phase column using MeCN/water (5→95%) containing 0.1% formic acid, at either 0.5 mL min<sup>-1</sup> over a period of five minutes or 1.0 mL min<sup>-1</sup> over a period of 30 minutes. All compounds with reported HPLC retention times are >95% pure unless otherwise stated.

High resolution electrospray (ESI+) mass spectrometry was performed on a Bruker MaXis Impact QTOF mass spectrometer, and *m/z* values are reported in Daltons to four decimal places. FTIR were acquired using a Bruker Platinum-ATR. <sup>1</sup>H and <sup>13</sup>C NMR spectra were recorded in deuterated solvents on a Bruker Avance 500, Bruker Avance 400 or Bruker Avance DPX 300. Chemical shifts are quoted in parts per million downfield of tetramethylsilane and referenced to residual solvent peaks (CDCl<sub>3</sub>: <sup>1</sup>H = 7.26 ppm, <sup>13</sup>C = 77.16 ppm, DMSO-d<sub>6</sub>: <sup>1</sup>H = 2.50 ppm, <sup>13</sup>C = 39.52 ppm) and coupling constants (*J*) are reported to the nearest 0.1 Hz. The following abbreviations are used: s, singlet; d, doublet; t, triplet; q, quartet; m, multiplet; app. apparent. Assignment of spectra was based on expected chemical shifts and coupling constants, aided by COSY, HMQC and HMBC measurements where appropriate.

## 7.1.2 Ionic Solutions

### Standard Bath Solution (SBS) for Ca<sup>2+</sup> imaging and measurement experiments

SBS: NaCl 130 mM, KCl 5 mM, MgCl<sub>2</sub> 1.2 mM, CaCl<sub>2</sub> 1.5 mM, HEPES 10 mM, D-Glucose 8 mM; pH was titrated to 7.4 with 1 M NaOH.

Ca<sup>2+</sup>-free SBS was prepared by omitting CaCl<sub>2</sub> and adding 0.4 mM EGTA.

### Dulbecco's Phosphate Buffered Saline (DPBS)

Dulbecco's Phosphate Buffered Saline (DPBS) without magnesium (Mg<sup>2+</sup>) and Ca<sup>2+</sup> (Lonza) contained: KCl 2.68 mM, KH<sub>2</sub>PO<sub>4</sub> 1.47 mM, NaCl 136.89 mM and Na<sub>2</sub>HPO<sub>4</sub>·7H<sub>2</sub>O 8.06 mM. DPBS was used for cell culture purposes including washing of cells during passage and photocrosslinking experiments.

## 7.1.3 Chemicals and reagents

All general salts, solvents and compounds were purchased from Sigma-Aldrich unless stated otherwise.

Fura-2 acetoxymethyl ester (fura-2 AM, Invitrogen) and fluo-4 acetoxymethyl ester dye (fluo-4 AM, Invitrogen) were prepared as 1 mM stock solutions in 100% dimethyl sulfoxide (DMSO) and stored at -20 °C protected from light. Fura-2 AM was utilised at a concentration of 2 µM for experiments mixed with pluronic acid. Pluronic acid is a non-ionic surfactant required to enhance the water solubility of fura-2 AM. A stock solution of 10% pluronic acid diluted in water was prepared and a final concentration of 0.01% was used in experiments. Fluo-4 AM was used at a concentration of 2 µM for experimentation, with 2.5 mM probenecid and 0.01% pluronic acid. Probenecid was used as an inhibitor of non-specific plasma membrane anion transport and was used to reduce leakage of fluo-4 AM. Probenecid was prepared fresh in 1 M NaOH and diluted to a final concentration of 2.5 mM.

(-)-Englerin A ((-)-EA) was supplied by PhytoLAB. Stock solutions were prepared at a concentration of 10 mM dissolved in 100% DMSO and stored at -80 °C. (-)-EA was diluted to working concentration in the experimental buffer (SBS) containing 0.1% DMSO and 0.01% pluronic acid. Pluronic acid was used as a dispersing agent to minimise aggregation of (-)-EA. (-)-EA was utilised at a concentration of 10 nM to induce Ca<sup>2+</sup> entry in HEK-293-TRPC5 and TRPC5-SYFP2, 30 nM to induce Ca<sup>2+</sup> entry in TRPC4-SYFP2 and TRPC5/C1 cells and 100nM to induce Ca<sup>2+</sup> entry in TRPC4/C1 cells.

## 7.1.4 Cell Culture

### Human Embryonic Kidney-293 (HEK-293) Cells

HEK-293 cells (ATCC) were maintained in Dulbecco's Modified Eagle's Medium (DMEM; Gibco) supplemented with 10% Fetal Bovine Serum (FBS) and 100 unit/ml penicillin-streptomycin. Cells were grown to 95% confluence before passage and utilised at 95% confluence for experiments.

### TRPC5

HEK-293 cells stably expressing a tetracycline inducible over-expression of TRPC5 were created as previously described.<sup>33</sup>

## 7.1.5 Intracellular calcium measurements

The changes in the intracellular ionized calcium concentration upon agonist evoked channel activation were measured using the fura-2 (or fluo-4 in Section 3.3.5) calcium indicator dye and the FlexStationII<sup>384</sup>/FlexStationIII<sup>384</sup>.

### 7.1.5.1 Fura-2 acetoxymethyl ester (Fura-2 AM)

The acetoxymethyl ester (AM) form is membrane permeable and once inside the cell, the AM group is cleaved by non-specific esterases to produce the charged and active form (fura-2) able to bind  $\text{Ca}^{2+}$  with high affinity. Fura-2 is one of the most popular ratiometric calcium indicator dyes. It has a high affinity for calcium, binding with a  $K_d$  value of 140 nM.<sup>172</sup> Upon calcium binding the excitation spectrum shifts, resulting in an increase in fluorescence emission at 340 nm and a decrease in fluorescence emission at 380 nm. Fura-2 fluorescence is recorded as a ratio of 340/380 and thus, there is an overall increase in the ratio that indicates an increase in intracellular calcium.<sup>269</sup> Emitted light is collected at 510 nm. The use of a ratiometric indicator is advantageous as it allows the accurate measurement intracellular  $\text{Ca}^{2+}$  concentrations whilst minimising the effects of unequal dye loading, leakage, photobleaching and varying cell thickness, delivering more reproducible results.<sup>173</sup>

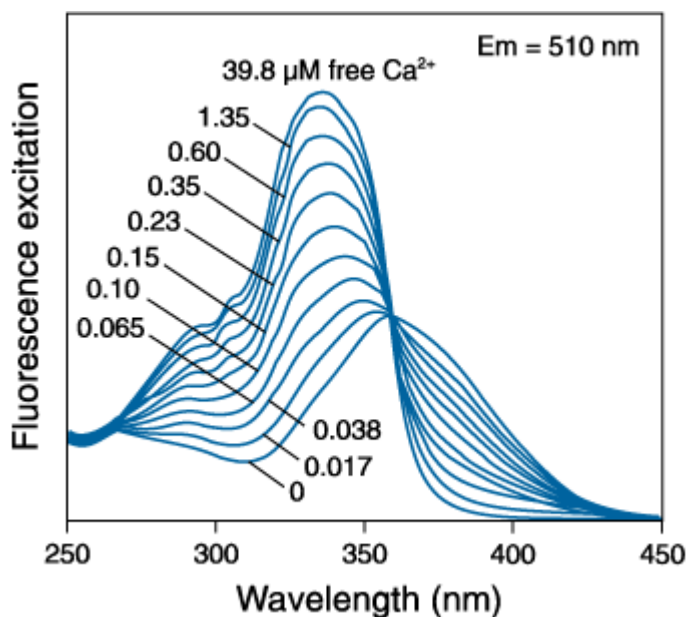


**Figure 68: Fluorescence excitation spectra of fura-2 in varying free  $\text{Ca}^{2+}$  concentrations.**<sup>269</sup> An increase in intracellular  $\text{Ca}^{2+}$  will cause fura-2 fluorescence emission intensity at 510 nm to increase at excitation wavelength 340 nm and decrease at 380 nm. Image reference: [www.thermofisher.com](http://www.thermofisher.com).

#### 7.1.5.2 High throughput $\text{Ca}^{2+}$ measurement using the FlexStation II<sup>384</sup>/FlexStation III<sup>384</sup>

The FlexStation (Molecular Devices, USA) is a bench-top scanning fluorimeter. It provides integrated fluid transfer from a compound plate to an assay plate whilst taking measurements of fluorescence. All experiments for this study used 96-well based assay. The FlexStation has 3 drawers designed to hold the tips, the assay plate and the compound plate. The automated device has a built-in 8-head dispenser that can be programmed to add compounds from a compound plate into a prepared assay plate containing cells at designated time points and measure any subsequent changes in fluorescence. Softmax Pro 4.7.1 software (Molecular Devices) was used in order to select the desired excitation wavelengths (Fura-2 - 340 nm and 380 nm), the emission wavelength (Fura-2 - 510 nm), the time course of the experiment, the timing of compound addition and sampling frequency. Experiments were performed at room temperature (RT:  $21 \pm 2$  °C) unless stated otherwise.

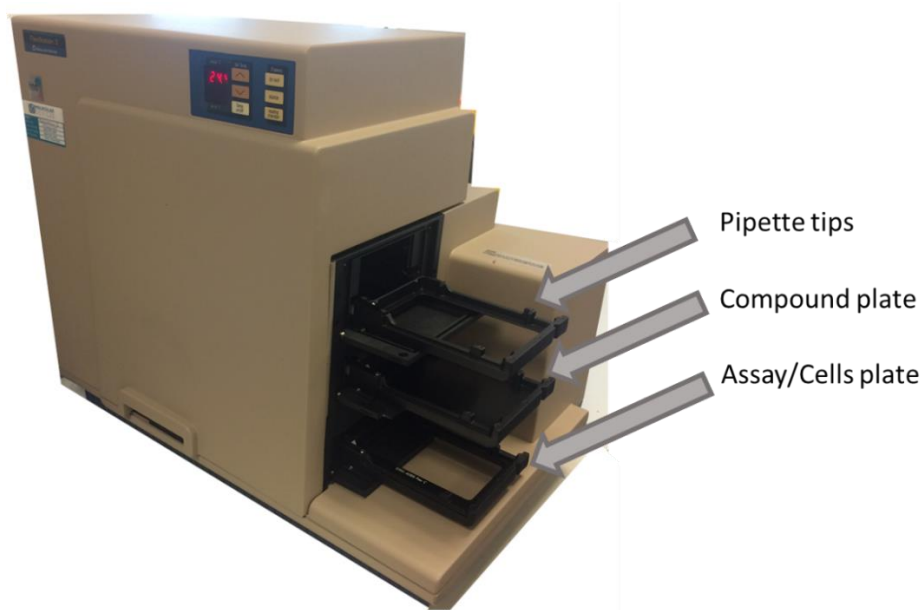


**Figure 69: FlexStation III<sup>384</sup>/FlexStation III<sup>384</sup> benchtop microplate reader.** Highlighting the positions of Pipette tips, compound plate and the Assay/cells plate.

### 7.1.5.3 Experimental protocol

#### Cell plates

HEK-293-TRPC5, HEK-293-TRPC5-SYFP2, HEK-293-TRPC4-SYFP2, HEK-293-TRPC4/C1 and C5/C1 cells were seeded onto Cellcoat Poly-D-Lysine 96-well plates (Greiner Bio-One, UK). A seeding density of 60,000 cells per well was used for HEK cells in a 96-well plate format. Cells were plated from a 70-80% confluent T75 flask. Trypsin-EDTA (0.05%) (Sigma, UK) was used to detach cells.  $1\mu\text{g}\cdot\text{ml}^{-1}$  tetracycline (tet+) was applied or not (tet-) 18 hr prior to experimentation to induce TRPC5, TRPC5-SYFP2, TRPC4, TRPC4-SYFP2, TRPC5-C1 or TRPC4-C1 expression. All cells were grown to confluency overnight at 37 °C, 5% CO<sub>2</sub> levels.

#### Fura-2 loading

On the day of experimentation cells were incubated with fura-2. Cells were incubated for 1 hour at 37 °C in standard bath solution (SBS) containing 2  $\mu\text{M}$  fura-2 and 0.01% pluronic acid. Pluronic acid is a mild detergent that was used to facilitate the solubility of the dye. All loading was carried out under low light conditions and the plates were wrapped in aluminium foil.

#### Pre-incubation

Cells were then washed with 1.5 mM Ca<sup>2+</sup> SBS (3x) to minimise background fluorescence. Cells were then pre-incubated according to the experiment being

carried out (compounds incubated in SBS at desired concentration for antagonist mode, or cell incubated with DMSO control in SBS for agonist mode). All pre-incubations were carried out at room temperature ( $21 \pm 2$  °C) for 30 minutes prior to recordings and protected from the light.

#### Compound Plate

The compound plate contained 1.5 mM  $\text{Ca}^{2+}$  SBS for all experiments. Automated compound transfer from the compound plate into the assay plate involved a 1:2 dilution. For experiments that involved the addition of a fresh compound to the assay plate (without prior incubation of the compound), the compound was prepared at 2x the desired final concentration for addition to the test plate, where it underwent a 1:2 dilution to the final required concentration. The FlexStation was programmed to transfer 80  $\mu\text{l}$  from the compound plate to the assay plate wells containing 80  $\mu\text{l}$  (hence, a 1:2 dilution).

For experiments involving pre-treatment with test compounds, it was important to maintain the concentration of the compound in question in the 1.5 mM  $\text{Ca}^{2+}$  SBS in the compound plate in line with that in the assay plate. The DMSO concentration should also remain consistent throughout each experiment. After pre-incubation, the assay plate along with the compound plate and FlexStation tips were loaded into the FlexStation. Baseline fluorescence ratios were recorded before addition of the compound solution to the assay plate after 60 seconds.  $\Delta F$  ratio values at peak (150-200 seconds)  $\text{Ca}^{2+}$  entry was used for statistical comparison, unless stated otherwise. 'Zero baseline' traces are displayed throughout where baseline  $\text{Ca}^{2+}$  levels are consistent.  $\text{Ca}^{2+}$  traces displaying 'absolute' values are used when the baseline  $\text{Ca}^{2+}$  level is altered, or to confirm no alteration of basal  $\text{Ca}^{2+}$  levels.

Cells that had no induction of the channels, *i.e.* no pre-treatment with tetracycline (tet-) were included in each experiment to ensure there was low levels of leak in the expression system and the  $\text{Ca}^{2+}$  entry responses observed were attributable to the TRPC channel of interest (TRPC5, TRPC4, TRPC5-YSFP2, TRPC4-SYFP2, TRPC5:C1 or TRPC4:C1).

#### **7.1.5.4 Data Analysis**

Mean data are presented as mean  $\pm$  standard error of the mean, where n represents the number of independent experiments and the N represents the number of wells of a 96-well plate used in a single experiment. The data (mean  $\pm$  standard error of the mean) from a minimum of three independent replicates was transferred in Origin Pro

8.5. The Hill equation was fitted using Origin software (Microcal Inc. USA) (*Equation 1*). The Hill equation is based on the principle that a physiological response is the result of ligand binding and therefore dose-response curves reflect binding curves.<sup>270</sup> In the Hill equation the  $K_d$  is the equilibrium dissociation, which in terms of a dose-response curve is the  $EC_{50}$  or  $IC_{50}$ .

$$\text{Fraction of bound ligand} = \frac{[L]^n}{(K_d + [L]^n)} \quad \text{Equation 1}$$

The Hill equation; where  $K_d$  is the equilibrium dissociation constant,  $[L]$  is the free (unbound) ligand concentration and  $n$  is the Hill coefficient.<sup>270</sup>

## 7.1.6 Automated electrophysiology

### 7.1.6.1 Cell culture

All cells were cultured in HAM/nut mix F12 with Glutamax-1 supplemented with 10% fetal bovine serum, 1% non-essential amino acids and; 0.6 mg/mL Hygromycin B (hERG cell line), or 1.1 mg/mL Geneticin (hNav1.5 cell line), or 1.1 mg/mL Geneticin and 0.6 mg/mL Hygromycin B ( $I_{to}$  cell line), or 0.4 mg/mL Geneticin and 0.1 mg/mL Hygromycin B ( $I_{Ks}$  cell line).

#### *Cell preparation for the IonWorks*

All cells were cultured in T75 or T175 flasks. Fresh cell suspensions were prepared immediately prior to use in the IonWorks™ system as follows. Cells were removed from semi-confluent flasks by initial washing with 3-5 mL pre-warmed (37 °C) D-PBS, and then incubated in 2-3 mL of Versene (1:5,000 DMSO, Invitrogen 15040-03) at 37 °C for 6 minutes. Cells are lifted by gentle agitation followed by addition of 10 mL DPBS. The resultant cell suspension was centrifuged (50 xg, 3 minutes) and the cell pellet was re-suspended in 3 mL of DPBS. The final cell suspension is adjusted such that the final cell concentration is as desired for the corresponding cell type. This suspension is added directly into the IonWorks™ prior to the start of the experiment.

#### hERG

The cell line stably expressing hERG was made by transfecting CHO K1 cells with 1.25 µg hERG cDNA per mL of cell culture medium as described by Jacobson and co-workers.<sup>271</sup>

The hERG cells were kept at 30 °C for 2–3 days prior to voltage clamp experiments and the final cell count was adjusted to  $0.5 \times 10^6$  cells per mL.



### hNav1.5

The cell line stably expressing hNav1.5 was created by transfecting CHO K1 cells with 4 µg hNav1.5 cDNA per mL of cell culture medium as described by Jacobson and co-workers.<sup>271</sup>

The hNav1.5 cells were seeded 2-3 days prior to voltage clamp experiments and the final cell count adjusted to  $1.0 \times 10^6$  cells per mL.

### I<sub>KS</sub>

CHO cells stably expressing human K<sub>v</sub>LQT1 plus minK sub-unit were used for voltage clamp experiments. Cells were seeded 2-3 days prior to voltage clamp experiments and the final cell count adjusted to  $1.0 \times 10^6$  cells per mL.

Cell line was obtained from Cytomyx (CYL3007), now Millipore.

### I<sub>to</sub>

CHO cells stably expressing human K<sub>v</sub>4.3/KChIP2.2 were used for voltage clamp experiments. The hERG cells were kept at 30 °C for 2–3 days prior to voltage clamp experiments and the final cell count was adjusted to  $1.0 \times 10^6$  cells per mL.

Cell line was obtained from CVGI, Mölndal.

#### **7.1.6.2 Experimental protocol for IonWorks HT system<sup>272</sup>**

Each sample was initially dissolved in DMSO to generate a 50 mM stock solution. These stock solutions were then serially diluted in DMSO to give 8 concentrations at half-log<sub>10</sub>-concentrations in a 96-well plate, which were used to determine dose-response curves. The source plate also contained a positive control and DMSO control to act as negative control (*Figure 71*). The source plate was then used to generate a series of PBS solutions in a 96-well plate (called the destination plate). This was achieved by transferring 3 µL of DMSO stock solutions from the source plate into 297 µL of PBS in the corresponding well of the destination plate (i.e. the result is a destination plate in which the DMSO stock solutions have been diluted 1:100 in PBS). The final dilution was then made during the IonWorks experiment in the Patchplate,

A boat containing the cell suspension and the PBS destination plate were placed in the machine. A 384-well PatchPlate was placed in the IonWorks above the ground electrode. From this point the experiment was started and progressed automatically.

Initially, the fluidics head (F-Head) (*Figure 70*) of the IonWorks system adds 3  $\mu$ L of PBS to each well of the PatchPlate, and then performs a 'hole test'. This allows any blocked holes to be detected. Subsequently, 3  $\mu$ L of the cell suspension was added to each of the 384-wells of the PatchPlate and the device then aims to seal a cell to the hole(s) at the bottom of each well. The underside of the PatchPlate is then exposed to the Amphotericin B (Saturating concentration (18-22mg/650 $\mu$ l DMSO) Sigma A4888) containing Access solution in order to obtain a perforated-patch whole-cell recording. The electronics head (E-head) of IonWorks then moves around all 384 wells of the PatchPlate to obtain pre-compound current measurements. The fluidics head (F-head) then adds 3  $\mu$ l of solution from each well of the compound plate to 4 wells on the PatchPlate. After approximately three minutes incubation, the E-head moves around all 384-wells of the PatchPlate to obtain post-compound current measurements. Thus, depending on the number of successful recordings in the four wells containing the same solution, between 0 and 4 data points were obtained.

Using this workflow four cell lines were investigated: hERG, Nav1.5,  $I_{KS}$  and  $I_{to}$ . For these cell lines individual voltage protocols were used to activate the channels, which are described below. The voltage protocol was applied pre-compound addition and currents were recorded. The compound was applied, and the cell membranes were not voltage-clamped during the incubation time. The voltage protocol was repeated post-compound addition. Compounds were tested at eight separate concentrations at half- $\log_{10}$  intervals. For each compound, the percentage inhibition is determined as a ratio of the pre- and post-compound current metric and is taken from up to 4 wells (depending on the success rate of the seal formation). Using  $n/N \geq 1/3$  from independent experiment repeats  $IC_{50}$  curves were generated.

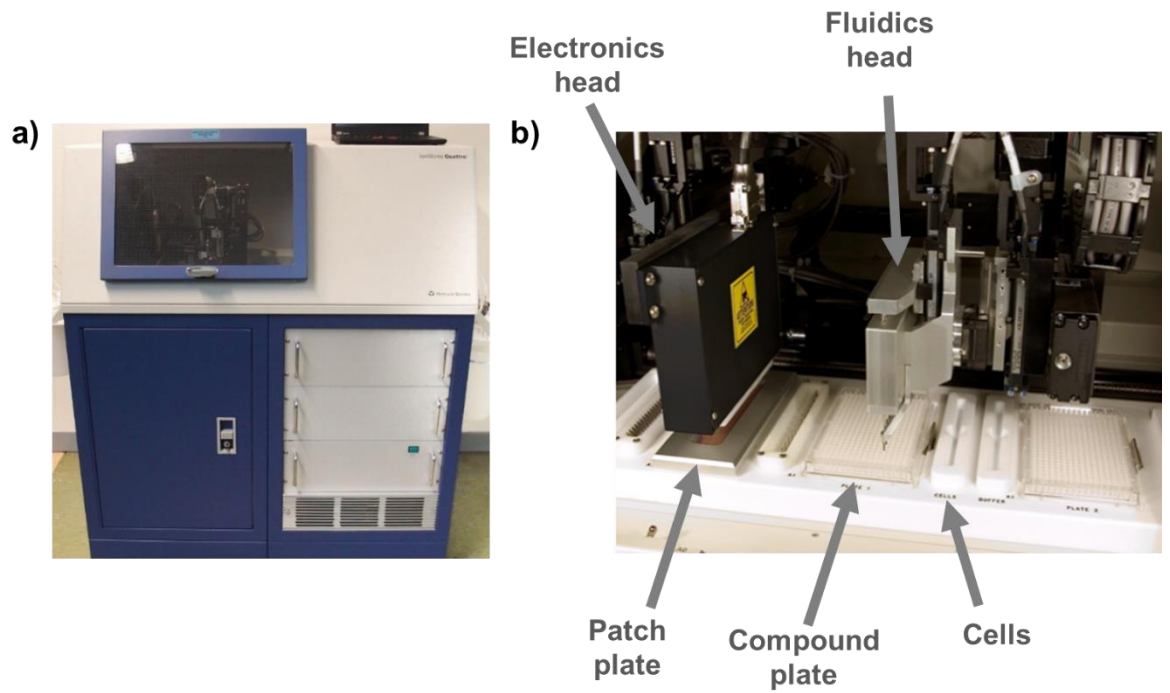


**Figure 70: The IonWorks Quattro instrument.** a) Photograph of the instrument b) photograph of the experimental deck inside the instrument, showing the electronic and fluidic heads, compound plates and PatchPlate PPC. Figures adapted from <sup>273</sup>

**a)**

**Test compound concentrations (mM)**

**Positive control  
(full curve)  
(mM)**

0.5 log<sub>10</sub>  
serial  
dilution  
(DMSO)

A	0.02	0.02	0.02	0.02	0.02	0.02	0.02	0.02	0.02	0.02	0.02	0.02	0.02	0.02	0.02	0.03	100% DMSO
B	0.05	0.05	0.05	0.05	0.05	0.05	0.05	0.05	0.05	0.05	0.05	0.05	0.05	0.05	0.05	0.1	100% DMSO
C	0.16	0.16	0.16	0.16	0.16	0.16	0.16	0.16	0.16	0.16	0.16	0.16	0.16	0.16	0.16	0.3	100% DMSO
D	0.5	0.5	0.5	0.5	0.5	0.5	0.5	0.5	0.5	0.5	0.5	0.5	0.5	0.5	0.5	1	100% DMSO
E	1.6	1.6	1.6	1.6	1.6	1.6	1.6	1.6	1.6	1.6	1.6	1.6	1.6	1.6	1.6	3	control
F	5	5	5	5	5	5	5	5	5	5	5	5	5	5	5	10	control
G	15.8	15.8	15.8	15.8	15.8	15.8	15.8	15.8	15.8	15.8	15.8	15.8	15.8	15.8	15.8	30	control
H	50	50	50	50	50	50	50	50	50	50	50	50	50	50	50	100	control
	1	2	3	4	5	6	7	8	9	10		11				12	

**b)**

	Test compounds ( $\mu\text{M}$ )	Positive control ( $\mu\text{M}$ )
A	0.05	0.1
B	0.16	0.3
C	0.53	1
D	1.67	3
E	5.2	10
F	16.7	30
G	53	100
H	167	330

**Figure 71: Compound dilutions.** **a)** Layout of the DMSO source plate showing concentrations in mM; **b)** final IC<sub>50</sub> concentrations of compounds tested and the positive control in the Patchplate. Where (positive) control compound refers to the reference compounds used: cisapride (hERG), flecainide (Na<sub>v</sub>1.5 and I<sub>to</sub>) and XE-991 (I<sub>Ks</sub>) (chemical structures shown in Section 2.3.2)

### 7.1.6.3 Voltage protocols

#### *hERG*

The *hERG* voltage protocol is as described by Persson *et al.*<sup>271</sup> Outward currents in *hERG* transfected cells were activated using a single voltage pulse of a one second depolarisation to +40 mV, followed by a two second repolarisation to –30 mV and finally a 500 ms step to –70 mV (Figure 72). Initially, a 20 s period holding at –70 mV and a 160 ms step to –60 mV was performed to obtain an estimate of leak. Currents were leak-subtracted based on the estimate of current evoked during the +10mV step at the start of the voltage pulse protocol.

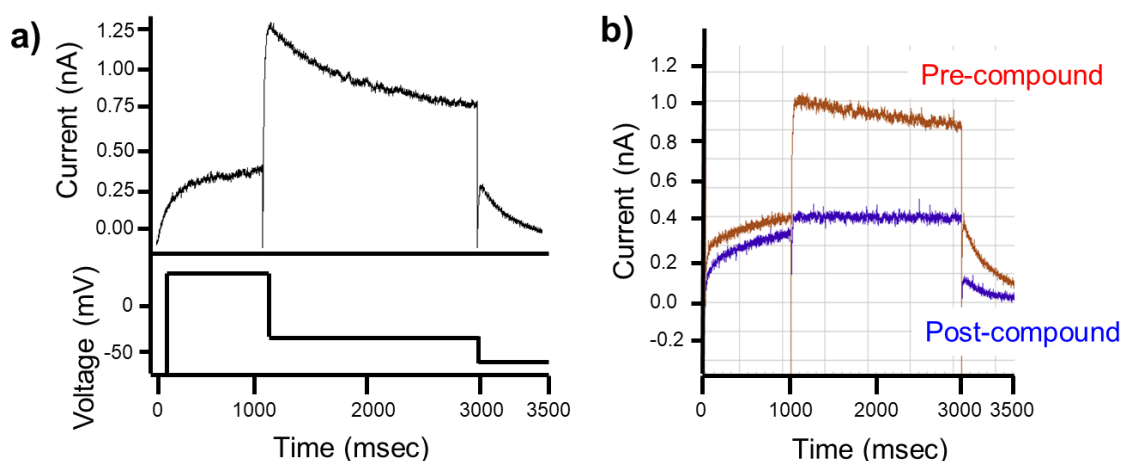


**Figure 72: *hERG* voltage protocol.** *a)* The voltage protocol (bottom) shown with the subsequent activation of *hERG* currents in CHO cells (top); *b)* Example data from an IonWorks assay using this voltage protocol, with pre-compound addition *hERG* currents shown in red and post-compound incubation *hERG* currents shown in blue.

#### *Duplex protocol*

Voltage protocols to activate Nav1.5 and hKv4.3-hKChIP2 ( $I_{to}$ ) currents were described by Persson *et al.*<sup>271</sup> Currents were activated in Nav1.5 transfected cells with a train of eight pulses from the holding potential –90 mV to –20 mV for 50 ms.  $I_{to}$  currents were evoked in cells expressing hKv4.3-hKChIP2 channels three pulses to +20 mV. These two protocols can be combined to independently activate and record currents from Nav1.5 and  $I_{to}$  during the same experiment. The  $I_{to}$  protocol can be applied directly after the Nav1.5 protocol to generate a ‘duplex’ protocol. Cells suspensions containing cells stably expressing Nav1.5 and hKv4.3-hKChIP2 ( $I_{to}$ ) are pre-mixed and added to the ‘cell boat’ in the IonWorks. This duplex protocol was used for all whole-cell patch recordings of Nav1.5 and  $I_{to}$ . The voltage protocol was applied pre-compound, and after three minutes of compound incubation.

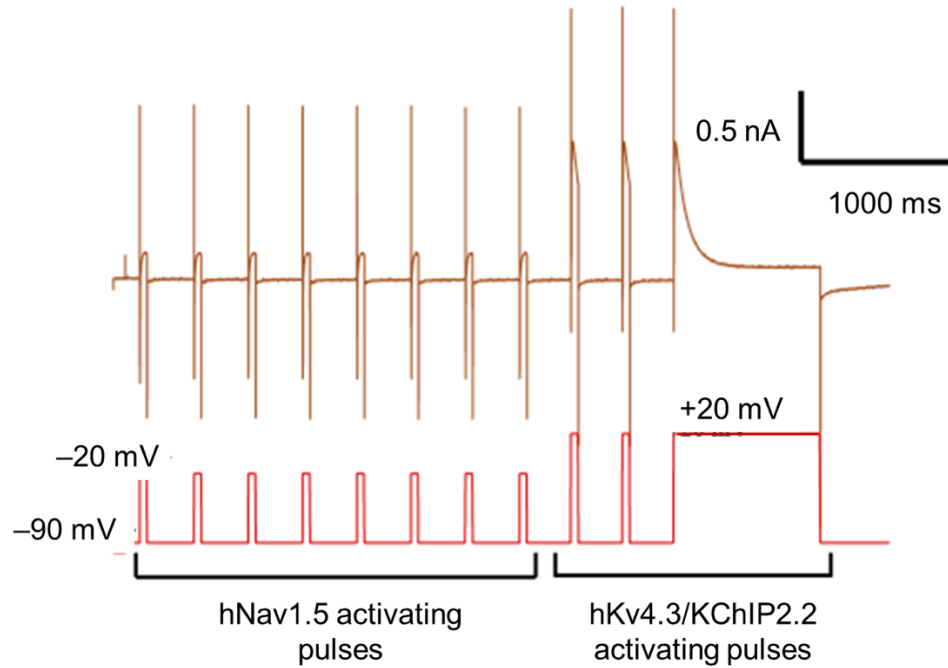


**Figure 73: Duplex voltage protocol;** *Nav1.5* and *I<sub>to</sub>* cells are mixed and independently activated and recorded. An eight-pulse sequence evoking the *Nav1.5* current is followed by three pulses to evoke the *I<sub>to</sub>* current.

#### *I<sub>KS</sub>* voltage protocol

Tristani-Firouzi and Sanguinetti describe a voltage protocol to evoke *KvLQT1* (*I<sub>KS</sub>*) channel currents.<sup>274</sup> Cells were initially voltage clamped at a holding potential of -80mV for 5 seconds, followed by a brief 100ms pulse to -90mV in order to measure the leak current. The slow outward *I<sub>KS</sub>* current was then evoked by a voltage step from the holding potential of -80mV to +40mV for 4000ms. The *I<sub>KS</sub>* current measurement was calculated by measuring the mean current towards the end of the pulse (3800-3900ms) and subtracting the mean current at the beginning of the pulse (110-150ms).

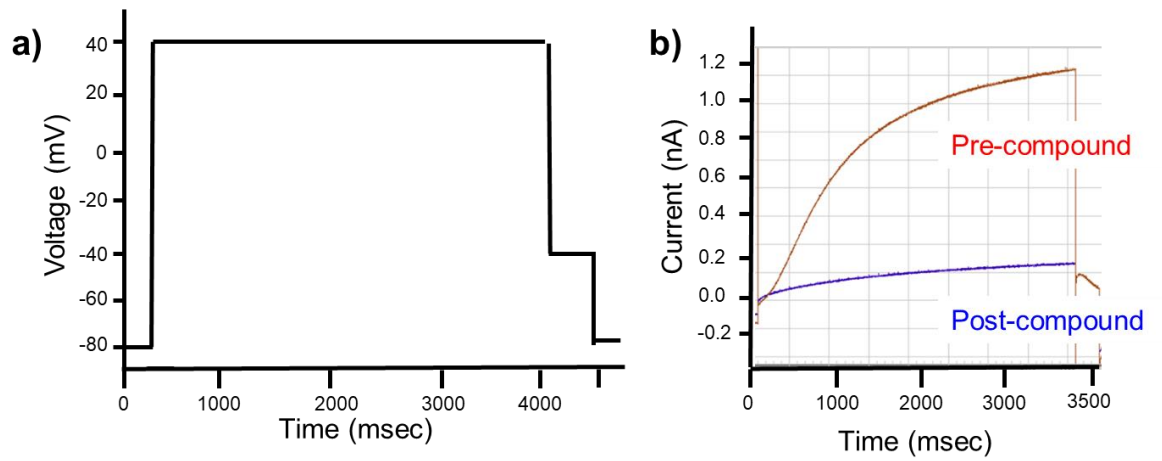


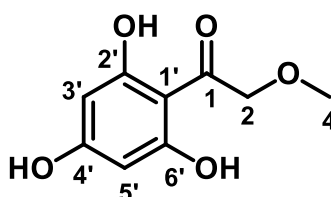
**Figure 74:  $I_{KS}$  voltage protocol; a)** Voltage protocol to evoke  $I_{KS}$  current; **b)** example current trace from an  $I_{KS}$  channel assay, where the red trace shows the current pre-compound and the blue trace shows the current after 3 minutes of compound incubation.

## 7.2 Experimental section for Chapter 3

Intracellular calcium measurements are explained in *Section 7.1.5*. Cardiac Safety assays are explained in *Section 7.1.6*.

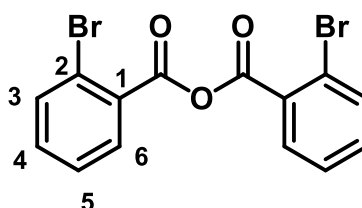
### 7.2.1 Organic synthesis

#### 2-methoxy-1-(2,4,6-trihydroxyphenyl)ethan-1-one, 71<sup>275</sup>



Phloroglucinol (2.5 g, 20.0 mmol) in dry diethyl ether (75 mL) was added to a stirred solution of aluminium chloride (11.0 g, 82.0 mmol) in DCM (40 mL) at  $-10\text{ }^{\circ}\text{C}$ . Methoxyacetyl chloride (2 mL) in ether (5 mL) was added dropwise to the stirred solution. The mixture was stirred at  $-10\text{ }^{\circ}\text{C}$  for 3-4 hr and then poured onto ice (70.0 g) and stirred in potassium sodium tartrate (50% in  $\text{H}_2\text{O}$ , 100 mL) for 1 hr. The aqueous layer was extracted with ether (4  $\times$  60 mL), the organic layers were combined, washed with water (2  $\times$  80 mL) and dried ( $\text{MgSO}_4$ ). The volatiles were evaporated *in vacuo* to yield the *title compound* as a yellow solid (0.92 g, 4.64 mmol, 23%); m.p. 154-155  $^{\circ}\text{C}$ ;  $R_f$  0.23 (75:25 EtOAc-Hexanes)  $\delta_{\text{H}}$  (300 MHz,  $d_6$ -DMSO) 12.18 (1H, s, OH), 10.43 (1H, s, OH), 8.95 (1H, s, OH), 5.81 (2H, app. s, 3'-CH and 5'-CH), 4.58 (2H, s, 2-CH<sub>2</sub>), 3.34 (3H, s, 4-CH<sub>3</sub>);  $\delta_{\text{C}}$  (125 MHz,  $d_6$ -DMSO) 164.9 (C=O), 164.0 (C-2' and C-6'), 158.9 (C-4'), 102.6 (C-1'), 94.5 (CH-3' or CH-5'), 94.0 (CH-3' or CH-5'), 77.0 (CH<sub>2</sub>-2), 58.5 (CH<sub>3</sub>-4);  $\nu_{\text{max}}/\text{cm}^{-1}$  (neat) 3280, 2920, 2852 and 1592; ESI-HRMS: calcd. for  $\text{C}_9\text{H}_{10}\text{O}_5$  [2M+Na]<sup>+</sup> 419.0964, found 419.0948. Data consistent with literature.

#### 2-bromobenzoyl 2-bromobenzoate, 68a<sup>204</sup>

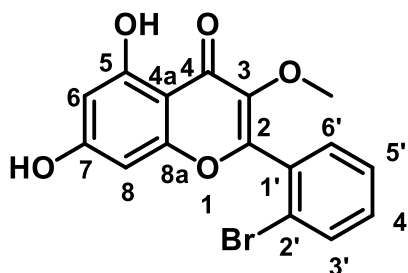


A solution of triethylamine (16 mL) in THF (14 mL) was added dropwise to a stirred solution of 2-bromobenzoic acid (8.21 g, 40.8 mmol) and methanesulfonyl chloride



(1.58 mL, 20.4 mmol) in THF (100 mL) at 0 °C. The resulting solution was allowed to warm to room temperature and stirred for 16 hr. The reaction mixture was concentrated *in vacuo*, NaHCO<sub>3</sub> (10% in H<sub>2</sub>O, 50 mL) was added and the aqueous layer was extracted with ethyl acetate (3 × 30 mL). The organic layers were combined and the volatiles evaporated *in vacuo* to yield the *title compound* as off-white crystals (7.41 g, 19.3 mmol, 95%); m.p. 70-71 °C; *R*<sub>f</sub> 0.29 (1:4 EtOAc–Hexanes) δ<sub>H</sub> (300 MHz, CDCl<sub>3</sub>) 8.07-7.93 (2H, m, 6-CH), 7.78-7.70 (2H, m, 3-CH), 7.48-7.40 (4H, m, 4-CH and 5-CH); δ<sub>C</sub> (125 MHz, CDCl<sub>3</sub>) 167.0 (C=O), 135.2 (CH-4 or CH-5), 134.3 (CH-4 or CH-5), 132.8 (CH-3), 130.1 (C-1), 127.7 (CH-6), 123.2 (C-2); ν<sub>max</sub>/cm<sup>-1</sup> (neat) 3064, 2982, 1784 and 1720; ESI-HRMS: calcd. for C<sub>14</sub>H<sub>8</sub>Br<sub>2</sub>O<sub>3</sub> [M+Na]<sup>+</sup> 404.8732 and 406.8712, found [M+Na]<sup>+</sup> 404.8747 and 406.8727. Data consistent with literature.

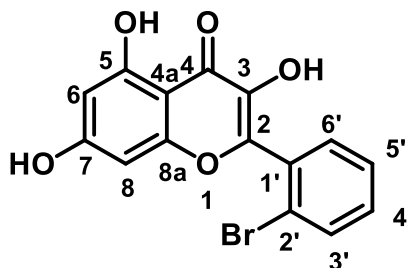
### 2-(2-bromophenyl)-5,7-dihydroxy-3-methoxy-4*H*-chromen-4-one, 77a



2-Bromobenzoic anhydride (2.33 g, 6.06 mmol) suspended in NEt<sub>3</sub> (5 mL) was added to 2-methoxy-1-(2,4,6-trihydroxyphenyl)ethan-1-one (400 mg, 2.02 mmol) and heated under reflux for 5 hr. The solution was allowed to cool to room temperature, followed by the addition of propanol (4 mL) and NaOH solution (2M, 5 mL) and refluxed for a further 14 hrs, forming an orange-brown solution. The solution was diluted with water (20 mL), followed by evaporation of the volatiles *in vacuo*. A solution of EtOH and water (1:1 v/v) was added to break up the precipitate that formed. Following this, saturation with cardice yielded a brown precipitate which was washed with cold water and dried over P<sub>2</sub>O<sub>5</sub> to yield the *title compound* as a pale brown solid (0.49 g, 1.38 mmol, 68%); m.p. 244-246 °C; *R*<sub>f</sub> 0.36 (1:3 EtOAc–hexanes); δ<sub>H</sub> (300 MHz, d<sub>6</sub>-DMSO) 12.47 (1H, s, OH), 11.00 (1H, s, OH), 7.83 (1H, dd, *J* 7.7, 1.5, 6'-CH), 7.68 (1H, dd, *J* 7.4 2.0, 3'-CH), 7.61-7.47 (2H, m, 4'-CH and 5'-CH), 6.38 (1H, d, *J* 2.0, 8-CH), 6.26 (1H, d, *J* 2.0, 6-CH), 3.68 (3H, s, O-CH<sub>3</sub>); δ<sub>C</sub> (125 MHz, d<sub>6</sub>-DMSO): 178.0 (C-4), 164.6 (C-7 or C-5), 161.4 (C-7 or C-5), 157.0 (C-8a or C-2), 156.6 (C-8a or C-2), 149.1 (C-3), 132.8 (CH-4' or CH-5' or CH-6'), 132.5 (CH-4' or CH-5' or CH-6'), 131.5 (CH-4' or CH-5' or CH-6'), 131.4 (C-1'), 127.9 (CH-3'), 122.1 (C-2'), 105.0 (C-4a), 98.9 (CH-6), 93.9 (CH-8), 60.25 (O-CH<sub>3</sub>); ν<sub>max</sub>/cm<sup>-1</sup> (neat) 3269,

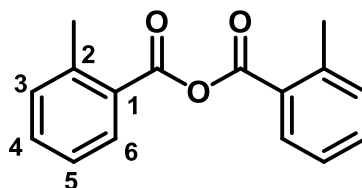
2973, 2931, 1742 and 1649; ESI-HRMS: calcd. for  $C_{16}H_{11}BrO_5$   $[M+Na]^+$  384.9682 and 386.9622, found 384.9697 and 386.9678.

### 2-(2-bromophenyl)-3,5,7-trihydroxy-4H-chromen-4-one, 78a (AM12)



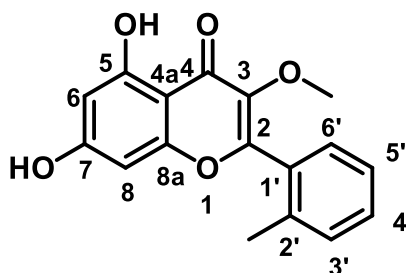
$BBr_3$  in DCM (1M, 0.63 mL) was added dropwise to a solution of 2-(2-bromophenyl)-5,7-dihydroxy-3-methoxy-4H-chromen-4-one (75.0 mg, 0.21 mmol) in DCM (10 mL) at 0 °C. The mixture was stirred for a further 1 hr at room temperature. The pH of the reaction mixture was confirmed to be pH 1 before quenching with water (30 mL) at 0 °C. The reaction mixture was diluted with DCM (30 mL), extracted with EtOAc (3 × 30 mL), washed with water (3 × 30 mL), dried ( $Na_2SO_4$ ) and the volatiles were evaporated *in vacuo* to yield a pale yellow solid. The crude product was purified by column chromatography ( $SiO_2$ ; eluting with 35:65 acetone–hexanes) to yield the *title compound* as a pale yellow solid (25 mg, 0.07 mmol, 33%); m.p. 245-246 °C;  $R_f$  0.30 (35:65 acetone–hexanes);  $\delta_H$  (300 MHz,  $d_6$ -acetone) 12.18 (1H, s, OH), 7.83 (1H, dd,  $J$  8.0, 1.3, 6'-CH), 7.74 (1H, dd,  $J$  7.5, 1.8, 3'-CH), 7.59 (1H, dd,  $J$  7.5, 1.3, 5'-CH or 4'-CH), 7.54-7.47 (1H, m, 5'-CH or 4'-CH), 6.44 (1H, d,  $J$  2.1, 8-CH), 6.31 (1H, d,  $J$  2.1, 6-CH);  $\delta_C$  (125 MHz,  $d_6$ -Acetone): 187.1 (C-4), 175.1 (C-7 or C-5), 168.3 (C-7 or C-5), 157.7 (C-8a or C-2), 148.1 (C-3), 134.1 (CH-4' or CH-5' or CH-6'), 133.0 (CH-4' or CH-5' or CH-6'), 132.8 (CH-4' or CH-5' or CH-6'), 132.6 (CH-1'), 128.5 (CH-3'), 124.6 (C-2'), 114.8 (C-4a), 109.3 (CH-6), 104.5 (CH-8) C-8a or C-2 not observed;  $\nu_{max}/cm^{-1}$  (solid state) 3228, 2961, 2922, 2850, 1709 and 1656. ESI-HRMS: calcd. for  $C_{15}H_9O_5Br$   $[M+H]^+$  348.9706 and 350.9686, found 348.9693 and 350.9675.

## 2-methylbenzoyl 2-methylbenzoate, 68b



Methanesulfonyl chloride (2.84 mL, 36.7 mmol) was added dropwise to a solution of 2-methylbenzoic acid (10.0 g, 73.5 mmol) in THF (100 mL) at 0 °C. A mixture of THF (14 mL) and Et<sub>3</sub>N (16 mL) was added dropwise to the solution and stirred for 1 hr at 0 °C. The solution was warmed to room temperature and stirred for a further 16 hr. The volatiles were evaporated *in vacuo*, and aqueous NaHCO<sub>3</sub> (10%, 50 mL) was added and the aqueous layer was extracted with EtOAc (3 × 75 mL). The organic layers were combined and washed with water (100 mL), brine (100 mL), dried (MgSO<sub>4</sub>) and the volatiles were evaporated *in vacuo* to yield a pale yellow oil, which cooled to form the *title compound* as pale yellow crystals (8.10 g, 32.1 mmol, 87%); *R*<sub>f</sub> 0.35 (1:9 EtOAc–hexanes); δ<sub>H</sub> (300 MHz, CDCl<sub>3</sub>) 8.06 (2H, dd, *J* 7.8, 1.4, 6-*CH*), 7.51 (2H, dd, *J* 7.5, 1.5, 4-*CH* or 5-*CH*), 7.35–7.31 (4H, m, 4-*CH* or 5-*CH* and 3-*CH*), 2.71 (6H, s, CH<sub>3</sub>); δ<sub>C</sub> (125 MHz, CDCl<sub>3</sub>) 162.9 (C=O), 142.6 (C-2), 133.7 (CH-3 or CH-4 or CH-5), 132.3 (CH-3 or CH-4 or CH-5), 131.5 (CH-3 or CH-4 or CH-5), 127.8 (C-1), 126.1 (CH-6), 22.0 (CH<sub>3</sub>); ν<sub>max</sub>/cm<sup>-1</sup> (neat) 3061, 2983, 2965, 1940, 1770 and 1715; ESI-HRMS: calcd. for C<sub>16</sub>H<sub>14</sub>O<sub>3</sub> [M+Na]<sup>+</sup> 277.0833, found 277.0835.

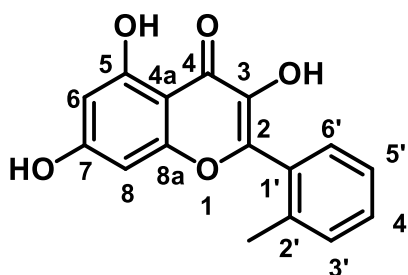
## 7-dihydroxy-3-methoxy-2-(2-methylphenyl)-4H-chromen-4-one, 77b



2-methoxy-1-(2,4,6-trihydroxyphenyl)ethan-1-one (350 mg, 1.76 mmol) and 2-methylbenzoyl 2-methylbenzoate (1.34 g, 5.30 mmol) were dissolved in NEt<sub>3</sub> (5 mL) and heated to reflux for 5 hrs. Upon cooling propanol (4 mL) and aqueous NaOH (2M, 5 mL) were added and the mixture was refluxed for 14 hours yielding an orange/brown solution. The solution was diluted with water (20 mL), and the volatiles were evaporated *in vacuo*, producing a solid residue, a mixture of EtOH and water (1:1 v/v) was added to break up the residue. Saturation with cardice yielded the *title compound*

as a pale brown solid which was dried over P<sub>2</sub>O<sub>5</sub> (90 mg, 0.30 mmol, 18%); m.p. 208-209 °C; *R*<sub>f</sub> 0.33 (3:7 EtOAc–hexanes); δ<sub>H</sub> (300 MHz, *d*<sub>6</sub>-DMSO): 12.58 (1H, s, OH), 7.52-7.45 (2H, m, 6'-CH and 3'-CH), 7.42-7.32 (2H, m, 4'-CH and 5'-CH), 6.37 (1H, d, *J* 2.1, 8-CH), 6.23 (1H, d, *J* 2.1, 6-CH), 3.62 (3H, s, Ar-CH<sub>3</sub>), 2.28 (3H, s, O-CH<sub>3</sub>); δ<sub>C</sub> (125 MHz, *d*<sub>6</sub>-DMSO) 178.3 (C=O), 165.0 (C-7 or C-5), 161.7 (C-7 or C-5), 158.2 (C-8a or C-2), 157.3 (C-8a or C-2), 139.1 (C-3), 137.1 (C-2'), 130.8 (CH-4' or CH-5' or CH-6'), 130.7 (CH-1'), 130.1 (CH-4' or CH-5' or CH-6'), 129.9 (CH-4' or CH-5' or CH-6'), 126.0 (CH-3'), 105.1 (C-4a), 99.2 (CH-6), 94.2 (CH-8), 60.3 (O-CH<sub>3</sub>), 19.6 (Ar-CH<sub>3</sub>); ν<sub>max</sub>/cm<sup>-1</sup> (neat) 3131, 2978, 1739 and 1646; ESI-HRMS: calcd. for C<sub>17</sub>H<sub>14</sub>O<sub>5</sub> [2M+Na]<sup>+</sup> 619.1575, found 619.1584.

### 3,5,7-trihydroxy-2-(2-methylphenyl)-4H-chromen-4-one, 78b (AM13)



7-Dihydroxy-3-methoxy-2-(2-methylphenyl)-4H-chromen-4-one (70.0 mg, 0.23 mmol) was suspended in DCM (10 mL) and cooled to 0 °C. BBr<sub>3</sub> in DCM (1.00 M, 0.70 mL) was added dropwise, the solution was allowed to warm to room temperature and stirred for a further 1 hr. The pH of the reaction mixture was confirmed to be pH 1 before quenching with water (30 mL) at 0 °C. The reaction mixture was diluted with DCM (30 mL), extracted with EtOAc (3 × 30 mL), washed with water (3 × 30 mL), dried (Na<sub>2</sub>SO<sub>4</sub>) and the volatiles were evaporated *in vacuo* to yield a pale yellow solid (59.3 mg). The crude product was purified by column chromatography (eluting with 3:7 ethyl acetate–hexane), and prep TLC (SiO<sub>2</sub>; eluting with 4:6 acetone–hexanes) to yield the *title compound* as a pale yellow solid (10.0 mg, 0.04 mmol, 15%); *R*<sub>f</sub> 0.33 (4:6 acetone–hexanes); δ<sub>H</sub> (300 MHz, *d*<sub>6</sub>-acetone): 12.22 (1H, s, OH), 9.89 (1H, s, OH), 7.61 (1H, dd, *J* 7.4, 1.4, 3'-CH) 7.47-7.32 (3H, m, 4'-H, 5'-CH and 6'-CH), 6.44 (1H, d, *J* 2.1, 8-CH), 6.30 (1H, d, *J* 2.1, 6-CH), 2.39 (3H, s, Ar-CH<sub>3</sub>); δ<sub>C</sub> (125 MHz, *d*<sub>6</sub>-acetone) 177.5 (C=O), 163.1 (C-7 or C-5), 162.8 (C-7 or C-5), 158.9 (C-8a or C-2), 157.9 (C-8a or C-2), 138.8 (C-3), 131.7 (CH-4' or CH-5' or CH-6'), 131.3 (CH-4' or CH-5' or CH-6'), 131.1 (CH-4' or CH-5' or CH-6'), 126.8 (CH-3'), 108.0 (C-1'), 105.2 (C-4a), 99.6 (CH-6), 94.9 (CH-8), 20.4 (Ar-CH<sub>3</sub>) C-2' not observed; ν<sub>max</sub>/cm<sup>-1</sup> (neat)

3324, 3078, 2953, 2919, 2850, 1732 and 1654; ESI-HRMS: calcd. for  $C_{16}H_{12}O_5$   $[M+H]^+$  285.0757, found 285.0750.

## 7.2.2 Chemicals and reagents

2-APB was dissolved in methanol and stored as a 10 mM stock solution. Galangin, apigenin, kaempferol, quercetin, myricetin, and luteolin were used as 10 mM stocks in ethanol for FlexStation experiments and as 50 mM stock solutions in DMSO for cardiac safety experiments.  $Gd^{3+}$  was used as an aqueous solution of  $GdCl_3$ .

## 7.2.3 Cell Culture

Details of TRPC5 cell line is explained in *Section 7.1.4*.

### TRPC3

HEK-293 cells stably expressing tetracycline-regulated human TRPC3 were prepared by Dr Melanie Ludlow. Inducible TRPC3 cells were maintained in DMEMF12 + GlutaMAX-1 (ThermoFisher Scientific) supplemented with 10% fetal calf serum (FCS) and penicillin/streptomycin at 37 °C in a 5% CO<sub>2</sub> incubator. For selection, 400  $\mu\text{g mL}^{-1}$  zeocin and 5  $\mu\text{g mL}^{-1}$  blasticidin S were included in the cell medium.

### TRPM2

HEK-293 cells stably expressing tetracycline-regulated human TRPM2 were prepared by Dr Melanie Ludlow, and have been described previously by McHugh *et al.*<sup>276</sup>

### TRPV4

TRPV4 was studied in CHO K1 cells stably expressing human TRPV4 and maintained in Ham's F12 (ThermoFisher Scientific) in the presence of 1  $\text{mg mL}^{-1}$  G418 (Sigma-Aldrich). TRPV4 cells were prepared by Dr Melanie Ludlow.

## 7.2.4 Manual electrophysiology

Manual electrophysiology experiments were performed by Dr Katsuhiko Muraki. Current recordings were made from outside-out configuration patch clamp at room temperature. Cells were seeded on glass coverslips at 20–30% density. Signals were amplified and sampled using an Axopatch 200B amplifier and pCLAMP 8 or 10 software (Molecular Devices). Data were filtered at 2 kHz and digitally sampled at

4 kHz. The voltage protocol comprised voltage ramps applied from  $-100$  to  $+100$  mV. The extracellular solution was SBS. The patch pipette solution contained the following: 135 mM CsCl, 2 mM MgCl<sub>2</sub>, 1 mM EGTA, 10 mM HEPES, 5 mM Na<sub>2</sub>ATP and 0.1 mM Na<sub>2</sub>GTP, titrated to pH 7.2 with NaOH. TRPC4 or TRPC5 cells were induced by tetracycline 24 h before experiments. For TRPC1–TRPC5 whole-cell recordings, HEK-293-MSR cells were transiently transfected with TRPC1-SYFP2 and TRPC5-mTurquoise2 according to the manufacturer's instructions, with the following modifications: 4.5  $\mu$ g of each construct and 5.5  $\mu$ L Lipofectamine®2000 (ThermoFisher Scientific) were used. Cells were transfected at 90–95% confluence in a 35 mm culture dish, and transfection was performed for 4 h. Patch clamp experiments were performed on the cells 24–48 hours post transfection.<sup>198</sup>

### **7.2.5 Rapid cyclic voltammetry experiments**

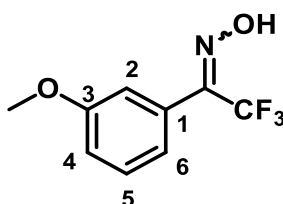
Experiments were performed in collaboration with Dr Shahrzad Mohamadi. A fabricated Pt/Hg electrode was contained in a flow cell and a constant flow of PBS passed over the electrode (flow rate 5-10 cm<sup>3</sup> min<sup>-1</sup>) maintained by a peristaltic pump. The peristaltic pump was used to flow compounds (all tested at 8 $\mu$ M) into the cell, following successful formation of a DOPC monolayer. The Pt/Hg electrode in the flow cell was connected to the PGSTAT12 potentiostat where the input voltage functions are applied through Scope™ software (AD Instruments). Capacitance current vs. potential profiles were monitored with Scope™ software using rapid cyclic voltammetry (RCV) at scan rate 40 V s<sup>-1</sup>. In the RCV experiments the fabricated Pt electrode was employed as a counter electrode and 3.5 mol dm<sup>-3</sup> KCl Ag/AgCl inserted into the flow cell was used as reference electrode. A blanket of argon gas was maintained above the control, sample electrolytes and DOPC dispersion, 20 minutes prior to experiments and maintained throughout the experiment; to exclude O<sub>2</sub>.

## 7.3 Experimental section for Chapter 4

Intracellular calcium measurements are explained in *Section 7.1.5*. Cell culture for WT HEK-293 and TRPC5 cell lines is described in *Section 7.1.4*.

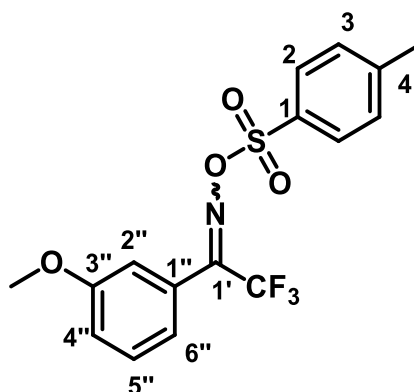
### 7.3.1 Organic synthesis

#### N-[2,2,2-trifluoro-1-(3-methoxyphenyl)ethylidene]hydroxylamine, **84**<sup>277</sup>



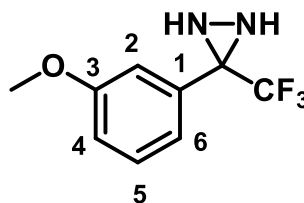
Hydroxylamine hydrochloride (340 mg, 4.90 mmol) was added to a stirred solution of 3'-methoxy-2,2,2-trifluoroacetophenone (500 mg, 2.45 mmol) in anhydrous EtOH (8 mL) and anhydrous pyridine (2 mL). The reaction mixture was under reflux for 18 hr, after which the reaction mixture was allowed to cool to room temperature and the solvents were evaporated *in vacuo*. The residue was dissolved in ether (30 mL), washed with water (2 × 20 mL), dried (MgSO<sub>4</sub>) and concentrated *in vacuo*, to yield a pale orange oil (557 mg, 2.54 mmol, quantitative)  $\delta_{\text{H}}$  (500 MHz, CDCl<sub>3</sub>) 7.39 (1H, app. t, *J* 8.0, 5-CH), 7.10 (1H, ddd, *J* 8.0, 1.9, 0.8, 4-CH), 7.07 (1H, app. t, *J* 1.9, 2-CH), 7.00 (1H, ddd, *J* 8.0, 1.9, 0.8, 6-CH), 3.83 (3H, s, CH<sub>3</sub>);  $\delta_{\text{C}}$  (125 MHz, CDCl<sub>3</sub>) 159.6 (C-3), 129.6 (CH-5), 128.6 (C-1), 121.2 (q, *J* 274.3, CF<sub>3</sub>), 120.9 (CH-4), 115.9 (CH-2), 114.3 (CH-6), 55.3 (C-H<sub>3</sub>) C=N-OH not observed,;  $\delta_{\text{F}}$  (235 MHz, CDCl<sub>3</sub>) -66.5;  $\nu_{\text{max}}/\text{cm}^{-1}$  (neat) 2837, 1595, 1343. Crude product taken forward with traces of pyridine in NMR. Data consistent with literature.

**[2,2,2-trifluoro-1-(3-methoxyphenyl)ethylidene]amino 4-methylbenzene-1-sulfonate, 85<sup>277</sup>**



*p*-Toluenesulfonyl chloride (3.83 g, 20.1 mmol) was added to a solution of N-[2,2,2-trifluoro-1-(3-methoxyphenyl)ethylidene]hydroxylamine (3.00 g, 14.7 mmol), DMAP (118 mg, 0.97 mmol) and anhydrous triethylamine (2.25 mL, 22.1 mmol) in DCM (70 mL) at 0 °C. The mixture was stirred for 3 hours, over which time it was allowed to warm to room temperature and stirred for 16 hr. The reaction mixture was washed with water (3 × 100 mL), dried (Na<sub>2</sub>SO<sub>4</sub>) and concentrated *in vacuo*. The crude material was purified by column chromatography (SiO<sub>2</sub>; hexanes-DCM 7:3) to yield the *title compound* as a pale yellow solid (5.02 g, 14.0 mmol, 96%). *R*<sub>f</sub> 0.19 (3:7 DCM:hexanes); δ<sub>H</sub> (400 MHz, CDCl<sub>3</sub>) 7.81 (2H, d, *J* 8.3, 2-*CH*), 7.35-7.26 (3H, m, 3-*CH*, 5''-*CH*), 6.98 (1H, dd, *J* 8.3, 2.0, 6''-*CH*), 6.83 (1H, app. d, *J* 8.3, 4''-*CH*), 6.81 (1H, t, *J* 2.0, 2''-*CH*), 3.75 (s, 3H, OCH<sub>3</sub>), 2.41 (s, 3H, CH<sub>3</sub>); δ<sub>C</sub> (100 MHz, CDCl<sub>3</sub>) 159.7 (C-3''), 154.1 (app. d, *J* 33.7, C-1'), 146.3 (C-1''), 131.4 (C-1), 130.2 (CH-5''), 130.0 (CH-2), 129.4 (CH-3), 125.8 (C-4), 120.7 (CH-4''), 119.0 (q, *J* 277.7, CF<sub>3</sub>), 117.4 (CH-6''), 114.1 (CH-2''), 55.6 (OCH<sub>3</sub>), 22.0 (CH<sub>3</sub>); δ<sub>F</sub> (235 MHz, CDCl<sub>3</sub>) -66.9; ν<sub>max</sub>/cm<sup>-1</sup> (neat) 2953, 1576, 1386, 1191; ESI-HRMS: calcd. for C<sub>16</sub>H<sub>14</sub>F<sub>3</sub>NO<sub>4</sub>SNa [M+Na]<sup>+</sup> 396.0488, found 396.0482. Data consistent with literature.

**3-(3-methoxyphenyl)-3-(trifluoromethyl)diaziridine, 86<sup>230</sup>**

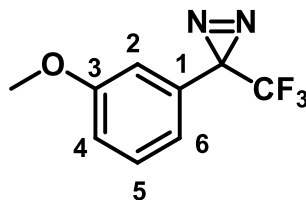


[2,2,2-trifluoro-1-(3-methoxyphenyl)ethylidene]amino 4-methylbenzene-1-sulfonate (1.60 g, 4.55 mmol) was dissolved in 7 M ammonia in methanol solution (15 mL) at



0 °C under a gaseous ammonia atmosphere. The reaction mixture was stirred vigorously to dissolve [2,2,2-trifluoro-1-(3-methoxyphenyl)ethylidene]amino 4-methylbenzene-1-sulfonate, whilst bubbling ammonia through the solution. The reaction mixture was allowed to warm to room temperature after 6 hr and stirred for a further 16 hr at room temperature. The reaction was left open to allow the ammonia to evaporate, sodium bicarbonate (sat. aq. soln., 2 mL) was added to the mixture and a white precipitate formed. The white precipitate was filtered off and the crude product was extracted with DCM (30 mL) and concentrated *in vacuo*. The crude material was purified by column chromatography (SiO<sub>2</sub>; hexanes-EtOAc 85:15) to give the title compound as a colourless oil (860 mg, 4.25 mmol, 94%) *R*<sub>f</sub> 0.37 (CH<sub>2</sub>Cl<sub>2</sub>-Hex 9:1); δ<sub>H</sub> (400 MHz, CDCl<sub>3</sub>) 7.34 (1H, app. t, *J* 8.0, 5-CH), 7.20 (1H, ddd, *J* 8.0, 2.1, 0.9, 6-CH), 7.15 (1H, app. t, *J* 2.1, 2-CH), 6.98 (1H, ddd, *J* 8.0, 2.1, 0.9, 4-CH), 3.83 (3H, s, O-CH<sub>3</sub>), 2.79 (1H, d, *J* 8.8, NH), 2.26 (1H, d, *J* 8.8, NH); δ<sub>C</sub> (100 MHz, CDCl<sub>3</sub>) 159.7 (C-3), 133.0 (C-1), 129.9 (CH-5), 123.5 (q, *J* 278.4, CF<sub>3</sub>), 120.3 (CH-6), 115.8 (CH-4), 113.6 (CH-2), 58.0 (app. d, *J* 36.1, diaziridine-C) 55.4 (O-CH<sub>3</sub>); δ<sub>F</sub> (235 MHz, CDCl<sub>3</sub>) -75.48; ν<sub>max</sub>/cm<sup>-1</sup> (neat) 3254, 1604, 1586, 1458, 1394, 1215, 1134; ESI-HRMS: calcd. for C<sub>9</sub>H<sub>10</sub>F<sub>3</sub>N<sub>2</sub>O [M+H] 219.0740, found 219.0675. Data consistent with literature.

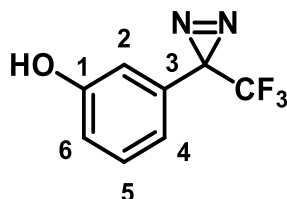
### 3-(3-methoxyphenyl)-3-(trifluoromethyl)-3H-diazirine, 87<sup>227</sup>



3-(3-methoxyphenyl)-3-(trifluoromethyl)diaziridine (1.6 g, 7.30 mmol) was dissolved in MeOH (10 mL) and stirred at 0 °C for 5 min. Triethylamine (1.5 mL, 11.0 mmol) was added to the reaction mixture and stirring continued for 5 min. Small portions of iodine (2.22 g in total, 8.76 mmol) were added until a deep red colour persisted. EtOAc (5 mL) was added to the solution and the mixture was washed with 1M HCl (15 mL), sodium thiosulfate aq. solution (10% w/w, 3 x 10 mL or until solution turns colourless) brine (15 mL), dried (Na<sub>2</sub>SO<sub>4</sub>) and concentrated *in vacuo* to yield the title compound as a pale yellow oil (1.35g, 6.25 mmol, 86%); *R*<sub>f</sub> 0.10 (Hex-EtOAc 9:1); δ<sub>H</sub> (500 MHz, CDCl<sub>3</sub>) 7.31 (1H, app. t, *J* 8.1, 5-CH) 6.95 (1H, dd, *J* 8.1, 2.1, 4-CH), 6.78 (1H, app d, *J* 8.1, 6-CH), 6.70 (1H, d, *J* 2.1, 2-CH), 3.81 (3H, s, O-CH<sub>3</sub>); δ<sub>C</sub> (125 MHz, CDCl<sub>3</sub>) 159.9 (C-3), 130.7 (C-1), 129.9 (CH-5), 122.5 (q, *J* 274.6, CF<sub>3</sub>), 118.9 (CH-6), 115.4 (CH-4), 112.4 (CH-2), 55.5 (O-CH<sub>3</sub>) 28.6 (app d., *J* 36.1, diazirine-C); δ<sub>F</sub> (235 MHz,

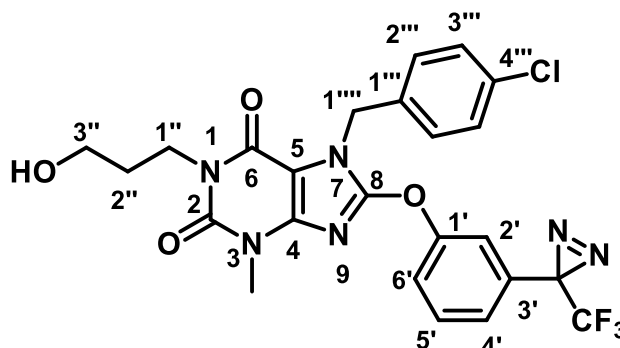
$\text{CDCl}_3$ ) -65.20;  $\nu_{\text{max}}/\text{cm}^{-1}$  (neat) 2840, 1693, 1583, 1211 ; ESI-HRMS: calcd. for  $\text{C}_9\text{H}_8\text{F}_3\text{N}_2\text{O}$   $[\text{M}+\text{H}]$  217.0583, found 217.0599. Data consistent with literature.

**3-[3-(trifluoromethyl)-3H-diazirin-3-yl]phenol, 88**<sup>231</sup>



$\text{BBr}_3$  (1.0 M in DCM, 7.40 mL, 7.40 mmol) was added dropwise to a solution of 3-(3-methoxyphenyl)-3-(trifluoromethyl)-3H-diazirine (0.82 g, 3.70 mmol) in DCM (10 mL) over 5 minutes, at 0 °C. The reaction mixture was stirred for 2 hours at 0 °C, then allowed to warm to room temperature and stirred for a further 12 hours. Water was added to the mixture and the organic compounds were extracted with diethyl ether (3 × 20 mL). The combined organic layers were washed with water (3 × 20 mL) and brine (20 mL), the ethereal layer was dried ( $\text{Na}_2\text{SO}_4$ ) and concentrated *in vacuo* to yield the title compound as a brown oil (754 mg, 3.70 mmol, quantitative).  $R_f$  0.19 (Hex-EtOAc 9:1);  $\delta_{\text{H}}$  (500 MHz,  $\text{CDCl}_3$ ) 7.26 (1H, t,  $J$  8.0, 5-CH), 6.88 (1H, dd,  $J$  8.0, 2.1, 6-CH), 6.73 (1H, dd,  $J$  8.0, 2.1, 4-CH), 6.67 (1H, t,  $J$  2.1, 2-CH);  $\delta_{\text{C}}$  (125 MHz,  $\text{CDCl}_3$ )  $\delta$  155.9 (C-1), 131.0 (C-3), 130.4 (CH-5), 122.2 (d,  $J$  274.9,  $\text{CF}_3$ ), 120.8 (CH-4), 118.1 (CH-6), 113.7 (CH-2), 28.4 (q,  $J$  40.4, diazirine-C);  $\delta_{\text{F}}$  (235 MHz,  $\text{CDCl}_3$ ) -71.6;  $\nu_{\text{max}}/\text{cm}^{-1}$  (neat) 3329, 1693, 1588, 1199 ; ESI-HRMS could not be obtained. Data consistent with literature.

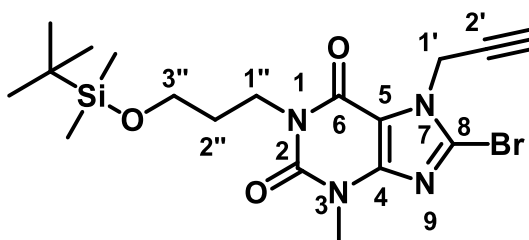
**7-[(4-chlorophenyl)methyl]-1-(3-hydroxypropyl)-3-methyl-8-{3-[3-(trifluoromethyl)-3H-diazirin-3-yl]phenoxy}-2,3,6,7-tetrahydro-1H-purine-2,6-dione, 81 (Pico145-DA)**



$\text{Cs}_2\text{CO}_3$  (286 mg, 0.81 mmol) was added to a solution of 8-bromo-7-[(4-chlorophenyl)methyl]-1-(3-hydroxypropyl)-3-methyl-2,3,6,7-tetrahydro-1H-purine-2,6-dione<sup>59</sup> (289 mg, 0.67 mmol) in DMF (6 mL). After 5 minutes, 3-[3-(trifluoromethyl)-3H-diazirin-3-yl]phenol (150 mg, 0.74 mmol) was added to the reaction mixture, and the reaction mixture was heated to 40 °C for 1 hour. The mixture was cooled, partitioned between EtOAc (10 mL) and water (10 mL). The organics were washed with LiCl (1 M aq. solution, 3 × 10 mL), dried ( $\text{Na}_2\text{SO}_4$ ) and concentrated *in vacuo* to yield the title compound (220.7 mg, 40.2 mmol, 60%);  $R_f$  0.18 (7:3 EtOAc:hexanes);  $\delta_H$  (400 MHz,  $\text{CDCl}_3$ ) 7.39 (1H, app. t,  $J$  8.1, 5'-CH), 7.33 (2H, d,  $J$  8.5, 3'''-CH), 7.26 (3H, d,  $J$  8.5, 2'''-CH and 6'-CH), 7.13 (1H, app. s, 2'-CH), 7.01 (1H, dd,  $J$  8.1, 1.8, 4'-CH), 5.35 (2H, s, 1'''-CH<sub>2</sub>), 4.13 (2H, t,  $J$  6.1, 1''-CH<sub>2</sub>), 3.46 (2H, t,  $J$  5.7, 3''-CH<sub>2</sub>), 3.37 (3H, s, CH<sub>3</sub>) 1.83 (2H, tt,  $J$  5.7, 6.1, 2''-CH<sub>2</sub>);  $\delta_C$  (100 MHz,  $\text{CDCl}_3$ ) 155.4 (C-6), 153.3 (C-8), 153.1 (C-1'), 151.8 (C-2), 146.4 (C-4), 134.7 (C-4'''), 134.3 (C-1'''), 131.4 (C-3'), 130.6 (CH-5'), 129.7 (CH-2'''), 129.3 (CH-3'''), 124.0 (CH-4'), 122.0 (app. d,  $J$  274.7, CF<sub>3</sub>), 121.6 (CH-6'), 118.2 (CH-2''), 103.1 (C-5), 58.7 (CH<sub>2</sub>-3''), 46.8 (CH<sub>2</sub>-1'''), 37.9 (CH<sub>2</sub>-1''), 31.0 (CH<sub>2</sub>-2''), 30.1 (CH<sub>3</sub>) 28.4 (app. d,  $J$  40.4, diazirine-C);  $\delta_F$  (235 MHz,  $\text{CDCl}_3$ ) -65.11;  $\nu_{\text{max}}/\text{cm}^{-1}$  (neat) 3536, 1890, 1699, 1649, 1579, 1320; ESI-HRMS: calcd. for  $\text{C}_{24}\text{H}_{21}\text{ClF}_3\text{N}_6\text{O}_4$   $[\text{M}+\text{H}]^+$  549.1259 and 551.1230 found 549.1266 and 551.1241. HPLC: RT = 1.93 min.

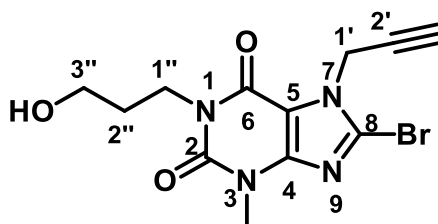
*NMR and HPLC data shown in Appendix VI*

**8-bromo-1-{3-[(tert-butyldimethylsilyl)oxy]propyl}-3-methyl-7-(prop-2-yn-1-yl)-2,3,6,7-tetrahydro-1H-purine-2,6-dione, 92**



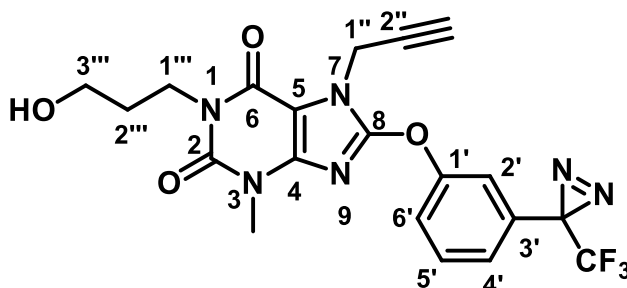
Propargyl bromide (80% in toluene, 1.36 mL, 12.2 mmol) was added to a solution of 8-bromo-3-methyl-1H-purine-2,6(3H,7H)-dione (3 g, 12.2 mmol) and N,N-diisopropylethylamine (2.14 mL, 12.2 mmol) in DMF (25 mL) and the reaction mixture was stirred for 16 hr. Water was added to the reaction mixture and the crude product was isolated by filtration, washed with water (10 mL), ethanol (10 mL) and ether (10 mL). The crude product was carried forward without purification. All crude material ('12.2 mmol') was dissolved in DMF (30 mL), K<sub>2</sub>CO<sub>3</sub> (1.6 g, 12.2 mmol) and (3-Bromopropoxy)-tert-butyldimethylsilane (2.97 g, 12.2 mmol) was added and the mixture stirred at 60 °C for 16hr. The reaction mixture was poured into H<sub>2</sub>O and the organics extracted with EtOAc (4 × 100 mL), washed with LiCl (1M aq. solution, 2 × 50 mL), brine (50 mL) and dried (Na<sub>2</sub>SO<sub>4</sub>) and concentrated *in vacuo*. The crude material was purified by column chromatography (SiO<sub>2</sub>; hexanes-EtOAc 95:5 →1:1) to yield the title compound as a white solid (3.8 g, 8.3 mmol, 67%). *R*<sub>f</sub> 0.32 (7:3 hexanes:EtOAc); δ<sub>H</sub> (400 MHz, CDCl<sub>3</sub>) 5.15 (2H, d, *J* 2.5, 1'-CH<sub>2</sub>), 4.07 (2H, t, *J* 7.2, 1''-CH<sub>2</sub>), 3.69 (2H, t, *J* 6.2, 3''-CH<sub>2</sub>), 3.51 (3H, s, CH<sub>3</sub>), 2.38 (1H, t, *J* 2.5, alkyne-CH), 1.85 (2H, tt, *J* 7.2, 6.2, 2''-CH<sub>2</sub>), 0.84 (9H, s, tert-butyl-CH), 0.00 (6H, s, dimethyl-CH<sub>3</sub>); δ<sub>C</sub> (100 MHz, CDCl<sub>3</sub>) 154.1 (C-6), 151.0 (C-2), 148.2 (C-4), 127.4 (C-8), 108.5 (C-5), 75.7 (C-2'), 74.3 (CH-alkyne), 61.3 (CH<sub>2</sub>-3''), 39.4 (CH<sub>2</sub>-1''), 36.5 (CH<sub>2</sub>-1'), 31.0 (CH<sub>2</sub>-2''), 29.8 (CH<sub>3</sub>), 25.9 (C-tert-butyl), 18.3 (C-quaternary-tert-butyl), 0.0 (C-dimethyl); ν<sub>max</sub>/cm<sup>-1</sup> (neat) 3232, 1665, 1609, 1379, 658; ESI-HRMS: calcd. for C<sub>18</sub>H<sub>27</sub>BrN<sub>4</sub>O<sub>3</sub>SiNa [M+Na] 477.0928, 479.0908, found 477.0920, 479.0902.

**8-bromo-1-(3-hydroxypropyl)-3-methyl-7-(prop-2-yn-1-yl)-2,3,6,7-tetrahydro-1H-purine-2,6-dione, 93**



8-bromo-1-{3-[(tert-butyldimethylsilyl)oxy]propyl}-3-methyl-7-(prop-2-yn-1-yl)-2,3,6,7-tetrahydro-1H-purine-2,6-dione (1g, 2.2 mmol) and HCl (conc.aq solution, 4 mL) were suspended in EtOH (20 mL) and refluxed for 1.5 hrs. The reaction mixture was concentrated *in vacuo* and the crude material was triturated (Et<sub>2</sub>O), filtered and washed with Et<sub>2</sub>O (2 × 5 mL) and concentrated *in vacuo* to yield the title compound as a white solid (682 mg, 1.99 mmol, 91 %).  $\delta_{\text{H}}$  (400 MHz, CDCl<sub>3</sub>) 5.18 (2H, d, *J* 2.5, 1'-CH), 4.19 (2H, t, *J* 5.8, 1''-CH<sub>2</sub>), 3.56 (3H, s, CH<sub>3</sub>) 3.54 (2H, t, *J* 5.7, 3''-CH<sub>2</sub>), 2.43 (1H, t, *J* 2.5, alkyne-H), 1.90 (2H, tt, *J* 5.8, 5.7 2''-CH<sub>2</sub>)  $\delta_{\text{C}}$  (100 MHz, CDCl<sub>3</sub>) 154.8 (C-6), 151.5 (C-2), 148.6 (C-4), 128.4 (C-8), 108.4 (C-5), 75.5 (C-2'), 74.6 (CH-alkyne), 58.8 (CH<sub>2</sub>-3''), 38.2 (CH<sub>2</sub>-1''), 36.6 (CH<sub>2</sub>-2''), 35.6 (CH<sub>2</sub>-1'), 30.2 (CH<sub>3</sub>);  $\nu_{\text{max}}/\text{cm}^{-1}$  (neat) 3227, 2953, 1698, 1655, 1381, 664; ESI-HRMS: calcd. for C<sub>12</sub>H<sub>13</sub>BrN<sub>4</sub>O<sub>3</sub>Na [M+Na] 363.0063, 365.0043, found 363.0057, 365.0037.

**1-(3-hydroxypropyl)-3-methyl-7-(prop-2-yn-1-yl)-8-{3-[3-(trifluoromethyl)-3H-diazirin-3-yl]phenoxy}-2,3,6,7-tetrahydro-1H-purine-2,6-dione, 82 (Pico145-DAAIk)**

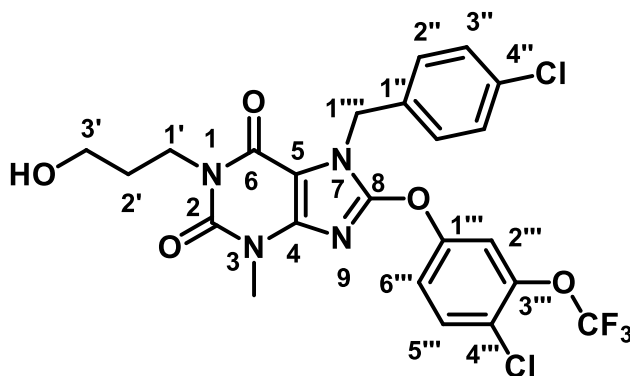


Cs<sub>2</sub>CO<sub>3</sub> (381 mg, 1.08 mmol) was added to a solution of 8-bromo-1-(3-hydroxypropyl)-3-methyl-7-(prop-2-yn-1-yl)-2,3,6,7-tetrahydro-1H-purine-2,6-dione (307 mg, 0.90 mmol) in DMF (8 mL). After 5 minutes, 3-[3-(trifluoromethyl)-3H-diazirin-3-yl]phenol (200 mg, 0.99 mmol) was added to the reaction mixture, and the reaction mixture was heated to 40 °C for 1 hour. The mixture was cooled, partitioned between EtOAc (10 mL) and water (10 mL). The organics were washed with LiCl (1 M aq.

solution, 3 × 10 mL), dried (Na<sub>2</sub>SO<sub>4</sub>) and concentrated *in vacuo*. The crude material was purified by column chromatography (SiO<sub>2</sub>; eluting with 3:7 EtOAc:hexanes) to yield the *title compound* as an off-white solid (135 mg, 0.30 mmol, 33%). *R*<sub>f</sub> 0.28 (3:7 EtOAc:hexanes); δ<sub>H</sub> (600 MHz, CDCl<sub>3</sub>) 7.48 (1H, t, *J* 7.7, 5'-CH), 7.43 (1H, dd, *J* 7.7, 2.1 6'-CH), 7.30 (1H, t, *J* 2.1, 2'-CH), 7.09 (1H, app. d, *J* 7.7, 4'-CH), 5.11 (2H, d, *J* 2.5, 1''-CH<sub>2</sub>), 4.19 (2H, t, *J* 6.2, 1'''-CH<sub>2</sub>), 3.54 (2H, td, *J* 6.1, 5.7, 3'''-CH<sub>2</sub>), 3.46 (3H, s, CH<sub>3</sub>), 2.40 (1H, d, *J* 2.5, alkyne-*H*), 1.91 (3H, tt, *J* 6.2, 5.7, 2'''-CH<sub>2</sub>); δ<sub>C</sub> (150 MHz, CDCl<sub>3</sub>) 155.3 (C-6) 153.3 (C-8) 153.1 (C-1' or C-3') 151.8 (C-2) 150.5 (C-1' or C-3') 146.4 (C-4), 131.3 (C-5), 130.5 (CH-4'), 124.0 (CH-6'), 122.0 (app. d, *J* 275.0, CF<sub>3</sub>), 121.3 (CH-2'), 118.4 (C-5'), 102.9 (C-2''), 73.9 (CH-alkyne), 58.7 (CH<sub>2</sub>-3'''), 37.9 (CH<sub>2</sub>-1'''), 33.5 (CH<sub>2</sub>-1''), 31.0 (CH<sub>2</sub>-2'''), 30.1 (CH<sub>3</sub>), 28.4 (app. d, *J* 40.5, C-diazirine); δ<sub>F</sub> (235 MHz, CDCl<sub>3</sub>) 65.0; ν<sub>max</sub>/cm<sup>-1</sup> (neat); 3235, 2938, 1655, 1635, 1586, 1345; ESI-HRMS: calcd. for C<sub>20</sub>H<sub>18</sub>F<sub>3</sub>N<sub>6</sub>O<sub>4</sub> [M+H]<sup>+</sup> 485.1156, found 485.1154. HPLC: RT = 0.85 min.

*NMR and HPLC data shown in Appendix VI*

**8-[4-chloro-3-(trifluoromethoxy)phenoxy]-7-[(4-chlorophenyl)methyl]-1-(3-hydroxypropyl)-3-methyl-2,3,6,7-tetrahydro-1H-purine-2,6-dione, 98 (AM237)<sup>65</sup>**



4-Chloro-3-(trifluoromethyl)phenol (127 mg, 0.64 mmol) was added to a suspension of 8-bromo-7-[(4-chlorophenyl)methyl]-1-(3-hydroxypropyl)-3-methyl-2,3,6,7-tetrahydro-1H-purine-2,6-dione<sup>59</sup> (250 mg, 0.59 mmol) and K<sub>2</sub>CO<sub>3</sub> (162 mg, 1.17 mmol) in DMF (3.5 mL) and the reaction mixture was stirred at 80 °C for 4 hours. After cooling to room temperature, the reaction mixture was diluted with water (30 mL) and extracted with EtOAc (30 mL, then 3 × 20 mL). The combined organic layers were washed with aqueous LiCl solution (1M aq. solution 3 × 20 mL), brine (20 mL), dried (Na<sub>2</sub>SO<sub>4</sub>) and concentrated *in vacuo*. The crude material was purified by column chromatography (SiO<sub>2</sub>; eluting with 2:8 EtOAc:hexanes) to yield the *title compound*

as an off-white solid (152 mg, 0.27 mmol, 46%).  $R_f$  0.35 (2:8 EtOAc:hexanes);  $\delta_H$  (400 MHz,  $CDCl_3$ ) 7.51 (1H, d,  $J$  8.9, 5'''-CH), 7.40 (1H, d,  $J$  2.8, 2'''-CH), 7.38 (2H, d,  $J$  8.4, 3'''-CH), 7.30 (2H, d,  $J$  8.4, 2'''-CH), 7.20 (1H, dd,  $J$  8.9, 2.8, 6'''-CH), 5.41 (2H, s, 1''''-CH<sub>2</sub>) 4.17 (2H, t,  $J$  5.4, 1'-CH<sub>2</sub>), 3.52 (2H, t,  $J$  5.9, 3'-CH<sub>2</sub>), 3.42 (3H, s, CH<sub>3</sub>) 1.88 (2H, tt,  $J$  5.9, 5.4 2'-CH<sub>2</sub>);  $\delta_C$  (100 MHz,  $CDCl_3$ ) 155.3 (C-6), 152.6 (C-8), 151.6 (C-2), 146.2 (C-4), 145.4 (C-1'''), 134.7 (C-4''), 134.1 (C-1''), 131.4 (CH-5'''), 129.9 (C-4'''), 129.8 (CH-2''), 129.3 (CH-3''), 124.7 (C-5), 120.43 (q,  $J$  260.3, CF<sub>3</sub>), 119.2 (CH-6'''), 114.9 (CH-2'''), 103.1 (C-3'''), 58.7 (CH<sub>2</sub>-1'), 46.8 (CH<sub>2</sub>-1'''), 37.9 (CH<sub>2</sub>-3'), 31.0 (CH<sub>2</sub>-2'), 30.0 (CH<sub>3</sub>)  $\delta_F$  (235 MHz,  $CDCl_3$ ) -57.9;  $\nu_{max}/cm^{-1}$  (neat); 3495, 1891, 1693, 1652; ESI-HRMS: calcd. for C<sub>23</sub>H<sub>20</sub>Cl<sub>2</sub>F<sub>3</sub>N<sub>4</sub>O<sub>5</sub> [M+H]<sup>+</sup> 559.0757 and 561.0278, found 559.0766 and 561.0727. HPLC: RT = 1.99 min.

*NMR and HPLC data shown in Appendix IV*

### 7.3.2 Solutions

*NP-40 lysis buffer:* 10 mM Tris, pH 7.4, 150 mM NaCl, 0.5 mM EDTA, 0.5% Nonidet P40 substitute, protease inhibitor cocktail (Sigma) and phosphatase inhibitor cocktail (Sigma).

*Triton X-100 lysis buffer:* 1 x PBS, 0.1% SDS, 1% TritonX-100, 1 EDTA-free protease inhibitor cocktail.

*DDM-CHS lysis buffer:* 1% Dodecyl Maltoside (DDM), 0.1% Cholesteryl Hemisuccinate (CHS), 100 nM NaCl, 20 mM TRis pH7.5, EDTA free protease inhibitor cocktail (Thermo Scientific)

*TGS-T running buffer:* 25 mM Tris, 192 mM Glycine, 0.1% (w/v) SDS, pH 8.3

*Dilution buffer:* 10 mM Tris/Cl pH7.5, 150 mM NaCl, 0.5 mM EDTA.

*Coomassie Blue Stain:* (45% (v/v) methanol, 10% (v/v) acetic acid, 0.25% (w/v) Coomassie Brilliant Blue R-250)

*De-stain solution:* (30% (v/v) methanol, 10% acetic acid)

*WET transfer buffer:* 48 mM Tris/Trizma-base, 39 mM glycine, 20% methanol, 0.05% SDS

### 7.3.3 Chemicals and reagents

Azide-fluor-545 and Tris(benzyltriazolylmethyl)amine (TBTA) were prepared as 10 mM stock solutions in DMSO. CuSO<sub>4</sub> and tris(2-carboxyethyl)phosphine (TCEP)

were prepared as 50 mM stock solutions in degassed double-distilled water. All click reagents were made up fresh on the day of experimentation.

### 7.3.4 Cell Culture

#### TRPC4/5-SYFP2

To facilitate cloning of TRPC4-SYFP2 and TRPC5-SYFP2, a four amino acid linker (ASAS) flanked by AgeI and SacII restriction sites was introduced into the pcDNA™4/TO expression vector (ThermoFisher Scientific, Waltham, MA, USA) between EcoRI and XhoI restriction sites using Gibson Assembly® (New England Biolabs, Ipswich, MA, USA) (forward oligonucleotide: 5' CCACTAGTCCAGTGTGGTGGGAATTCACCGGTGCCAGCGCATCCCGC 3', and reverse oligonucleotide: 5' GTTTAAACGGGCCCTCTAGACTCGAGCCGCGGGATGCGCTGGCACC 3').<sup>198</sup>

Human TRPC4β, including an N-terminal Kozak sequence, was inserted between BamHI and AgeI restriction sites using hTRPC4β/pcDNA4/TO<sup>21</sup> as a PCR template (forward primer, 5' AGTCGGATCCGCCACCATGGCTCAGTTCTATTACAAAAG 3'; reverse primer, 5' AGTTACCGGTCAATCTTGTGGTCACGTAATCTTC 3').<sup>22</sup> Human TRPC5 (forward primer: 5' GCTTGGTACCGCCACCATG 3', and reverse primer: 5' TGACACCGGTGAGGCGAGTTGTAAGTTGTTCTTC 3') was inserted upstream of the linker between KpnI and AgeI restriction sites using hTRPC5/pcDNA™4/TO<sup>33</sup> as a PCR template. All constructs contained an N-terminal Kozak sequence. (Performed by Dr Melanie Ludlow)

T-Rex™ cell line was transfected with TRPC5-SYFP2 or TRPC4-SYFP2 using FuGENE® HD transfection reagent. After 48 hrs cells were put under antibiotic selection using 400 µg/ml zeocin and 5 µg/ml Blasticidin S (Invitrogen, Thermo Fisher Scientific). Medium changes were carried out regularly to remove dead cells. (Performed by Dr Eulashini Chuntharpursat)

#### TRPC4/C1 and TRPC5/C1 Tetracycline-Inducible Human Embryonic Kidney-293 cells (HEK-293-TRPC4/C1 and HEK-293-TRPC5/C1)

The T-Rex system was used to create HEK-293 cells conditionally over-expressing TRPC4/C1 and TRPC5/C1 concatamers (Katie Musialowski (2015) and Nicola Blythe (2015) Beech Laboratory, respectively). To generate chimeric TRPC4/C1 and TRPC5/C1 under a tetracycline-inducible promoter T-Rex-293 cells were purchased from Thermo Fisher Scientific (R710-07) and transfected with pcDNA4/TA-TRPC4-TRPC1 or pcDNA4/TA-TRPC5-TRPC1 concatamer constructs (as described below)



using Lipofectamine 2000 (Thermo Fisher Scientific) for 24 hours. Subsequently, cells were treated with blasticidin and Zeocin (Invitrogen, Thermo Fisher Scientific) to select stably transfected cells.

Generation of TRPC4-TRPC1 and TRPC5-TRPC1 concatemers — Human TRPC4 and TRPC1 were cloned upstream and downstream respectively of a four amino linker (ASAS), flanked by AgeI and SacII restriction endonuclease sites, that had previously been introduced into pcDNAT M4/TO. TRPC4 $\beta$ , including an N-terminal Kozak sequence, was inserted between BamHI and AgeI restriction sites using hTRPC4 $\beta$ /pcDNAT M4/TO (8) a PCR template (forward primer: 5' AGTCGGATCC GCCACCATGGCTCAGTTCTATTACAAAAG 3' and reverse primer: 5' AGTT ACCGGTCAATCTTGTGGTCACGTAATCTTC 3'). TRPC1 was inserted between SacII and XbaI restriction sites using hTRPC1/pIRES as a PCR template (forward primer: 5' ACTCCGCGGCATGATGGCGGCCCTG 3' and reverse primer: 5' AGTCTCTAGATTAATTTCTTGGATAAAACATAGCATATTTAG 3'). HEK-293 cells stably expressing the TRPC5-TRPC1 and TRPC4-TRPC1 constructs were then generated for tetracycline-regulated expression as for TRPC5 HEK-293 Tet cells.<sup>59,33</sup>

### **7.3.5 Photoaffinity labelling experiments**

#### **7.3.5.1 Photoaffinity labelling in cells and lysis**

HEK-293 T-REx TRPC5-SYFP2 cells were seeded either onto coated 10cm petri dishes (Nunclon™ Delta surface treatment, Corning) or 6-well plates (tissue culture treated, Corning™ Costar™). Prior to use, the 6 well plates were coated with poly-D-lysine (wells were coated with ~0.5 mL poly-D-lysine (VWR) 0.1 mg/mL in DPBS for 30 minutes and then washed with DPBS before use). A seeding density of  $6 \times 10^6$  cells per petri dish or  $1.5 \times 10^6$  per well was used for HEK-293 T-REx TRPC5-SYFP2 cells. Cells were plated from a 70-80% confluent T75 flask. Trypsin-EDTA (0.05%) (Sigma, UK) was used to detach cells.  $1 \mu\text{g}\cdot\text{ml}^{-1}$  tetracycline (tet+) was applied 18 hr prior to experimentation to induce TRPC5-SYFP2 expression. WT HEK-293 cells were used as a control for no expression of TRPC5. All cells were grown to confluency overnight at 37 °C, 5% CO<sub>2</sub> levels. Cells were washed with DPBS, Pico145-DAAIk or DMSO control (final concentration of 300 nM, from a 300  $\mu\text{M}$  stock in DMSO) was added to each well/dish and cells were incubated at 37 °C, 5% CO<sub>2</sub> levels for 5 minutes. Plates were placed on ice and irradiated at 365 nm for 25 minutes (UVP-Crosslinker cl-1000, *Figure 75*). Cells were washed with DPBS and lysed with Triton-X100 (1 x PBS, 0.1% SDS, 1% TritonX-100, 1 EDTA-free protease inhibitor cocktail) or DDM-CHS (1% DDM, 0.1% CHS, 100 nM NaCl, 20 mM Tris pH7.5, EDTA free

protease inhibitor cocktail (Thermo Scientific)) lysis buffer. The cells were transferred with gentle scraping to an Eppendorf and incubated in the lysis buffer at 4 °C for 1 hour under constant mixing. Cell lysates were centrifuged at 10,000 ×g for 10 min at 4 °C in order to pellet large debris. The supernatant was transferred to a fresh tube and protein concentration measured using DC protein quantification.



**Figure 75: Photograph of UVP crosslinker cl-1000**

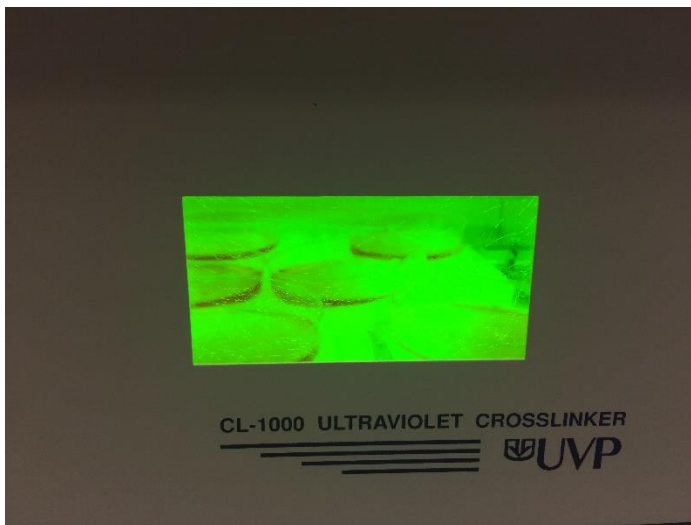


**Figure 76: Photograph of cells in 10cm petri dishes on ice in UVP crosslinker machine**

### 7.3.5.1 DC protein quantification assay

The DC (detergent compatible) protein assay (Bio-Rad) is a colorimetric assay for protein concentration following detergent solubilization. The assay is based on the reaction of protein with an alkaline copper tartrate solution (Reagent A) and Folin reagent (Reagent B). There are 2 steps which lead to colour development: the

reaction between protein and copper at alkaline pH, and the subsequent reduction of Folin reagent by the copper-treated protein.

Reagent A and a surfactant (Reagent S) were added to lysates which were serially diluted in a mixture of water and lysis buffer. Subsequently, Reagent B was added to the mixtures and absorbance was measured at 750 nm (iMark Microplate Reader, BioRad).

### **7.3.5.2 CuAAC**

Lysate concentration was adjusted to 1 mg/mL. Click reagents were premixed in the following order and added to the lysate (50 µg) at the indicated final concentrations: 100 µM azide reagent (10 mM stock in DMSO, see below), 1 mM CuSO<sub>4</sub> (50 mM stock in water), 1 mM TCEP (50 mM stock in water) and 100 µM TBTA (10 mM stock in DMSO). Samples were incubated for 1 hr with gentle agitation, at room temperature. The azide reagent used for all fluorescence gel experiments was Fluor-Azide-545. Following CuAAC, proteins were precipitated with ice-cold acetone (4 volumes) at -20 °C overnight, centrifuged at 16,000 xg, 10 min, 4 °C and the pellet was then washed twice with ice-cold MeOH. Proteins were resuspended in equal volumes of 2% SDS in PBS and 2× SDS sample loading buffer (SLB: 4% SDS, 20% glycerol, 10% 2-mercaptoethanol, 0.004% bromphenol blue and 0.125 M Tris HCl, pH approx. 6.8.) by vortexing.

### **7.3.5.3 SDS-PAGE**

Mini-PROTEAN TGX Precast Gels (4-20%, 10-well comb, 50 µl/well, Bio-Rad) were used in analysis and purification of TRPC5-SYFP2 and analysis of all photolabelling reactions. The gel was placed inside an electrophoresis tank and TGS-T running buffer was added (25 mM Tris, 192 mM Glycine, 0.1% (w/v) SDS, pH 8.3). Samples (previously mixed with an equal volume of 2× SDS SLB) were heated to 95 °C for 5 minutes and loaded onto gel. SDS binds to polypeptides applying an overall negative charge, allowing the protein to unravel. Proteins must be negatively charged to run the gel electrophoresis. 5-10 µg of the protein sample, along with a molecular weight marker were loaded onto precast gels. Electrophoresis was performed at a constant voltage of 170V for approximately 60 minutes, or until the loading buffer had reached the bottom of the gel. Proteins were visualised using Coomassie Blue Stain (45% (v/v) methanol, 10% (v/v) acetic acid, 0.25% (w/v) Coomassie Brilliant Blue R-250) and

destained (30% (v/v) methanol, 10% acetic acid), or alternatively using Instant Blue (TripleRed) for peptide mapping experiments.

The molecular weight marker used for fluorescence gels was Precision Plus Protein™ All Blue Prestained Protein Standards, Bio-Rad. The molecular weight marker used for western blot analysis was Precision Plus Protein™ Dual Color Standards, Bio-Rad.

#### **7.3.5.4 Fluorescence Gel**

Samples have undergone Photoaffinity labelling (7.3.5.1), CuAAC (7.3.5.2) and SDS-PAGE (7.3.5.3). Fluorescently modified proteins were analysed using a Molecular Imager ChemiDoc XRS System (Bio-Rad, CA). After obtaining the fluorescence image, the same gel was stained with Coomassie Brilliant Blue (CBB) and visualised on a Molecular Imager ChemiDoc XRS System.

#### **7.3.5.5 Western blotting**

Following SDS-PAGE (7.3.5.3) some samples were analysed by Western blot. Samples were transferred to a PVDF membrane (Immobilon) by WET transfer at constant current of 250 mA for 120 minutes per membrane in transfer buffer containing 48 mM Tris/Trizma-base, 39 mM glycine, 20% methanol, 0.05% SDS. The membrane was then incubated for 1 hour in PBST (consisting of 0.05% Tween in DPBS) containing 5% milk (GFP Western Blot) to block non-specific binding sites. Membranes were then labelled overnight with anti-GFP (1:2,000, Abcam (ab1218)) in 5% milk in PBST. After three washes with PBST, the membrane was incubated with secondary horse radish-peroxidase anti-mouse secondary antibodies (1:5,000, Invitrogen (A16160)) in 5% milk in PBST for 1 hour at room temperature. It was then washed three times with PBST and twice with PBS prior to visualisation with SuperSignal Pico/Femto detection reagents (Pierce).

#### **7.3.6 Peptide mapping of TRPC5-SYFP2**

Immunoprecipitation experiments were performed in collaboration with Dr David Wright. In-gel digestion, on-bead digestion and MS/MS analysis performed by Dr Rachel George.

### **7.3.6.1 Immunoprecipitation**

HEK-293-TRPC5-SYFP2 cells were seeded either onto coated (Nunclo<sup>TM</sup> Delta surface treatment, Corning) 10cm petri dishes. A seeding density of  $6 \times 10^6$  cells per petri dish was used for HEK cells. Cells were plated from a 70-80% confluent T75 flask. Trypsin-EDTA (0.05%) (Sigma, UK) was used to detach cells.  $1 \mu\text{g} \cdot \text{ml}^{-1}$  tetracycline (tet+) or not (tet-) was applied 18 hr prior to experimentation to induce TRPC5-sYFP2 expression. All cells were grown to confluency overnight at 37 °C, 5% CO<sub>2</sub> levels. Cells were washed with DPBS, and lysis buffer containing 10 mM Tris, pH 7.4, 150 mM NaCl, 0.5 mM EDTA, 0.5% Nonidet P40 substitute, protease inhibitor cocktail (Sigma) and phosphatase inhibitor cocktail (Sigma) was added. Cells were transferred with gentle scraping to an Eppendorf. Cell lysates were centrifuged at 10,000  $\times g$  for 10 min at 4 °C in order to pellet large debris. The supernatant was transferred to a fresh tube and protein concentration measured using DC protein quantification.

GFP-Trap beads were equilibrated in dilution buffer (10 mM Tris/Cl pH7.5, 150 mM NaCl, 0.5 mM EDTA) by resuspending in dilution buffer, beads were centrifuged at 2500  $\times g$  for 2 min at 4 °C. The supernatant was discarded, and beads washed twice with ice cold dilution buffer. Lysates (3 mg/mL) were added to GFP-trap beads and incubated for 3 hr at 4 °C under constant mixing. Samples were centrifuged at 2500  $\times g$  for 2 minutes at 4 °C, supernatant discarded, and samples were washed twice with ice cold dilution buffer. Beads were resuspended in 2 $\times$  SDS sample loading buffer (SLB: 4% SDS, 20% glycerol, 10% 2-mercaptoethanol, 0.004% bromophenol blue and 0.125 M Tris HCl, pH approx. 6.8.) and boiled at 95 °C for 10 minutes to dissociate immunocomplexes from GFP-trap beads. GFP-trap beads were collected by centrifugation at 2,500  $\times g$  for 2 minutes and SDS-PAGE (7.3.5.3) was performed.

### **7.3.6.2 In-gel digestion**

In-gel digestion was performed by Dr Rachel George. Proteins were resolved using SDS-PAGE and the gel was washed with PBS and stained with InstantBlue<sup>TM</sup> Coomassie Protein Stain (Expedeon). Gel bands were excised and chopped into small pieces ( $\sim 1 \text{ mm}^3$ ), covered with 30 % ethanol in a 1.5 mL microcentrifuge and heated to 70 °C for 30 min with shaking. The supernatant was removed and replaced with fresh ethanol solution and heated to 70 °C for 30 min with shaking. This was repeated until all coomassie stain was removed from the gel. The gel slices were covered with ammonium bicarbonate (25 mM): acetonitrile (1:1 v/v) and incubated for

ten min with shaking. The gel slices were then covered with 100% acetonitrile and left for five minutes before the supernatant was discarded and replaced with a fresh aliquot of acetonitrile. 100  $\mu\text{L}$  20 mM dithiothreitol (DTT) solution was then added and the sample was incubated at 57 °C for 1 hr with shaking. The supernatant was removed and once the gel pieces were at room temperature iodoacetic acid (55 mM, 100  $\mu\text{L}$ ) was added. The samples were then incubated at room temperature in the dark for 30 min with shaking. After removing the supernatant, the gel slices were covered with acetonitrile and left for five minutes. The acetonitrile was removed, and the gel pieces were left to dry in a laminar flow hood for 60 min. Once dry, the gel slices were cooled on ice then they were then covered with ice-cold protease...

- trypsin solution (20 ng  $\mu\text{L}^{-1}$  in 25 mM ammonium bicarbonate)
- chymotrypsin (25 ng  $\mu\text{L}^{-1}$  in 25 mM ammonium bicarbonate)
- glu-C (10 ng  $\mu\text{L}^{-1}$  in 25 mM ammonium bicarbonate)

...and left on ice for 10 mins to rehydrate. Excess protease solution was removed, and the gel slices were covered with a minimal amount of ammonium bicarbonate (25 mM). After briefly vortexing and centrifuging, the gel slices were incubated at 37 °C with shaking for 18 hours. Double digests were performed by adding chymotrypsin at this stage and incubating for a further 18 hours at 37 °C. The resulting digest was vortexed and centrifuged. The supernatant was recovered and added to an eppendorf containing 5  $\mu\text{L}$  acetonitrile/ water/ formic acid (60/35/5; v/v). 50  $\mu\text{L}$  acetonitrile/ water/ formic acid (60/35/5; v/v) was added to the gel slices and vortexed for an additional 10 mins. The supernatant was pooled with the previous wash and one additional wash of the gel slices was performed. The pool of three washes was dried by vacuum centrifugation. The peptides were reconstituted in 20  $\mu\text{L}$  0.1% aqueous trifluoroacetic acid.

### **7.3.6.3 In-Gel Digestion Protocol – ProteaseMax**

Proteins were resolved using SDS-PAGE and the gel was washed with PBS and stained with InstantBlue™ Coomassie Protein Stain (Expedeon). Gel bands were excised and chopped into small pieces ( ~ 1 mm<sup>3</sup> ) and transferred to a 0.5 or 1.5ml microcentrifuge tube. Bands were washed with NANOpure® water (200 $\mu\text{l}$ ) with vortex mixing for 30 seconds. After washing discard the water. Proteins were destained with methanol: $\text{NH}_4\text{HCO}_3$  (50 mM) (1:1 v/v, 200  $\mu\text{l}$ ) for 1 minute with intermittent vortex mixing. The supernatant was discarded and the wash repeated. Acetonitrile:50mM  $\text{NH}_4\text{HCO}_3$  (1:1 v/v, 200  $\mu\text{l}$ ) was added to the gel slices with intermittent vortexing for

5 minutes. The supernatant was discarded, fresh acetonitrile (200µl) was added and the incubated for 30 seconds. The supernatant was discarded and the gel slices were dried in a Speed Vac® vacuum centrifuge for 5 minutes or until sample is dry. The gel slices were rehydrated in a freshly prepared solution of DTT (25 mM) in NH<sub>4</sub>HCO<sub>3</sub> (25 mM) (100 µl), and incubated for 20 minutes at 56 °C.

The supernatant was discarded and a freshly prepared solution of iodoacetamide (55 mM) in NH<sub>4</sub> HCO<sub>3</sub> (50 mM) (100 µl) was added and incubated in the dark for 20 minutes at room temperature. Note: Alkylation with iodoacetamide increases peptide mass by 57.02 for each cysteine. The supernatant was discarded, and gel slices were washed with NANOpure® water (400 µl) by vortex mixing briefly. The supernatant was discarded and the wash step repeated once. The gel slices were dehydrated for 5 minutes in a solution of acetonitrile:NH<sub>4</sub>HCO<sub>3</sub> (50 mM) (1:1 v/v, 200 µl) with intermittent vortex mixing. Discard supernatant. Add 200µl of 100% acetonitrile, mix and incubate for 30 seconds. Discard the supernatant. Gel slices were dried in a Speed Vac® vacuum centrifuge for 5 minutes or until sample is dry.

Gel slices were rehydrated in a solution of trypsin (12ng/µl) in 0.01% ProteaseMAX™ Surfactant:NH<sub>4</sub>HCO<sub>3</sub> (50 mM) (20 µl) for 10 minutes. Overlaid with 0.01% ProteaseMAX™ Surfactant:NH<sub>4</sub>HCO<sub>3</sub> (50 mM) (30 µl) and gently mixed for several seconds. Gel slices were incubated for two hours at 37 °C. The condensate was collected from tube walls by centrifuging at 12,000–16,000 × g for 10 seconds. The digested peptides were mixed for a few seconds, and transferred into a new tube. Trifluoroacetic acid (TFA) was added to a final concentration of 0.5% to inactivate trypsin. The digested peptides were mixed and kept on ice.

#### **7.3.6.4 On-bead digestion<sup>278</sup>**

On-bead digestion was performed by Dr Rachel George. Proteins are purified using immunoprecipitation with GFP-trap beads. Proteins were equilibrated with GFP-trap beads as described in *Section 7.3.6.1*. Following incubation of lysates with the GFP-trap beads, samples were centrifuged at 2500 ×g for 2 minutes at 4 °C, supernatant discarded, and samples were washed twice with ice cold dilution buffer (10 mM Tris/Cl pH7.5, 150 mM NaCl, 0.5 mM EDTA). Samples were heated at 60 °C for 10 minutes. Proteins were resuspended in a protein reconstitution buffer (2% acetonitrile (ACN) and 0.1% TFA). Proteases were added...

- trypsin solution (20 ng µL<sup>-1</sup> in 25 mM ammonium bicarbonate)
- chymotrypsin (25 ng µL<sup>-1</sup> in 25 mM ammonium bicarbonate)

- glu-C (10 ng  $\mu\text{L}^{-1}$  in 25 mM ammonium bicarbonate)

... and samples were shaken (RT; 500 rpm; 10 min). Peptides were acidified to a final concentration of 0.1% TFA. The resulting digest was centrifuged (RT; 2,500 rcf; 2 min) to pellet beads. The supernatant was transferred to an equilibrated cartridge (14-gauge StageTip plug, iST Kit for Proteomic Sample Preparation, PreOmics). Ethylacetate/1% TFA (125 ml) was added, and the StageTips were centrifuged. The StageTips were washed using two wash steps of ethylacetate with 1% TFA (100 ml) and one of 1 ddH<sub>2</sub>O with 0.2% TFA (100 ml) consecutively, purified peptides were eluted by 60 ml of elution buffer (80% acetonitrile, 19% ddH<sub>2</sub>O, 1% ammonia).

### **7.3.6.5 Sep-Pak C18 Purification**

Sep-Pak purification was performed by Dr Rachel George. The Sep-Pak column was equilibrated with 1mL acetonitrile followed by 1mL 0.1% trifluoroacetic acid. 500 $\mu\text{L}$  0.1% trifluoroacetic acid was added to the peptide digest, this mix was passed through the column. The column was washed with 1mL 0.1% trifluoroacetic acid. Peptides were then eluted from the column with 500 $\mu\text{L}$  50% acetonitrile, 50% water, 0.1% formic acid. The eluent was dried by vacuum centrifugation. The peptides were reconstituted in 20  $\mu\text{L}$  0.1% aqueous trifluoroacetic acid.

### **7.3.6.6 Liquid chromatography-mass spectrometry**

LC-MS analysis was performed by Dr Rachel George on an ACQUITY M-Class UPLC (Waters UK, Manchester). 1  $\mu\text{L}$  of each sample was loaded onto a Symmetry C18 trap column (180  $\mu\text{M}$  i.d. \* 20 mm) and washed with 1% acetonitrile/0.1% formic acid for 5 min at 5  $\mu\text{L min}^{-1}$ . After valve switching, the peptides were then separated on a HSS T3 C18, 75  $\mu\text{m}$  i.d. x 150 mm analytical column (Waters UK, Manchester) by gradient elution of 1-60% solvent B in A over 30 min. at 0.3  $\mu\text{L min}^{-1}$ . Solvent A was 0.1% formic acid in water, solvent B was 0.1% formic acid in acetonitrile.

The column eluent was directly interfaced to a Xevo G2-XS Q-TOF mass spectrometer via a Z-spray nanoflow electrospray source. The MS was operated in positive TOF mode using a capillary voltage of 3.0 kV, cone voltage of 40 V, source offset of 80 V, backing pressure of 3.58 mbar and a trap bias of 2 V. The source temperature was 80 °C. Argon was used as the buffer gas at a pressure of  $8.6 \times 10^{-3}$  mbar in the trap and transfer regions. Mass calibration was performed using [Glu]-fibrinopeptide (GFP) at a concentration of 100 fmol  $\mu\text{L}^{-1}$ . GFP was also used as a lock mass calibrant with a one second lock spray scan taken every 30 s during



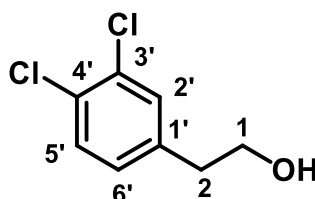
acquisition. Ten scans were averaged to determine the lock mass correction factor. Data acquisition was using data dependent analysis with a 0.2 s scan MS over  $m/z$  350-2000 being followed by five 0.5 s MS/MS taken of the five most intense ions in the MS spectrum. CE applied was dependent upon charge state and mass of the ion selected. Dynamic exclusion of 60 s was used. Data processing was performed using the MassLynx v4.1 suite of software supplied with the mass spectrometer. Peptide MS/MS data were processed with PEAKS Studio (Bioinformatic Solutions Inc, Waterloo, Ontario, Canada) and searched against the Uniprot database for TRPC5. Carbamidomethylation was selected as a fixed modification, variable modifications were set for oxidation of methionine and deamidation of glutamine and asparagine. (Carbamidomethyl: 57.02, Oxidation: 15.99, and Deamidation : 0.98). MS mass tolerance was 20 ppm, and fragment ion mass tolerance was 0.05 Da. The false discovery rate was set to 1%.

## 7.4 Experimental Section for Chapter 5

Cell culture for TRPC5 is explained in *Section 7.1.4*. Details for intracellular calcium measurements are explained in *Section 7.1.5*. Automated electrophysiology experiments and cell culture for cell lines expressing hERG, Nav1.5,  $I_{to}$  and  $I_{KS}$  are explained in *Section 7.1.5.4*.

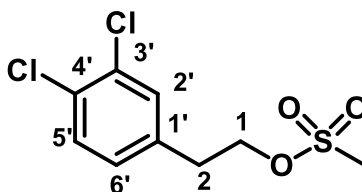
### 7.4.1 Organic synthesis

#### 2-(3,4-dichlorophenyl)ethan-1-ol, 111<sup>279</sup>



3,4-dichlorophenyl acetic acid (3.0 g, 14.6 mmol) dissolved in THF (20 mL) was added dropwise to a solution of lithium aluminium hydride (0.83 g, 21.9 mmol) in THF (20 mL) at 0 °C, over 10 minutes. The reaction was stirred at room temperature for 18 hr, then quenched with an aqueous sodium thiosulfate solution (sat., 10 mL). The reaction mixture was filtered, and the filter cake washed with ether. The filtrate was evaporated *in vacuo* to yield the *title compound* as a pale yellow oil (4.43 g, 23.2 mmol, 80%);  $R_f$  0.50 (75:25 EtOAc–Hexanes);  $\delta_H$  (500 MHz,  $CDCl_3$ ) 7.33 (1H, d,  $J$  8.2, 5'-H), 7.29 (1H, d,  $J$  1.9, 2'-CH), 7.02 (1H, dd,  $J$  8.2, 1.9, 6'-CH), 3.75 (2H, t,  $J$  6.5, 1- $CH_2$ ), 2.75 (2H, t,  $J$  6.5, 2- $CH_2$ ), 2.45 (1H, s, OH);  $^{13}C$  NMR (125 MHz,  $CDCl_3$ ) 139.1 (C-3' or C-4'), 132.3 (C-3' or C-4'), 130.9 (CH-2' or CH-5'), 130.4 (CH-2' or CH-5'), 128.5 (CH-6'), 62.9 (CH<sub>2</sub>-1), 38.1 (CH<sub>2</sub>-2) C-1' not observed;  $\nu_{max}/cm^{-1}$  (neat) 2938 and 1595. HRMS could not be obtained. Data consistent with literature.

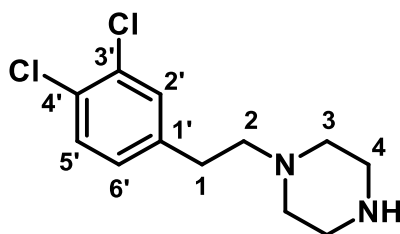
#### 2-(3,4-dichlorophenyl)ethyl methanesulfonate, 112<sup>279</sup>



2-(3,4-dichlorophenyl)ethan-1-ol (2.8 g, 14.7 mmol) and methane sulfonyl chloride (1.25 mL, 16.1 mmol) were dissolved in THF (30 mL) at 0 °C. Triethylamine (3.79 mL,

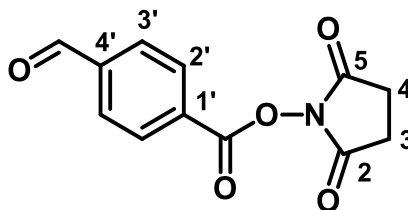
27.2 mmol) was added dropwise to the solution over 10 minutes and allowed to stir for 30 minutes. The precipitate was filtered off, the filter cake washed with THF, and the filtrate evaporated *in vacuo* to give the *title compound* as a pale yellow oil (3.75 g, 13.9 mmol, 95%);  $R_f$  0.28 (2:3 EtOAc–Hexanes);  $\delta_H$  (500 MHz,  $CDCl_3$ )  $\delta$  7.38 (1H, d,  $J$  8.2, 5'-CH), 7.33 (1H, d,  $J$  2.1, 2'-CH), 7.08 (1H, dd,  $J$  8.2, 2.1 Hz, 6'-CH), 4.38 (2H, t,  $J$  6.7, 1-CH<sub>2</sub>), 3.01 (2H, t,  $J$  6.7, 2-CH<sub>2</sub>), 2.92 (s, 3H, CH<sub>3</sub>);  $^{13}C$  NMR (125 MHz,  $CDCl_3$ ): 136.7 (C-3' or C-4'), 132.7 (C-3' or C-4'), 131.3 (C-1'), 130.9 (CH-2' or CH-5'), 130.7 (CH-2' or CH-5'), 128.4 (CH-6'), 69.2 (CH<sub>2</sub>-1), 37.5 (CH<sub>2</sub>-2), 34.8 (CH<sub>3</sub>);  $\nu_{max}/cm^{-1}$  (neat) 1594 and 1060; ESI-HRMS: calcd. for  $C_9H_{10}Cl_2NaO_3S$  [M+Na]<sup>+</sup> 290.9620 and 292.9590, found 290.9615 and 292.9584. Data consistent with literature.

### 1-[2-(3,4-dichlorophenyl)ethyl]piperazine, 113<sup>260</sup>



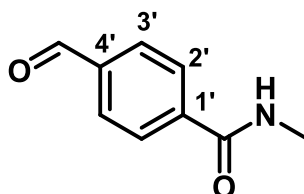
Piperazine (6.5 g, 75.0 mmol) was dissolved in acetonitrile (80 mL) at 75 °C. 3,4-Dichlorophenylethyl methane sulfonate (4 g, 15.0 mmol) was added dropwise to the solution, and left to stir at 60°C for 1 hr. The mixture was poured over ice (40 g) and extracted with EtOAc (3 × 50 mL). The organic extracts were washed with water (2 × 40 mL), dried ( $Na_2SO_4$ ) and the volatiles evaporated *in vacuo* to yield the *title compound* as a colourless oil (3.30 g, 12.7 mmol, 85%);  $R_f$  0.19 (1:5:94  $NH_3$ –MeOH–DCM);  $\delta_H$  (500 MHz,  $CDCl_3$ ) 7.31 (1H, d,  $J$  8.2, 5'-CH), 7.27 (1H, d,  $J$  2.1, 2'-CH), 7.01 (1H, dd,  $J$  8.2, 2.1, 6'-CH), 2.88 (4H, t,  $J$  4.9, 4-CH<sub>2</sub>), 2.76-2.68 (2H, m, 1-CH<sub>2</sub>), 2.55-2.50 (2H, m, 2-CH<sub>2</sub>), 2.42-2.48 (4H, m, 3-CH<sub>2</sub>), 1.79 (1H, br.s, NH);  $\delta_C$  (125 MHz,  $CDCl_3$ ): 141.1 (C-3' or C-4'), 132.5 (C-3' or C-4'), 131.0 (CH-2' or CH-5'), 130.6 (CH-2' or CH-5'), 130.3 (C-1'), 128.5 (CH-6'), 60.8 (CH<sub>2</sub>-2), 54.8 (CH<sub>2</sub>-3 or CH<sub>2</sub>-4), 46.4 (CH<sub>2</sub>-3 or CH<sub>2</sub>-4), 32.8 (CH<sub>2</sub>-1);  $\nu_{max}/cm^{-1}$  (neat) 3265, 2940 and 2808; ESI-HRMS: calcd. ( $C_{12}H_{16}Cl_2N_2$ ) [M+H]<sup>+</sup>  $m/z$  259.0775 and 261.0734, found 259.0763 and 261.0740. Data consistent with literature.

### 2,5-dioxopyrrolidin-1-yl 4-formylbenzoate, 125<sup>262</sup>



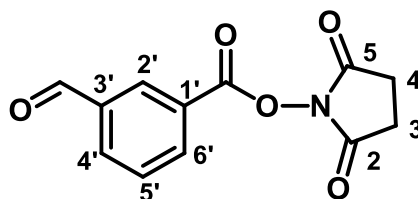
N-hydroxysuccinimide (380 mg, 3.30 mmol), 4-carboxybenzaldehyde (500 mg, 3.3 mmol) and EDCI (1.27 g, 6.6 mmol) were dissolved in DCM (15 mL). The reaction was stirred at room temperature for 2 hours. The reaction mixture was washed with sodium bisulfate (2.5% aq. soln. w/w, 7 mL) to remove the excess EDCI. The organic phase was washed with brine (10 mL), dried ( $\text{Na}_2\text{SO}_4$ ) and evaporated *in vacuo*, to yield the *title compound* as a pale yellow solid (570 mg, 2.3 mmol, 70%);  $\delta_{\text{H}}$  (500 MHz,  $\text{DMSO}-d_6$ ) 10.17 (1H, s, C=O-H), 8.31 (2H, d,  $J$  8.2, 3'-CH), 8.16 (2H, d,  $J$  8.2, 2'-CH), 2.92 (4H, s, 3- $\text{CH}_2$  and 4- $\text{CH}_2$ );  $\delta_{\text{C}}$  (125 MHz,  $\text{DMSO}-d_6$ ): 192.8 (C=O aldehyde), 170.1 (C-2 and C-5), 161.1 (C=O ester), 140.5 (C-4'), 130.7 (CH-3'), 130.1 (CH-2'), 128.9 (C-1'), 25.6 (CH<sub>2</sub>-3 and CH<sub>2</sub>-4). Data consistent with literature. Compound was carried onto the next step without further characterisation.

### 4-formyl-N-methylbenzamide, 124<sup>261</sup>



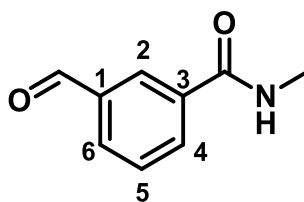
2,5-dioxopyrrolidin-1-yl 4-formylbenzoate (450 mg, 1.8 mmol) was dissolved in DMF (5 mL) and added dropwise to methylamine (40% w/w aq. soln., 0.16 mL, 1.8 mmol). The reaction was left for 1 hr then diluted with water (15 mL) and extracted with ethyl acetate (3 x 20 mL). The organic were then evaporated *in vacuo* to give the crude product, which was recrystallized from toluene to yield the *title compound* as a pale yellow solid (110 mg, 0.68 mmol, 38%);  $\delta_{\text{H}}$  (500 MHz,  $\text{DMSO}-d_6$ ) 10.07 (1H, s, C=O-H), 8.65 (1H, br s, NH), 8.03 – 7.97 (4H, m, 2'-CH and 3'-CH), 2.81 (3H, d,  $J$  4.6 Hz, CH<sub>3</sub>);  $\delta_{\text{C}}$  (125 MHz,  $\text{DMSO}-d_6$ ) 193.4 (C=O aldehyde), 166.2 (C=O ester), 140.0 (C-4'), 138.2 (C-1'), 129.9 (CH-3' or CH-2'), 128.3 (CH-3' or CH-2'), 26.8 (CH<sub>3</sub>);  $\nu_{\text{max}}/\text{cm}^{-1}$  (neat) 3343, 1693, 1634; ESI-HRMS: calcd. for  $\text{C}_9\text{H}_{10}\text{NO}_2$  [M+H]<sup>+</sup>  $m/z$  164.0706, found 164.0700. Data consistent with literature.

**2,5-dioxopyrrolidin-1-yl 3-formylbenzoate, 127<sup>262</sup>**



N-hydroxysuccinimide (380 mg, 3.30 mmol), 3-carboxybenzaldehyde (500 mg, 3.3 mmol) and EDCI (1.27 g, 6.6 mmol) were dissolved in DCM (15 mL). The reaction was stirred at room temperature for 2 hours. The reaction mixture was washed with sodium bisulfate (2.5% aq. soln. w/w, 7 mL) to remove the excess EDCI. The organic phase was washed with brine (10 mL), dried ( $\text{Na}_2\text{SO}_4$ ) and evaporated *in vacuo*, to yield the *title compound* as a cream solid (395 mg, 1.6 mmol, 49%);  $\delta_{\text{H}}$  (500 MHz,  $\text{DMSO}-d_6$ ) 10.13 (1H, s, O=CH), 8.57 (1H, t,  $J$  1.5, 2'-CH), 8.39 (1H, app. dt,  $J$  7.8, 1.5, 4'-CH), 8.33 (1H, app. dt,  $J$  7.8, 1.5, 6'-CH), 7.89 (1H, app. t,  $J$  7.8, 5'-CH), 2.91 (4H, s, 3- $\text{CH}_2$  and 4- $\text{CH}_2$ );  $\delta_{\text{C}}$  (125 MHz,  $\text{DMSO}-d_6$ ): 192.3 (C=O aldehyde), 170.2 (C-2 and C-5), 161.1 (C=O ester), 136.9 (C-3'), 135.3 (CH-4' or CH-6'), 135.2 (CH-4' or CH-6'), 130.9 (CH-2'), 130.7 (CH-5'), 125.4 (C-1'), 25.6 (CH<sub>2</sub>-3 and CH<sub>2</sub>-4). Data consistent with literature. Compound was carried onto the next step without further characterisation.

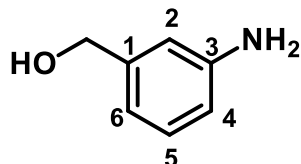
**3-formyl-N-methylbenzamide, 128<sup>262</sup>**



2,5-dioxopyrrolidin-1-yl 3-formylbenzoate (370 mg, 1.5 mmol) was dissolved in DMF (5 mL) and added dropwise to methylamine (40% w/w aq. soln., 0.13 mL, 1.5 mmol). The reaction was left for 1 hr then diluted with water (15 mL) and extracted with ethyl acetate (3 x 20 mL). The solvent was then evaporated *in vacuo* to give the crude product, which was recrystallized from toluene to yield the *title compound* as a pale yellow solid (165 mg, 1.01 mmol, 67%);  $\delta_{\text{H}}$  (400 MHz,  $\text{CDCl}_3$ ) 9.99 (1H, s, O=CH), 8.24 (1H, app. t,  $J$  1.2, 2-CH), 8.08 (1H, app. dt,  $J$  7.7, 1.2, 4-CH), 8.00 (1H, dt,  $J$  7.7, 1.2, 6-CH), 7.62 (1H, t,  $J$  7.7, 5-CH), 6.37 (1H, br. s, NH), 2.91 (s, 1H, CH<sub>3</sub>);  $\delta_{\text{C}}$  (100 MHz,  $\text{CDCl}_3$ ) 193.4 (C=O aldehyde), 165.6 (C=O amide), 136.2 (C-3), 133.0 (CH-4), 132.3 (CH-6), 129.4 (CH-5), 125.4 (C-1), 128.7 (CH-2), 26.8 (CH<sub>3</sub>);  $\nu_{\text{max}}/\text{cm}^{-1}$  (neat)

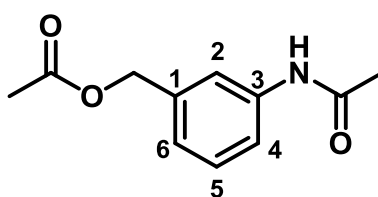
3293, 1709, 1632 and 1608; ESI-HRMS: calcd. for  $C_9H_{10}NO_2$   $[M+H]^+$   $m/z$  164.0706, found 164.0703. Data consistent with literature.

**(3-aminophenyl)methanol, 130**<sup>264</sup>



Ammonium chloride (7.0 g, 130 mmol) was added to a solution of 3-nitrobenzyl alcohol (1.55 mL, 13.1 mmol) in methanol (150 mL). The mixture was stirred at room temperature for 10 minutes. Zinc powder (17.0 g, 260.2 mmol) was added portion wise and the reaction was stirred vigorously at room temperature for 1 hr. The heterogeneous mixture was filtered through celite and the filter cake washed with methanol. The filtrate was collected and evaporated *in vacuo*, to yield the *title compound* as a pale yellow solid (1.61 g, 13.1 mmol, quantitative);  $\delta_H$  (500 MHz, MeOD- $d_4$ ) 7.07 (1H, app. t,  $J$  7.7, 5-CH), 6.74 (1H, app. t,  $J$  0.8, 2-CH), 6.70 – 6.67 (1H, app. m, 4-CH), 6.66 (1H, app. dt,  $J$  7.7, 0.8, 6-CH), 4.55 (1H, s,  $CH_2$ );  $\delta_C$  (125 MHz, MeOD- $d_4$ ) 148.5 (C-3), 143.6 (C-1), 130.0 (CH-5), 118.1 (CH-4), 115.7 (CH-6), 115.3 (CH-2), 65.4 ( $CH_2$ );  $\nu_{max}/cm^{-1}$  (neat) 3352, 3274 and 1736; ESI-HRMS: calcd. for  $C_7H_{10}NO$   $[M+H]^+$  124.0757, found 124.0755. Data consistent with literature.

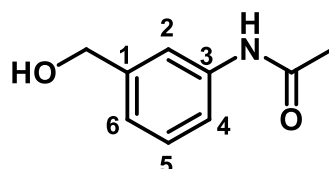
**(3-acetamidophenyl)methyl acetate, 131**<sup>264</sup>



Acetic anhydride (0.15 mL, 1.6 mmol) and DMAP (10 mg, 0.08 mmol) were added to a solution of (3-aminophenyl)methanol (50 mg, 0.4 mmol) in DCM (10 mL) and stirred for 18 hr. The reaction mixture was washed with an aqueous solution of  $NaHCO_3$  (sat. 15 mL). The aqueous layer was extracted with DCM (2  $\times$  10 mL). The organic layers were combined and washed with HCl (1 M, 15 mL), dried ( $Na_2SO_4$ ) evaporated *in vacuo*, to yield the *title compound* as a pale yellow solid (99 mg, 0.4 mmol, quantitative);  $\delta_H$  (500 MHz, DMSO- $d_6$ )  $\delta$  9.95 (1H, br. s, NH), 7.57 (1H, app. t,  $J$  1.8, 2-CH), 7.53 (1H, app. dt,  $J$  7.7, 1.8, 4-CH), 7.28 (1H, app. t,  $J$  7.8, 5-CH), 7.01 (1H, app. d,  $J$  7.7, 6-CH), 5.03 (2H, s,  $CH_2$ ), 2.06 (3H, s, ester- $CH_3$ ), 2.03 (3H, s, amide-

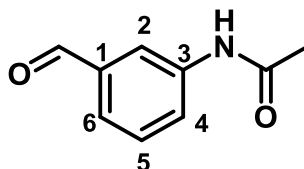
$CH_3$ );  $\delta_C$  (125 MHz, DMSO- $d_6$ ) 170.1 (C=O amide), 168.3 (C=O ester), 139.4 (C-3), 136.7 (C-1), 128.7 (CH-5), 122.5 (CH-6), 118.5 (CH-4), 118.3 (CH-2), 65.3 (CH<sub>2</sub>), 24.0 (CH<sub>3</sub> amide), 20.78 (CH<sub>3</sub> ester);  $\nu_{max}/cm^{-1}$  (neat) 3435, 1737, 1654 and 1611; ESI-HRMS: calcd. for C<sub>11</sub>H<sub>14</sub>NO<sub>3</sub> [M+H]<sup>+</sup> 208.0968, found 208.0968. Data consistent with literature.

***N*-[3-(hydroxymethyl)phenyl]acetamide, 132<sup>263</sup>**



Sodium hydroxide (780 mg, 19.5 mmol) was added to a solution of (3-acetamidophenyl)methyl acetate (1.35 g, 6.5 mmol) in methanol (50 mL), and stirred for 2.5 hr. After evaporation of the solvent *in vacuo*, water (40 mL) was added and extracted with ethyl acetate (3 × 25 mL). The combined organic layers were washed with brine (20 mL), dried (Na<sub>2</sub>SO<sub>4</sub>) and evaporated *in vacuo* to yield the *title compound* as a cream solid (815 mg, 4.90 mmol, 76%);  $\delta_H$  (500 MHz, MeOD- $d_4$ ) 7.54 (1H, app. t, *J* 1.6, 2-CH), 7.44 (1H, app. dt, *J* 7.8, 1.6, 4-CH), 7.27 (1H, app. t, *J* 7.8, 5-CH), 7.09 (1H, app. dt, *J* 7.8, 1.6, 6-CH), 4.58 (2H, s, CH<sub>2</sub>), 2.12 (3H, s, CH<sub>3</sub>);  $\delta_C$  (125 MHz, MeOD- $d_4$ ) 171.6 (C=O), 143.5 (C-3), 139.9 (C-1), 129.8 (CH-5), 123.6 (CH-6), 120.1 (CH-4), 119.7 (CH-2), 65.1 (CH<sub>2</sub>), 23.8 (CH<sub>3</sub>);  $\nu_{max}/cm^{-1}$  (neat) 3198, 3148, 1655 and 1616; ESI-HRMS: calcd. for C<sub>9</sub>H<sub>12</sub>NO<sub>2</sub> [M+H]<sup>+</sup> 166.0863, found 166.0857. Data consistent with literature.

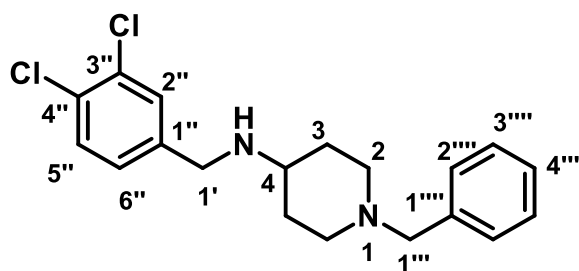
***N*-[3-(formylphenyl)phenyl]acetamide, 133<sup>263</sup>**



Dess-Martin periodinane (2.79 g, 6.59 mmol) was added to a solution of *N*-[3-(hydroxymethyl)phenyl]acetamide (725 mg, 4.39 mmol) in DCM (100 mL) and stirred for 30 min. The mixture was washed with Na<sub>2</sub>SO<sub>3</sub> (4.90 g, 19.8 mmol) in a saturated solution of sodium carbonate (aq., 30 mL) and extracted with DCM (3 × 15 mL). The combined organic layers were dried (Na<sub>2</sub>SO<sub>4</sub>) and evaporated *in vacuo* to yield the *title compound* as a cream solid (405 mg, 2.48 mmol, 57%); *R<sub>f</sub>* 0.47 (1:9 MeOH-DCM);  $\delta_H$  (500 MHz, MeOD- $d_4$ ) 9.94 (1H, s, O=CH), 8.81 (1H, s, NH), 8.14 (1H, app. t, *J* 1.4,

2-CH), 7.81 (1H, app. dt, *J* 7.6, 1.4, 6-CH), 7.62 (1H, app. dt, *J* 7.6, 1.4, 4-CH), 7.50 (1H, app. t, *J* 7.6, 5-CH), 2.15 (3H, s, CH<sub>3</sub>);  $\delta_{\text{C}}$  (125 MHz, MeOD-*d*<sub>4</sub>) 192.4 (C=O aldehyde), 170.5 (C=O amide), 139.6 (C-3), 137.2 (C-1), 129.2 (CH-5), 125.0 (CH-6), 122.1 (CH-4), 119.6 (CH-2), 22.4 (CH<sub>3</sub>);  $\nu_{\text{max}}/\text{cm}^{-1}$  (neat) 3282, 1737 and 1663; ESI-HRMS: calcd. for C<sub>9</sub>H<sub>10</sub>NO<sub>2</sub> [M+H]<sup>+</sup> 164.0706, found 164.0707. Characterisation confirmed by comparison with literature data.<sup>263</sup>

### 1-benzyl-N-[(3,4-dichlorophenyl)methyl]piperidin-4-amine, 139



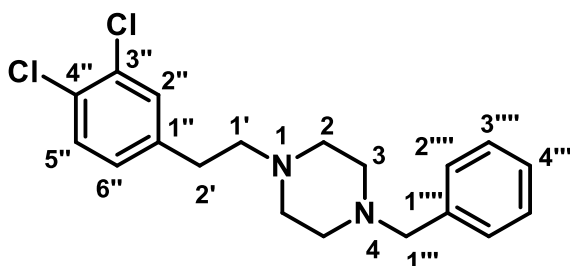
4-Amino-1-benzaldehyde (0.55 mL, 2.86 mmol) was added to a solution of 3,4-dichlorobenzaldehyde (500 mg, 2.80 mmol) in MeOH:acetic acid (15:1 v:v, 25 mL) and stirred for 10 minutes. Sodium cyanoborohydride (120 mg, 1.91 mmol) was added in portions and the reaction mixture was stirred for 3 hr. The reaction mixture was diluted with ice-cold water (25 mL), basified to pH 9 (1M NaOH) and the organics were extracted with EtOAc (3 x 30 mL). The organics were washed with brine (20 mL), dried (Na<sub>2</sub>SO<sub>4</sub>) and concentrated *in vacuo*. The crude material was purified by column chromatography (SiO<sub>2</sub>, eluting with CH<sub>2</sub>Cl<sub>2</sub>-MeOH-NEt<sub>3</sub> 90:9:1) to yield the *title compound* as a pale yellow solid (366 mg, 1.05 mmol, 37%). *R*<sub>f</sub> 0.33 (CH<sub>2</sub>Cl<sub>2</sub>-MeOH-NEt<sub>3</sub> 90:9:1);  $\delta_{\text{H}}$  (500 MHz, CDCl<sub>3</sub>) 7.43 (1H, d, *J* 1.9, 2''-CH), 7.35 (1H, d, *J* 8.2, 5''-CH), 7.30-7.21 (5H, m, 2'''-CH, 3'''-CH and 4'''-CH), 7.14 (1H, dd, *J* 8.2, 1.9, 6''-CH), 3.74 (2H, s, 1'-CH<sub>2</sub>), 3.49 (2H, s, 1'''-CH<sub>2</sub>), 2.83 (2H, dt, *J* 11.5, 3.7, 2-CH ax.or eq.), 2.47 (1H, tt, *J* 10.3, 4.0, 4-CH), 2.01 (2H, td, *J* 11.5, 2.7, 2-CH ax.or eq.), 1.90-1.80 (2H, m, 3-CH ax.or eq.), 1.48-1.34 (2H, m, 3-CH ax.or eq.);  $\delta_{\text{C}}$  (125 MHz, CDCl<sub>3</sub>) 141.4 (C-1''), 138.5 (C-1'''), 132.4 (C-3''), 130.7 (C-4''), 130.3 (CH-5'' or CH-2''), 129.9 (CH-5'' or CH-2''), 129.2 (C-2'''), 128.3 (C-3'''), 127.4 (CH-6''), 127.0 (CH-4'''), 63.1 (CH<sub>2</sub>-1'''), 54.3 (C-4), 52.4 (CH<sub>2</sub>-2), 49.7 (CH<sub>2</sub>-1'), 32.8 (CH<sub>2</sub>-3);  $\nu_{\text{max}}/\text{cm}^{-1}$  (neat) 3323, 1678; ESI-HRMS: calcd. for C<sub>19</sub>H<sub>23</sub>Cl<sub>2</sub>N<sub>2</sub> [M+H]<sup>+</sup> 349.1233 and 351.1203, found 349.1238 and 351.1209. HPLC: RT = 1.75 min.



### General Procedure for reductive amination's<sup>266</sup>

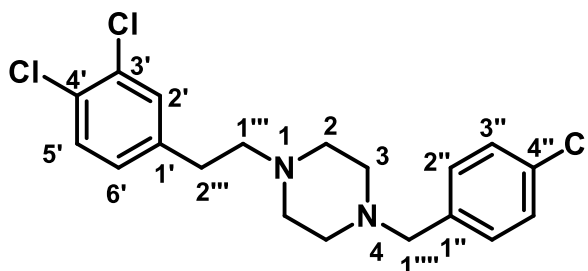
A solution of amine (1 equiv), the carbonyl analogue (1.2 equiv), and acetic acid (1 equiv) in DCM was treated with  $\text{NaBH}(\text{OAc})_3$  (1.6 equiv). After 16 h, the resulting mixture was treated with 10% sodium hydroxide (5 mL), and the mixture was extracted with DCM (3 x 10 mL). The combined organic phases were dried ( $\text{Na}_2\text{SO}_4$ ) and evaporated *in vacuo* to yield the crude product. Chromatography of the residue (EtOAc + 1%  $\text{NEt}_3$ ) provided the desired product.

#### 1-benzyl-4-[2-(3,4-dichlorophenyl)ethyl]piperazine, 141



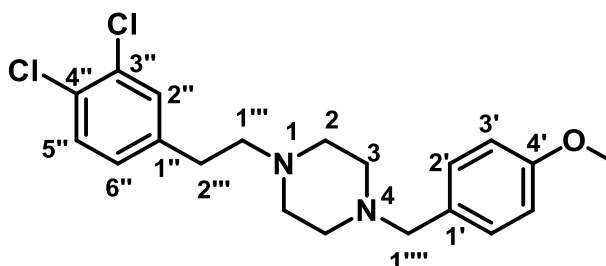
Prepared using general procedure for reductive aminations from 1-[2-(3,4-dichlorophenyl)ethyl]piperazine (250 mg, 0.97 mmol) and chromatography of the crude residue (1:2:97  $\text{NEt}_3$ :MeOH:EtOAc) provided the *title compound* as a pale yellow oil (186 mg, 0.53 mmol, 66%);  $R_f$  0.36 (1:2:97  $\text{NEt}_3$ :MeOH:EtOAc);  $\delta_H$  (400 MHz,  $\text{CDCl}_3$ ); 7.28 – 7.17 (7H, m, 2''-CH, 5''-CH, 2'''-CH, 3'''-CH and 4'''-CH), 6.95 (1H, dd,  $J$  8.2, 2.1, 6''-CH), 3.45 (2H, s, 1'''-CH<sub>2</sub>), 2.67 (2H, t,  $J$  7.1, 2'-CH<sub>2</sub>), 2.54 – 2.42 (10H, m, 1'-CH, 2-CH and 3-CH);  $\delta_C$  (100 MHz,  $\text{CDCl}_3$ ) 140.8 (C-1''), 138.1 (C-1'''), 132.3 (C-3'' or C-4''), 130.6 (CH-5'' or CH-2''), 130.2 (CH-5'' or CH-2''), 130.0 (C-3'' or C-4''), 129.2 (CH-2'''), 128.2 (CH-3'''), 128.1 (CH-4'''), 127.1 (CH-6''), 63.2 (CH<sub>2</sub>-1'''), 59.9 (CH<sub>2</sub>-1'), 53.3 (CH<sub>2</sub>-2 or CH<sub>2</sub>-3), 53.2 (CH<sub>2</sub>-2 or CH<sub>2</sub>-3), 32.8 (CH<sub>2</sub>-2');  $\nu_{\text{max}}/\text{cm}^{-1}$  (neat) 1628; ESI-HRMS: calcd. for  $\text{C}_{19}\text{H}_{23}\text{Cl}_2\text{N}_2$   $[\text{M}+\text{H}]^+$  349.1233 and 351.1203, found 349.1223 and 351.1214; HPLC: RT = 2.04 min.

**1-[(4-chlorophenyl)methyl]-4-[2-(3,4-dichlorophenyl)ethyl]piperazine,  
114**



Prepared using general procedure for reductive aminations from 1-[2-(3,4-dichlorophenyl)ethyl]piperazine (70 mg, 0.27 mmol) and chromatography of the crude residue (1:2:97 NEt<sub>3</sub>:MeOH:EtOAc) provided the *title compound* as a pale yellow oil (24 mg, 0.06 mmol, 13%); *R<sub>f</sub>* 0.29 (1:2:97 NEt<sub>3</sub>:MeOH:EtOAc); δ<sub>H</sub> (500 MHz, CDCl<sub>3</sub>) 7.33 (1H, d, *J* 8.2, 5'-CH), 7.29 (1H, d, *J* 2.1, 2'-CH), 7.28-7.23 (4H, m, 2''-CH and 3''-H), 7.02 (1H, dd, *J* 8.2, 2.0, 6'-H), 3.47 (2H, s, 1''''-CH<sub>2</sub>), 2.74 (2H, t, *J* 7.2, 2''''-CH<sub>2</sub>), 2.64-2.41 (10H, m, 1''''-CH<sub>2</sub>, 2-CH<sub>2</sub> and 3-CH<sub>2</sub>); δ<sub>C</sub> (125 MHz, CDCl<sub>3</sub>) 140.8 (C-1'), 136.8 (C-1''), 132.8 (C-4''), 132.3 (C-3'), 130.8 (CH-2' or CH-5'), 130.5 (CH-2''), 130.4 (CH-2' or CH-5'), 130.1 (C-4'), 128.5 (CH-3''), 128.3 (CH-6'), 62.2 (CH<sub>2</sub>-1'''), 59.8 (CH<sub>2</sub>-1'''), 53.1 (CH<sub>2</sub>-2 or CH<sub>2</sub>-3), 52.9 (CH<sub>2</sub>-2 or CH<sub>2</sub>-3) 32.7 (CH<sub>2</sub>-2'''); ν<sub>max</sub>/cm<sup>-1</sup> (neat) 1636; ESI-HRMS: calcd. for C<sub>19</sub>H<sub>22</sub>Cl<sub>3</sub>N<sub>2</sub> [M+H]<sup>+</sup> 338.0843 and 385.0814, found 383.0862 and 385.0834. HPLC: RT = 2.33 min.

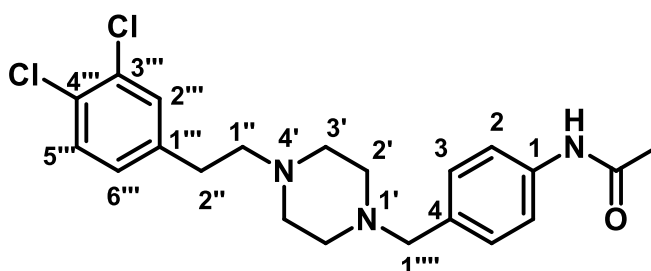
**1-[2-(3,4-dichlorophenyl)ethyl]-4-[(4-methoxyphenyl)methyl]piperazine,  
115**



Prepared using general procedure for reductive aminations from 1-[2-(3,4-dichlorophenyl)ethyl]piperazine (150 mg, 0.58 mmol) and chromatography of the crude residue (1:2:97 NH<sub>3</sub>:MeOH:DCM) provided the *title compound* as a pale yellow solid (30 mg, 0.08 mmol, 35%); *R<sub>f</sub>* 0.37 (1:2:97 NH<sub>3</sub>:MeOH:DCM); δ<sub>H</sub> (400 MHz, CDCl<sub>3</sub>) δ 7.32 (1H, d, *J* 8.2, 5''-CH), 7.28 (1H, d, *J* 2.0, 2''-CH), 7.23 (2H, d, *J* 8.6, 2'-CH), 7.02 (1H, dd, *J* 8.2, 2.0, 6''-CH), 6.85 (2H, d, *J* 8.6, 3'-CH), 3.79 (3H, s, CH<sub>3</sub>),

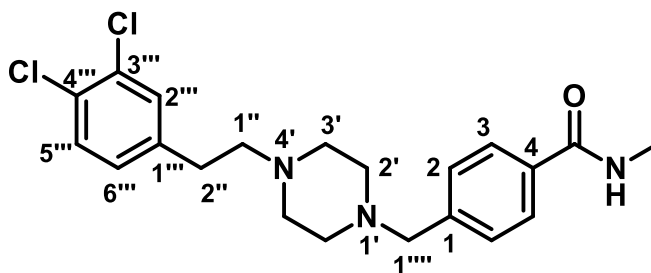
3.45 (2H, s, 1''''-CH<sub>2</sub>), 2.73 (2H, t, *J* 7.3, 2'''-CH<sub>2</sub>), 2.61 – 2.43 (10H, m, 2-CH<sub>2</sub>, 3-CH<sub>2</sub> and 1'''-CH<sub>2</sub>); δ<sub>C</sub> (125 MHz, CDCl<sub>3</sub>) 158.8 (C-4'), 140.7 (C-1''), 132.2 (C-3''), 130.8 (CH-2'' or CH-5''), 130.5 (CH-2'), 130.3 (CH-2'' or CH-5''), 130.2 (C-4''), 130.1 (C-1'), 128.6 (CH-6''), 113.6 (CH-3'), 62.4 (CH<sub>2</sub>-1'''), 59.8 (CH<sub>2</sub>-1''), 55.3 (CH<sub>3</sub>), 53.1 (CH<sub>2</sub>-2 or CH<sub>2</sub>-3), 52.9 (CH<sub>2</sub>-2 or CH<sub>2</sub>-3), 32.7 (CH<sub>2</sub>-2'''); ν<sub>max</sub>/cm<sup>-1</sup> (neat) 1684 and 1599; ESI-HRMS: calcd. for C<sub>20</sub>H<sub>25</sub>Cl<sub>2</sub>N<sub>2</sub>O [M+H]<sup>+</sup> 379.1338 and 381.1309 found 379.1356 and 381.1321. HPLC: RT = 2.09 min

**N-[4-({4-[2-(3,4-dichlorophenyl)ethyl]piperazin-1-yl)methyl}phenyl)acetamide, 118**



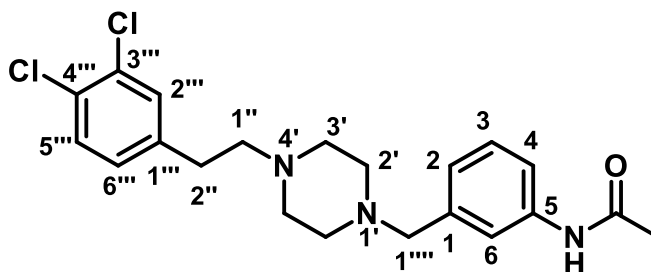
Prepared using general procedure for reductive aminations from 1-[2-(3,4-dichlorophenyl)ethyl]piperazine (190 mg, 0.74 mmol) and chromatography of the crude residue (1:2:97 NEt<sub>3</sub>:MeOH:EtOAc) provided the *title compound* as a pale yellow solid (142 mg, 0.35 mmol 47%); R<sub>f</sub> 0.18 (1:2:97 NEt<sub>3</sub>:MeOH:EtOAc); δ<sub>H</sub> (400 MHz, CDCl<sub>3</sub>) δ 7.82 (1H, s, NH), 7.37 (2H, d, *J* 8.1, 2-CH), 7.27 – 7.11 (4H, m, 2'''-CH, 5'''-CH and 3-CH), 6.94 (1H, dd, *J* 8.1, 2.0, 6'''-CH), 3.38 (2H, s, 1''''-CH<sub>2</sub>), 2.65 (2H, t, *J* 7.6, 2''-CH), 2.51 – 2.37 (10H, m, 1''-CH<sub>2</sub>, 2'-CH<sub>2</sub> and 3'-CH<sub>2</sub>), 2.06 (3H, s, CH<sub>3</sub>); δ<sub>C</sub> (125 MHz, CDCl<sub>3</sub>) 168.7 (C=O), 140.7 (C-1'''), 137.0 (C-1), 134.0 (C-4), 132.2 (C-3'''), 130.6 (CH-2''' or CH-5'''), 130.2 (CH-2''' or CH-5'''), 129.8 (C-4'''), 129.9 (CH-3), 128.2 (CH-6'''), 119.9 (CH-2), 62.5 (CH<sub>2</sub>-1'''), 59.8 (CH<sub>2</sub>-1''), 53.2 (CH<sub>2</sub>-2' or CH<sub>2</sub>-3'), 53.0 (CH<sub>2</sub>-2' or CH<sub>2</sub>-3'), 32.7 (CH<sub>2</sub>-2''), 21.1 (CH<sub>3</sub>); ν<sub>max</sub>/cm<sup>-1</sup> (neat) 3450, 1660 and 1598; ESI-HRMS: calcd. for C<sub>21</sub>H<sub>26</sub>Cl<sub>2</sub>N<sub>3</sub>O [M+H]<sup>+</sup> 406.1447 and 408.1418, found 406.1449 and 408.1430. HPLC: RT = 1.87 min

**4-({4-[2-(3,4-dichlorophenyl)ethyl]piperazin-1-yl}methyl)-N-methylbenzamide,  
116**



Prepared using general procedure for reductive aminations from 1-[2-(3,4-dichlorophenyl)ethyl]piperazine (161 mg, 0.63 mmol) and chromatography of the crude residue (1:10:89 NEt<sub>3</sub>:MeOH:EtOAc) provided the *title compound* as a cream solid (64 mg, 0.16 mmol, 31%); *R<sub>f</sub>* 0.24 (1:10:89 NEt<sub>3</sub>:MeOH:EtOAc); δ<sub>H</sub> (400 MHz, CDCl<sub>3</sub>) 7.72 (2H, d, *J* 8.2, 3-CH), 7.37 (2H, d, *J* 8.2 Hz, 2-CH), 7.32 (1H, d, *J* 8.2, 5'''-CH), 7.28 (1H, d, *J* 1.9, 2'''-CH), 7.02 (1H, dd, *J* 8.2, 1.9, 6'''-CH), 6.44 (1H, q, *J* 4.8, NH), 3.54 (2H, s, 1'''-CH<sub>2</sub>), 2.99 (3H, d, *J* 4.8, CH<sub>3</sub>), 2.74 (2H, t, *J* 7.4, 2''-CH) 2.60 – 2.47 (m, 10H, 1''-CH<sub>2</sub>, 2'-CH<sub>2</sub> and 3'-CH<sub>2</sub>); δ<sub>C</sub> (125 MHz, CDCl<sub>3</sub>) 168.2 (C=O), 141.8 (C-1), 140.6 (C-1'''), 133.5 (C-4), 132.2 (C-3'''), 130.7 (CH-5''' or CH-2'''), 130.3 (CH-5''' or CH-2'''), 130.0 (C-4'''), 129.2 (CH-2), 128.3 (CH-6'''), 126.9 (CH-3), 62.6 (CH<sub>2</sub>-1'''), 59.7 (CH<sub>2</sub>-1''), 53.1 (CH<sub>2</sub>-2' or CH<sub>2</sub>-3'), 53.0 (CH<sub>2</sub>-2' or CH<sub>2</sub>-3'), 32.7 (CH<sub>2</sub>-2''), 26.9 (CH<sub>3</sub>); ν<sub>max</sub>/cm<sup>-1</sup> (neat) 3316, 1632 and 1571; ESI-HRMS: calcd. for C<sub>21</sub>H<sub>26</sub>Cl<sub>2</sub>N<sub>3</sub>O [M+H]<sup>+</sup> *m/z* 406.1447 and 408.1418, found 406.1456 and 408.1412. HPLC: RT = 1.84 min.

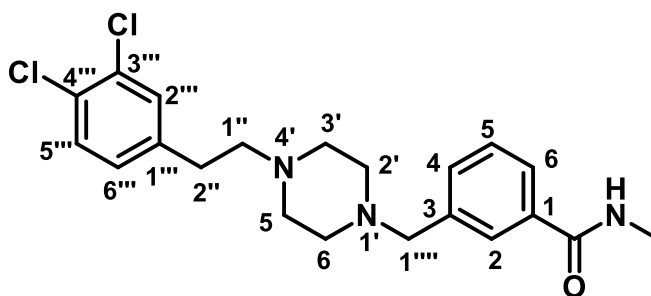
**N-[3-({4-[2-(3,4-dichlorophenyl)ethyl]piperazin-1-yl}methyl)phenyl]acetamide,  
119**



Prepared using general procedure for reductive aminations from 1-[2-(3,4-dichlorophenyl)ethyl]piperazine (190 mg, 0.74 mmol) and chromatography of the crude residue (1:99 NEt<sub>3</sub>:EtOAc) provided the *title compound* as a pale yellow oil (127 mg, 0.32 mmol, 51%); *R<sub>f</sub>* 0.19 (1:99 NEt<sub>3</sub>:EtOAc); δ<sub>H</sub> (300 MHz, CDCl<sub>3</sub>) δ 7.52 (1H, s,

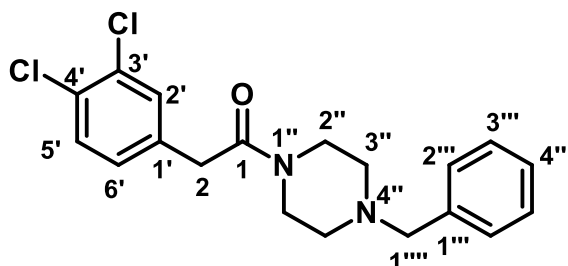
6-CH), 7.44 (1H, d,  $J$  7.0, 4-CH), 7.32 (1H, app. t,  $J$  7.0, 3-CH), 7.28 (1H, d,  $J$  1.9, 2'''-CH), 7.24 (1H, d,  $J$  8.2, 5'''-CH), 7.06 (1H, d,  $J$  7.0, 2-CH), 7.02 (1H, dd,  $J$  8.2, 1.9, 6'''-CH), 3.48 (2H, s, 1''''-CH<sub>2</sub>), 2.73 (2H, t,  $J$  7.3, 2''-CH), 2.63 – 2.41 (10H, m, 10H, 1''-CH<sub>2</sub>, 2'-CH<sub>2</sub> and 3-CH<sub>2</sub>) 2.16 (3H, s, CH<sub>3</sub>);  $\delta_c$  (75 MHz, CDCl<sub>3</sub>) 168.4 (C=O), 140.7 (C-1'''), 139.2 (C-5), 137.9 (C-1), 132.1 (C-3'''), 130.7 (CH-2''' or CH-5'''), 130.3 (CH-5''' or CH-2'''), 130.0 (C-4'''), 128.8 (CH-6'''), 128.2 (CH-3), 125.1 (CH-2), 120.5 (CH-6), 118.7 (CH-4), 62.7 (CH<sub>2</sub>-1'''), 59.8 (CH<sub>2</sub>-1''), 53.1 (CH<sub>2</sub>-2' or CH<sub>2</sub>-3'), 53.0 (CH<sub>2</sub>-2' or CH<sub>2</sub>-3'), 32.7 (CH<sub>2</sub>-2''), 24.6 (CH<sub>3</sub>);  $\nu_{\max}/\text{cm}^{-1}$  (neat) 3306, 1666 and 1594; ESI-HRMS: calcd. for C<sub>21</sub>H<sub>26</sub>Cl<sub>2</sub>N<sub>3</sub>O [M+H]<sup>+</sup> 406.1447 and 408.1418, found 406.1447 and 408.1428. HPLC: RT = 1.91 min.

**3-({4-[2-(3,4-dichlorophenyl)ethyl]piperazin-1-yl}methyl)-N-methylbenzamide,  
117**



Prepared using general procedure for reductive aminations from 1-[2-(3,4-dichlorophenyl)ethyl]piperazine (190 mg, 0.74 mmol) and chromatography of the crude residue (1:99 NEt<sub>3</sub>:EtOAc) provided the *title compound* as a pale yellow oil (112 mg, 0.28 mmol, 45%);  $R_f$  0.10 (1:99 NEt<sub>3</sub>:EtOAc);  $\delta_H$  (400 MHz, CDCl<sub>3</sub>)  $\delta$  7.71 (1H, s, 2-CH), 7.64 (1H, d,  $J$  7.7, 6-CH), 7.43 (1H, d,  $J$  7.7, 4-CH), 7.35 (1H, t,  $J$  7.7, 5-CH), 7.30 (1H, d,  $J$  8.3, 5'''-CH), 7.26 (1H, app. s, 2'''-CH), 7.00 (1H, d,  $J$  8.3, 1H, 6'''-CH), 6.36 (1H, br. s, NH), 3.51 (2H, s, 1''''-CH<sub>2</sub>), 2.98 (3H, d,  $J$  4.9, CH<sub>3</sub>), 2.71 (2H, t,  $J$  7.2, 2''-CH<sub>2</sub>), 2.62 – 2.39 (10H, m, 1''-CH<sub>2</sub>, 2'-CH<sub>2</sub> and 3'-CH<sub>2</sub>);  $\delta_c$  (125 MHz, CDCl<sub>3</sub>) 168.3 (C=O), 140.7 (C-1'''), 138.8 (C-3), 134.7 (C-1), 132.2 (C-3'''), 132.1 (CH-4), 130.7 (CH-2''' or CH-5'''), 130.3 (CH-2''' or CH-5'''), 130.0 (C-4'''), 128.6 (C-6'''), 128.3 (CH-6), 127.5 (CH-2), 125.7 (CH-5), 62.7 (CH<sub>2</sub>-1'''), 59.8 (CH<sub>2</sub>-1''), 53.2 (CH<sub>2</sub>-2' or CH<sub>2</sub>-3'), 53.1 (CH<sub>2</sub>-2' or CH<sub>2</sub>-3'), 32.7 (CH<sub>2</sub>-2''), 26.9 (CH<sub>3</sub>);  $\nu_{\max}/\text{cm}^{-1}$  (neat) 3322, 1639 and 1607; ESI-HRMS: calcd. for C<sub>21</sub>H<sub>26</sub>Cl<sub>2</sub>N<sub>3</sub>O [M+H]<sup>+</sup> 406.1447 and 408.1418, found 406.1458 and 408.1430. HPLC: RT = 1.88 min.

**1-(4-benzylpiperazin-1-yl)-2-(3,4-dichlorophenyl)ethan-1-one**



EDC·HCl (331 mg, 1.73 mmol) and HOBt·H<sub>2</sub>O (233 mg, 1.73 mmol) were added to a solution of 3,4-dichlorophenylacetic acid (353 mg, 1.73 mmol) in DCM:DMF (1:1, 10 mL). The reaction mixture was stirred for 30 minutes before 1-benzylpiperazine (0.2 mL, 1.15 mmol) was added dropwise and the reaction mixture was stirred for 72 hr. The mixture was diluted with DCM (40 mL), washed with NaHCO<sub>3</sub> (sat. aq. soln, 40 mL), water (5 × 20 mL), brine (40 mL), dried (Na<sub>2</sub>SO<sub>4</sub>) and concentrated *in vacuo* to give a pale yellow solid (385 mg). The crude product was purified by column chromatography (SiO<sub>2</sub>; eluting with 10:90:1 MeOH–EtOAc–NEt<sub>3</sub>) to yield the *title compound* as a pale yellow solid (271mg, 0.75 mmol, 65 %); R<sub>f</sub> 0.63 (10:90:1 MeOH–EtOAc–NEt<sub>3</sub>); δ<sub>H</sub> (400 MHz, CDCl<sub>3</sub>) δ 7.38 (1H, d, *J* 8.2, 5'-CH), 7.35 – 7.23 (6H, m, 2'-CH, 2'''-CH, 3'''-CH and 4'''-CH), 7.07 (1H, dd, *J* 8.2, 2.1, 6'-CH), 3.67 – 3.62 (4H, m, 1''''-CH<sub>2</sub> and 2''-CH eq. or ax.), 3.50 (2H, s, 2-CH<sub>2</sub>), 3.46-3.40 (2H, m, 2''-CH eq. or ax.), 2.45-2.39 (2H, m, 3''-CH eq. or ax.), 2.37 – 2.29 (2H, m, 3''-CH eq. or ax.); δ<sub>C</sub> (125 MHz, CDCl<sub>3</sub>) 168.3 (C=O), 137.7 (C-1'), 135.3 (C-1'''), 132.6 (C-3'), 131.0 (C-4'), 130.8 (CH-2' or CH-5'), 130.5 (CH-2' or CH-5'), 129.1 (CH-2'''), 128.4 (CH-3'''), 128.3 (CH-4'''), 127.3 (CH-6'), 62.8 (CH<sub>2</sub>-1'''), 52.9 (CH<sub>2</sub>-2'' or CH<sub>2</sub>-3''), 52.7 (CH<sub>2</sub>-2'' or CH<sub>2</sub>-3''), 46.1 (CH<sub>2</sub>-2); ν<sub>max</sub>/cm<sup>-1</sup> (neat) 1738 and 1635; ESI-HRMS: calcd. for C<sub>19</sub>H<sub>21</sub>Cl<sub>2</sub>N<sub>2</sub>O [M+H]<sup>+</sup> 406.1447 and 408.1418, found 406.1456 and 408.1428. HPLC: RT = 2.29 min.

## Appendix I

### Cardiac safety screening data for reference compounds

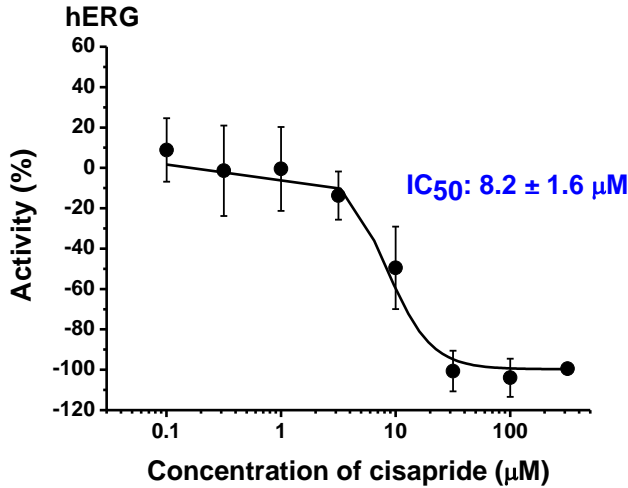


**Figure 77: Cisapride inhibition of hERG channel;** Concentration-response data for cisapride on hERG channel. Whole-cell voltage clamp recordings were taken from CHO cells over-expressing hERG under control conditions and then following three minutes incubation with cisapride (0.1, 0.3, 1, 3, 10, 30, 100 and 300 µM). The current amplitude at the end of 3.5 seconds activating clamp step was recorded and plotted as a percentage of the pre-compound current. The fitted curve is a Hill equation with a half-maximal inhibitory concentration (IC<sub>50</sub>) of 8.2 ± 1.6 µM. (Mean ± SD of mean) (n/N = 4/16)

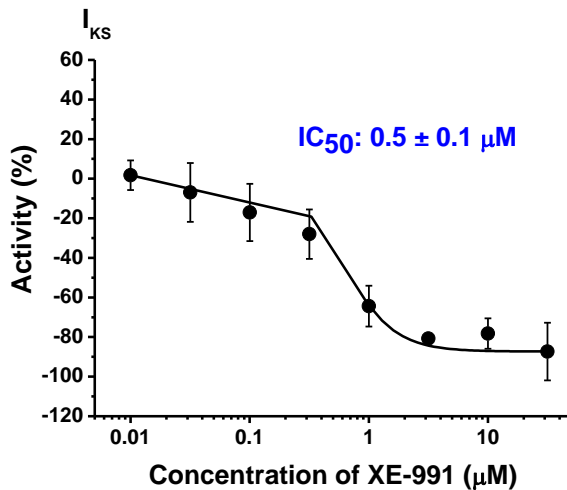


**Figure 78: XE-991 inhibition of I<sub>KS</sub> channel;** Concentration-response data for XE-991 on I<sub>KS</sub> channel. Whole-cell voltage clamp recordings were taken from CHO cells over-expressing hKvLQT1/hminK under control conditions and then following three minutes incubation with XE-991 (0.01, 0.03, 0.1, 0.3, 1, 3, 10 and 30 µM). The current amplitude at the end of 4.5 seconds activating clamp step was recorded and plotted as a percentage of the pre-compound current. The fitted curve is a Hill equation with an IC<sub>50</sub> of 0.5 ± 0.1 µM. (Mean ± SD of mean) (n/N = 4/16).

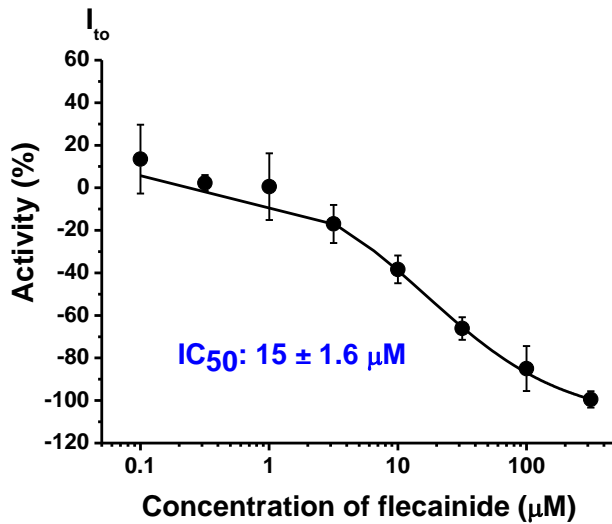


**Figure 79: flecainide inhibition of  $I_{to}$  channel;** Concentration-response data for flecainide on  $I_{to}$  channel. Whole-cell voltage clamp recordings were taken from CHO cells over-expressing  $K_v4.3/KChIP2.2$  under control conditions and then following three minutes incubation with flecainide (0.01, 0.03, 0.1, 0.3, 1, 3, 10 and 30  $\mu\text{M}$ ). The current amplitude at the end of the 2 seconds activating clamp step was recorded and plotted as a percentage of the pre-compound current. The fitted curve is a Hill equation with an  $IC_{50}$  of  $15 \pm 1.6 \mu\text{M}$ . (Mean  $\pm$  SD of mean) ( $n/N = 4/16$ ).

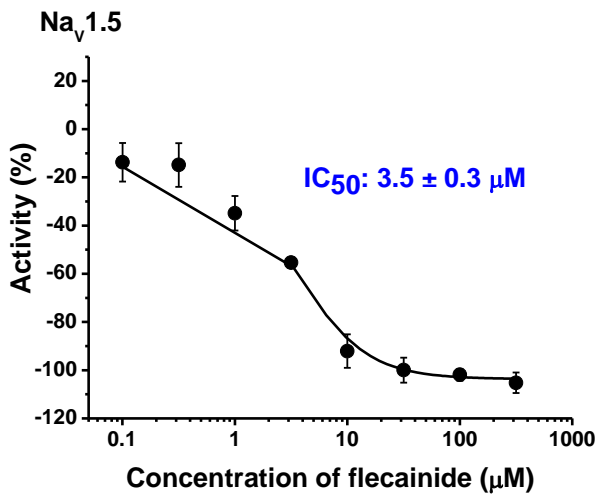


**Figure 80: flecainide inhibition of  $Na_v1.5$  channel;** Concentration-response data for flecainide on  $Na_v1.5$  channel. Whole-cell voltage clamp recordings were taken from CHO cells over-expressing  $Na_v1.5$  under control conditions and then following three minutes incubation with flecainide (0.1, 0.3, 1, 3, 10, 30, 100 and 300  $\mu\text{M}$ ). The current amplitude at the end of the 3 seconds activating clamp step was recorded and plotted as a percentage of the pre-compound current. The fitted curve is a Hill equation with an  $IC_{50}$  of  $3.5 \pm 0.3 \mu\text{M}$ . (Mean  $\pm$  SD of mean) ( $n/N = 4/16$ ).



### Cardiac safety screening data for flavonol compounds

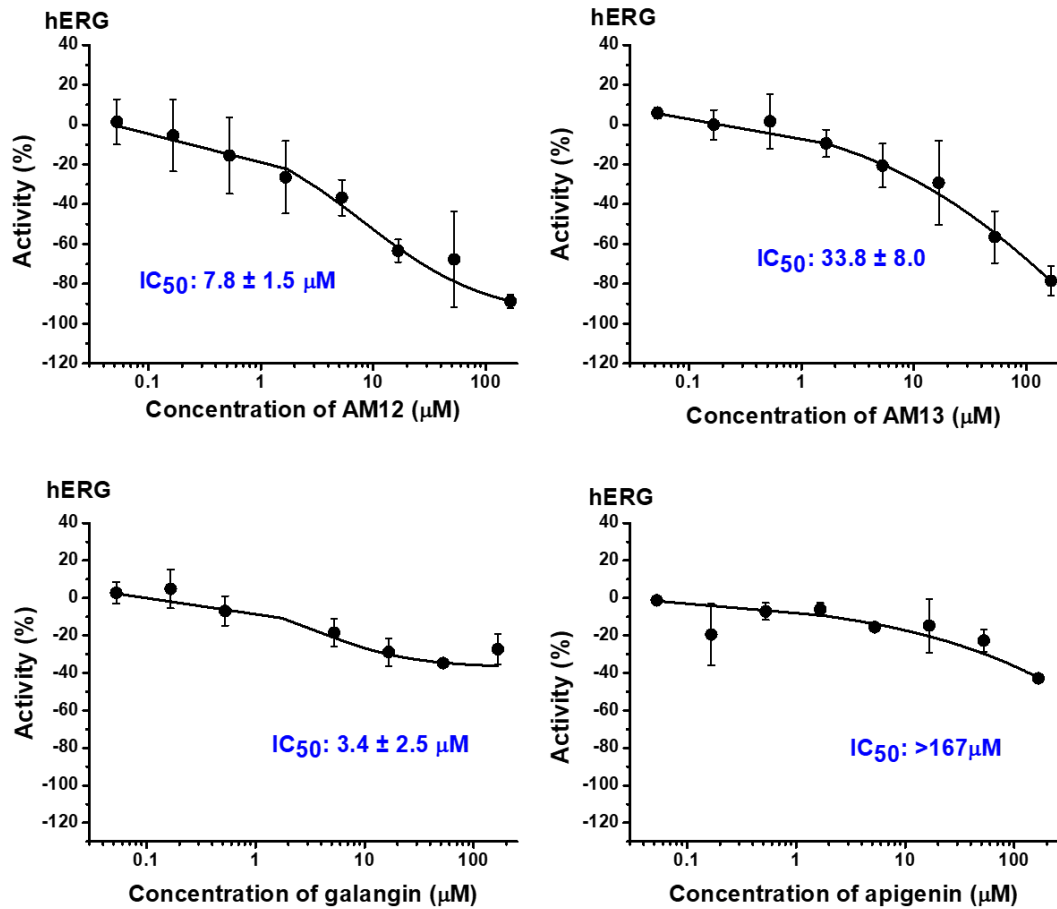


**Figure 81: Concentration-response data for AM12, AM13, galangin and apigenin against the hERG channel.** Whole-cell voltage clamp recordings were taken from CHO cells over-expressing hERG under control conditions and then following three minutes incubation with AM12, AM13, galangin and apigenin (0.05, 0.17, 0.5, 1.7, 5, 16, 50 and 167 μM). The current amplitude at the end of 3.5 seconds activating clamp step was recorded and plotted as a percentage of the pre-compound current. The fitted curve is a Hill equation with an IC<sub>50</sub> for AM12 of 7.8 ± 1.5 μM (n/N=2/6), AM13: 33.8 ± 8.0 μM (n/N=2/6), galangin: 3.4 ± 2.5 μM (n/N=1/3) and apigenin: >167 μM (n/N=1/3). (Mean ± SD of mean)

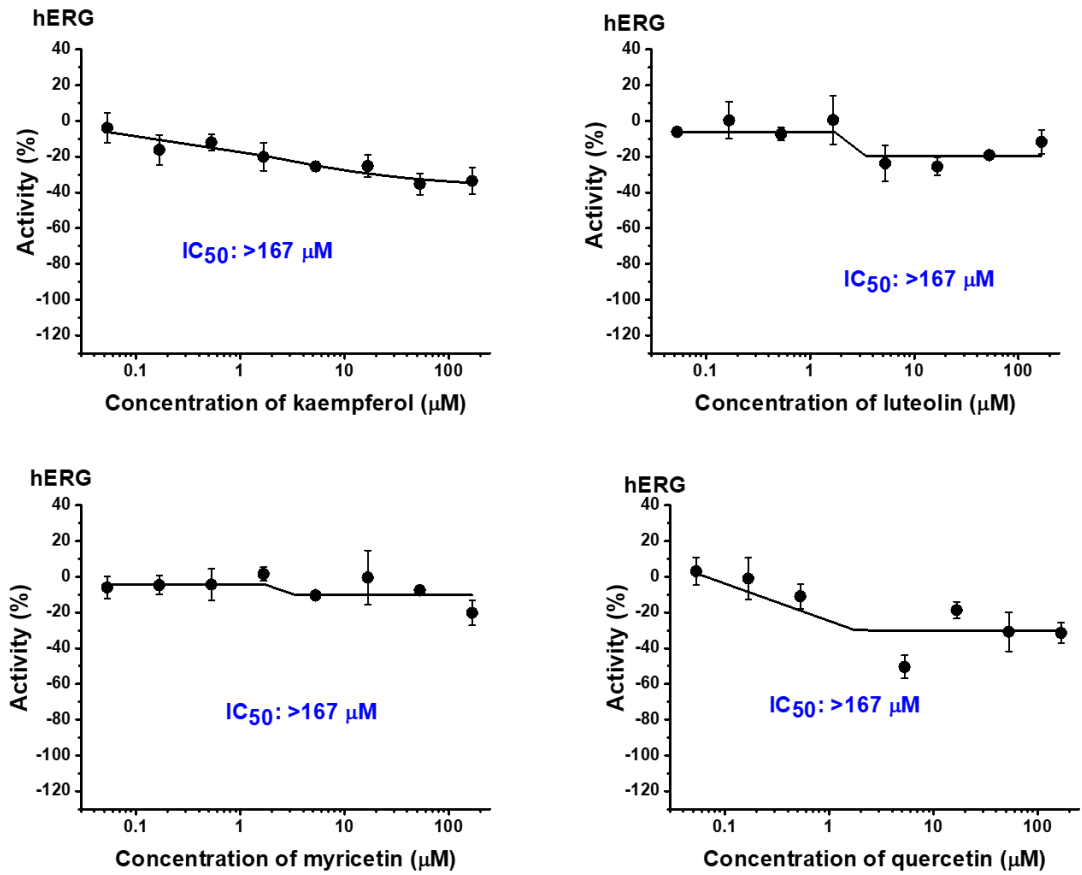


**Figure 82: Concentration-response data for kaempferol, luteolin, myricetin and quercetin against the hERG channel.** Whole-cell voltage clamp recordings were taken from CHO cells over-expressing hERG under control conditions and then following three minutes incubation with kaempferol, luteolin, myricetin and quercetin (0.05, 0.17, 0.5, 1.7, 5, 16, 50 and 167 μM). The current amplitude at the end of 3.5 seconds activating clamp step was recorded and plotted as a percentage of the pre-compound current. The fitted curve is a Hill equation with an  $IC_{50}$  of >167 μM for kaempferol ( $n/N=1/3$ ), luteolin ( $n/N=1/3$ ), myricetin( $n/N=1/3$ ) and quercetin( $n/N=1/3$ ).

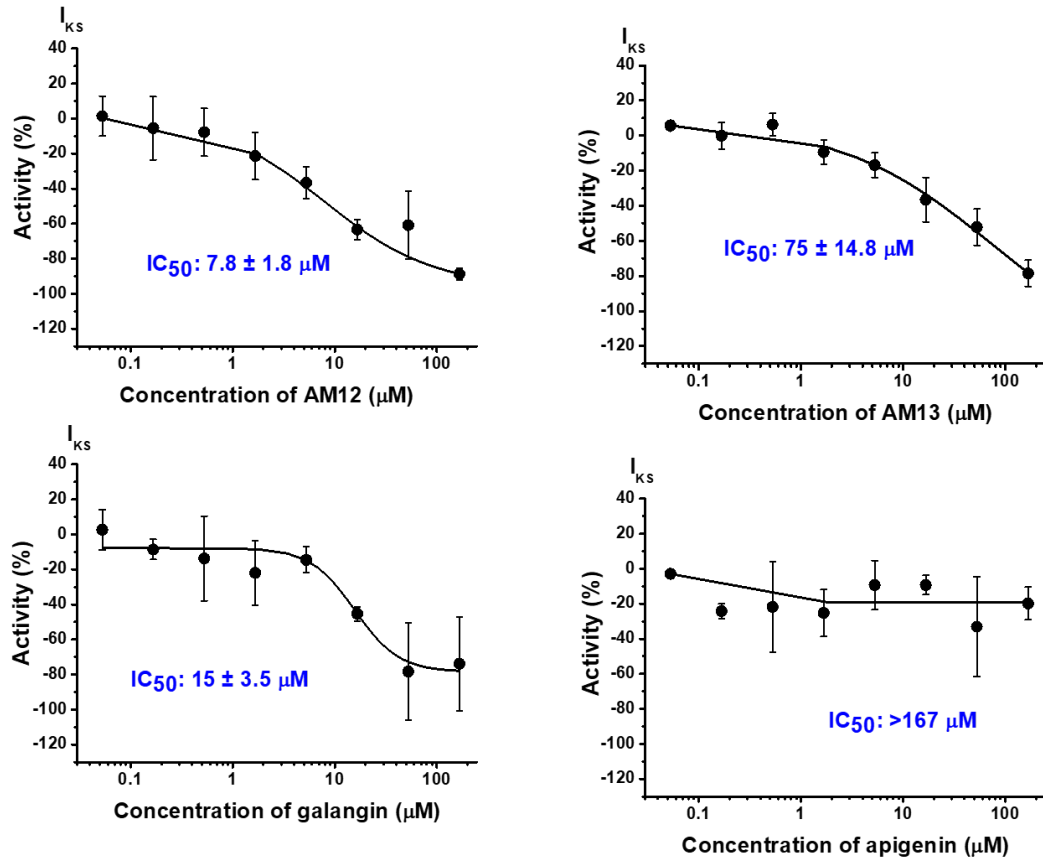


**Figure 83: Concentration-response data for AM12, AM13, galangin and apigenin against the  $I_{Ks}$  channel.** Whole-cell voltage clamp recordings were taken from CHO cells over-expressing hKvLQT1/hminK under control conditions and then following three minutes incubation with AM12, AM13, galangin and apigenin (0.05, 0.17, 0.5, 1.7, 5, 16, 50 and 167  $\mu M$ ). The current amplitude at the end of 3.5 seconds activating clamp step was recorded and plotted as a percentage of the pre-compound current. The fitted curve is a Hill equation with an  $IC_{50}$  for AM12 of  $7.8 \pm 1.8 \mu M$  ( $n/N=2/6$ ), AM13:  $75 \pm 15 \mu M$  ( $n/N=2/6$ ), galangin:  $15 \pm 3.5 \mu M$  ( $n/N=1/3$ ) and apigenin:  $>167 \mu M$  ( $n/N=1/3$ ). (Mean  $\pm$  SD of mean)

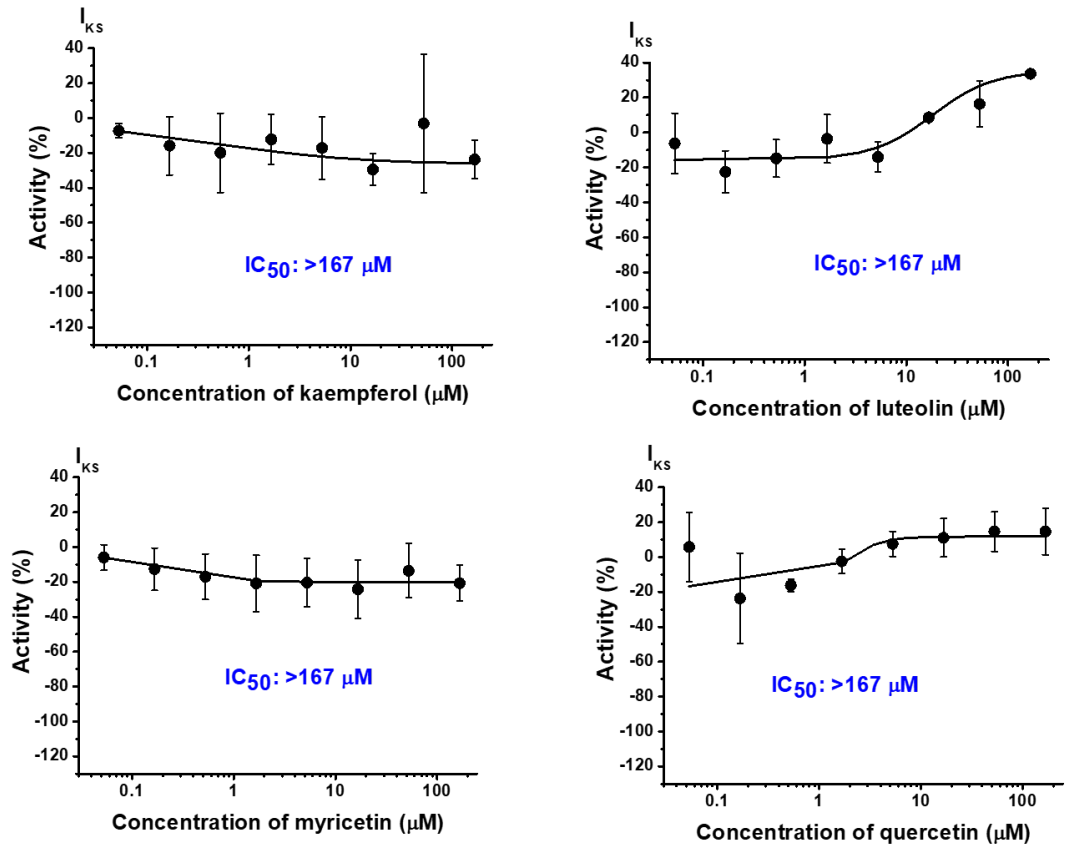


**Figure 84: Concentration-response data for kaempferol, luteolin, myricetin and quercetin against the  $I_{KS}$  channel.** Whole-cell voltage clamp recordings were taken from CHO cells over-expressing hKvLQT1/hminK under control conditions and then following three minutes incubation with kaempferol, luteolin, myricetin and quercetin (0.05, 0.17, 0.5, 1.7, 5, 16, 50 and 167  $\mu\text{M}$ ). The current amplitude at the end of 3.5 seconds activating clamp step was recorded and plotted as a percentage of the pre-compound current. The fitted curve is a Hill equation with an  $\text{IC}_{50}$  of >167  $\mu\text{M}$  for kaempferol ( $n/N=1/3$ ), luteolin ( $n/N=1/3$ ), myricetin( $n/N=1/3$ ) and quercetin( $n/N=1/3$ ).

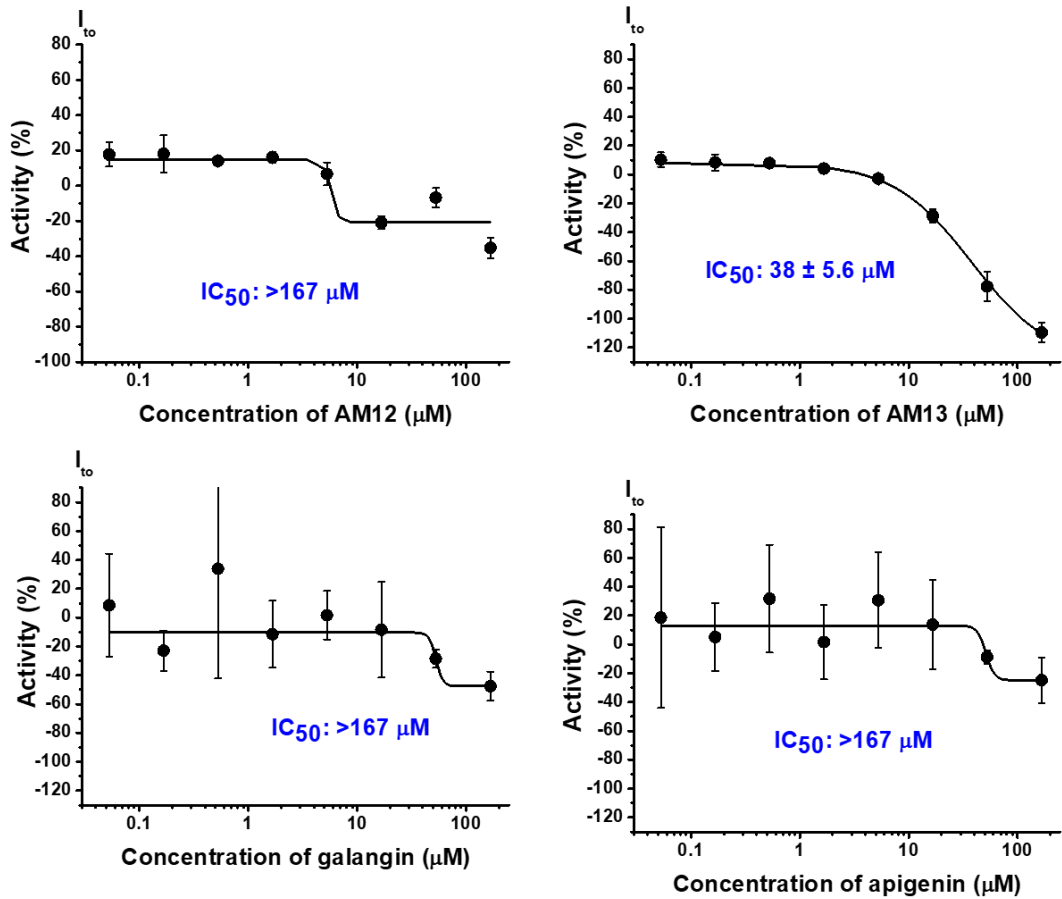


**Figure 85: Concentration-response data for AM12, AM13, galangin and apigenin against the  $I_{to}$  channel.** Whole-cell voltage clamp recordings were taken from CHO cells over-expressing  $K_v4.3/KChIP2.2$  under control conditions and then following three minutes incubation with AM12, AM13, galangin and apigenin (0.05, 0.17, 0.5, 1.7, 5, 16, 50 and 167 μM). The current amplitude at the end of the 2 seconds activating clamp step was recorded and plotted as a percentage of the pre-compound current. The fitted curve is a Hill equation with an  $IC_{50}$  for AM12 of  $>167 \mu M$  ( $n/N=2/6$ ), AM13:  $38 \pm 5.6 \mu M$  ( $n/N=2/6$ ), galangin:  $>167 \mu M$  ( $n/N=1/3$ ) and apigenin:  $>167 \mu M$  ( $n/N=1/3$ ). (Mean  $\pm$  SD of mean)

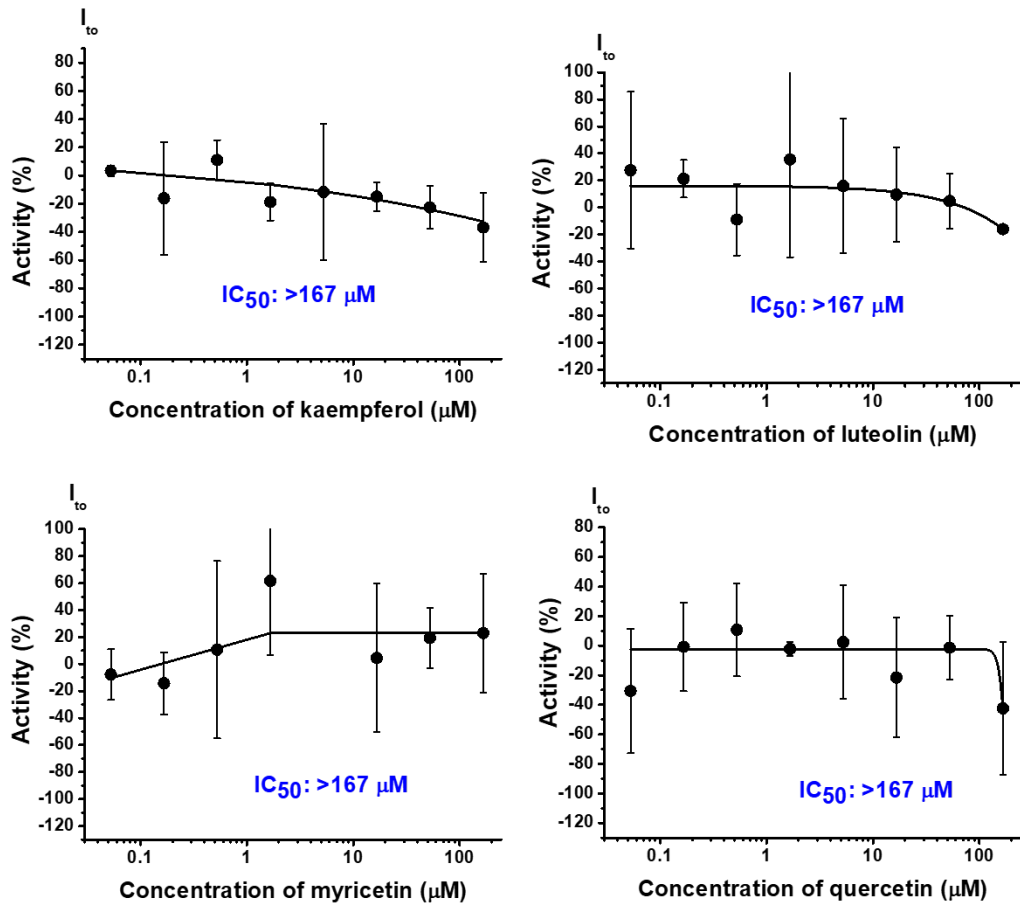


**Figure 86: Concentration-response data for kaempferol, luteolin, myricetin and quercetin against the  $I_{to}$  channel.** Whole-cell voltage clamp recordings were taken from CHO cells over-expressing  $K_{v4.3}/K\text{ChIP}2.2$  under control conditions and then following three minutes incubation with kaempferol, luteolin, myricetin and quercetin (0.05, 0.17, 0.5, 1.7, 5, 16, 50 and 167  $\mu\text{M}$ ). The current amplitude at the end of the 2 seconds activating clamp step was recorded and plotted as a percentage of the pre-compound current. The fitted curve is a Hill equation with an  $\text{IC}_{50}$  of  $>167 \mu\text{M}$  for kaempferol ( $n/N=1/3$ ), luteolin ( $n/N=1/3$ ), myricetin( $n/N=1/3$ ) and quercetin( $n/N=1/3$ ).

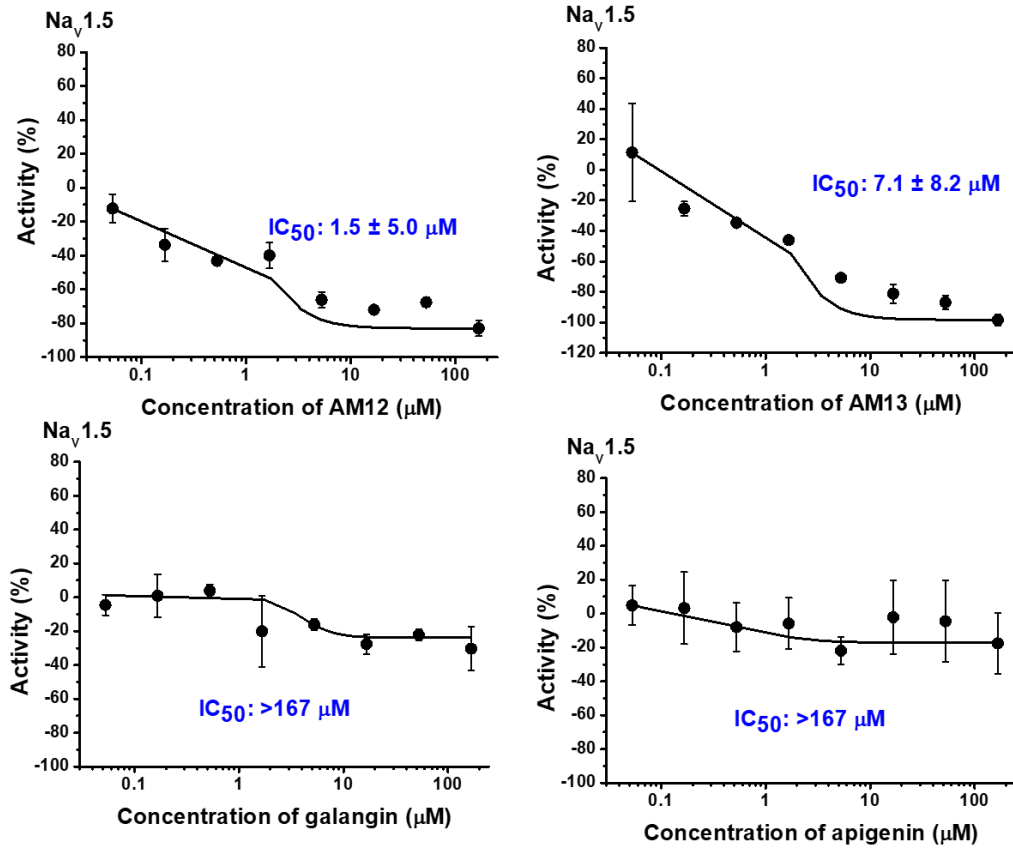


**Figure 87: Concentration-response data for AM12, AM13, galangin and apigenin against the Nav<sub>v</sub>1.5 channel.** Whole-cell voltage clamp recordings were taken from CHO cells over-expressing Nav<sub>v</sub>1.5 under control conditions and then following three minutes incubation with AM12, AM13, galangin and apigenin (0.05, 0.17, 0.5, 1.7, 5, 16, 50 and 167 μM). The current amplitude at the end of the 3 seconds activating clamp step was recorded and plotted as a percentage of the pre-compound current. The fitted curve is a Hill equation with an IC<sub>50</sub> for AM12 of 1.5 ± 5.0 μM (n/N=2/6), AM13: 7.1 ± 8.2 μM (n/N=2/6), galangin: >167 μM (n/N=1/3) and apigenin: >167 μM (n/N=1/3). (Mean ± SD of mean)

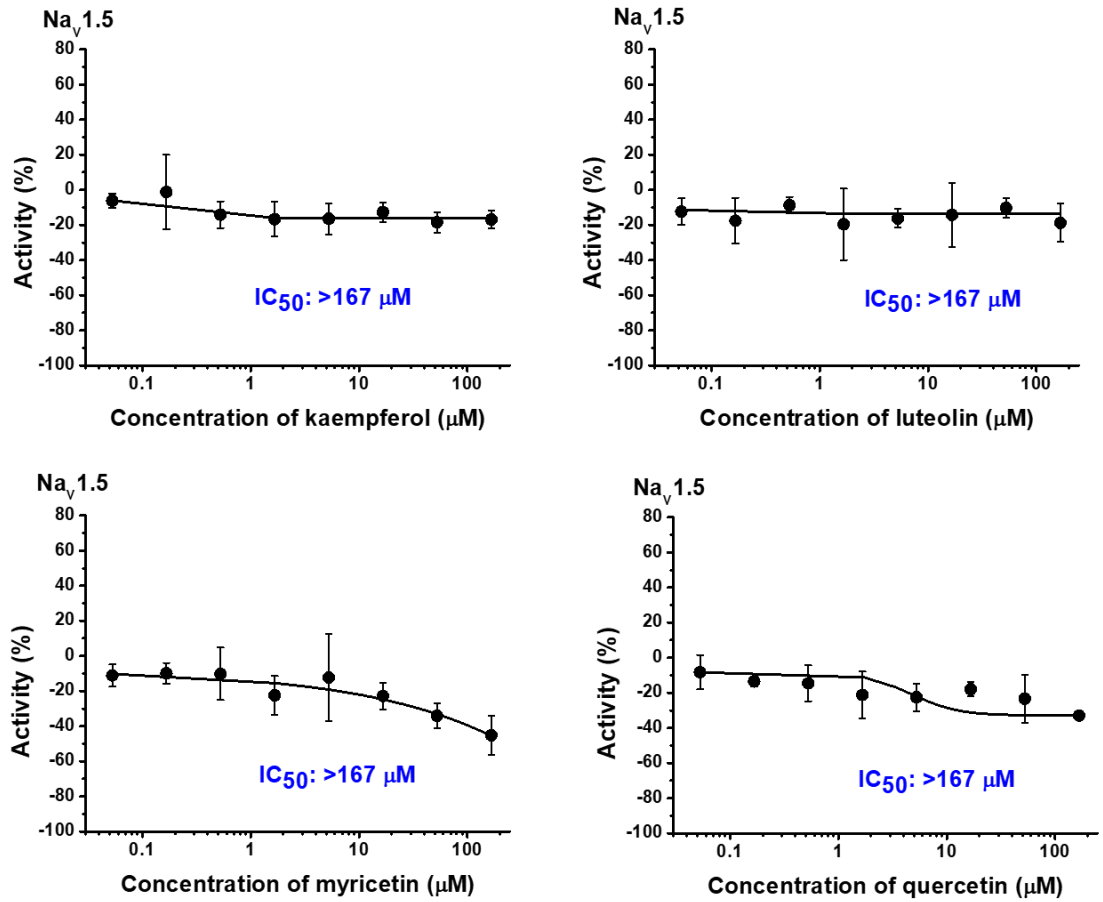


**Figure 88: Concentration-response data for kaempferol, luteolin, myricetin and quercetin against the  $Na_v1.5$  channel.** Whole-cell voltage clamp recordings were taken from CHO cells over-expressing  $Na_v1.5$  under control conditions and then following three minutes incubation with kaempferol, luteolin, myricetin and quercetin (0.05, 0.17, 0.5, 1.7, 5, 16, 50 and 167  $\mu M$ ). The current amplitude at the end of the 3 seconds activating clamp step was recorded and plotted as a percentage of the pre-compound current. The fitted curve is a Hill equation with an  $IC_{50}$  of  $>167 \mu M$  for kaempferol ( $n/N=1/3$ ), luteolin ( $n/N=1/3$ ), myricetin( $n/N=1/3$ ) and quercetin( $n/N=1/3$ ).



### Cardiac safety screening data for piperazine/piperidine compounds

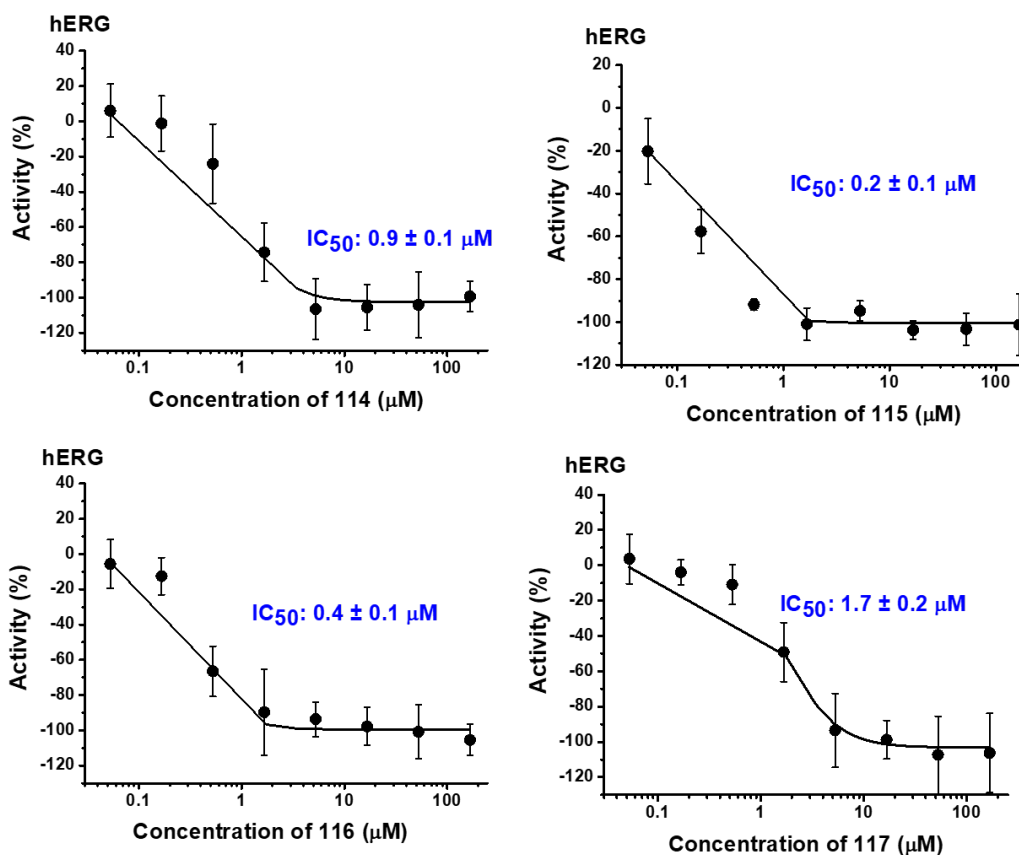


**Figure 89: Concentration-response data for 114, 115, 116 and 117 against the hERG channel.** Whole-cell voltage clamp recordings were taken from CHO cells over-expressing hERG under control conditions and then following three minutes incubation with 114, 115, 116 and 117 (0.05, 0.17, 0.5, 1.7, 5, 16, 50 and 167 μM). The current amplitude at the end of 3.5 seconds activating clamp step was recorded and plotted as a percentage of the pre-compound current. The fitted curve is a Hill equation with an IC<sub>50</sub> for 114: of 0.9 ± 0.1 μM (n/N=2/7), 115: 0.2 ± 0.1 μM (n/N=2/6), 116: 0.4 ± 0.1 μM (n/N=2/6) and 117: 1.7 ± 0.2 μM (n/N=4/12). (Mean ± SD of mean)

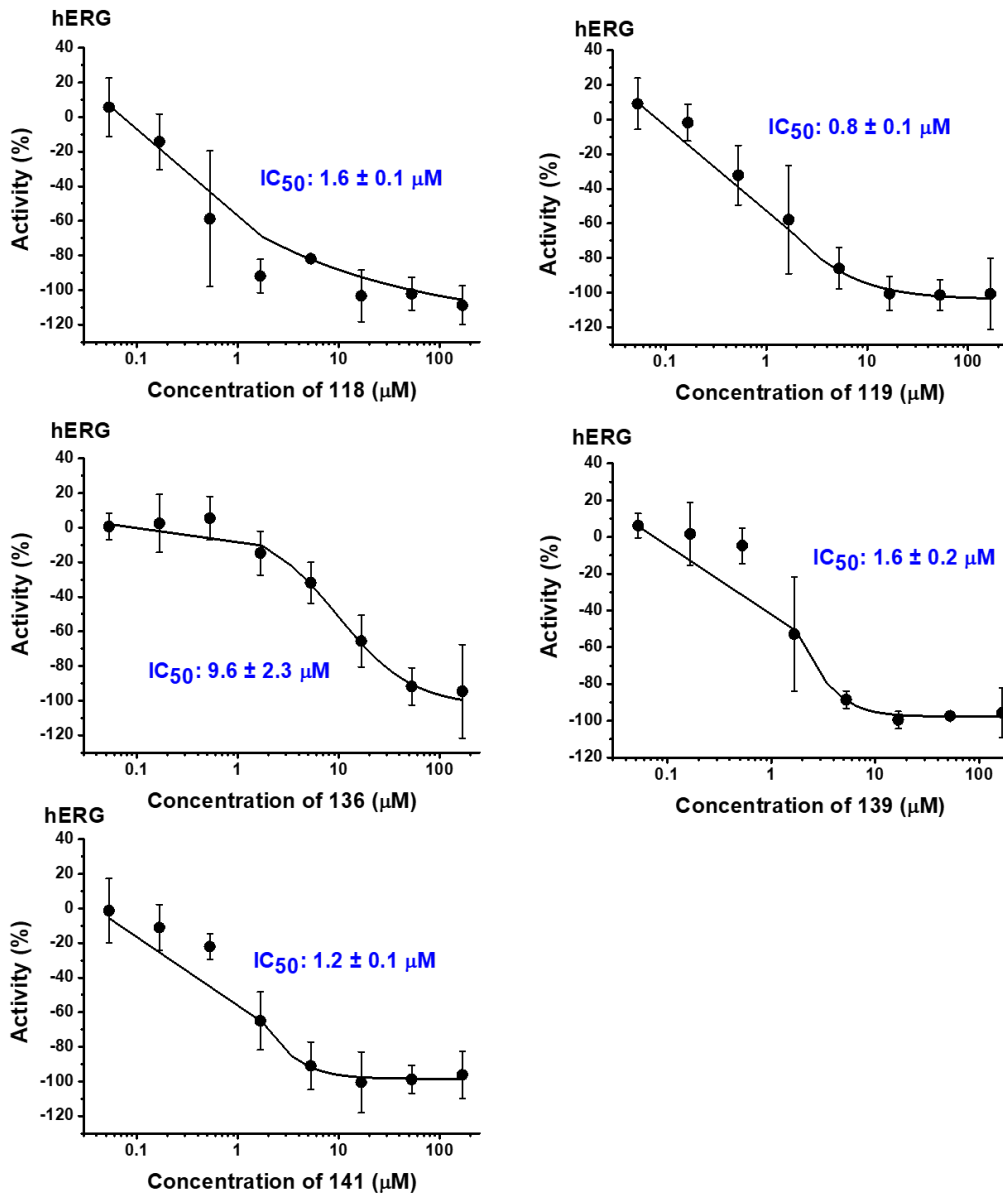


**Figure 90: Concentration-response data for 118, 119, 136, 139 and 141 against the hERG channel.** Whole-cell voltage clamp recordings were taken from CHO cells over-expressing hERG under control conditions and then following three minutes incubation with 118, 119, 136, 139 and 141 (0.05, 0.17, 0.5, 1.7, 5, 16, 50 and 167 μM). The current amplitude at the end of 3.5 seconds activating clamp step was recorded and plotted as a percentage of the pre-compound current. The fitted curve is a Hill equation with an IC<sub>50</sub> for 118: of 1.6 ± 0.1 μM (n/N=4/10), 119: 0.8 ± 0.1 μM (n/N=4/12), 136: 9.6 ± 2.3 μM (n/N=4/12), 139: 1.6 ± 0.2 μM (n/N=2/6) and 141: 1.2 ± 0.1 μM (n/N=4/10). (Mean ± SD of mean)

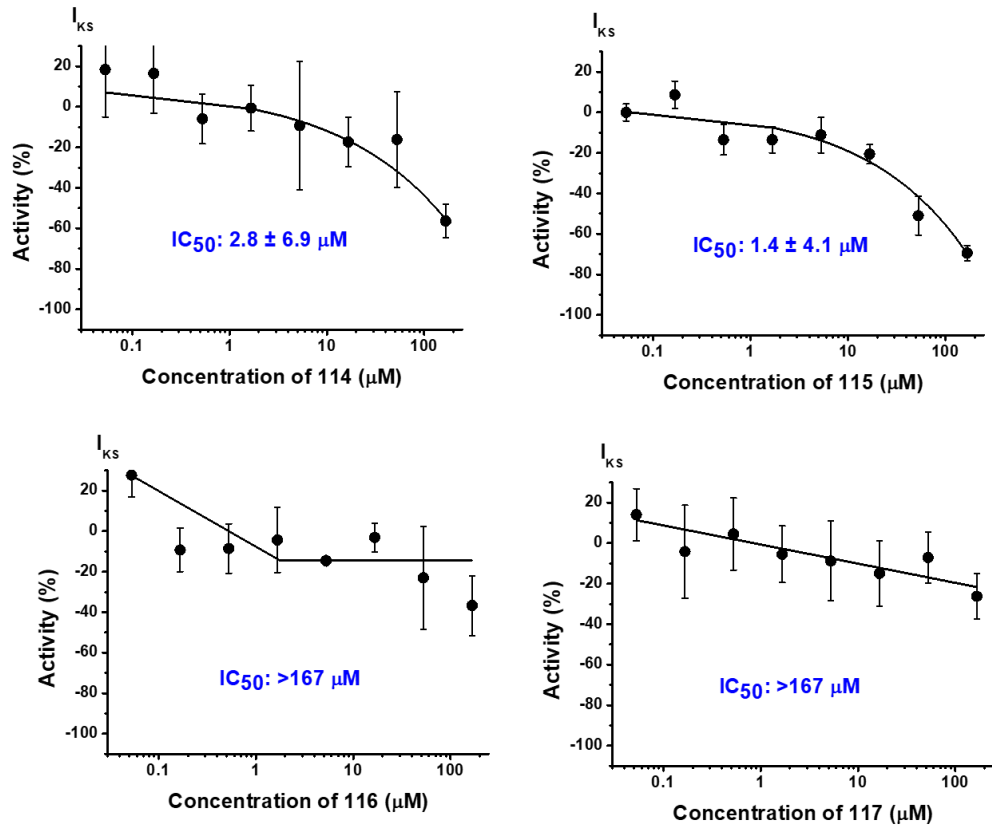


**Figure 91: Concentration-response data for 114, 115, 116 and 117 against the  $I_{Ks}$  channel.** Whole-cell voltage clamp recordings were taken from CHO cells over-expressing *hKvLQT1/hminK* under control conditions and then following three minutes incubation with 114, 115, 116 and 117 (0.05, 0.17, 0.5, 1.7, 5, 16, 50 and 167  $\mu M$ ). The current amplitude at the end of 3.5 seconds activating clamp step was recorded and plotted as a percentage of the pre-compound current. The fitted curve is a Hill equation with an  $IC_{50}$  of 114: of  $2.8 \pm 6.9 \mu M$  ( $n/N=2/7$ ), 115:  $1.4 \pm 4.1 \mu M$  ( $n/N=2/6$ ), 116:  $>167 \mu M$  ( $n/N=2/6$ ) and 117:  $>167 \mu M$  ( $n/N=4/12$ ). (Mean  $\pm$  SD of mean).

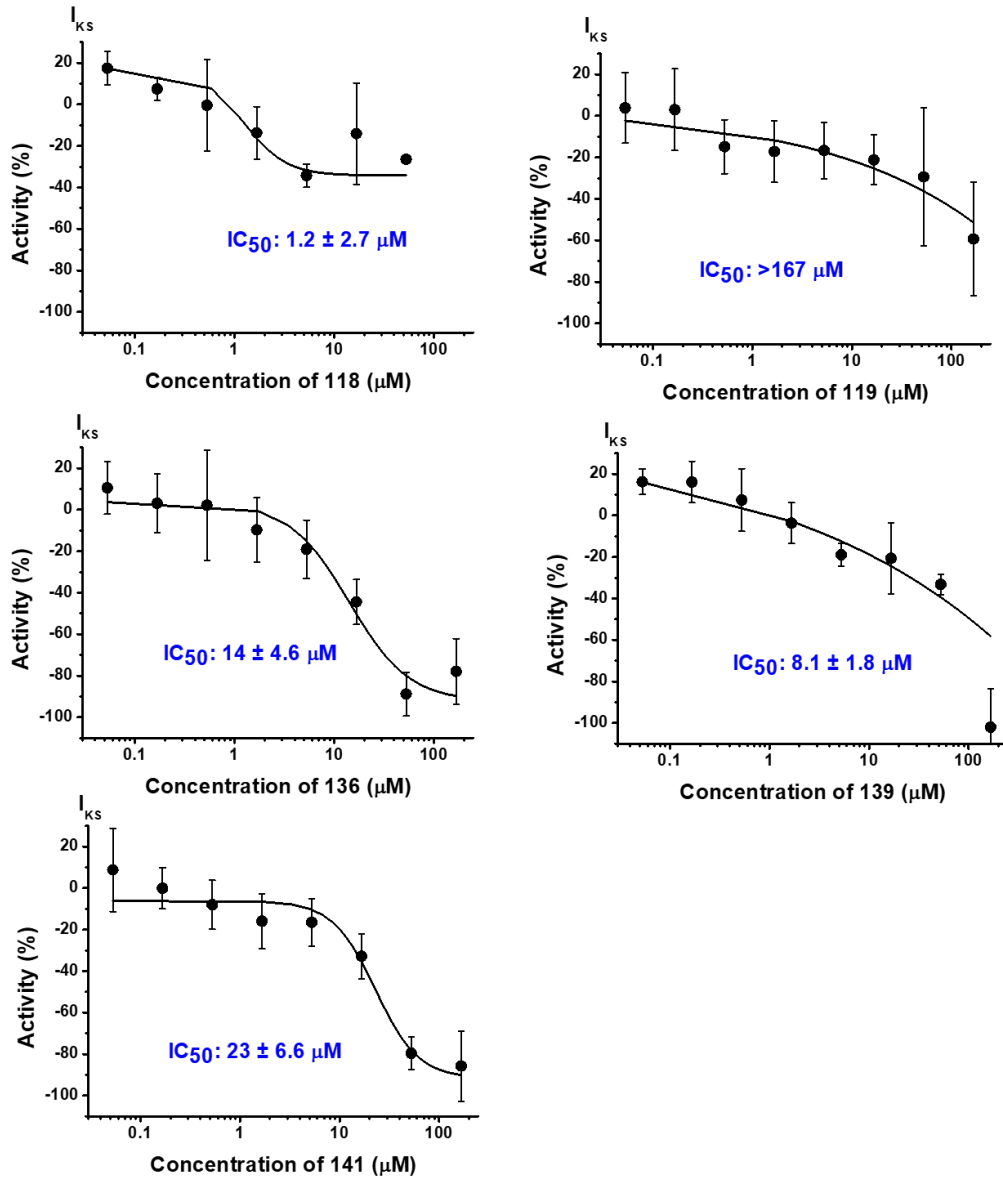


**Figure 92: Concentration-response data for 118, 119, 136, 139 and 141 against the  $I_{KS}$  channel.** Whole-cell voltage clamp recordings were taken from CHO cells over-expressing *hKvLQT1/hminK* under control conditions and then following three minutes incubation with 118, 119, 136, 139 and 141 (0.05, 0.17, 0.5, 1.7, 5, 16, 50 and 167  $\mu\text{M}$ ). The current amplitude at the end of 3.5 seconds activating clamp step was recorded and plotted as a percentage of the pre-compound current. The fitted curve is a Hill equation with an  $IC_{50}$  of 118: of  $1.2 \pm 2.7$   $\mu\text{M}$  ( $n/N=4/10$ ), 119:  $>167$   $\mu\text{M}$  ( $n/N=4/12$ ), 136:  $14 \pm 4.6$   $\mu\text{M}$  ( $n/N=4/12$ ), 139:  $8.1 \pm 1.8$   $\mu\text{M}$  ( $n/N=2/6$ ) and 141:  $23 \pm 6.6$   $\mu\text{M}$  ( $n/N=4/10$ ). (Mean  $\pm$  SD of mean).

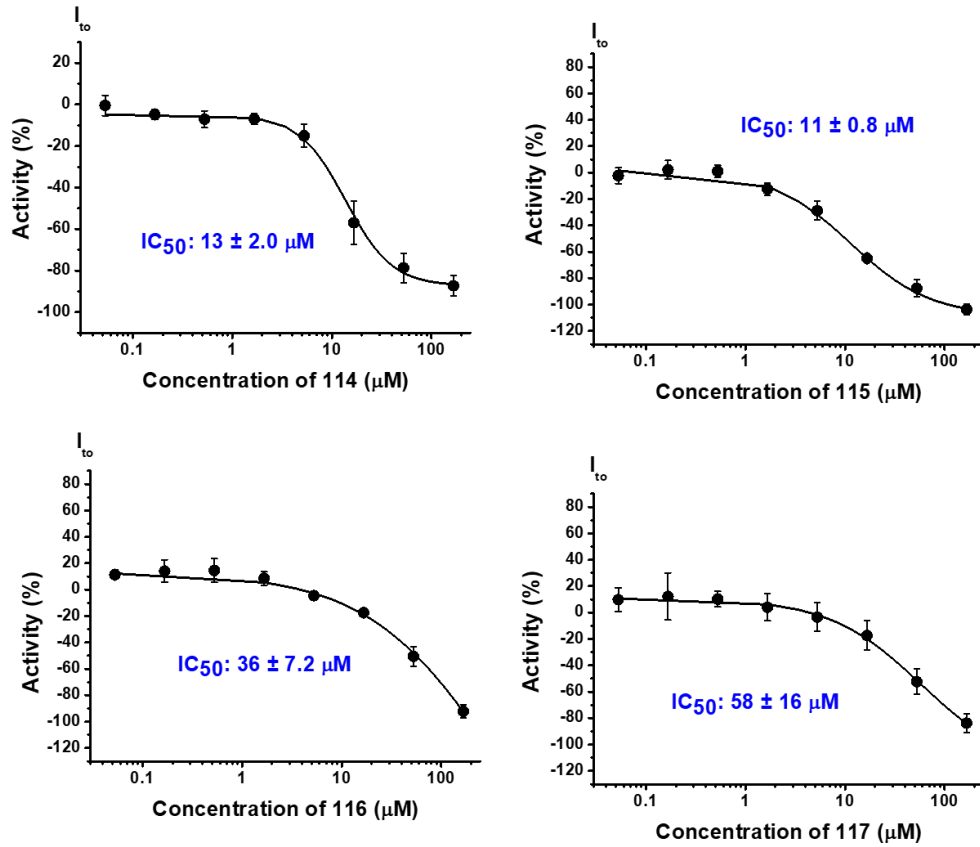


**Figure 93: Concentration-response data for 114, 115, 116 and 117 against the  $I_{to}$  channel.** Whole-cell voltage clamp recordings were taken from CHO cells over-expressing  $K_{v4.3}/KChIP2.2$  under control conditions and then following three minutes incubation with 114, 115, 116 and 117 (0.05, 0.17, 0.5, 1.7, 5, 16, 50 and 167  $\mu\text{M}$ ). The current amplitude at the end of the 2 seconds activating clamp step was recorded and plotted as a percentage of the pre-compound current. The fitted curve is a Hill equation with an  $\text{IC}_{50}$  of 114: of  $13 \pm 2.0 \mu\text{M}$  ( $n/N=2/7$ ), 115:  $11 \pm 0.8 \mu\text{M}$  ( $n/N=2/6$ ), 116:  $36 \pm 7.2 \mu\text{M}$  ( $n/N=2/6$ ) and 117:  $58 \pm 16 \mu\text{M}$  ( $n/N=4/12$ ). (Mean  $\pm$  SD of mean).

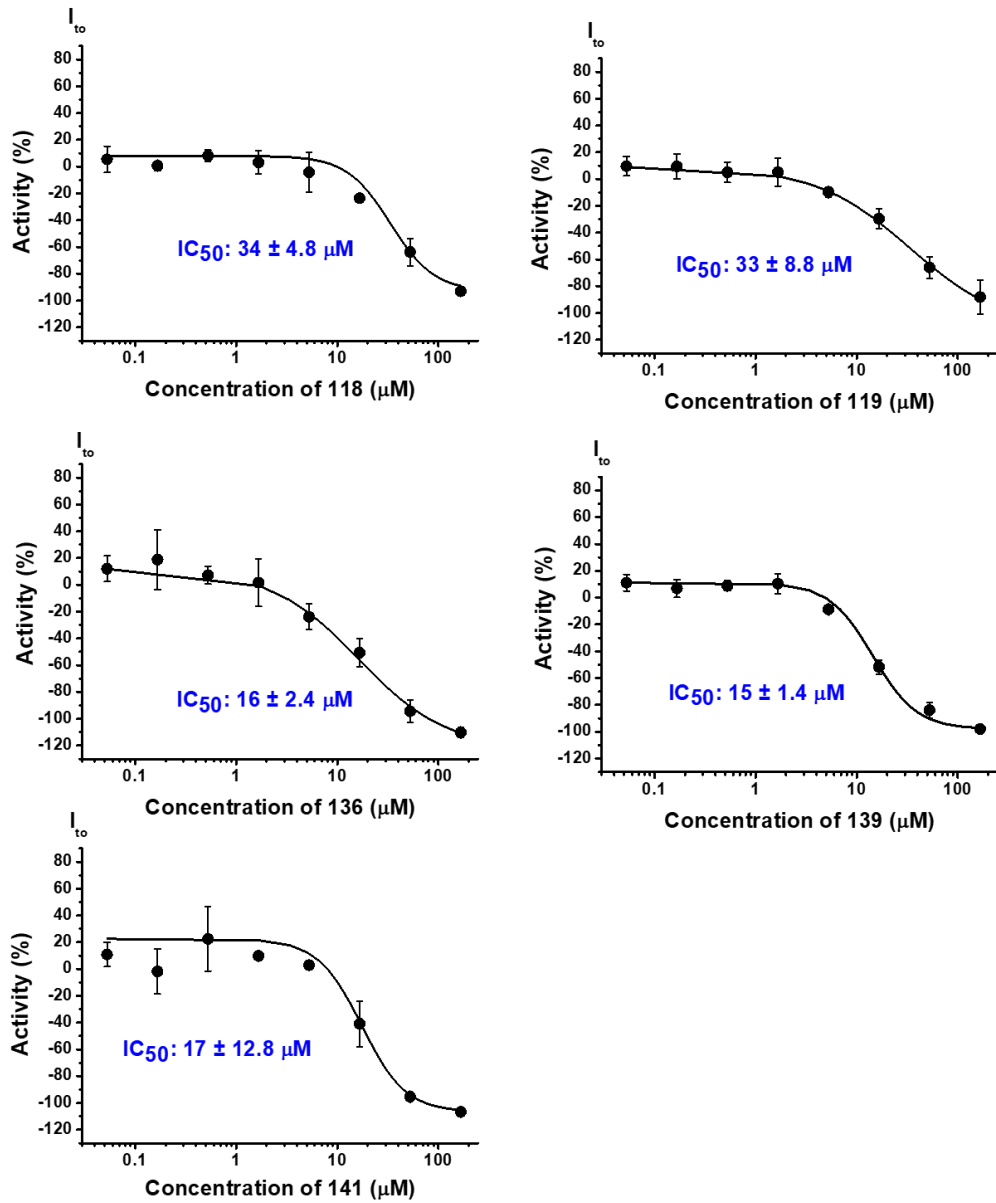


**Figure 94: Concentration-response data for 118, 119, 136, 139 and 141 against the  $I_{to}$  channel.** Whole-cell voltage clamp recordings were taken from CHO cells over-expressing  $K_{V4.3}/KChIP2.2$  under control conditions and then following three minutes incubation with 118, 119, 136, 139 and 141 (0.05, 0.17, 0.5, 1.7, 5, 16, 50 and 167 µM). The current amplitude at the end of the 2 seconds activating clamp step was recorded and plotted as a percentage of the pre-compound current. The fitted curve is a Hill equation with an  $IC_{50}$  of 118: of  $34 \pm 4.8$  µM ( $n/N=4/10$ ), 119:  $33 \pm 8.8$  µM ( $n/N=4/12$ ), 136:  $16 \pm 2.4$  µM ( $n/N=4/12$ ), 139:  $15 \pm 1.4$  µM ( $n/N=2/6$ ) and 141:  $17 \pm 12.8$  µM ( $n/N=4/10$ ). (Mean  $\pm$  SD of mean).

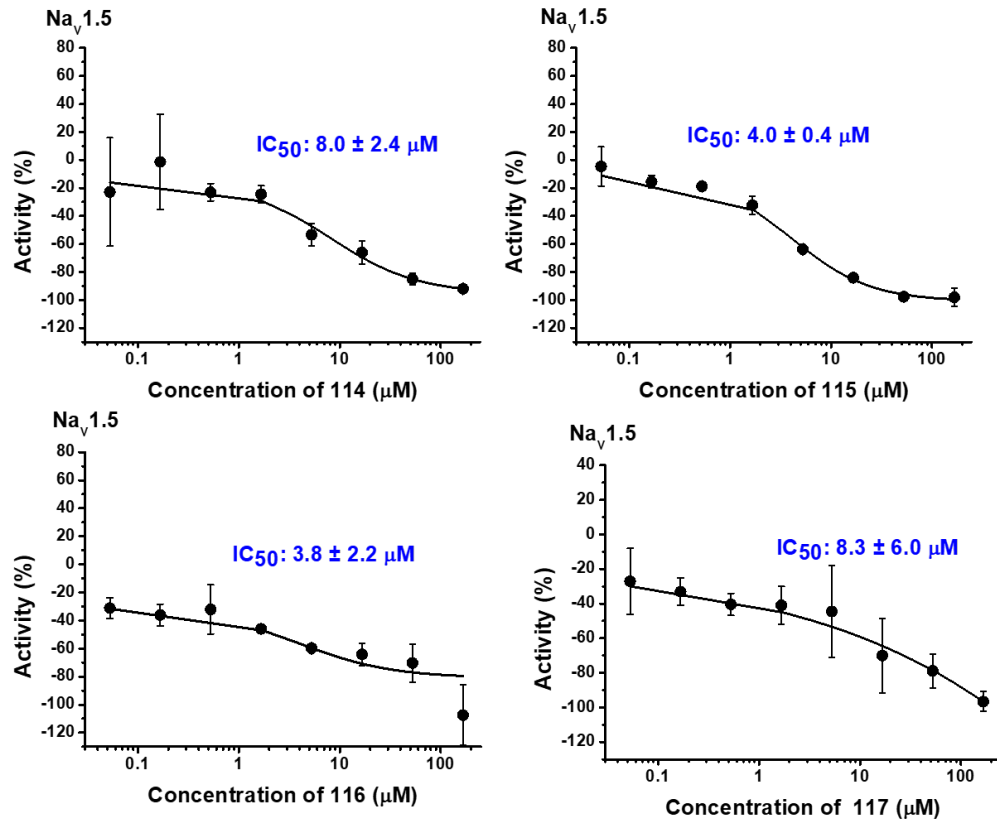


**Figure 95: Concentration-response data for 114, 115, 116 and 117 against the  $Na_v 1.5$  channel.** Whole-cell voltage clamp recordings were taken from CHO cells over-expressing  $Na_v 1.5$  under control conditions and then following three minutes incubation with 114, 115, 116 and 117 (0.05, 0.17, 0.5, 1.7, 5, 16, 50 and 167  $\mu M$ ). The current amplitude at the end of the 3 seconds activating clamp step was recorded and plotted as a percentage of the pre-compound current. The fitted curve is a Hill equation with an  $IC_{50}$  of 114: of  $8.0 \pm 2.4 \mu M$  ( $n/N=2/7$ ), 115:  $4.0 \pm 0.4 \mu M$  ( $n/N=2/6$ ), 116:  $3.8 \pm 2.2 \mu M$  ( $n/N=2/6$ ) and 117:  $8.3 \pm 6.0 \mu M$  ( $n/N=4/12$ ). (Mean  $\pm$  SD of mean).

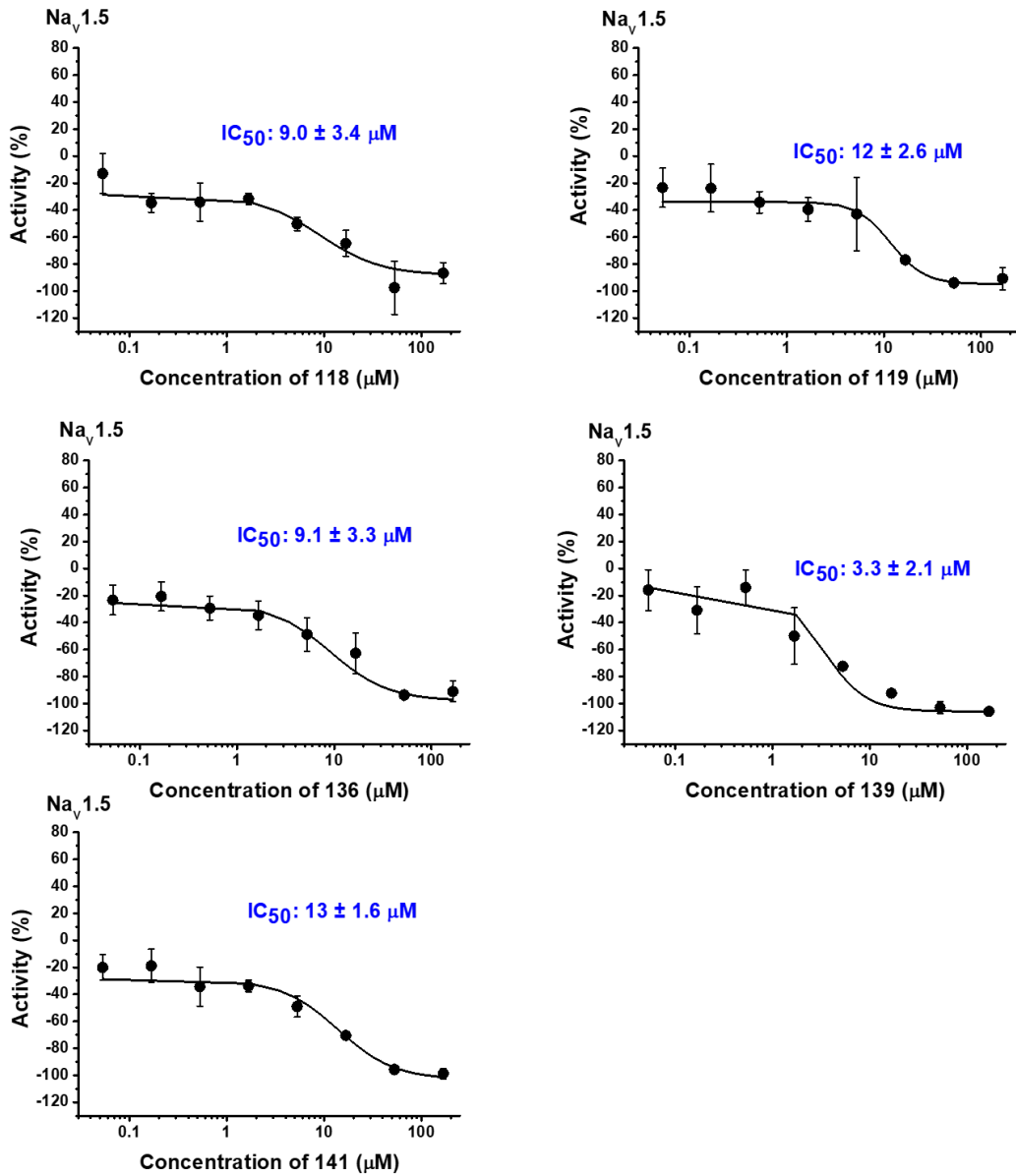


**Figure 96: Concentration-response data for 118, 119, 136, 139 and 141 against the Nav<sub>v</sub>1.5 channel.** Whole-cell voltage clamp recordings were taken from CHO cells over-expressing Nav<sub>v</sub>1.5 under control conditions and then following three minutes incubation with 118, 119, 136, 139 and 141 (0.05, 0.17, 0.5, 1.7, 5, 16, 50 and 167 μM). The current amplitude at the end of the 3 seconds activating clamp step was recorded and plotted as a percentage of the pre-compound current. The fitted curve is a Hill equation with an IC<sub>50</sub> of 118: of 9.0 ± 3.4 μM (n/N=4/12), 119: 12 ± 2.6 μM (n/N=4/12), 136: 9.1 ± 3.3 μM (n/N=4/12), 139: 3.3 ± 2.1 μM (n/N=2/6) and 141: 13 ± 1.6 μM (n/N=4/10). (Mean ± SD of mean).



## Appendix II

### Optimisation of activation of TRPC4-SYFP2.

Differing concentrations of (-)-EA were tested on HEK-293 T-REx cells with a tetracycline inducible system to overexpress TRPC4-SYFP2. By comparing cells lacking channel induction (tet-) with cells where the TRPC4-SYFP2 channel is induced with tetracycline (18-24 hours prior to experimentation) indicated a concentration for optimal size and clarity of the fluorescence measurements, where low levels of fluorescence are observed in the tet- cells. Increased calcium entry is observed in tet- cells with high concentrations of (-)-EA due to leaky expression of the channels. Many promoters can show some degree of expression without the addition of an inducer, which can cause an increase in the response of TRPC4-SYFP2 channels in comparison to endogenous levels.<sup>280</sup> Tet- cells should see low levels of fluorescence at the desired concentration of (-)-EA, therefore meaning there little leak in the expression system and the  $\text{Ca}^{2+}$  entry responses observed are attributable to the TRPC4-SYFP2 channels.

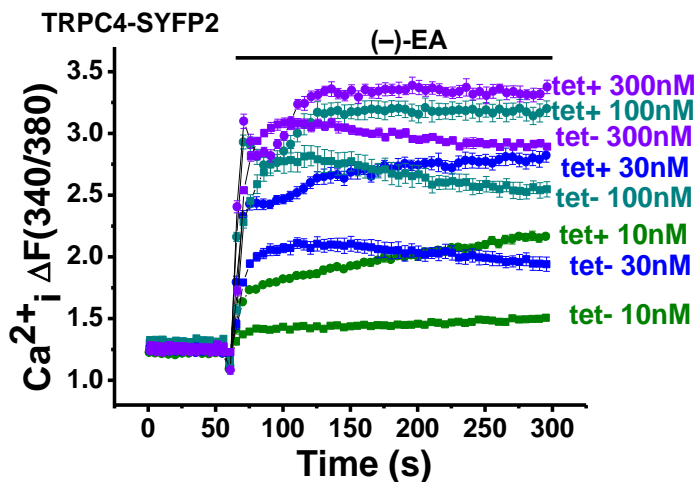


**Figure 97:** (-)-EA evoked  $\text{Ca}^{2+}$  entry in TRPC4-SYFP2 cells. Calcium measurement of the free intracellular calcium concentration in HEK-293 T-REx cells over-expressing TRPC4-SYFP2 (tet+) or no channel induction (tet-), with extracellular application of (-)-EA at 300, 100, 30 and 10 nM.

## Appendix III

### Identification of TRPC4-SYFP2 by immunoprecipitation.

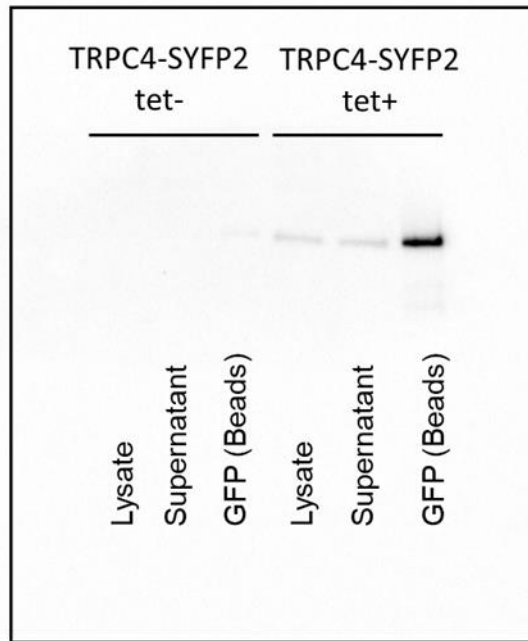
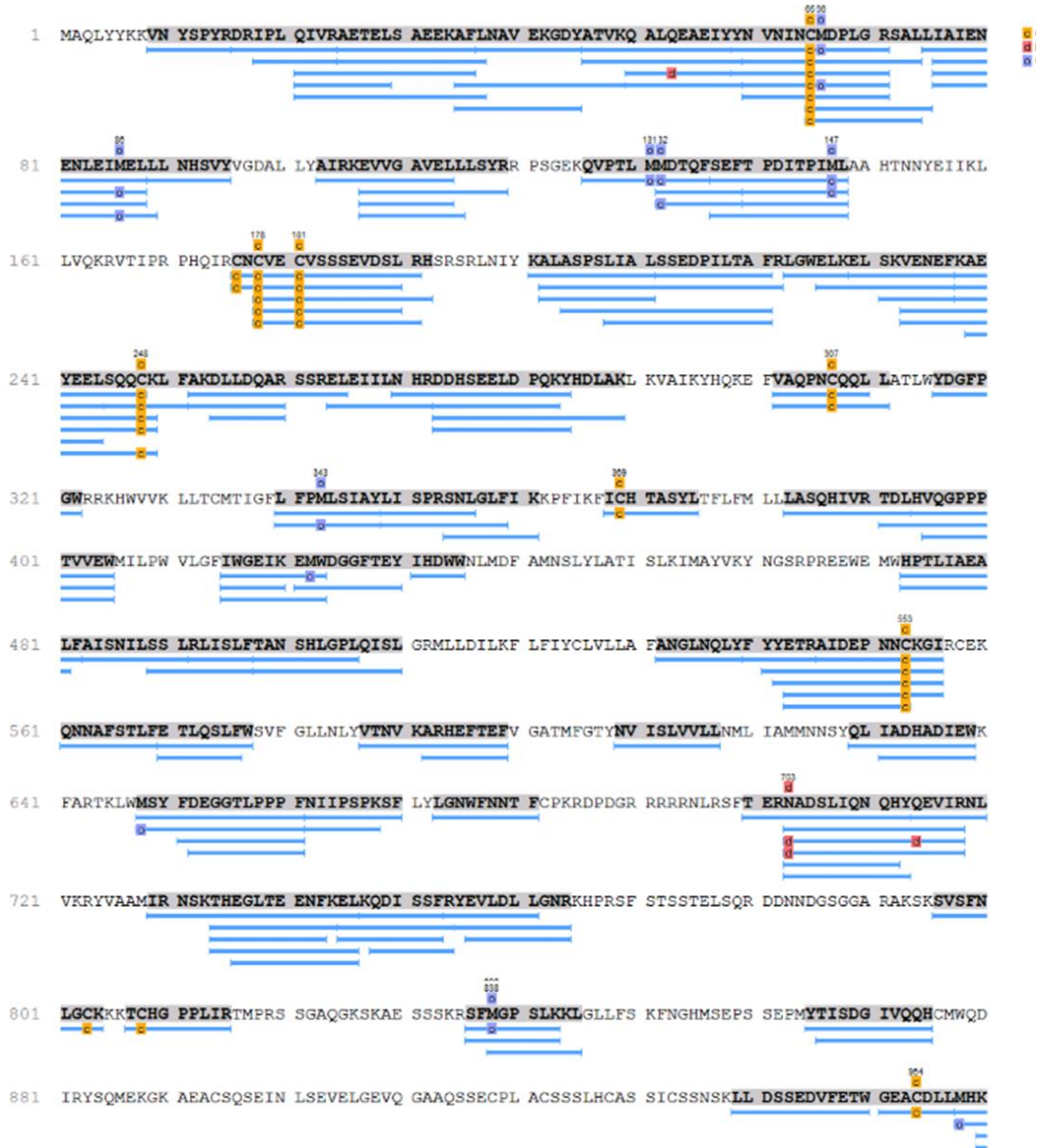


**Figure 98: Western blot analysis of immunoprecipitation of TRPC4-SYFP2.** HEK-293 T-REx cells over-expressing TRPC4-SYP2 (*tet+*) or no channel induction (*tet-*) were purified using GFP-trap beads and SDS-PAGE. Western blot analysis was performed with an anti-GFP antibody to confirm the presence of TRPC4-SYFP2.

## Appendix IV

Peptide mapping for TRPC5-SYFP2 using in-gel proteolytic digestion with chymotrypsin and trypsin proteases combined.



(Continued on page 202)

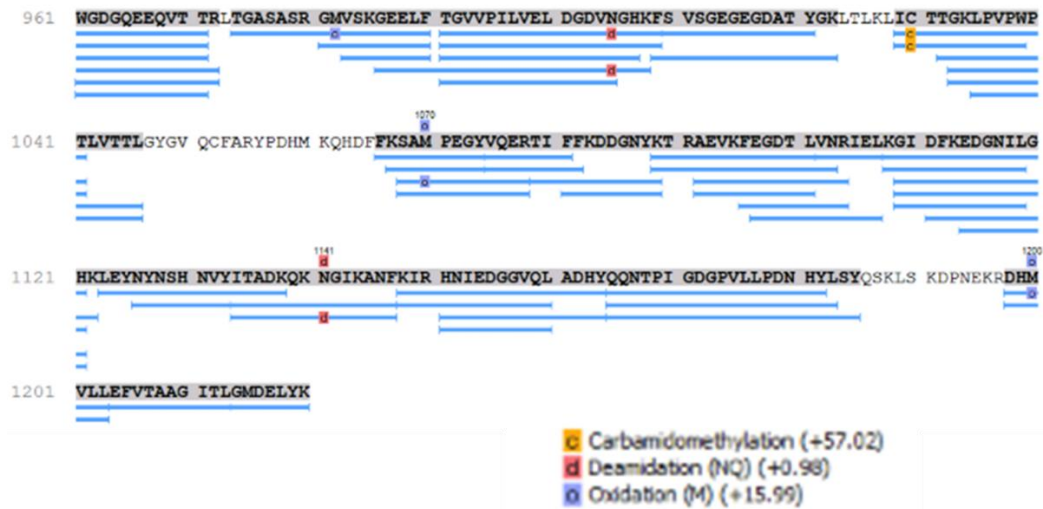


**Figure 99:** Peptide mapping for TRPC5-SYFP2 using in-gel proteolytic digestion with chymotrypsin and trypsin proteases combined to give a sequence coverage of 62%. Peptides detected in MS shown in blue, with post-translational modifications carbamidomethylation, deamidation and oxidation indicated by an orange 'c', red 'd' and blue 'o' respectively.

**Peptide mapping for TRPC5-SYFP2 using in-gel proteolytic digestion using ProteaseMAX surfactant with chymotrypsin and trypsin proteases.**



**Figure 100:** Peptide mapping for TRPC5-SYFP2 using in-gel proteolytic digestion using ProteaseMAX surfactant with chymotrypsin and trypsin proteases to give a combined sequence coverage of 54%. Peptides detected in MS shown in blue, with post-translational modifications carbamidomethylation and oxidation indicated by an orange 'c', and blue 'o' respectively.

**Peptide mapping for TRPC5-SYFP2 using on-bead proteolytic digestion with pepsin protease.**



**Figure 101:** Peptide mapping for TRPC5-SYFP2 using on-bead proteolytic digestion using pepsin protease to give a sequence coverage of 65%. Peptides detected in MS shown in blue, with post-translational modifications of oxidation indicated by a pink 'o'.

Peptide mapping for TRPC5-SYFP2 using on-bead proteolytic digestion using pepsin protease.



(continued on page 206)

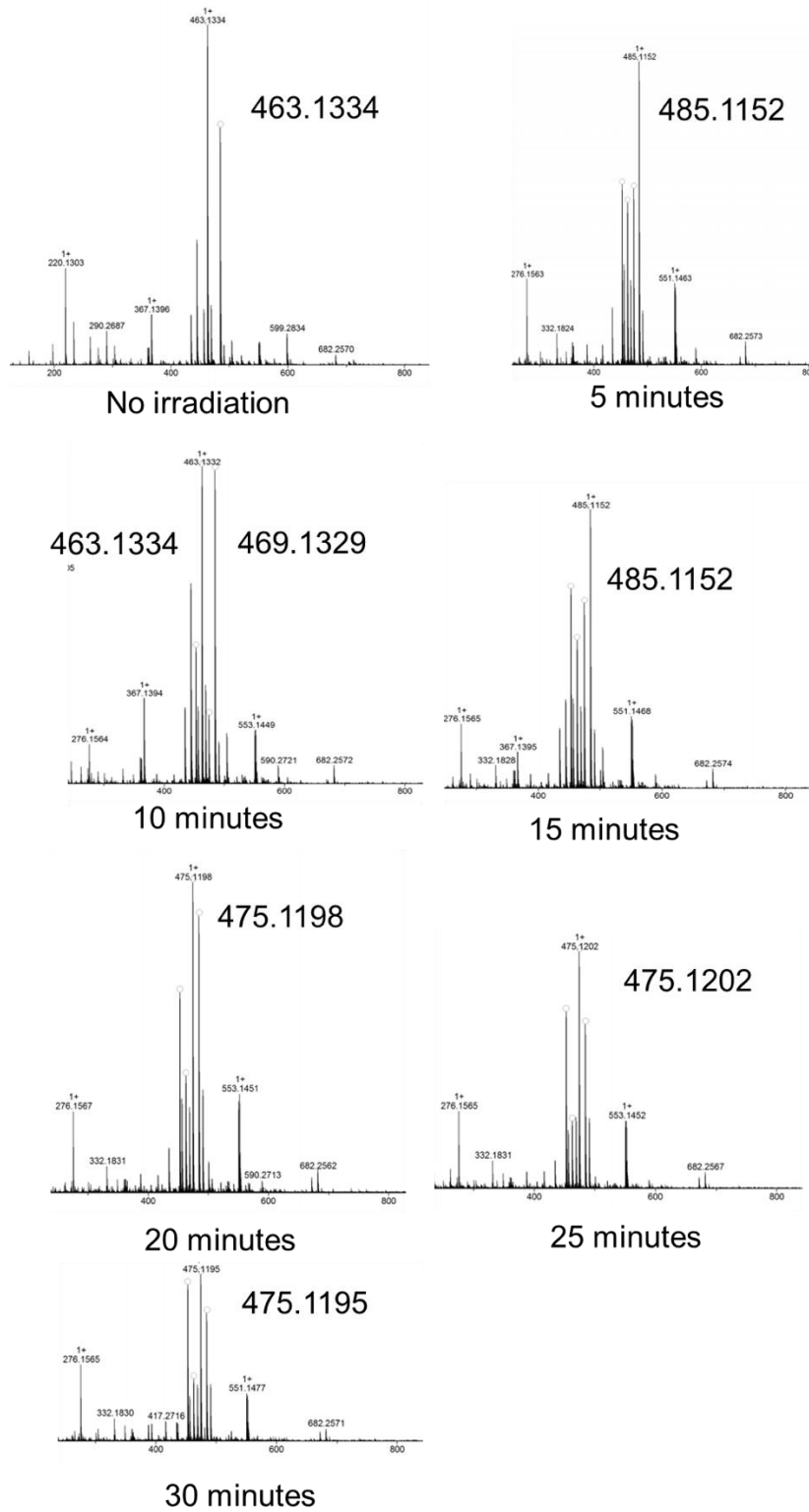


**Figure 102:** Peptide mapping for TRPC5-SYFP2 using on-bead proteolytic digestion using a combination of chymotrypsin, trypsin and Glu-C proteases to give a sequence coverage of 65%. Peptides detected in MS shown in blue, with post-translational modifications of carbamidomethylation, deamidation and oxidation indicated by an blue 'c', red 'd' and orange 'o' respectively.



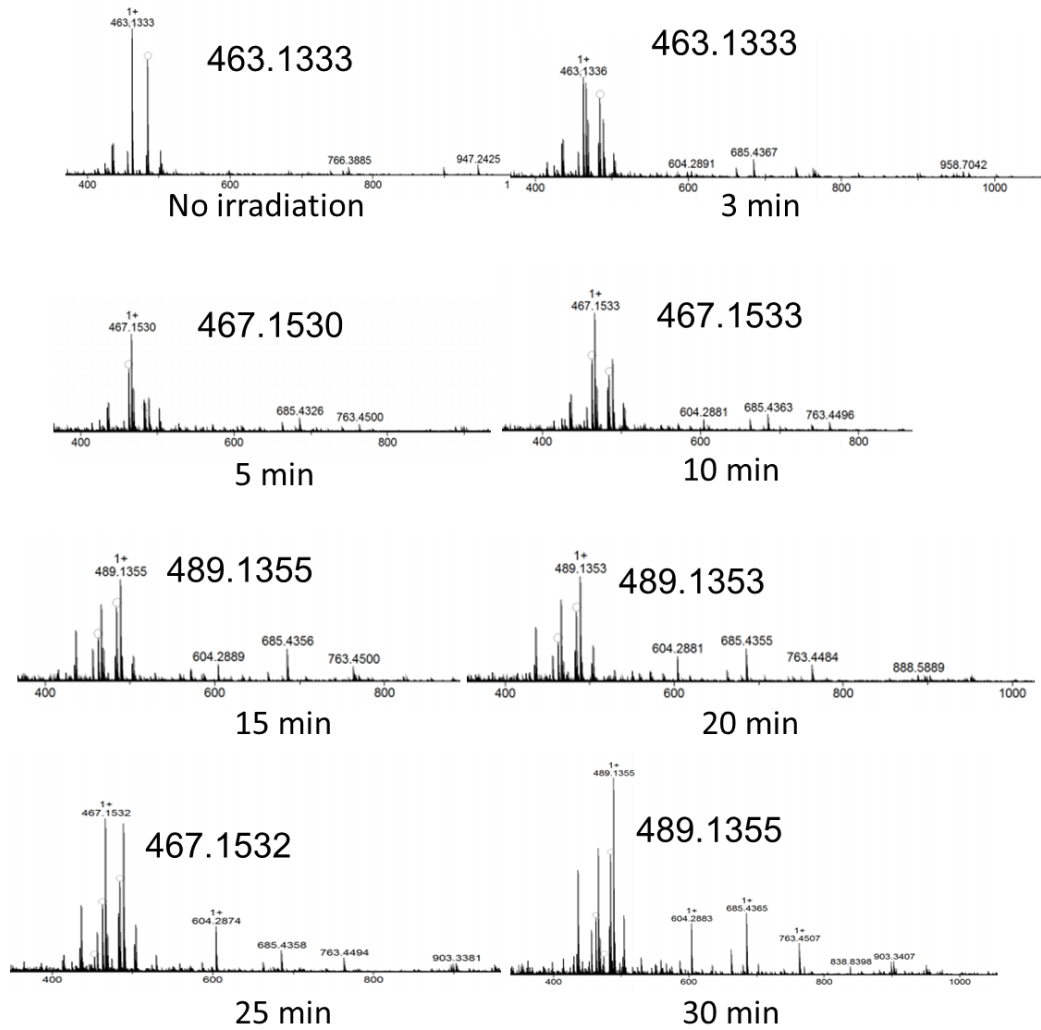
## Appendix V

Irradiation of Pico145-DAAlk in H<sub>2</sub>O at 365 nm.



**Figure 103:** MS spectra of Pico145-DAAlk in H<sub>2</sub>O with irradiation at 365 nm, for 0, 5, 10, 15, 20, 25 and 30 minutes.

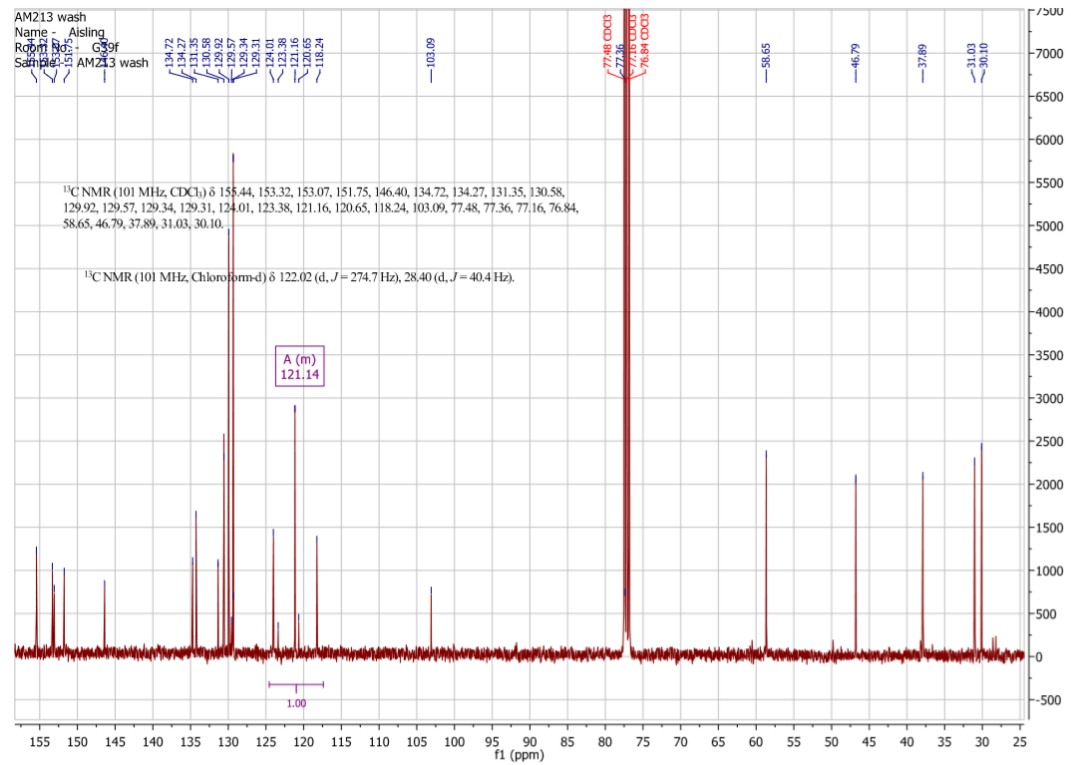
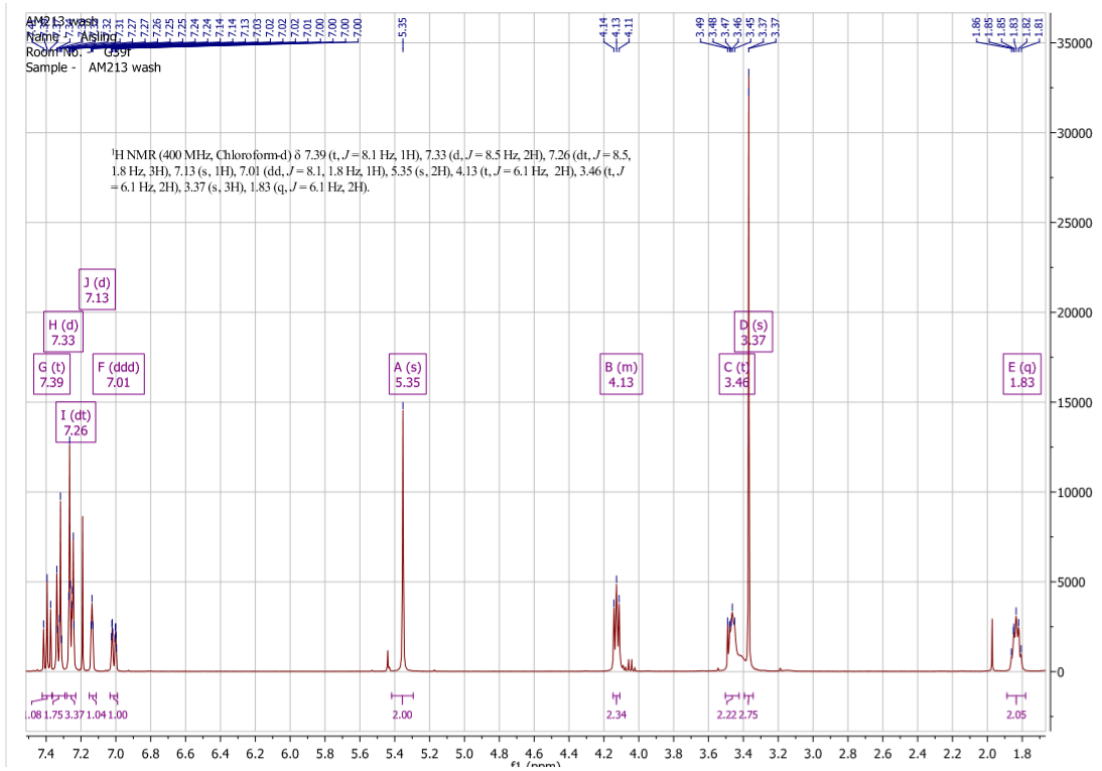
**Irradiation of Pico145-DAAlk in MeOH at 365 nm.**

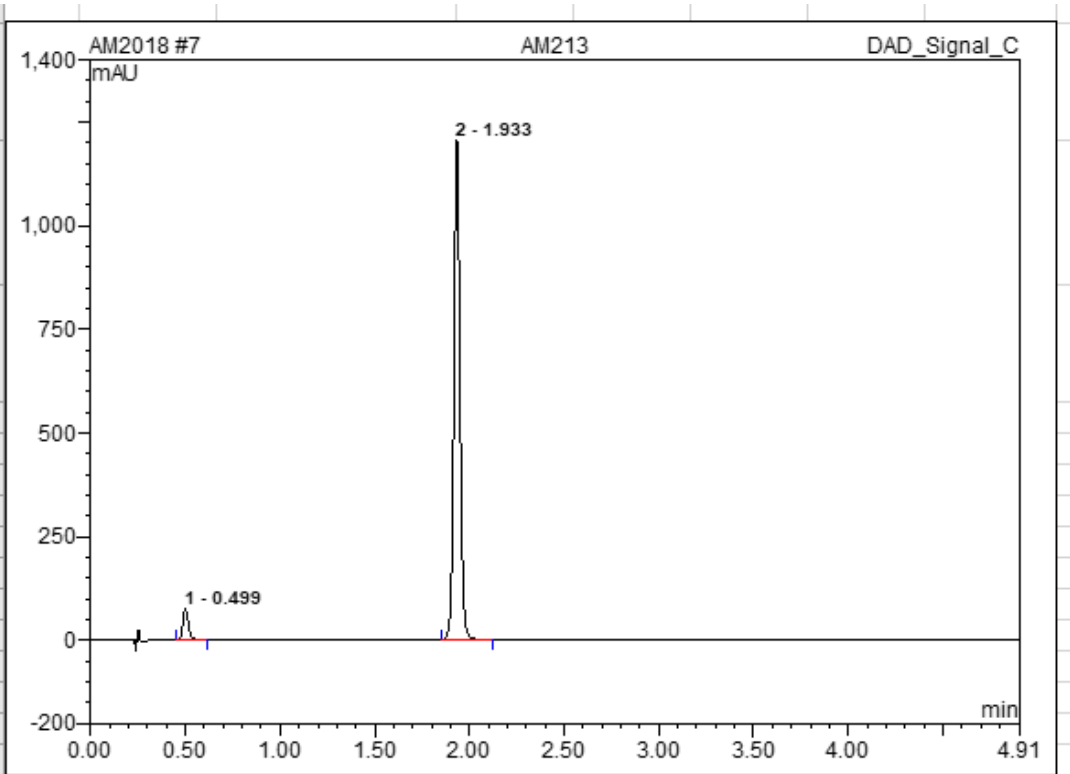
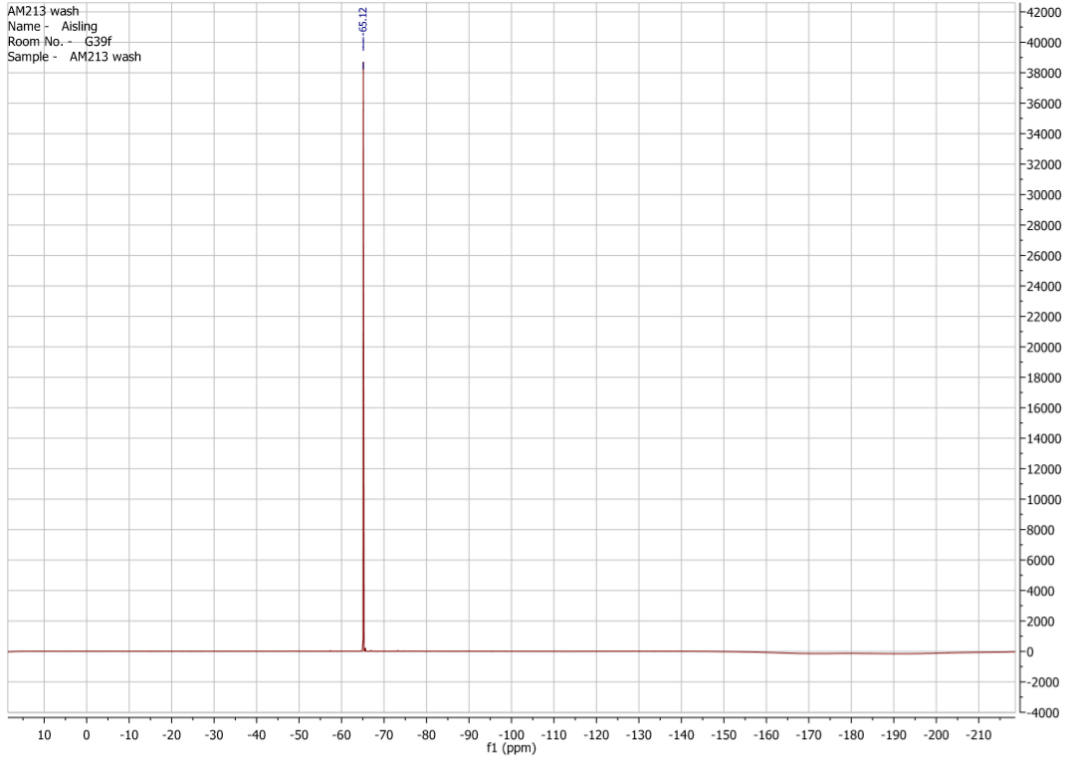


**Figure 104:** MS spectra of Pico145-DAAlk in MeOH with irradiation at 365 nm, for 0, 3, 5, 10, 15, 20, 25 and 30 minutes.

# Appendix VI

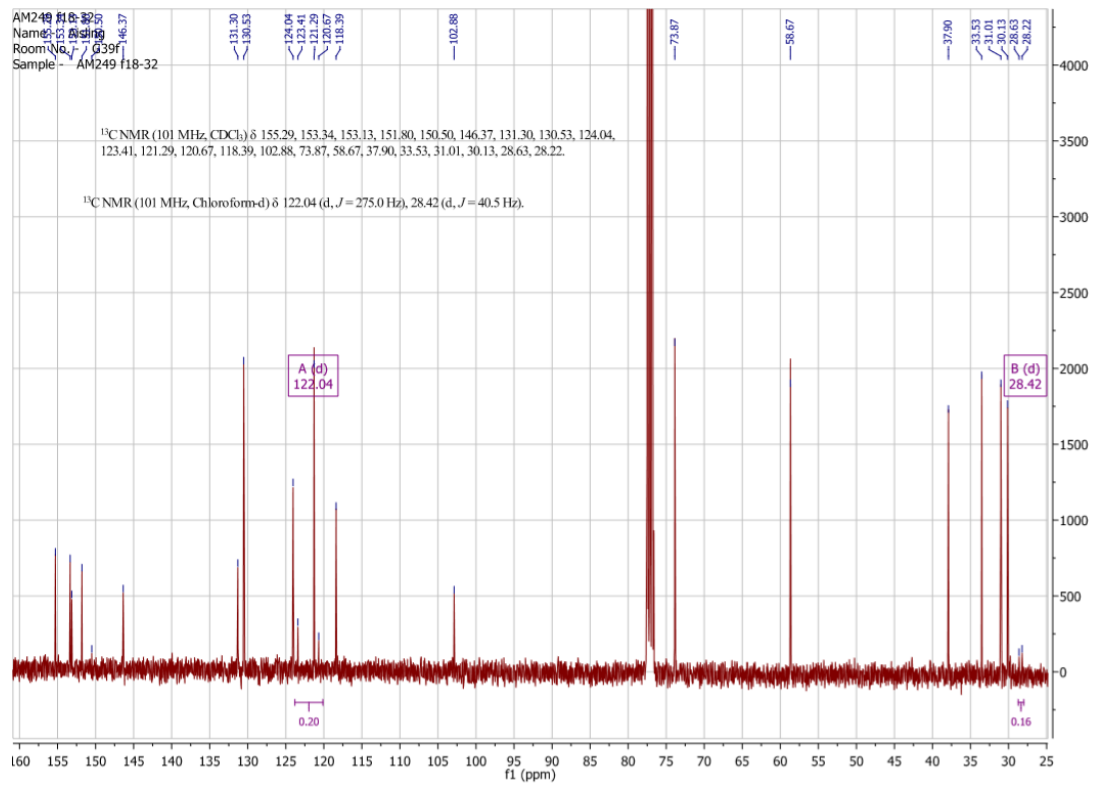
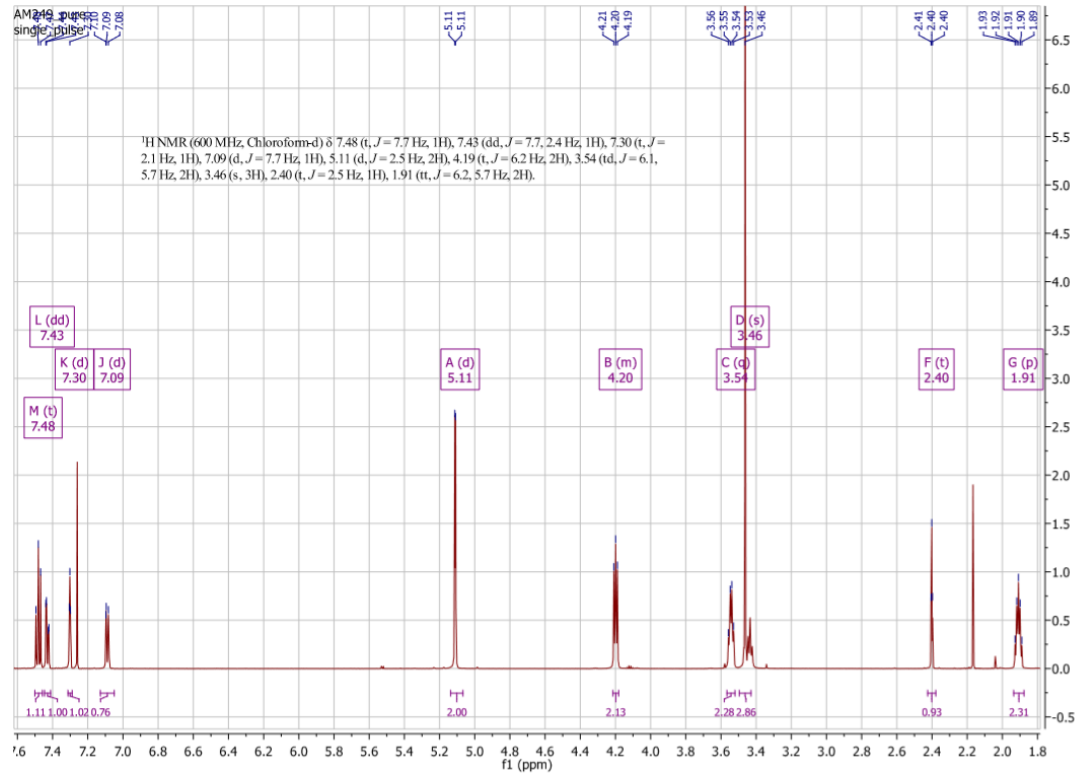
## NMR and HPLC data for Pico145-DA

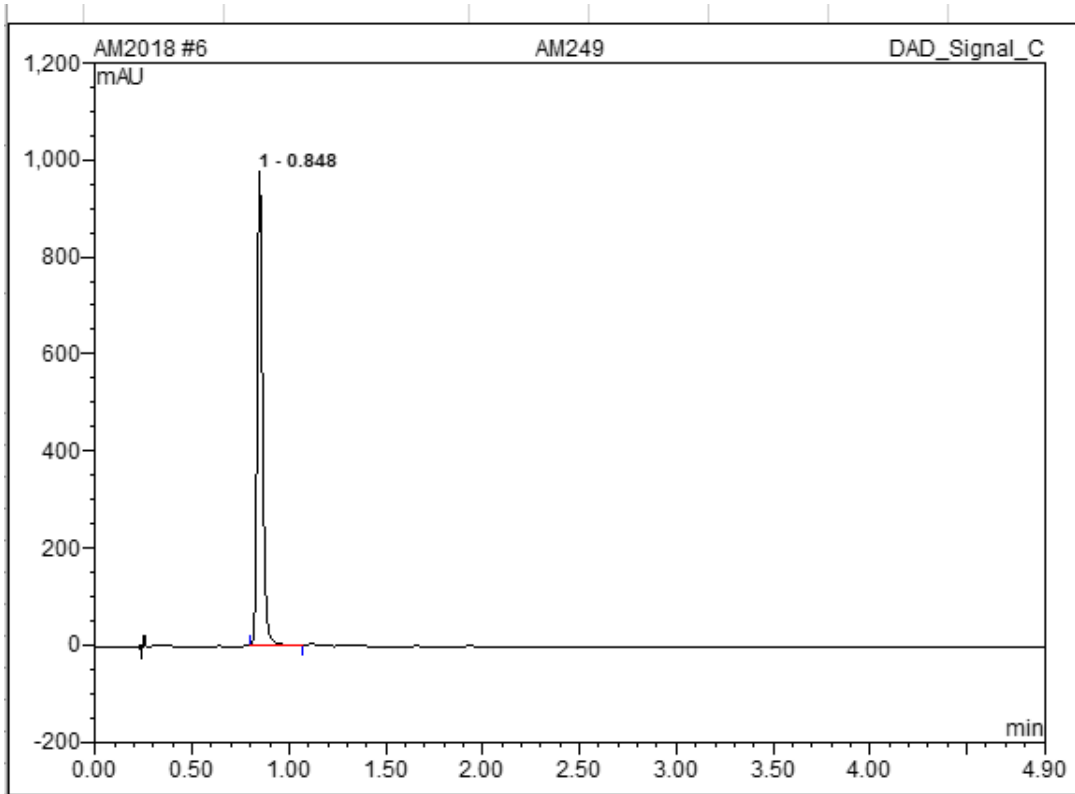
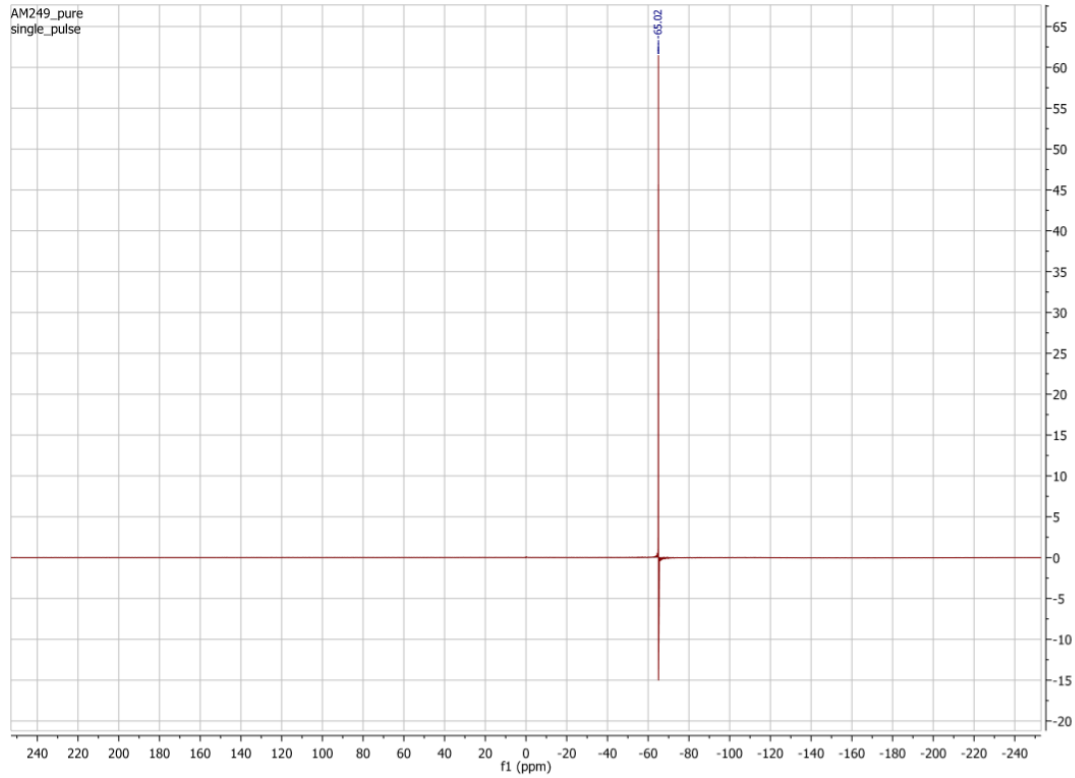




No.	Ret.Time min	Peak Name	Height mAU	Area mAU*min	Rel.Area %	Amount	Type
1	0.50	n.a.	76.231	2.537	5.36	n.a.	BMB
2	1.93	n.a.	1207.351	44.826	94.64	n.a.	BMB
<b>Total:</b>			1283.582	47.363	100.00	0.000	

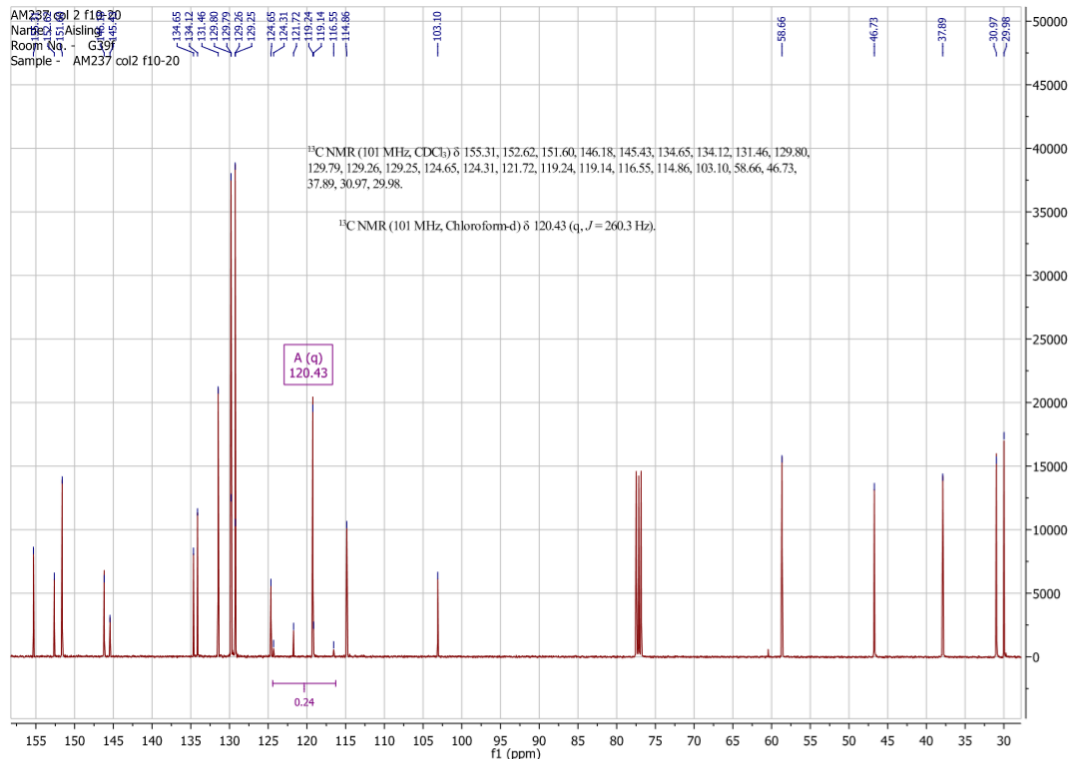
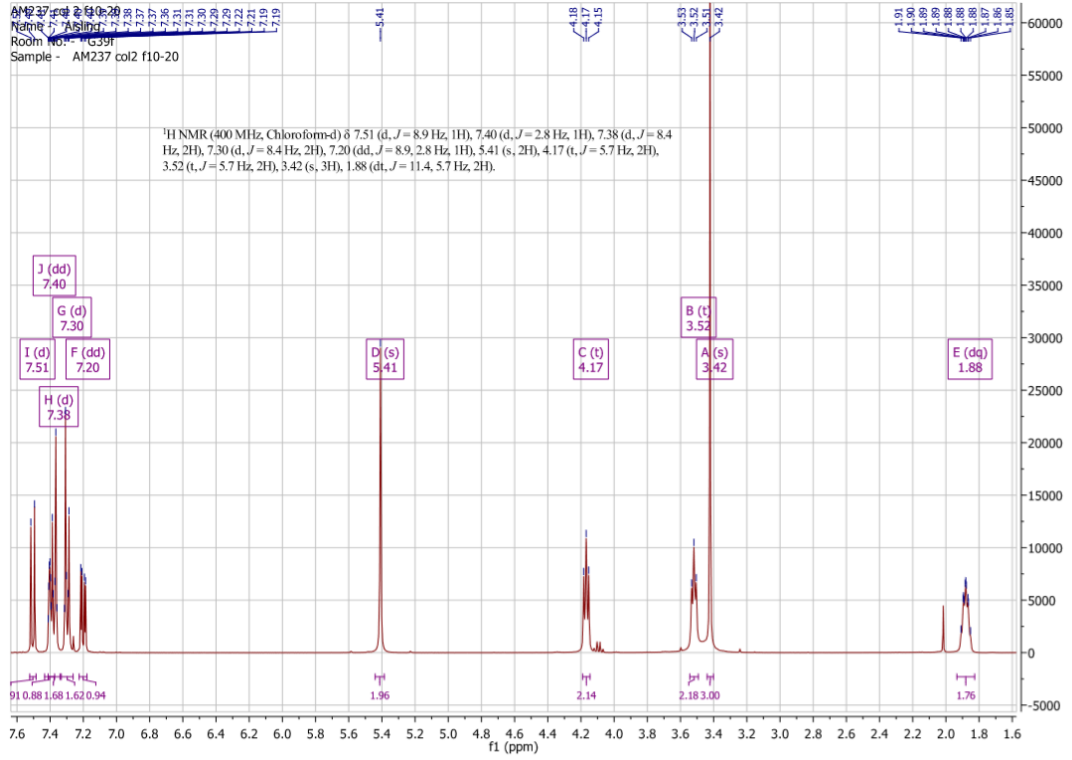
### NMR and HPLC data for Pico145-DAAIk

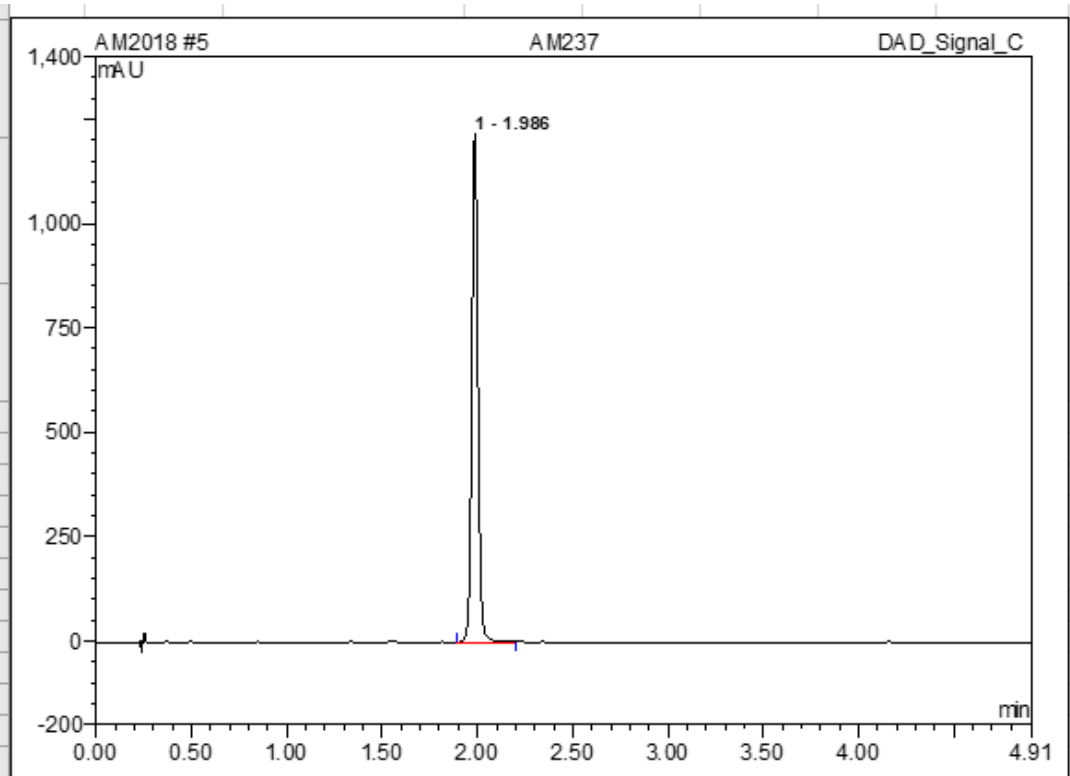
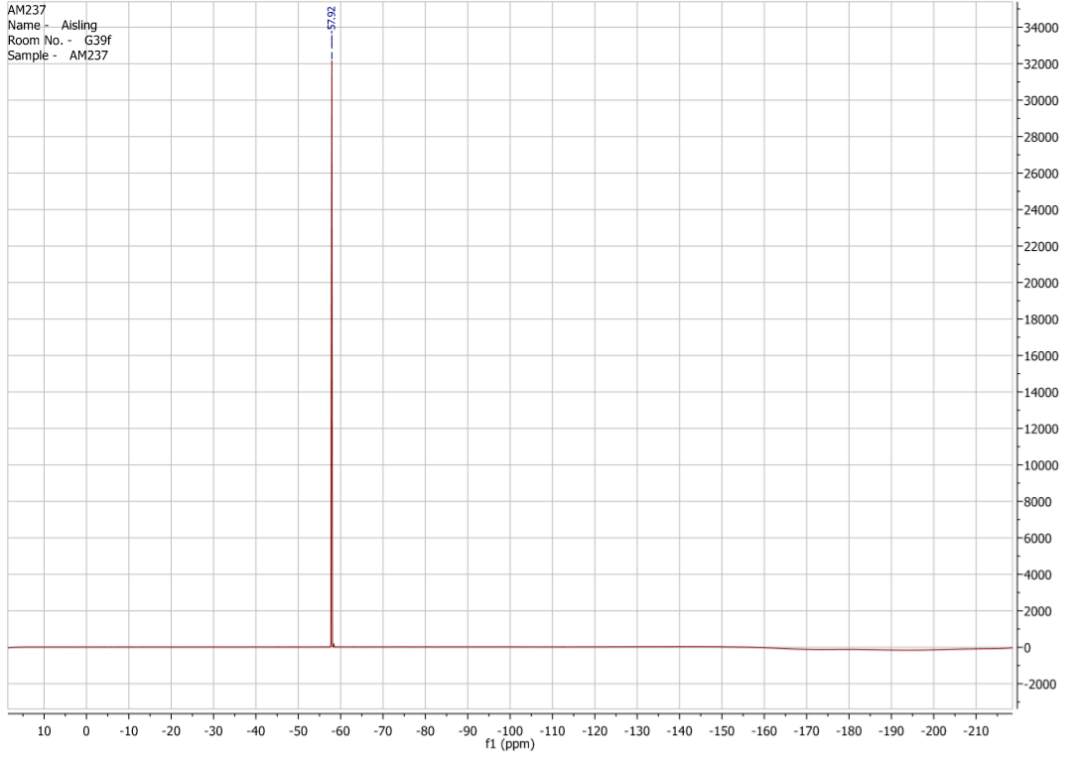




No.	Ret.Time min	Peak Name	Height mAU	Area mAU*min	Rel.Area %	Amount	Type
1	0.85	n.a.	976.748	31.389	100.00	n.a.	BMB
<b>Total:</b>			976.748	31.389	100.00	0.000	

### NMR and HPLC data for AM237





No.	Ret.Time min	Peak Name	Height mAU	Area mAU*min	Rel.Area %	Amount	Type
1	1.99	n.a.	1218.831	45.200	100.00	n.a.	BMB
<b>Total:</b>			1218.831	45.200	100.00	0.000	



## Bibliography

1. Clapham, D. E., Runnels, L. W. & Strübing, C. The TRP ion channel family. *Nat. Rev. Neurosci.* **2**, 387–396 (2001).
2. Bootman, M. D. *et al.* Calcium signalling — an overview. *Cell Dev. Biol.* **12**, 3–10 (2001).
3. Watanabe, H., Murakami, M., Ohba, T., Takahashi, Y. & Ito, H. TRP channel and cardiovascular disease. *Pharmacol. Ther.* **118**, 337–351 (2008).
4. Clapham, D. E. Calcium signalling. *Cell* **131**, 1047–1058 (2007).
5. Bon, R. S. & Beech, D. J. In pursuit of small molecule chemistry for calcium-permeable non-selective TRPC channels -- mirage or pot of gold? *Br. J. Pharmacol.* **170**, 459–474 (2013).
6. Cosens, D. J. & Manning, A. Abnormal Electroretinogram from a *Drosophila* Mutant. *Nature* **224**, 285–287 (1969).
7. Montell, C. The TRP Superfamily of Cation Channels. *Sci. Signal.* **2005**, re3-re3 (2005).
8. Eder, P. & Molkenin, J. D. TRPC channels as effectors of cardiac hypertrophy. *Circ. Res.* **108**, 265–272 (2011).
9. Wes, P. D. *et al.* TRPC1, a human homolog of a *Drosophila* store-operated channel. *Proc. Natl. Acad. Sci.* **92**, 9652–6 (1995).
10. Gaunt, H. J., Vasudev, N. S. & Beech, D. J. Transient receptor potential canonical 4 and 5 proteins as targets in cancer therapeutics. *Eur. Biophys. J.* **45**, 611–620 (2016).
11. Okada, T. *et al.* Molecular Cloning and Functional Characterization of a Novel Receptor-activated TRP Ca<sup>2+</sup> Channel from Mouse Brain \*. *J. Biol. Chemistry* **273**, 10279–10287 (1998).
12. Ramsey, I. S., Delling, M. & Clapham, D. E. An introduction to TRP channels. *Annu. Rev. Physiol.* **68**, 619–647 (2006).
13. Rosenberg, P. *et al.* TRPC3 channels confer cellular memory of recent neuromuscular activity. *Proc. Natl. Acad. Sci.* **101**, 9387–9392 (2004).

14. Vannier, B. *et al.* Mouse *trp2*, the homologue of the human *trpc2* pseudogene, encodes mTrp2, a store depletion-activated capacitative Ca<sup>2+</sup> entry channel. *Proc. Natl. Acad. Sci.* **96**, 2060–2064 (1999).
15. Vazquez, G., Wedel, B. J., Aziz, O., Trebak, M. & Putney Jr., J. W. The mammalian TRPC cation channels. *Biochim. Biophys. Acta* **1742**, 21–36 (2004).
16. Bai, C. X. *et al.* Formation of a new receptor-operated channel by heteromeric assembly of TRPP2 and TRPC1 subunits. *EMBO Rep.* **9**, 472–479 (2008).
17. Ma, X. *et al.* Functional Role of Vanilloid Transient Receptor Potential 4-Canonical Transient Receptor Potential 1 Complex in Flow-Induced Ca<sup>2+</sup> Influx. *Arterioscler. Thromb. Vasc. Biol.* **30**, 851–858 (2010).
18. Liao, Y. *et al.* A role for Orai in TRPC-mediated Ca<sup>2+</sup> entry suggests that a TRPC:Orai complex may mediate store and receptor operated Ca<sup>2+</sup> entry. *Proc. Natl. Acad. Sci.* **106**, 3202–3206 (2009).
19. Lee, K. P., Yuan, J. P., So, I., Worley, P. F. & Muallem, S. STIM1-dependent and STIM1-independent function of Transient Receptor Potential Canonical (TRPC) channels tunes their store-operated mode. *J. Biol. Chem.* **285**, 38666–38673 (2010).
20. Strübing, C., Krapivinsky, G., Krapivinsky, L. & Clapham, D. E. TRPC1 and TRPC5 form a novel cation channel in mammalian brain. *Neuron* **29**, 645–655 (2001).
21. Akbulut, Y. *et al.* (–)-Englerin A is a Potent and Selective Activator of TRPC4 and TRPC5 Calcium Channels. *Angew. Chem. Int. Ed.* **54**, 3787–3791 (2015).
22. Ludlow, M. J. *et al.* (–)-Englerin A-evoked Cytotoxicity Is Mediated by Na<sup>+</sup> Influx and Counteracted by Na<sup>+</sup>/K<sup>+</sup> -ATPase. *J. Biol. Chem.* **292**, 723–731 (2017).
23. Muraki, K. *et al.* Na<sup>+</sup> entry through heteromeric TRPC4/C1 channels mediates (–) Englerin A-induced cytotoxicity in synovial sarcoma cells. *Sci. Rep.* **7**, 16988 (2017).
24. Sukumar, P. *et al.* Constitutively active TRPC channels of adipocytes confer a mechanism for sensing dietary fatty acids and regulating adiponectin. *Circ.*

Res. **111**, 191–200 (2012).

25. Bröker-Lai, J. *et al.* Heteromeric channels formed by TRPC1, TRPC4 and TRPC5 define hippocampal synaptic transmission and working memory. *EMBO J.* **36**, e201696369 (2017).
26. Moran, M. M., McAlexander, M. A., Bíró, T. & Szallasi, A. Transient receptor potential channels as therapeutic targets. *Nat. Rev. Drug Discov.* **10**, 601–620 (2011).
27. Shirakawa, H. *et al.* Transient Receptor Potential Canonical 3 (TRPC3) Mediates Thrombin-Induced Astrocyte Activation and Upregulates Its Own Expression in Cortical Astrocytes. *J. Neurosci.* **30**, 13116–13129 (2010).
28. Birnbaumer, L. The TRPC class of ion channels: a critical review of their roles in slow, sustained increases in intracellular Ca(2+) concentrations. *Annu. Rev. Pharmacol. Toxicol.* **49**, 395–426 (2009).
29. Jung, S. *et al.* Lanthanides potentiate TRPC5 currents by an action at extracellular sites close to the pore mouth. *J. Biol. Chem.* **278**, 3562–3571 (2003).
30. Abramowitz, J. & Birnbaumer, L. Physiology and pathophysiology of canonical transient receptor potential channels. *FASEB J.* **23**, 297–328 (2009).
31. Beech, D. J. Characteristics of Transient Receptor Potential Canonical Calcium-Permeable Channels and Their Relevance to Vascular Physiology and Disease. *Circ. J.* **77**, 570–579 (2013).
32. Gautier, M. *et al.* New insights into pharmacological tools to TR(i)P cancer up. *Br. J. Pharmacol.* **171**, 2582–2592 (2014).
33. Zeng, F. *et al.* Human TRPC5 channel activated by a multiplicity of signals in a single cell. *J. Physiol.* **559**, 739–750 (2004).
34. Majeed, Y. *et al.* Rapid and Contrasting Effects of Rosiglitazone on Transient Receptor Potential TRPM3 and TRPC5 Channels. *Mol. Pharmacol.* **79**, 1023–1030 (2011).
35. Carson, C. *et al.* Englerin A Agonizes the TRPC4/C5 Cation Channels to Inhibit Tumor Cell Line Proliferation. *PLoS One* **1**, 1–21 (2015).

36. Altschul, S. F., Gish, W., Miller, W., Myers, E. W. & Lipman, D. J. Basic Local Alignment Search Tool. *J. Mol. Biol.* **215**, 403–410 (1990).
37. Sourbier, C. *et al.* Englerin A stimulates PKC $\theta$  to inhibit insulin signaling and simultaneously activate HSF1: An example of pharmacologically induced synthetic lethality. *Cancer Cell* **11**, 228–237 (2013).
38. Cheung, S. Y. *et al.* TRPC4/TRPC5 channels mediate adverse reaction to the cancer cell cytotoxic agent (-)-Englerin A. *Oncotarget* **9**, 29634–29643 (2018).
39. Busch, T. *et al.* Synthesis and antiproliferative activity of new tonantzitlolone-derived diterpene derivatives. *Org. Biomol. Chem.* **14**, 9040–9045 (2016).
40. Jasper, C., Wittenberg, R., Quitschalle, M., Jakupovic, J. & Kirschning, A. Total synthesis and elucidation of the absolute configuration of the diterpene tonantzitlolone. *Org. Lett.* **7**, 479–482 (2005).
41. Sourbier, C. *et al.* Tonantzitlolone cytotoxicity toward renal cancer cells is PKC $\theta$ - and HSF1-dependent. *Oncotarget* **6**, 29963–29974 (2015).
42. Rubaiy, H. N. *et al.* Tonantzitlolone is a nanomolar potency activator of transient receptor potential canonical 1/4/5 channels. *Br. J. Pharmacol.* **175**, 3361–3368 (2018).
43. Richter, J. M., Schaefer, M. & Hill, K. Riluzole activates TRPC5 channels independently of PLC activity. *Br. J. Pharmacol.* **171**, 158–170 (2014).
44. Schuster, J., Fu, R., Siddique, T. & Heckmann, C. Effect of prolonged riluzole exposure on cultured motoneurons in a mouse model of ALS. *J Neurophysiol* **107**, 484–482 (2012).
45. Grant, P., Song, J. Y. & Swedo, S. E. Review of the Use of the Glutamate Antagonist Riluzole in Psychiatric Disorders and a Description of Recent Use in Childhood Obsessive-Compulsive Disorder. *J. Child Adolesc. Psychopharmacol.* **20**, 309–315 (2010).
46. Bellingham, M. C. A Review of the Neural Mechanisms of Action and Clinical Efficiency of Riluzole in Treating Amyotrophic Lateral Sclerosis: What have we Learned in the Last Decade? *CNS Neurosci. Ther.* **17**, 4–31 (2011).
47. Beckmann, H. *et al.* A benzothiadiazine derivative and methylprednisolone are

novel and selective activators of transient receptor potential canonical 5 (TRPC5) channels. *Cell Calcium* **66**, 10–18 (2017).

48. Richter, J. M., Schaefer, M. & Hill, K. Clemizole Hydrochloride is a Novel and Potent Inhibitor of Transient Receptor Potential Channel TRPC5. *Mol. Pharmacol.* **86**, 514–521 (2014).
49. Bootman, M. D. *et al.* 2-Aminoethoxydiphenyl borate (2-APB) is a reliable blocker of store-operated Ca<sup>2+</sup> entry but an inconsistent inhibitor of InsP<sub>3</sub>-induced Ca<sup>2+</sup> release. *FASEB J.* **16**, 1145–1150 (2002).
50. Xu, S.-Z. *et al.* Block of TRPC5 channels by 2-aminoethoxydiphenyl borate: a differential, extracellular and voltage-dependent effect. *Br. J. Pharmacol.* **145**, 405–414 (2005).
51. Peppiatt, C. M. *et al.* 2-Aminoethoxydiphenyl borate (2-APB) antagonises inositol 1,4,5-trisphosphate-induced calcium release, inhibits calcium pumps and has a use-dependent and slowly reversible action on store-operated calcium entry channels. *Cell Calcium* **34**, 97–108 (2003).
52. Kiyonaka, S. *et al.* Selective and direct inhibition of TRPC3 channels underlies biological activities of a pyrazole compound. *Proc. Natl. Acad. Sci.* **106**, 5400–5405 (2009).
53. Singh, A., Hildebrand, M. E., Garcia, E. & Snutch, T. P. The transient receptor potential channel antagonist SKF96365 is a potent blocker of low-voltage-activated T-type calcium channels. *Br. J. Pharmacol.* **160**, 1464–1475 (2010).
54. Radtke, L. *et al.* Total synthesis and biological evaluation of (-)-englerin A and B: Synthesis of analogues with improved activity profile. *Angew. Chem. Int. Ed.* **50**, 3998–4002 (2011).
55. Willot, M. *et al.* Total synthesis and absolute configuration of the guaiane sesquiterpene englerin A. *Angew. Chem. Int. Ed.* **48**, 9105–9108 (2009).
56. Wu, Z. *et al.* Englerins: A Comprehensive Review. *J. Nat. Prod.* **80**, 771–781 (2017).
57. Rubaiy, H. N. *et al.* Identification of an (-)-englerin A analogue, which antagonizes (-)-englerin A at TRPC1/4/5 channels. *Br. J. Pharmacol.* **175**, 830–839 (2018).

58. Miller, M. *et al.* Identification of ML204, a novel potent antagonist that selectively modulates native TRPC4/C5 ion channels. *J. Biol. Chem.* **286**, 33436–33446 (2011).
59. Rubaiy, H. N. *et al.* Picomolar, selective, and subtype specific small-molecule inhibition of TRPC1/4/5 channels. *J. Biol. Chem* **292**, 8158–8173 (2017).
60. Einav, S., Sobol, H. D., Gehrig, E. & Glenn, J. S. The Hepatitis C virus (HCV) NS4B RNA binding inhibitor, clemizole, is highly synergistic with HCV protease inhibitors. *J Infect Dis* **202**, 65–74 (2010).
61. Pollard, C. E. *et al.* An introduction to QT interval prolongation and non-clinical approaches to assessing and reducing risk. *Br. J. Pharmacol.* **159**, 12–21 (2010).
62. Zhu, Y. *et al.* Identification and optimization of 2-aminobenzimidazole derivatives as novel inhibitors of TRPC4 and TRPC5 channels. *Br. J. Pharmacol.* **172**, 3495–3509 (2015).
63. Yang, L. *et al.* Acute Treatment with a Novel TRPC4/C5 Channel Inhibitor Produces Antidepressant and Anxiolytic-Like Effects in Mice. *PLoS One* 1–15 (2015). doi:10.1371/journal.pone.0136255
64. Zhou, Y. *et al.* A small-molecule inhibitor of TRPC5 ion channels suppresses progressive kidney disease in animal models. *Science (80-. )*. **358**, 1332–1336 (2017).
65. Chenard, B. & Gallaschun, R. Substituted xanthines and methods of use thereof. WO2014143799 (2014).
66. Just, S. *et al.* Treatment with HC-070, a potent inhibitor of TRPC4 and TRPC5, leads to anxiolytic and antidepressant effects in mice. *PLoS One* **1**, 1–32 (2018).
67. Ratnayake, R., Covell, D., Ransom, T. T., Gustafson, K. R. & Beutler, J. A. Englerin A, a selective inhibitor of renal cancer cell growth, from *Phyllanthus engleri*. *Org. Lett.* **11**, 57–60 (2009).
68. Earley, S. & Brayden, J. E. Transient Receptor Potential Channels in the Vasculature. *Physiol. Rev.* **95**, 645–690 (2015).

69. Yue, Z. *et al.* Role of TRP channels in the cardiovascular system. *Am. J. Physiol. - Hear. Circ. Physiol.* **308**, H157–H182 (2015).
70. Camacho Londoño, J. E. *et al.* A background Ca<sup>2+</sup> entry pathway mediated by TRPC1/TRPC4 is critical for development of pathological cardiac remodelling. *Eur. Heart J.* **36**, 2257–2266 (2015).
71. Alzoubi, A. *et al.* TRPC4 Inactivation Confers a Survival Benefit in Severe Pulmonary Arterial Hypertension. *Am. J. Pathol.* **183**, 1779–1788 (2013).
72. Francis, M., Xu, N., Zhou, C. & Stevens, T. Transient Receptor Potential Channel 4 Encodes a Vascular Permeability Defect and High-Frequency Ca<sup>2+</sup> Transients in Severe Pulmonary Arterial Hypertension. *Am. J. Pathol.* **186**, 1701–1709 (2016).
73. Chen, G.-L., Jiang, H. & Zou, F. Upregulation of Transient Receptor Potential Canonical Channels Contributes to Endotoxin-Induced Pulmonary Arterial Stenosis. *Med. Sci. Monit.* **22**, 2679–2684 (2016).
74. Riccio, A. *et al.* Essential role for TRPC5 in amygdala function and fear-related behavior. *Cell* **137**, 761–772 (2009).
75. Riccio, A. *et al.* Decreased Anxiety-Like Behavior and G<sub>q</sub>/11-Dependent Responses in the Amygdala of Mice Lacking TRPC4 Channels. *J. Neurosci.* **34**, 3653–3667 (2014).
76. Tian, D. *et al.* Antagonistic regulation of actin dynamics and cell motility by TRPC5 and TRPC6 channels. *Sci. Signal.* **3**, 1–14 (2010).
77. Schaldecker, T. *et al.* Inhibition of the TRPC5 ion channel protects the kidney filter. *J. Clin. Investig.* **123**, 5298–5309 (2013).
78. Wang, X. *et al.* TRPC5 Does Not Cause or Aggravate Glomerular Disease. *J. Am. Soc. Nephrol.* ASN.2017060682 (2017). doi:10.1681/ASN.2017060682
79. Van Der Wijst, J. & Bindels, R. J. M. Renal physiology: TRPC5 inhibition to treat progressive kidney disease. *Nat. Rev. Nephrol.* **14**, 145–146 (2018).
80. Piast, M., Kustrzeba-Wójcicka, I., Matusiewicz, M. & Banaś, T. Astex, Structural Genomix, and Syrrx. I Can See Clearly Now: Structural Biology and Drug Discovery. *Chem. Biol.* **10**, 95–98 (2003).

81. Scapin, G., Potter, C. S. & Carragher, B. Perspective Cryo-EM for Small Molecules Discovery, Design, Understanding, and Application. *Cell Chem. Biol.* 1–8 (2018). doi:10.1016/j.chembiol.2018.07.006
82. Liao, M., Cao, E., Julius, D. & Cheng, Y. Structure of the TRPV1 ion channel determined by electron cryo-microscopy. *Nature* **504**, 107–112 (2013).
83. Shen, P. S. *et al.* The Structure of the Polycystic Kidney Disease Channel PKD2 in Lipid Nanodiscs. *Cell* **167**, 763–773.e11 (2016).
84. Guo, J. *et al.* Structures of the calcium-activated, non-selective cation channel TRPM4. *Nature* **552**, 205–209 (2017).
85. Hirschi, M. *et al.* Cryo-electron microscopy structure of the lysosomal calcium-permeable channel TRPML3. *Nature* **550**, 411–414 (2017).
86. Frank, J. Advances in the field of single-particle cryo-electron microscopy over the last decade. *Nat. Protoc.* **12**, 209–212 (2017).
87. Nogales, E. & Scheres, S. H. W. Cryo-EM: A Unique Tool for the Visualization of Macromolecular Complexity. *Mol. Cell* **58**, 677–689 (2015).
88. Chen, X., Wang, Q., Ni, F. & Ma, J. Structure of the full-length Shaker potassium channel Kv1.2 by normal-mode-based X-ray crystallographic refinement. *Proc. Natl. Acad. Sci.* **107**, 11352–11357 (2010).
89. Paulsen, C. E., Armache, J. P., Gao, Y., Cheng, Y. & Julius, D. Structure of the TRPA1 ion channel suggests regulatory mechanisms. *Nature* **520**, 511–517 (2015).
90. Zubcevic, L. *et al.* Cryo-electron microscopy structure of the TRPV2 ion channel. *Nat. Struct. Mol. Biol.* **23**, 180–186 (2016).
91. Huynh, K. W. *et al.* Structure of the full-length TRPV2 channel by cryo-EM. *Nat. Commun.* **7**, 1–8 (2016).
92. Zubcevic, L., Le, S., Yang, H. & Lee, S. Y. Conformational plasticity in the selectivity filter of the TRPV2 ion channel. *Nat. Struct. Mol. Biol.* **25**, 405–415 (2018).
93. Deng, Z. *et al.* Cryo-EM and X-ray structures of TRPV4 reveal insight into ion permeation and gating mechanisms. *Nat. Struct. Mol. Biol.* **25**, 252–260



(2018).

94. Hughes, T. E. T. *et al.* Structural basis of TRPV5 channel inhibition by econazole revealed by cryo-EM. *Nat. Struct. Mol. Biol.* **25**, 53–60 (2018).
95. McGoldrick, L. L. *et al.* Opening of the human epithelial calcium channel TRPV6. *Nature* **553**, 233–237 (2018).
96. Singh, A. K., Saotome, K., McGoldrick, L. L. & Sobolevsky, A. I. Structural bases of TRP channel TRPV6 allosteric modulation by 2-APB. *Nat. Commun.* **9**, 1–11 (2018).
97. Zhang, S., Li, N., Zeng, W., Gao, N. & Yang, M. Cryo-EM structures of the mammalian endo-lysosomal TRPML1 channel elucidate the combined regulation mechanism. *Protein Cell* **8**, 834–847 (2017).
98. Zhou, X. *et al.* Cryo-EM structures of the human endolysosomal TRPML3 channel in three distinct states. *Nat. Struct. Mol. Biol.* **24**, 1146–1154 (2017).
99. Autzen, H. E. *et al.* Structure of the human TRPM4 ion channel in a lipid nanodisc. *Science (80-. )*. **359**, 228–232 (2018).
100. Fan, C., Choi, W., Sun, W., Du, J. & Lu, W. Structure of the human lipid-gated cation channel TRPC3. *Elife* **7**, e36852 (2018).
101. Tang, Q. *et al.* Structure of the receptor-activated human TRPC6 and TRPC3 ion channels. *Cell Res.* **28**, 746–755 (2018).
102. Cao, E., Liao, M., Cheng, Y. & Julius, D. TRPV1 structures in distinct conformations reveal activation mechanisms. *Nature* **504**, 113–118 (2013).
103. Gao, Y., Cao, E., Julius, D. & Cheng, Y. TRPV1 structures in nanodiscs reveal mechanisms of ligand and lipid action. *Nature* **534**, 347–351 (2016).
104. Vinayagam, D. *et al.* Electron cryo-microscopy structure of the canonical TRPC4 ion channel. *Elife* **7**, e36615 (2018).
105. Duan, J. *et al.* Structure of the mouse TRPC4 ion channel. *Nat. Commun.* **9**, 3102 (2018).
106. Xu, S.-Z. *et al.* TRPC channel activation by extracellular thioredoxin. *Nature* **451**, 69–72 (2008).

107. Phulera, S. *et al.* Cryo-EM structure of the benzodiazepine-sensitive  $\alpha 1\beta 1\gamma 2$  heterotrimeric GABAA receptor in complex with GABA illuminates mechanism of receptor assembly and agonist binding. *bioRxiv* (2018).
108. Karakas, E. & Furukawa, H. Crystal structure of a heterotetrameric NMDA receptor ion channel. *Science* (80-. ). **344**, 992–997 (2014).
109. Lü, W., Du, J., Goehring, A. & Gouaux, E. Cryo-EM structures of the triheteromeric NMDA receptor and its allosteric modulation. *Science* (80-. ). **355**, (2017).
110. Morales-Perez, C. L., Noviello, C. M. & Hibbs, R. E. X-ray structure of the human  $\alpha 4\beta 2$  nicotinic receptor. *Nature* **538**, 411–415 (2016).
111. Apsel, B. *et al.* Targeted polypharmacology: Discovery of dual inhibitors of tyrosine and phosphoinositide kinases. *Nat. Chem. Biol.* **4**, 691–699 (2008).
112. Cravatt, B. F., Wright, A. T. & Kozarich, J. W. Activity-based protein profiling: from enzyme chemistry to proteomic chemistry. *Annu. Rev. Biochem.* **77**, 383–414 (2008).
113. Wright, M. H. & Sieber, S. A. Chemical proteomics approaches for identifying the cellular targets of natural products. *Nat. Prod. Rep.* **33**, 681–708 (2016).
114. Rix, U. & Superti-furga, G. Target profiling of small molecules by chemical proteomics. *Nat. Chem. Biol.* **5**, 616–624 (2009).
115. Zheng, X. S., Chan, T.-F. & Zhou, H. H. Genetic and Genomic Approaches to Identify and Study the Targets of Bioactive Small Molecules. *Chem. Biol.* **11**, 609–618 (2004).
116. Boutros, M. & Ahringer, J. The art and design of genetic screens: RNA interference. *Nat. Rev. Genet.* **9**, 554–566 (2008).
117. Young, D. W. *et al.* Integrating high-content screening and ligand-target prediction to identify mechanism of action. *Nat. Chem. Biol.* **4**, 59–68 (2008).
118. Hughes, T. R. *et al.* Functional discovery via a compendium of expression profiles. *Cell* **102**, 109–126 (2000).
119. Weinstein, J. N. *et al.* An Information-Intensive Approach to the Molecular Pharmacology of Cancer. *Science* (80-. ). **275**, 343–349 (1997).

120. Schenone, M., Dančik, V., Wagner, B. K. & Clemons, P. A. Target identification and mechanism of action in chemical biology and drug discovery. *Nat. Chem. Biol.* **9**, 232–240 (2013).
121. Cong, F., Cheung, A. K. & Huang, S.-M. A. Chemical Genetics–Based Target Identification in Drug Discovery. *Annu. Rev. Pharmacol. Toxicol.* **52**, 57–78 (2012).
122. Weiss, W. A., Taylor, S. S. & Shokat, K. M. Recognizing and exploiting differences between RNAi and small-molecule inhibitors. *Nat. Chem. Biol.* **3**, 739–744 (2007).
123. Colquhoun, D. Binding , gating , activity and efficacy: The interpretation of structure-activity relationships for agonists and of the effects of mutating receptors. *Br. J. Pharmacol.* **125**, 923–947 (1998).
124. Robinette, D., Neamati, N., Tomer, K. B. & Borchers, C. H. Photoaffinity labeling combined with mass spectrometric approaches as a tool for structural proteomics. *Expert Rev. Proteomics* **3**, 399–408 (2006).
125. Sletten, E. M. & Bertozzi, C. R. From mechanism to mouse: A tale of two bioorthogonal reactions. *Acc. Chem. Res.* **44**, 666–676 (2011).
126. Smith, E. & Collins, I. Photoaffinity labeling in target- and binding-site identification. *Futur. Med. Chem.* **7**, 159–183 (2015).
127. Gregory, K. J. *et al.* Clickable Photoaffinity Ligands for Metabotropic Glutamate Receptor 5 Based on Select Acetylenic Negative Allosteric Modulators. *ACS Chem. Biol.* **11**, 1870–1879 (2016).
128. Yip, G. M. S. *et al.* A propofol binding site on mammalian GABA A receptors identified by photolabeling. *Nat. Chem. Biol.* **9**, 715–720 (2013).
129. Chen, Z.-W., Fuchs, K., Sieghart, W., Townsend, R. R. & Evers, A. S. Deep Amino Acid Sequencing of Native Brain GABA<sub>A</sub> Receptors Using High-Resolution Mass Spectrometry. *Mol. Cell. Proteomics* **11**, M111.011445 (2012).
130. Woll, K. A. *et al.* Photoaffinity Ligand for the Inhalational Anesthetic Sevoflurane Allows Mechanistic Insight into Potassium Channel Modulation. *ACS Chem. Biol.* **12**, 1353–1362 (2017).

131. Kalia, J. & Swartz, K. J. Exploring structure-function relationships between TRP and Kv channels. *Sci. Rep.* **3**, 1523- (2013).
132. Liang, Q. *et al.* Positive allosteric modulation of Kv channels by sevoflurane: Insights into the structural basis of inhaled anesthetic action. *PLoS One* **10**, 1–20 (2015).
133. Park, J., Koh, M., Koo, J. Y., Lee, S. & Park, S. B. Investigation of Specific Binding Proteins to Photoaffinity Linkers for Efficient Deconvolution of Target Protein. *ACS Chem. Biol.* **11**, 44–52 (2016).
134. Kambe, T., Correia, B. E., Niphakis, M. J. & Cravatt, B. F. Mapping the protein interaction landscape for fully functionalized small-molecule probes in human cells. *J. Am. Chem. Soc.* **136**, 10777–10782 (2014).
135. Das, J. Aliphatic diazirines as photoaffinity probes for proteins: Recent developments. *Chem. Rev.* **111**, 4405–4417 (2011).
136. Staros, J. V. Aryl azide photolabels in biochemistry. *Trends Biochem. Sci.* **5**, 320–322 (1980).
137. Brunner, J. New photolabeling and crosslinking methods. *Annu. Rev. Biochem.* **62**, 483–514 (1993).
138. Geurink, P. P., Prely, L. M., van der Marel, G. A., Bischoff, R. & Overkleeft, H. S. in *Activity-Based Protein Profiling* 85–113 (2011).
139. Ghosh, B. & Jones, L. H. Target validation using in-cell small molecule clickable imaging probes. *Medchemcomm* **5**, 247–254 (2014).
140. Borden, W. T. *et al.* The interplay of theory and experiment in the study of phenylnitrene. *Acc. Chem. Res.* **33**, 765–771 (2000).
141. Preston, G. W. & Wilson, A. J. Photo-induced covalent cross-linking for the analysis of biomolecular interactions. *Chem. Soc. Rev.* **42**, 3289–301 (2013).
142. Dubinsky, L., Krom, B. P. & Meijler, M. M. Diazirine based photoaffinity labeling. *Bioorganic Med. Chem.* **20**, 554–570 (2012).
143. Galardy, E., Craig, C., Jamieson, J. D. & Printz, P. Photoaffinity Labeling of Peptide Hormone Binding Sites. *J. Biol. Chem* **249**, 3510–3518 (1974).

144. Terstappen, G. C., Schlüpen, C., Raggiaschi, R. & Gaviraghi, G. Target deconvolution strategies in drug discovery. *Nat. Rev. Drug Discov.* **6**, 891–903 (2007).
145. Sadakane, Y. & Hatanaka, Y. Photochemical Fishing Approaches for Identifying Target Proteins and Elucidating the Structure of a Ligand-binding Region Using Carbene-generating Photoreactive Probes. *Anal. Sci.* **22**, 209–218 (2006).
146. Young, T. S. *et al.* Evolution of cyclic peptide protease inhibitors. *Proc. Natl. Acad. Sci.* **108**, 11052–11056 (2011).
147. Bethell, D., Stevens, G. & Tickle, P. The reaction of diphenylmethylene with isopropyl alcohol and oxygen: The question of reversibility of singlet-triplet interconversion of carbenes. *J. Chem. Soc. D Chem. Commun.* 792–794 (1970). doi:10.1039/C2970000792b
148. Rosenberg, M. G. & Brinker, U. H. Constrained carbenes. *European J. Org. Chem.* 5423–5440 (2006). doi:10.1002/ejoc.200600547
149. Hill, J. R. & Robertson, A. A. B. Fishing for Drug Targets: A Focus on Diazirine Photoaffinity Probe Synthesis. *J. Med. Chem.* **61**, acs.jmedchem.7b01561 (2018).
150. Preston, G. W., Radford, S. E., Ashcroft, A. E. & Wilson, A. J. Covalent cross-linking within supramolecular peptide structures. *Anal. Chem.* **84**, 6790–6797 (2012).
151. Brunner, J., Senn, H. & Richards, F. M. 3-Trifluoromethyl-3-phenyldiazirine. A new carbene generating group for photolabeling reagents. *J. Biol. Chem.* **255**, 3313–3318 (1980).
152. Hayashi, T. & Hamachi, I. Traceless affinity labeling of endogenous proteins for functional analysis in living cells. *Acc. Chem. Res.* **45**, 1460–1469 (2012).
153. Tsukiji, S. & Hamachi, I. Ligand-directed tosyl chemistry for in situ native protein labeling and engineering in living systems: from basic properties to applications. *Curr. Opin. Chem. Biol.* **21**, 136–143 (2014).
154. Tamura, T. *et al.* Rapid labelling and covalent inhibition of intracellular native proteins using ligand-directed N-Acyl-N-Alkyl sulfonamide. *Nat. Commun.* **9**,

- 1–12 (2018).
155. Hamachi, I., Nagase, T. & Shinkai, S. A general semisynthetic method for fluorescent saccharide-biosensors based on a lectin. *J. Am. Chem. Soc.* **122**, 12065–12066 (2000).
  156. Takaoka, Y., Tsutsumi, H., Kasagi, N., Nakata, E. & Hamachi, I. One-pot and sequential organic chemistry on an enzyme surface to tether a fluorescent probe at the proximity of the active site with restoring enzyme activity. *J. Am. Chem. Soc.* **128**, 3273–3280 (2006).
  157. Tsukiji, S., Miyagawa, M., Takaoka, Y., Tamura, T. & Hamachi, I. Ligand-directed tosyl chemistry for protein labeling in vivo. *Nat. Chem. Biol.* **5**, 341–343 (2009).
  158. Tsukiji, S. *et al.* Quenched ligand-directed tosylate reagents for one-step construction of turn-on fluorescent biosensors. *J. Am. Chem. Soc.* **131**, 9046–9054 (2009).
  159. Tamura, T., Tsukiji, S. & Hamachi, I. Native FKBP12 engineering by ligand-directed tosyl chemistry: Labeling properties and application to photo-cross-linking of protein complexes in vitro and in living cells. *J. Am. Chem. Soc.* **134**, 2216–2226 (2012).
  160. Fujishima, S., Yasui, R., Miki, T., Ojida, A. & Hamachi, I. Ligand-directed acyl imidazole chemistry for labeling of membrane-bound proteins on live cells. *J. Am. Chem. Soc.* **134**, 3961–3964 (2012).
  161. Matsuo, K. *et al.* One-step construction of caged carbonic anhydrase I using a ligand-directed acyl imidazole-based protein labeling method. *Chem. Sci.* **4**, 2573 (2013).
  162. Wakayama, S. *et al.* Chemical labelling for visualizing native AMPA receptors in live neurons. *Nat. Commun.* **8**, 1–14 (2017).
  163. Yamaura, K., Kiyonaka, S., Numata, T., Inoue, R. & Hamachi, I. Discovery of allosteric modulators for GABA A receptors by ligand-directed chemistry. *Nat. Chem. Biol.* **12**, 822–830 (2016).
  164. Takaoka, Y., Nishikawa, Y., Hashimoto, Y., Sasaki, K. & Hamachi, I. Ligand-directed dibromophenyl benzoate chemistry for rapid and selective acylation

- of intracellular natural proteins. *Chem. Sci.* **6**, 3217–3224 (2015).
165. Matsuo, K., Nishikawa, Y., Masuda, M. & Hamachi, I. Live-Cell Protein Sulfonation Based on Proximity-driven N-Sulfonyl Pyridone Chemistry. *Angew. Chem. Int. Ed.* **57**, 659–662 (2018).
  166. Koshi, Y. *et al.* Target-specific chemical acylation of lectins by ligand-tethered DMAP catalysts. *J. Am. Chem. Soc.* **130**, 245–251 (2008).
  167. Wang, H. *et al.* Chemical cell-surface receptor engineering using affinity-guided, multivalent organocatalysts. *J. Am. Chem. Soc.* **133**, 12220–12228 (2011).
  168. Song, Z. *et al.* Extended Affinity-guided DMAP Chemistry with a Finely Tuned Acyl Donor for Intracellular FKBP12 Labeling. *Chem. Lett.* **44**, 333–335 (2015).
  169. Tamura, T. *et al.* Affinity-Guided Oxime Chemistry for Selective Protein Acylation in Live Tissue Systems. *J. Am. Chem. Soc.* **139**, 14181–14191 (2017).
  170. Tamura, T., Kioi, Y., Miki, T., Tsukiji, S. & Hamachi, I. Fluorophore labeling of native FKBP12 by ligand-directed tosyl chemistry allows detection of its molecular interactions in vitro and in living cells. *J. Am. Chem. Soc.* **135**, 6782–6785 (2013).
  171. Hughes, C. C. *et al.* Marinopyrrole A target elucidation by acyl dye transfer. *J. Am. Chem. Soc.* **131**, 12094–12096 (2009).
  172. Paredes, R. M., Etzler, J. C., Watts, L. T. & Lechleiter, J. D. Chemical Calcium Indicators. *Methods* **46**, 143–151 (2008).
  173. Grynkiewicz, G., Poenie, M. & Tsien, R. Y. A new generation of Ca<sup>2+</sup> indicators with greatly improved fluorescence properties. *J. Biol. Chem.* **260**, 3440–3450 (1985).
  174. Kornreich, B. G. The patch clamp technique: Principles and technical considerations. *J. Vet. Cardiol.* **9**, 25–37 (2007).
  175. Sakmann, B. & Neher, E. Patch Clamp Techniques for Studying Ionic Channels in Excitable Membranes. *Annu. Rev. Physiol.* **46**, 455–472 (1984).
  176. Neher, E., Sakmann, B. & Steinbach, J. H. The extracellular patch clamp: A

method for resolving currents through individual open channels in biological membranes. *Pflügers Arch. Eur. J. Physiol.* **375**, 219–228 (1978).

177. Neher, E. Ion channels for communication between and within cells. *Science* (80- ). **256**, 498–502 (1992).
178. Hamill, O. P., Marty, A., Neher, E., Sakmann, B. & Sigworth, F. J. Improved patch-clamp techniques for high-resolution current recording from cells and cell-free membrane patches. *Pflügers Arch. Eur. J. Physiol.* **391**, 85–100 (1981).
179. Kiss, L. *et al.* High throughput ion-channel pharmacology: planar-array-based voltage clamp. *Assay Drug Dev Technol* **1**, 127–135 (2003).
180. Schroeder, K., Neagle, B., Trezise, D. J. & Worley, J. IonWorks™ HT : A New High-Throughput. *J. Biomol. Screen.* **8**, 50–64 (2003).
181. Linley, J. E. in *Ion Channels. Methods in Molecular Biology (Methods and Protocols)* 149–157 (Humana Press, Totowa, NJ, 2013). doi:10.1007/978-1-62703-351-0\_16
182. John, V. H. *et al.* Novel 384-well population patch clamp electrophysiology assays for Ca<sup>2+</sup>-Activated K<sup>+</sup> Channels. *J. Biomol. Screen.* **12**, 50–60 (2007).
183. Priest, B. T. & McDermott, J. S. Cardiac ion channels. *Channels* **9**, 352–359 (2015).
184. Redfern, W. S. *et al.* Relationships between preclinical cardiac electrophysiology, clinical QT interval prolongation and torsade de pointes for a broad range of drugs: Evidence for a provisional safety margin in drug development. *Cardiovasc. Res.* **58**, 32–45 (2003).
185. Hinard, V. *et al.* ICEPO: The ion channel electrophysiology ontology. *Database* **2016**, 1–7 (2016).
186. Dunlop, J., Bowlby, M., Peri, R., Vasilyev, D. & Arias, R. High-throughput electrophysiology: an emerging paradigm for ion-channel screening and physiology. *Nat. Rev. Drug Discov.* **7**, 358–368 (2008).
187. Yao, J.-A. *et al.* Estimation of potency of HERG channel blockers: Impact of



- voltage protocol and temperature. *J. Pharmacol. Toxicol. Methods* **52**, 146–153 (2005).
188. Nelson, A. Electrochemical analysis of a phospholipid phase transition. *Journal of Electroanalytical Chemistry* **601**, 83–93 (2007).
189. Mohamadi, S., Tate, D. J., Vakurov, A. & Nelson, A. Electrochemical screening of biomembrane-active compounds in water. *Anal. Chim. Acta* **813**, 83–89 (2014).
190. Berg, R. & Straub, B. F. Advancements in the mechanistic understanding of the copper-catalyzed azide-alkyne cycloaddition. *Beilstein J. Org. Chem.* **9**, 2715–2750 (2013).
191. Wang, Q. *et al.* Bioconjugation by copper(I)-catalyzed azide-alkyne [3 + 2] cycloaddition. *J. Am. Chem. Soc.* **125**, 3192–3193 (2003).
192. Rostovtsev, V. V., Green, L. G., Fokin, V. V. & Sharpless, K. B. A Stepwise Huisgen Cycloaddition Process Catalyzed by Copper ( I ): Regioselective Ligation of Azides and Terminal Alkynes. *Angew. Chem. Int. Ed.* **41**, 2596–2599 (2002).
193. Naylor, J. *et al.* TRPC5 Channel Sensitivities to Antioxidants and Hydroxylated Stilbenes. *J. Biol. Chem* **286**, 5078–5086 (2011).
194. Goswami, S. K. & Das, D. K. Resveratrol and chemoprevention. *Cancer Lett.* **284**, 1–6 (2009).
195. Pietta, P. Flavonoids as Antioxidants. *J. Nat. Prod* **63**, 1035–1042 (2000).
196. Halake, K., Birajdar, M. & Lee, J. Structural implications of polyphenolic antioxidants. *J. Ind. Eng. Chem.* **35**, 1–7 (2016).
197. Al-shawaf, E. *et al.* Short-Term Stimulation of Calcium-Permeable Transient Receptor Potential Canonical 5 – Containing Channels by Oxidised Phospholipids. *Arter. Thromb. Vasc. Biol* **30**, 1453–1459 (2010).
198. Naylor, J. *et al.* Natural and synthetic flavonoid modulation of TRPC5 channels. *Br. J. Pharmacol.* **173**, 562–574 (2016).
199. Heo, M. Y., Sohn, S. J. & Au, W. W. Anti-genotoxicity of galangin as a cancer chemopreventive agent candidate. *Mutat. Res.* **488**, 135–150 (2001).

200. Wall, M. *et al.* Plant antimutagenic agents. 2. Flavonoids. *J. Nat. Prod.* **51**, 1084–1091 (1988).
201. Young, M., Hyung, L., Su, S. & Au, W. W. Anticlastogenic effects of galangin against mitomycin C-induced micronuclei in reticulocytes of mice. *Mutat. Res.* **360**, 37–41 (1996).
202. MR, C., M, P. & MJ, A. Inhibitory effects of phenolic compounds on CCl<sub>4</sub>-induced microsomal lipid peroxidation. *Experientia* **47**, 195–199 (1991).
203. Imamura, Y., Migita, T., Uriu, Y., Otagiri, M. & Okawara, T. Inhibitory of Flavonoids on Rabbit Carbonyl Reductase. *J. Biochem* **127**, 653–658 (2000).
204. Daskiewicz, J. B. *et al.* Effects of flavonoids on cell proliferation and caspase activation in a human colonic cell line HT29: An SAR study. *J. Med. Chem.* **48**, 2790–2804 (2005).
205. Carola, C., Toullec, A. & Buchholz, H. Google Patents. *Ger Offen* (2007).
206. Gerard, B., Cencic, R., Pelletier, J. & Porco, J. a. Enantioselective synthesis of the complex rocaglate (-)-silvestrol. *Angew. Chem. Int. Ed.* **46**, 7831–7834 (2007).
207. Kostanecki, S. & Rozycki, A. Ueber eine Bildungsweise von Chromonderivaten. *Chem. Ber.* **34**, 102–109 (1901).
208. Looker, J. H., Mcmechan, J. H. & Mader, J. W. An amine Solvent Modification of the Kostanecki-Robinson Reaction. Application to the Synthesis of Flavonols. *J. Org. Chem.* **43**, 2344–2347 (1978).
209. Szell, T., Dozai, L., Zarandy, M. & Menyharth, K. Cyclization of the Enol Esters of o-Acyloxyphenyl Alkyl Ketones-III. *Tetrahedron* **25**, 715–724 (1969).
210. Cook, D. & McIntyre, J. S. The Kostanecki-Robinson Acylation and Cyclization of 3-Acyl-4-hydroxy-2-pyrones. *J. Org. Chem.* **33**, 1746–1749 (1968).
211. Forbes, A. M., Meier, G. P., Haendiges, S. & Taylor, L. P. Structure – Activity Relationship Studies of Flavonol Analogues on Pollen Germination. *J. Agric. Food Chem.* **62**, 2175–2181 (2014).
212. AL-Shawaf, E. *et al.* GVI phospholipase A2 role in the stimulatory effect of sphingosine-1-phosphate on TRPC5 cationic channels. *Cell Calcium* **50**, 343–

350 (2011).

213. Xu, S.-Z. *et al.* A sphingosine-1-phosphate-activated calcium channel controlling vascular smooth muscle cell motility. *Circ. Res.* **98**, 1381–1389 (2006).
214. Hui, H. *et al.* Calcium-sensing mechanism in TRPC5 channels contributing to retardation of neurite outgrowth. *J. Physiol.* **572**, 165–172 (2006).
215. ICH Expert Working Group. S7B Nonclinical Evaluation of the Potential for Delayed Ventricular Repolarization (QT Interval Prolongation) by Human Pharmaceuticals. *Int. Conf. Harmon. Tech. Requir. Regist. Pharm. Hum. Use* **70**, 61133–61134 (2005).
216. Guth, B. D. Preclinical Cardiovascular Risk Assessment in Modern Drug Development. *Toxicol. Sci.* **97**, 4–20 (2007).
217. Hughes, J. P., Rees, S. S., Kalindjian, S. B. & Philpott, K. L. Principles of early drug discovery. *Br. J. Pharmacol.* **162**, 1239–1249 (2011).
218. Ingólfsson, H. I. *et al.* Phytochemicals perturb membranes and promiscuously alter protein function. *ACS Chem. Biol.* **9**, 1788–1798 (2014).
219. Andersen, O. S. & Koeppe, R. E. Bilayer Thickness and Membrane Protein Function: An Energetic Perspective. *Annu. Rev. Biophys. Biomol. Struct.* **36**, 107–130 (2007).
220. Lundbaek, J. a, Collingwood, S. a, Ingólfsson, H. I., Kapoor, R. & Andersen, O. S. Lipid bilayer regulation of membrane protein function: gramicidin channels as molecular force probes. *J. R. Soc. Interface* **7**, 373–395 (2010).
221. Košinová, P., Berka, K., Wykes, M., Otyepka, M. & Trouillas, P. Positioning of antioxidant quercetin and its metabolites in lipid bilayer membranes: Implication for their lipid-peroxidation inhibition. *J. Phys. Chem. B* **116**, 1309–1318 (2012).
222. Bahnasi, Y. M. *et al.* Modulation of TRPC5 cation channels by halothane , chloroform and propofol. 1505–1512 (2008). doi:10.1038/sj.bjp.0707689
223. Flemming, P. K. *et al.* Sensing of lysophospholipids by TRPC5 calcium channel. *J. Biol. Chem.* **281**, 4977–4982 (2006).

224. Coldrick, Z., Steenson, P., Millner, P., Davies, M. & Nelson, A. Phospholipid monolayer coated microfabricated electrodes to model the interaction of molecules with biomembranes. *Electrochim. Acta* **54**, 4954–4962 (2009).
225. Lapinsky, D. J. Tandem photoaffinity labeling–bioorthogonal conjugation in medicinal chemistry. *Bioorganic Med. Chem.* **20**, 6237–6247 (2012).
226. Fishwick, C. W. G. & Sanderson, J. M. An Efficient Route to S-N-(9-Fluorenylmethoxycarbonyl)-4'-((1-azido-2,2,2-trifluoroethyl)phenyl)alanine. *Tetrahedron Lett* **35**, 4611–4614 (1994).
227. Song, M. & Sheridan, R. S. Regiochemical Substituent Switching of Spin States in Aryl(trifluoromethyl)carbenes. *J. Am. Chem. Soc.* **133**, 19688–19690 (2011).
228. Lawrence, E. J. *et al.* 3-Aryl-3-(trifluoromethyl)diazirines as versatile photoactivated 'linker' molecules for the improved covalent modification of graphitic and carbon nanotube surfaces. *Chem. Mater.* **23**, 3740–3751 (2011).
229. Dash, C., Shaikh, M. M., Butcher, R. J. & Ghosh, P. Highly convenient regioselective intermolecular hydroamination of alkynes yielding ketimines catalyzed by gold(I) complexes of 1,2,4-triazole based N-heterocyclic carbenes. *Inorg. Chem.* **49**, 4972–4983 (2010).
230. Bond, M. R., Zhang, H., Vu, P. D. & Kohler, J. J. Photocrosslinking of glycoconjugates using metabolically incorporated diazirine-containing sugars. *Nat. Protoc.* **4**, 1044–1063 (2009).
231. Ghiassian, S. *et al.* Photoinduced carbene generation from diazirine modified task specific phosphonium salts to prepare robust hydrophobic coatings. *Langmuir* **28**, 12326–12333 (2012).
232. Black, J. Heinz Otto Schild. 18 May 1906-15 June 1984. *Biogr. Mem. Fellows R. Soc.* **39**, 383–415 (1994).
233. Wyllie, D. J. A. & Chen, P. E. Taking The Time To Study Competitive Antagonism. *Br. J. Pharmacol.* **150**, 541–551 (2009).
234. Kutter, E. in *Encyclopedia of Genetics* 435–436 (2001).
235. Storch, U., Forst, A. L., Philipp, M., Gudermann, T. & Mederos Y Schnitzler,

- M. Transient receptor potential channel 1 (TRPC1) reduces calcium permeability in heteromeric channel complexes. *J. Biol. Chem.* **287**, 3530–3540 (2012).
236. Thinon, E. *et al.* Global profiling of co- and post-translationally N-myristoylated proteomes in human cells. *Nat. Commun.* **5**, 1–13 (2014).
237. Wright, M. H. *et al.* Quantitative chemoproteomic profiling reveals multiple target interactions of spongiolactone derivatives in leukemia cells. *Chem. Commun.* **53**, 12818–12821 (2017).
238. Kanoh, N. *et al.* Distribution of photo-cross-linked products from 3-aryl-3-trifluoromethyldiazirines and alcohols. *Tetrahedron* **64**, 5692 (2008).
239. McDonald, R. S., Teo, K. C. & Stewart, R. Trifluoromethyl ketone hydration. Substituent effects of amino-groups and the hydrating properties of aqueous dimethyl sulphoxide. *J. Chem. Soc. Perkin Trans. 2* 297–299 (1983). doi:10.1039/P29830000297
240. Hashimoto, M. & Hatanaka, Y. Practical conditions for photoaffinity labeling with 3-trifluoromethyl-3-phenyldiazirine photophore. *Anal. Biochem.* **348**, 154–156 (2006).
241. Wright, M. H. *et al.* Global analysis of protein N-myristoylation and exploration of N-myristoyltransferase as a drug target in the neglected human pathogen leishmania donovani. *Chem. Biol.* **22**, 342–354 (2015).
242. Presolski, S. L., Hong, V. P. & Finn, M. G. Copper-Catalyzed Azide–Alkyne Click Chemistry for Bioconjugation. *Curr. Protoc. Chem. Biol.* **3**, 153–162 (2011).
243. Heal, W. P., Wright, M. H., Thinon, E. & Tate, E. W. Multifunctional protein labeling via enzymatic N-terminal tagging and elaboration by click chemistry. *Nat. Protoc.* **7**, 105–117 (2012).
244. Bak, D. W., Pizzagalli, M. D. & Weerapana, E. Identifying Functional Cysteine Residues in the Mitochondria. *ACS Chem. Biol.* **12**, 947–957 (2017).
245. Verhelst, S. H. L., Fonović, M. & Bogyo, M. A mild chemically cleavable linker system for functional proteomic applications. *Angew. Chem. Int. Ed.* **46**, 1284–1286 (2007).

246. Niphakis, M. J. *et al.* A Global Map of Lipid-Binding Proteins and Their Ligandability in Cells. *Cell* **161**, 1668–1680 (2015).
247. Wilchek, M. & Bayer, E. A. Introduction to avidin-biotin technology. *Methods Enzymol.* **184**, 5–13 (1990).
248. Golkowski, M., Pergola, C., Werz, O. & Ziegler, T. Strategy for catch and release of azide-tagged biomolecules utilizing a photolabile strained alkyne construct. *Org. Biomol. Chem.* **10**, 4496–4499 (2012).
249. Weerapana, E. *et al.* Quantitative reactivity profiling predicts functional cysteines in proteomes. *Nature* **468**, 790–797 (2010).
250. Szychowski, J. *et al.* Cleavable biotin probes for labeling of biomolecules via azide-alkyne cycloaddition. *J. Am. Chem. Soc.* **132**, 18351–18360 (2010).
251. Park, K. D., Liu, R. & Kohn, H. Useful Tools for Biomolecule Isolation, Detection, and Identification: Acylhydrazone-Based Cleavable Linkers. *Chem. Biol.* **16**, 763–772 (2009).
252. Yokoshima, S. *et al.* Development of photoaffinity probes for  $\gamma$ -secretase equipped with a nitrobenzenesulfonamide-type cleavable linker. *Bioorganic Med. Chem. Lett.* **19**, 6869–6871 (2009).
253. Fonović, M., Verhelst, S. H. L., Sorum, M. T. & Bogoy, M. Proteomics Evaluation of Chemically Cleavable Activity-based Probes. *Mol. Cell. Proteomics* **6**, 1761–1770 (2007).
254. Yang, Y. Y., Grammel, M., Raghavan, A. S., Charron, G. & Hang, H. C. Comparative analysis of cleavable azobenzene-based affinity tags for bioorthogonal chemical proteomics. *Chem. Biol.* **17**, 1212–1222 (2010).
255. Monnet, F. P. Sigma-1 receptor as regulator of neuronal intracellular  $\text{Ca}^{2+}$ : clinical and therapeutic relevance. *Biol. cell* **97**, 873–883 (2005).
256. Amer, M. S. *et al.* Inhibition of endothelial cell  $\text{Ca}^{2+}$  entry and transient receptor potential channels by Sigma-1 receptor ligands. *Br. J. Pharmacol.* **168**, 1445–1455 (2013).
257. Yoshida, T. *et al.* Nitric oxide activates TRP channels by cysteine S-nitrosylation. *Nat. Chem. Biol.* **2**, 596–607 (2006).

258. Wong, C. O., Sukumar, P., Beech, D. J. & Yao, X. Nitric oxide lacks direct effect on TRPC5 channels but suppresses endogenous TRPC5-containing channels in endothelial cells. *Pflugers Arch. Eur. J. Physiol.* **460**, 121–130 (2010).
259. Hecquet, C. M., Ahmmed, G. U., Vogel, S. M. & Malik, A. B. Role of TRPM2 channel in mediating H<sub>2</sub>O<sub>2</sub>-induced Ca<sup>2+</sup> entry and endothelial hyperpermeability. *Circ. Res.* **102**, 347–355 (2008).
260. Lorsbach, B. A. *et al.* N-Substituted Piperazines as insecticides or fungicides. US 2007/0004750 A1 (2007).
261. Abe, Y. *et al.* A Novel Class of Orally Active Non-Peptide Bradykinin B<sub>2</sub> Receptor Antagonists . 2 . Overcoming the Species Difference between Guinea Pig and Man. *J. Med. Chem.* **41**, 4053–4061 (1998).
262. Tang, Z. & Marx, A. Proline-Modified DNA as Catalyst of the Aldol Reaction. *Angew. Chem. Int. Ed.* **46**, 7297–7300 (2007).
263. Storz, M. P. *et al.* Validation of PqsD as an Anti-biofilm Target in *Pseudomonas aeruginosa* by Development of Small-Molecule Inhibitors. *J. Am. Chem. Soc.* **134**, 16143–16146 (2012).
264. Mccutcheon, D. C., Porterfield, W. B. & Prescher, J. A. Rapid and scalable assembly of firefly luciferase substrates. *Org. Biomol. Chem.* **13**, 2117–2121 (2015).
265. Chaturvedula, P. V *et al.* Constrained compounds as cgrp-receptor antagonists. Constrained compounds as cgrp-receptor antagonists (2007).
266. Dvorak, C. A. *et al.* 4-Phenoxypiperidines: Potent, Conformationally Restricted, Non-Imidazole Histamine H<sub>3</sub> Antagonists. *J. Med. Chem.* **48**, 2229–2238 (2005).
267. Minard, A. *et al.* Remarkable Progress with Small-Molecule Modulation of TRPC1/4/5 Channels: Implications for Understanding the Channels in Health and Disease. *Cells* **7**, 52–72 (2018).
268. Danker, T. & Möller, C. Early identification of hERG liability in drug discovery programs by automated patch clamp. *Front. Pharmacol.* **5 AUG**, 1–11 (2014).

269. Technologies, L. Fura-2 Calcium Indicator. <http://www.lifetechnologies.com/uk/en/home/life-science/drug-discovery/target-and-lead-identification-and-validation/g-protein-coupled-html> 2015-08-05 Available at: <http://www.lifetechnologies.com/uk/en/home/life-science/drug-discovery/target-and-lead-identification-and-validation/g-protein-coupled-html>. (Accessed: 5th August 2015)
270. Prinz, H. Hill coefficients, dose-response curves and allosteric mechanisms. *J. Chem. Biol.* **3**, 37–44 (2010).
271. Persson, F., Carlsson, L., Duker, G. & Jacobson, I. Blocking Characteristics of hERG, hNav1.5, and hKvLQT1/hminK after Administration of the Novel Anti-Arrhythmic Compound AZD7009. *J. Cardiovasc. Electrophysiol.* **16**, 329–341 (2005).
272. Schroeder, K., Neagle, B., Trezise, D. J. & Worley, J. IonWorks™ HT : A New High-Throughput Electrophysiology Measurement Platform Journal of Biomolecular. *J. Biomol. Screen.* **8**, 50–64 (2003).
273. Costantin, J., Handran, S., Yamane, D. & Yang, N. Primary screening of a 1564 compound focused diversity set against the human cardiac sodium channel Nav1.5 using the IonWorks Quattro system. Available at: <http://www.eposters.net/pdfs/primary-screening-of-a-1564-compound-focused-diversity-set-against-the-human-cardiac-sodium-channel.pdf>. (Accessed: 16th August 2016)
274. Tristani-Firouzi, M. & Sanguinetti, M. C. Voltage-dependent inactivation of the human K<sup>+</sup> channel KvLQT1 is eliminated by association with minimal K<sup>+</sup> channel (minK) subunits. *J. Physiol.* **510**, 37–45 (1998).
275. Urgaonkar, S. & Shaw, J. T. Synthesis of Kaempferitrin. *J. Org. Chem.* **72**, 4582–4585 (2007).
276. McHugh, D., Flemming, R., Xu, S. Z., Perraud, A. L. & Beech, D. J. Critical intracellular Ca<sup>2+</sup> dependence of transient receptor potential melastatin 2 (TRPM2) cation channel activation. *J. Biol. Chem.* **278**, 11002–11006 (2003).
277. Wang, L. *et al.* Alternative One-Pot Synthesis of (Trifluoromethyl)phenyldiazirines from Tosyloxime Derivatives: Application for New Synthesis of Optically Pure Diazirinyphenylalanines for Photoaffinity



Labeling. *Org. Lett.* **17**, 616–619 (2015).

278. Geyer, P. E. *et al.* Plasma Proteome Profiling to Assess Human Health and Disease. *Cell Syst.* **2**, 185–195 (2016).
279. Mosley, C. a *et al.* Synthesis, structural activity-relationships, and biological evaluation of novel amide-based allosteric binding site antagonists in NR1A/NR2B N-methyl-d-aspartate receptors. *Bioorganic Med. Chem.* **17**, 6463–6480 (2009).
280. Hosoda, H., Miyao, T., Uchida, S., Sakai, S. & Kida, S. Development of a tightly-regulated tetracycline-dependent transcriptional activator and repressor co-expression system for the strong induction of transgene expression. *Cytotechnology* **63**, 211–216 (2011).